IMPERIAL COLLEGE OF SCIENCE, TECHNOLOGY
AND MEDICINE

University of London

DYNAMIC ANALYSIS OF COUPLED STRUCTURES USING EXPERIMENTAL DATA,

by

António Paulo Vale Urgueira

A thesis submitred to rhe University of London for
the degree of Doctor of Philosophy and for the
Diploma of Imperial College.

Dynamics Section
Department of Mechanical Engineering
Imperial College of Science, Technology and Medicine
London SW7

October 1989

To my wife Cândida and my son Andre'

ABSTRACT

The work in this thesis is concerned with substructure coupling techniques which incorporate data readily available from modal tests. Two coupling techniques are investigated in detail, namely the Impedance and Modal Coupling techniques. In the former, different procedures for reducing models are described and the effects of the corresponding incompleteness - at this stage mainly relating to the **coordinates - are** investigated in order to detect and understand the main sources of errors in the predicted dynamic behaviour of different case studies. Additionally, alternative coupling algorithms are proposed to overcome numerical errors arising due to redundancy in the set of connection coordinates. In the second technique - Modal coupling - the investigation is concentrated on the effects of truncating the number of **modes.** A refined approach is presented for including residual flexibility equivalent to the omitted modes by incorporating a dummy flexible system between two components.

A common problem in all the investigated coupling techniques is that their validity may be reduced by using experimental data which **can** be measured rather than the data that **ought** to be measured. One of the most critical areas here is the formulation of meaningful constraint equations to express the actual physical connections between components. Sometimes, the number of measured junction coordinates can be excessive, thus provoking numerical difficulties during the coupling process. On other occasions, there are extreme situations where a lack of information causes a meaningless representation of the actual connection properties. Both situations are dealt with in the present work. The former is investigated by making use of a well established mathematical technique - the Singular Value Decomposition - which permits a confident inversion of ill-conditioned matrices and, additionally, detects the redundant coordinates responsible for the coupling numerical failures, when combined with a QR factorization. The latter aspect is related to the possibility of accurately measuring rotational coordinate

responses. These are important ingredients in a coupling process whenever moments must be transmitted through the connections. A new laser measurement technique is used for sensing the responses in the vicinity of a connecting region of a vibrating structure, which in this work is a simple straight beam. The rotational data are subsequently compared with theoretical values and with those estimated from accelerometer measurements made either with the transducers placed on one exciting block or closely-spaced near the coordinate of interest.

In order to assess the validity of the mathematical and experimental tools developed in this thesis, several case studies are presented. Some of them make use of theoretically-derived models to simulate practical conditions and others are experimentally-derived models of actual components which are used to predict the coupled structures responses, which in turn are compared with measured results on the actual assemblies.

ACKNOWLEDGMENTS

I am deeply grateful to my supervisor, Prof. D.J. Ewins, for his support, sustained interest and guidance throughout the duration of this work.

Thanks are also due to the members of the Dynamics Section, especially to Dr. M. Imregun and Mr. D.A. Robb, for their helpful advice and assistance over the years.

For their friendly coorperation and useful discussions throughout the duration of this work, I would also like to express my gratitude to many past and present colleagues in the Dynamics Section, in particular to W. Adam, N. Lieven, N.M.M. Maia, W.M. To and W.J. Visser.

I am especially grateful to Fundação Calouste Gulbenkian for the financial support provided over the period in which this work was carried out.

I am also indebted to the Reitoria da Universidade Nova de Lisboa for their scholarship equivalence granted during the course of the present work.

I would also like to acknowledge Ometron, Plc. for the loan of a Vibration Pattern Imager which has been used for the laser experiments.

Finally, I wish to express a word of special gratitude to my wife Cândida and my son Andre, to whom this thesis is dedicated. Without their patience, encouragement and invaluable support the work might never have culminated in this thesis.

NOMENCLATURE

DoF	- degree(s) of freedom
FRF	- frequency response function
SVD	- Singular Value Decomposition
${}_rA_{jk}$	- modal constant (mode r, FRF jk)
$\{{}_Af_c\}$, $\{{}_Bf_c\}$	- vector of interconnecting forces acting on component A and B, respectively
$H_{jk}(\omega)$, $[H(\omega)]$	- general FRF and FRF matrix (Receptance, Mobility and Accelerance)
$[H(\omega)]_{est}$, $[H(\omega)]_{meas}$	- estimated and measured FRF matrices
$[I]$	- identity matrix
$[K]$	- stiffness matrix
$[K_{cpl}]$	- stiffness matrix of the interconnecting system
m, m_k, m_e	- number of total, kept and eliminated modes
$[M]$	- mass matrix
N	- number of total coordinates
n_p, n_s	- number of primary (master) and secondary (slaves) coordinates, respectively
n_c, n_i	- number of connection and interior coordinates, respectively
$\{p_m\}$, $\{p_k\}$, $\{p_e\}$	- vector of principal coordinates referred to the m, m_k and m_e modes, respectively
$[P]$	- permutation matrix
r	- rank of a matrix
R_{jk}, S_{jk}	- high- and low-residual terms of FRF jk
$[{}_AR_{cc}]$, $[{}_BR_{cc}]$	- residual flexibility matrix referred to the connection coordinates of subsystem A and B, respectively
$\{u_i\}$, $\{u_c\}$	- vector of displacements referred to the interior and connection coordinates

[U], [V]	- matrices formed of left and right singular vectors, respectively
$[Z(\omega)]$	- general Impedance matrix (Dynamic Stiffness, Mechanical Impedance and Apparent Mass)
δ	- threshold to define rank of a matrix
ε	- machine precision
σ_i	- singular value i
ω	- circular frequency
ω_r	- undamped natural frequency
λ_r	- damped natural frequency
η_r	- damping factor for mode r
$\alpha_{jk}(\omega)$,$[\alpha(\omega)]$	- Receptance FRF, matrix
$[\Phi]$	- mass-normalised modal matrix
$[\Phi_m]$,$[\Phi_k]$,$[\Phi_e]$	- mass-normalised modal matrices corresponding to the total, kept and eliminated modes, respectively
$[\Psi]$	- non-normalised modal matrix
$[\ ]^T$	- transpose of a matrix
$[\ ]^H$	- complex conjugate transpose of a matrix
$[\ ]^+$	- pseudo-inverse of a rectangular matrix
$[\ ]^{-1}$	- inverse of a matrix
II II	- norm of a matrix
$\lvert\ \rvert$	- determinant of a matrix

TABLE OF CONTENTS

Chapter 1 INTRODUCTION

Chapter 2 STANDARD COUPLING TECHNIQUES

Chapter 3 IMPEDANCE COUPLING TECHNIQUES

Chapter 4 MODAL COUPLING TECHNIQUES

Chapter 5 SELECTION OF VALID CONNECTION COORDINATES

Chapter 6 EXPERIMENTAL DETERMINATION OF ROTATIONAL RESPONSES

Chapter 7 EXPERIMENTAL CASE STUDIES

Chapter 8 CLOSURE

1 INTRODUCTION

1.1 PREAMBLE

It is generally acknowledged that the advent of the Finite Element Method (FEM) constituted a major step towards the analysis of more complicated static and dynamic structural mechanics problems. Rather than trying to formulate the equilibrium equations of a given problem, treating the structure as a whole continuously defined entity, a new philosophy was then initiated which acted as a catalyst for several researchers. A basic principle inherent to this philosophy was the assumption of the whole structure being composed of individual analytical elements such as beams, plates or shells which, at a final stage, could be assembled to provide a model of the complete system.

Nevertheless, the complexity inherent in an increasing number of engineering problems still resulted in limitations of this type of 'discretised' structure when applied with the available computational means, mainly due to the large order of the matrices involved in the process. A more general approach was then necessary whereby a complex structure could be regarded as being formed of different substructures (or components), each of which could first be analysed individually and independently from the others. In this way, before being assembled to form the complete structure, each analysis could be done by whichever method was most convenient and eventually the substructure models could be assembled together to obtain the equations related to the complete structure. This is the idea underlying the nowadays well-known 'substructuring', 'building block' or 'coupling' approaches for solving static and dynamic problems.

Originally, the idea was restricted to the use of purely theoretical models but, as it was often found that certain substructure models could not be properly formulated due to their complexity, the method was developed so as to incorporate models derived by an experimental route also. This different route, can not only complement a subsystem theoretical model - by verifying and updating - but also can provide a suitable and reliable subsystem model for direct assembly in the coupling process. This route is nowadays firmly established and an experimental counterpart to the FE modelling is becoming widely used - the techniques being referred to as 'Modal Testing', 'Experimental Modal Analysis' or 'System Identification'. Recent advances in Modal Testing methods and in digital processing have reduced the time required and increased the accuracy and confidence associated with the experimental determination of modal parameters, which are the essential ingredients to construct an experimental model.

Accordingly, an ideal substructure approach should be versatile in terms of being able to incorporate data from either the sources - the FE method or Modal Testing. Such a method should yet provide other important benefits which may be outlined as,

- considerable insight into a complex system's dynamics can be obtained from the component or subsystem analyses which precede the system assembly level studies. In other words, each component can be treated by a more accurate and refined model. In certain cases, it may happen that components are still too large to be analysed by conventional experimental means, especially if they have to be suspended to simulate free-free support conditions. The substructure approach allows a further sub-division into other subsystems which are easier to measure.

- there is the possibility of creating a library of standard subsystems for which a high level of modelling has already been achieved. Such components can be input, as often as needed, into several assembly processes;

- the location and time for each component analysis may be selected during the design stage, since different organizations on different sites can perform the analysis for each part;

- each dynamic model may be obtained by theoretical analysis or by testing of the individual subsystems - these are easier to handle than the total system. A mixture of theoretical and experimental subsystem modelling is one of the main requirements for using coupling techniques; and

- any structural modification which has to be applied at any time only involves a re-analysis of the affected part. A design change in one part only implies new data for that modified part which can then be coupled with the remaining unmodified components, without requiring a reanalysis of the rest of the structure.

The possibility of attaining a more precise description of the component dynamic properties at the subsystem level leads to a better exploitation of the computational and experimental means available from an individual organization or team. However, it should be borne in mind that not all the thus-obtained information is necessarily incorporated into the system model, otherwise no gain would be obtained in terms of efficiently handling the size of matrices required for the formulation of the coupled structure final equation of motion. Thus, there is the necessity of reducing, in an optimum way, the size of the matrices at the subsystem level, while retaining a precise description of the dynamic properties. Any imprecise formulation of the reduced or condensed model will affect the predicted dynamic behaviour for the whole system.

Generally, the main steps involved in a substructuring technique may be described as;

System level

Step **1** - Partitioning of the whole physical system model into a number of substructures with a proper choice of connection and interior coordinates. At this stage, it must have already been decided which components are going to be subjected to a modal test and which ones are amenable to modelling by the finite element (or other analytical) method. In some cases, it may happen that both experimental and theoretical routes are chosen for the modelling phase of a given component.

Subsystem level

Step 2 - Derivation of the respective models, either by a theoretical or an experimental approach, with selection of an adequate number of coordinates and/or modes to be retained in the analysis and, whenever possible, with an evaluation of the effects of neglecting certain coordinates or modes.

Step 3 - Formulation of the subsystem equations of motion which are generally made by using physical or modal coordinates and, if possible, without requiring the knowledge of the dynamic properties of the remaining components forming the global structure. Such independency is an important requirement, although the interconnecting conditions must be commonly defined by some of the organizations involved in the design.

Sys tern level

Step 4 - Construction of reduced-order equations for the global structure (the assembly) by invoking interface displacement compatibility and force equilibrium conditions established for the different component models.

One can note that, the reduction or condensation process - performed at the subsystem stage - leads to a distinction between the different coupling techniques available which we shall divide into two major categories. One the one hand, there are techniques in which the order of the matrices involved in the final equation of motion is dictated by the number of kept (primary) coordinates pertaining to each subsystem (reduced) model. On the other hand, there is another category of techniques which also benefit from a reduction performed at the component level, but this time based on the number of modes included. In this thesis we shall refer to the former approach as “Impedance coupling” and to the latter one as “Modal coupling”. Before we proceed further to summarise the relevant works in both categories of methods, some terminology is necessary to characterize the subsystem models.

1.2 SUBSYSTEM MODELS

Essential to the communication among different organizations and research groups is the terminology and format used to describe the dynamic properties of a system or subsystem model, be it theoretically- or experimentally-derived. To start with, we shall present the different model formats using the same terminology as Ewins [1] and simultaneously, when pertinent, other similar designations will be referred to.

(i) Spatial Models

By discretising a given system, it is essential to assign to each of the N coordinates (or degrees-of-freedom (DoF)) the values of the spatially distributed properties i.e., the mass, stiffness and damping. The way to do so is by presenting each of those properties in a matrix form as follows,

$[M]_{NxN}$ - mass matrix which provides a means to define the inertia forces assigned to each DoF when they experience an acceleration (the off-diagonal terms contain the inertia coupling information),

$[K]_{NxN}$ - stiffness matrix providing a means to define the inherent restoring forces due to the relative displacements at each DoF (similarly to the previous one, the off-diagonal terms express the way the DoF are statically coupled)

$[C]_{NxN}$, $[H]_{NxN}$ - viscous and hysteretic damping matrices, respectively. They are not always used since damping is often neglected in theoretical modelling which means that the dissipative forces are negligible when compared to the previously mentioned ones.

It is important to note that the above mentioned definitions have a clear physical meaning in the case of lumped parameter systems whereby one can associate a DoF to a lumped region (such as in spring-mass models). This is not the case when matrices result from a

between the various finite elements connected at the so-called nodal points as described by Zienkiewicz [2].

A complete Spatial model has inherent to it N coordinates and N modes. As shown in chapter 3, Spatial models which are reduced or condensed to P primary or master coordinates will have order P (<N) i.e., they will possess information on P coordinates and P modes only.

Sometimes, Spatial models are referred to as Time Domain models, since equations of motion formulated by using Spatial properties contain the response motions of a system as functions of time.

(ii) Modal Models

There are situations where the dynamic properties are most conveniently described in terms of natural frequencies and associated mode shapes. Such convenience may arise from the need to compare data from different sources which use different routes to attain the modal description as mentioned by Ewins [3], or as a simple reason if it is intended to show an animated display of the structure at each corresponding natural frequency.

Mathematically, the mode shapes are represented as vectors in which each element represents a deflection of one DoF relative to the other (N-l) DoF in the model. The modal vectors (or eigenvectors) can be grouped together in the so-called Modal matrix which is represented by $[\Psi]_{NxM}$ - a square or rectangular matrix containing information on N coordinates and M modes. The eigenvalues, which are intimately related to the system natural frequencies, can be grouped together forming the diagonal terms of a diagonal matrix represented as $\left[\lambda_r^2\right]_{MxM}$. Generally, both are complex matrices whose real and imaginary parts have distinct physical meanings. Let us consider the k^{th} eigenvalue λ_k^2 and the corresponding mode shape $\{\psi\}_k$ as presented next for both matrices;

$$\left[\lambda_r^2\right]_{MxM} = \begin{bmatrix} \cdot & & \\ & \cdot & \\ & & \boxed{\omega_k^2(1+i\,\eta_k)} \\ & & & \cdot \end{bmatrix}$$

$$\left[\Psi\right]_{NxM} = \begin{bmatrix} \cdot & \cdot & \left\{ \begin{matrix} {}_k a_1 + i\,{}_k b_1 \\ {}_k a_2 + i\,{}_k b_2 \\ {}_k a_3 + i\,{}_k b_3 \\ \cdot \\ {}_k a_N + i\,{}_k b_N \end{matrix} \right\} & \cdot \\ \cdot & \cdot & & \cdot \\ \cdot & \cdot & & \cdot \\ \cdot & \cdot & & \cdot \\ \cdot & \cdot & & \cdot \end{bmatrix}$$

The k^{th} eigenvalue contains the information related simultaneously to the k^{th} natural frequency (ω_k) and modal damping (η_k) of the k^{th} mode $\{\psi\}_k$ which in turn is represented by a real part - the relative amplitude of motion at each DoF - and by an imaginary part which expresses the phase.

Since the mode shapes represent relative amplitudes at the DoF, rather than absolute deflections of the structure, the elements of each modal vector are scaled in some manner. Generally, they are scaled in such a way the largest element is made equal 1 (for instance for graphic visualisation purposes). On other occasions, when Modal models are obtained from different sources, it is convenient to have a consistent scaling factor. This can be achieved by making use of the concept of modal masses and modal stiffnesses. Due to the orthogonality of the mode shapes relative to the mass and stiffness matrices, the following relationships hold (if $M \leq N$):

$$\left[m_r\right]_{MxM} = \left[\Psi\right]^T_{MxN}\,[M]_{NxN}\,\left[\Psi\right]_{NxM}$$

$$\left[k_r\right]_{MXM} = \left[\Psi\right]^T_{MxN}\,[K]_{NxN}\,\left[\Psi\right]_{NxM}$$

being the modal masses and modal stiffnesses interrelated as $\lambda_r^2 = k_r / m_r = \omega_r^2(1+i\,\eta_r)$. If modal masses are used to scale the mode shapes, a new orthonormal set is obtained,

$$[\Phi]^{T}_{MxN}\,[M]_{NxN}\,[\Phi]_{NxM} = [I]_{MxM}$$

$$[\Phi]^{T}_{MxN}\,[K]_{NxN}\,[\Phi]_{NxM} = \left[\lambda_{r}^{2}\right]_{MxM}$$

which is here assumed to be the normalised format for the presentation of mode shapes. In fact, these are the mode shapes obtained from modal constants which are extracted from measured data by performing a Modal Analysis process, as shown by Ewins [1].

(iii) Response Models

According to the description in common use in the analysis of control systems and electrical circuits, we shall assume a structure possessing inputs and outputs which can be interrelated through a kind of 'black box' . The (input) forces {f(t)} applied to the system can be related to the (output) responses {x(t)} whenever the dynamic characteristics are known. Let us consider a **linear** system excited with harmonic forces for which the input/output relationship can be written in the frequency domain as,

$$\{X(\omega)\} = [H(\omega)]\,\{F(\omega)\}$$

or $$\{F(\omega)\} = [Z(\omega)]\,\{X(\omega)\}$$

where $[H(\omega)]$ and [Z(ω)] are frequency response transfer functions of the system related as,

$$[Z(\omega)] = [H(\omega)]^{-1}$$

From an experimental standpoint, either of these matrices could be measured directly on the structure. Depending on when displacement, velocity or acceleration is considered as the response, the transfer function matrix [H(w)] is called **Receptance** (or Admittance, Dynamic Compliance, Dynamic Flexibility), **Mobility** or **Inertance** (or Accelerance) respectively. In these matrices, each element is a complex ratio (response/force) which is

Due to the wide use of accelerometers to sense responses on structures, the FRFs are generally measured in terms of Inertance. The Response model is then expressed as a matrix - the **FRF matrix** - whose elements are measured FRFs. The corresponding inverses of the above mentioned matrices are called **Dynamic Stiffness, Mechanical Impedance** and **Apparent Mass,** respectively. Nevertheless, we shall refer to a generalised **Impedance matrix** as the inverse of whichever assumed FRF matrix.

It is important, however, to bear in mind that different practical constraints are associated with the measurement of either $[H(\omega)]$ or $[Z(\omega)]$. If, for instance, element H_{ij} is considered in matrix [H(W)], in physical terms this represents the amplitude and relative phase of a harmonic displacement at DoF i due to a harmonic force applied at DoF j (when no external forces are applied to any DoF other than j). A different physical meaning has Z_{ij} which represents the amplitude and relative phase of a harmonic force applied to or constraining DoF i such as DoF j executes a unit displacement (when no other **displacement** exists other than j). These two definitions explain two important distinctions between the FRF matrix and its inverse, the Impedance matrix.

- Firstly, to measure directly the elements in the Impedance matrix requires the displacements at numerous DoF to be held at zero. Conversely, direct measurement of the elements in the FRF matrix only requires an easy constraint to be satisfied in practical terms - only one force should be applied each time an (FRF) element is measured.

- Secondly, a measured FRF matrix at one stage of the design can be later expanded by simply performing new measurements at additional coordinates to form new rows and columns without modifying any existing elements. This is not the case whenever an Impedance matrix needs to be expanded, since all the existing elements have to be re-measured after the new constraints have been imposed to the structure.

Accordingly, the **Response models are** described by a **FRF matrix** whose elements (FRFs) can be either all measured or all analytically calculated or, sometimes, a mixture of both.

It is possible to derive a Response model theoretically by invoking the relationship between Response and Spatial or Response and Modal models as presented by Ewins [1] and outlined here for the Receptance matrix,

$$[\alpha(\omega)]_{NxN} = [[K] - \omega^2[M]\ ]^{-1}_{NxN}$$

$$[\alpha(\omega)]_{NxN} = [\Phi]_{NxM}\left[\ (\lambda_r^2-\omega^2)\ \right]^{-1}_{MxM}[\Phi]^T_{MxN}$$

where N and M are the numbers of coordinates and modes, respectively.

For simple components, however, a closed-form solution based on differential equations of equilibrium, can be used to relate 'exactly' the responses and excitations, as presented in textbooks by Bishop and Johnson [4] and Timoshenko [5].

All of the models previously mentioned may be interrelated as presented in fig. 1.1 for the particular case of undamped systems. Although it is assumed in the presented relationships that matrices have order N (number of coordinates = number of modes), they are still valid for reduced models whose number of coordinates (N) is less than the number of modes (M). Conversely, if M > N and an inverse (or pseudoinverse) has to be calculated to perform the necessary conversion, there is a numerical difficulty since the matrix to be inverted is rank deficient. This subject is discussed in more detail in chapter 3.

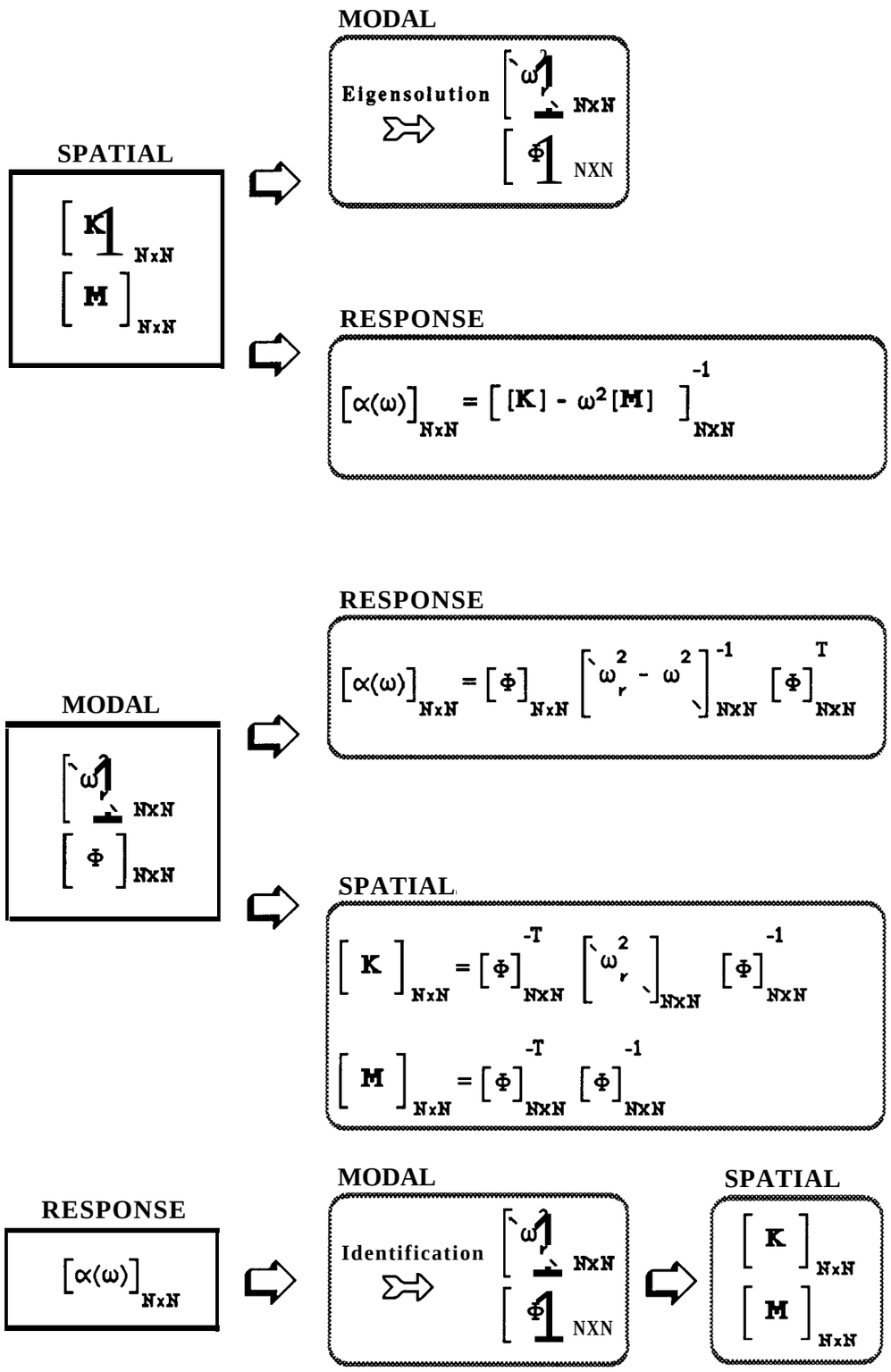
SPATIAL
[K] NxN
[M] NxN
MODAL
Eigensolution
[ω²] NxN
[Φ] NXN
RESPONSE
[α(ω)] NxN = [[K] - ω²[M]] -1 NxN
MODAL
[ω²] NxN
[Φ] NxN
RESPONSE
[α(ω)] NxN = [Φ] NxN [ω²r - ω²] -1 NxN [Φ] T NxN
SPATIAL
[K] NxN = [Φ] -T NxN [ω²r] NxN [Φ] -1 NxN
[M] NxN = [Φ] -T NxN [Φ] -1 NxN
RESPONSE
[α(ω)] NxN
MODAL
Identification
[ω²] NxN
[Φ] NXN
SPATIAL
[K] NxN
[M] NxN

1.3 SUMMARY OF PREVIOUS WORK

There have been numerous researchers addressing the substructuring method, especially since the early 1960's. A brief review is presented here, although a more thorough discussion is carried out in some later chapters when specific techniques are described or referred to in more detail.

To start with, we shall address the coupling techniques which exploit, in terms of computational efficiency, a reduction performed on the coordinates at the subsystem level. Depending on whether **Spatial** or **Response** component models are used directly as input data into the coupling process, the assembling techniques are here designated as **Spatial** or **FRF Coupling** techniques, respectively. The former is ideal for the use of FE methods whereas the latter comprises both theoretical and experimental fields of work. The FRF coupling technique is generally referred to as the "Impedance Coupling" technique since, at the system level, it assembles mathematically the generalised Impedance properties of each component although in practical terms, as mentioned in the previous section, they are not the directly measured ones. In chapter 3 a detailed discussion is devoted to the FRF Coupling method.

Early works were presented making an analogy between electrical circuits and vibrating systems, one of them from Duncan [6]. The concepts of linear operators and the principle of superposition were employed by Sykes [7] to develop linear multi-terminal network theory for solving periodic steady-state and transient vibration problems of mechanical systems synthesised from a number of small substructures. One of the most significant analytical works in the development of the Mobility (Impedance) concept is that by Bishop and Johnson [4]; from an 'exact' formulation of the Response model of a beam component, the properties of multi-beam assemblies could be formulated. The application of the conceptually-simple Impedance Coupling technique is straightforward when the components are amenable to theoretical modelling, but practical complex systems have demanded subsystem Impedances to be derived from measured data rather than a purely

models are necessarily an approximation of real structures, even if the solution of differential equations of motion are ‘exact’, whereas measuring a structure permits a description of its own equations of equilibrium and boundary conditions. Although models obtained via this latter approach have the advantage of more closely reflecting the ‘true’ dynamic characteristics of a structure, they are contaminated with errors arising during the acquisition and analysis of measure data. Consequently, the accuracy of the assembled structure results will be affected.

The experimental approach to the Impedance Coupling problem was one of the main reasons which motivated a breakthrough to the development of suitable techniques and equipment to measure, assess and analyse data. A comprehensive work was presented by Ewins [9] concerning ground rules, measurement techniques and interpretation and application of measured data with an extensive selected bibliography. The Impedance coupling technique was applied to many engineering problems, such those presented by Klosterman [10], Sainsbury and Ewins [11], Ewins, Silva and Maleci [12], Hunter and Otts [13] and Heer and Lutes [14], just to quote some of the earliest cases. The main difficulties encountered in those applications were mainly related to the mathematical inconsistency of the measured models and to the inadequacy of experimental means to measure some terms in the FRF matrices of certain components. Mostly, those FRFs were related to rotational response measurements.

The FRF matrix of a measured component tends to be ill-conditioned near each resonance frequency, especially when lightly-damped structures are dealt with. If any error in the FRFs is present in the vicinity of those regions, which is most likely in measured models causing the undesirable mathematical inconsistency, numerical failures will arise during the coupling process and, as a consequence, meaningless predicted results obtained. Lutes and Heer [15] addressed this problem by numerically ‘filtering out’ elements in the FRF matrix. Another approach was implemented in works by Ewins [16], Gleeson [17] and Imregun, Robb and Ewins [18], where the inconsistency was removed by subjecting raw data to modal analysis and then from the modal data base thus-obtained smoothed FRFs were regenerated to improve the predictions.

Rotational responses are necessary to formulate proper constraints between connected components. Success in the prediction of results for a coupled structure is dependent on how the connection coordinates are measured and included in a coupling process, as demonstrated in some practical applications undertaken by Ewins and Sainsbury [19], Henderson [20] and Maleci and Young [21]. For instance, by simply assuming one point-connected components, if they respond to excitations in all three planes, it is vital to include the three rotations in addition to the three translations in order to properly formulate the constraint conditions. In terms of Response models, the FRFs related to rotational response/excitations represent 75% (or 60% if symmetry properties are assumed) of total elements in the corresponding FRF matrix. Although simple to calculate those FRFs analytically, it is not an easy task to perform their measurement. This difficulty motivated a trend in the research procuring practical techniques and transducers to measure rotational quantities. Most of the reported works have tended to use translational transducers (coventional accelerometers) and from them the rotational quantities were derived. An early work in this field was carried out by Smith [22] who attempted to measure complete Mobility data from responses of two accelerometers and by producing an exciting couple with the use of two linear shakers vibrating in anti-phase. Later, a technique using a single shaker and an additional block attached to the structure was used by Sainsbury [23] who made use of different block configurations to minimise the errors, especially related to the FRF rotation/moment which is the most prone to errors. Further studies were carried out by Ewins and Gleeson [24] who developed an alternative technique, especially suitable for lightly-damped structures, which takes into account the special relationship between elements of point FRF matrices. However, this relationship could not be extended to the calculation of the residual flexibility associated with the out-of-range modes. Additionally, Gleeson [17] showed that base strain effects and cross-sensitivity of accelerometers are some of the causes of erroneous estimations of those FRFs. An alternative technique for measuring rotational responses was attempted by Licht [25] and Rorrer [26], who resorted to angular transducers instead of linear ones. The benefits achieved such as, no need to process data from linear responses and to cancel additional mass effects, were not compensatory if the ratio price/accuracy was

compared to the conventional approach. Yet another estimation of rotational responses on beam-type components is possible from the measurement of translational responses at closely-spaced locations near a point of interest. This alternative was attempted by Chen and Cherng [27] and Sattinger [28] by using first- and second-order approximations to estimate the rotational FRFs. Identical conclusions were found about the poor accuracy related to those FRFs, and the differentiation method was seen to accommodate considerable variation in measurement location spacings. The selection of response measurement and excitation location spacings must achieve a balance between resolution and proper approximation of derivatives across the number of natural modes of vibration to be encompassed in the frequency range of interest.

The other coupling method we shall be concerned with is the Modal Coupling technique, also referred to in the related literature as Time Domain or Component Mode Synthesis methods. The basic philosophy is the same as the previous one i.e., it permits the use of reduced component models in order to achieve a reduced order in the final equation of motion matrices of the assembled structure. However, unlike the Impedance based methods which take advantage on the reduction of the number of **coordinates,** these methods use a reduction performed on the number of **modes** used to describe each component model while still accounting for **all** the physical DoF. By using a Ritz-type transformation, the reduced number of principal coordinates is related to the number of modes that are taken into account for the modal estimation; generally, the information relating to the higher natural frequency modes is discarded. This feature in the method reduces the computational effort required in the system analysis and parallels the modal information in a real test, since it is only possible to measure some of the existing modes in a structure. The objective is to maintain a specified level of accuracy in the dynamic analysis, while using only the lower order modes for computational efficiency. Essentially, there are two Modal coupling approaches which differ from each other according to the dynamic displacement shapes used to form the truncated set of the natural modes. In the first approach, the elastic modes pertaining to a fixed-interface component

are retained, whereas in the second one, the modes are obtained by assuming the component to be vibrating in a freely-supported condition at its attachment points.

The basic idea for the fixed-interface method relies on the philosophy of the static substructuring technique proposed by Przemieniecki in 1963 [29]. It was mainly directed towards the use of the finite element technique with the total displacement for each component coordinate being calculated by a superposition of the displacements obtained with fixed and relaxed interface conditions. In 1965, Hurty [30] proposed the Normal mode or Component Mode Synthesis method, at this time focusing his work on dynamic structural systems and taking into account both the component's elastic and mass properties. Later, Craig and Bampton [31] re-formulated Hurty's method by simplifying the choice of the groups of modes for the transformation matrix construction.

In the second alternative - the free-interface method - the necessary natural modes incorporated in that matrix are those obtained from a subsystem vibrating either in its free-interface or completely free support condition. This being the most readily simulated condition during a experimental test, it constitutes an attractive technique for the use of combined experimental /theoretical analysis of dynamic structural systems.

Some of the early works reporting use of free-interface modes were presented by Gladwell [32] and Goldman [33]. The former was called the branch-mode analysis and was limited to the study of subsystems connected in a statically determinate condition, while the latter constituted the basis for more refined techniques. One of these was Hou's work [34] which presents some similarities with Goldman's method, but uses a less complicated procedure for generating the system transformation matrix. In some survey papers by Craig [35], Nelson [36], Goldenberg and Shapiro [37] and Hart, Hurty and Collins [38,39] it has been commonly stated that in the free-interface methods like Hou's and Goldman's procedures, very poor accuracy may be obtained for the overall system natural frequencies and mode shapes compared with the accuracy produced by the fixed-interface methods. However, it was then recognised that the free-interface methods could

the coupling process, which has led to an improvement of the existing methods by developing a great variety of approaches. Some of these presented by MacNeal [40], Kuhar and Stahle [41], Hintz [42], Benfield and Hruda[43] and Rubin [44] were primarily based on a purely analytical description and determination of the component characteristics in other words they are suitable for the theoretical route, while others tried to explore the use of experimentally-derived modal properties as a basis for the formulation of each subsystem's equations of motion. In this latter approach, one important early work is Klosterman's thesis [45] which provides a comprehensive study of the experimental determination of modal representations of components including the use of these models in the substructure coupling.

The structural definition of components from modal tests has been accomplished and successfully used by Klosterman and Lemon [10,461 for design purposes with relatively stiff structures connected with flexible elements such as an automobile frame and body connected by isolation mounts. For this situation, the subsystems can be tested with free boundaries to obtain a free-free modal data base which is sufficient for use in system synthesis. However, in the case where the components are rigidly connected, the use of a set of truncated modes to establish the compatibility equations sometimes leads to unacceptable errors in the system response predictions. In this case, a more accurate definition is necessary either by using more modes or, if these represent an unreasonable number, by providing some information about the effects of the neglected modes. The lack of definition of the component properties may be overcome in two ways; on the one hand, seeking to compensate for a lack of flexibility due to truncation of the set of natural modes by using an additional and important information concerning the flexibility effect of the out-of-range modes. On the other hand, by using additional masses attached to the connection points in an attempt to generate a more realistic condition for the component when it is vibrating together with the remaining parts, the localised flexibility properties near the connection area are better represented, since more modes are brought to the frequency range of interest.

The first alternative was presented by MacNeal [40] and Rubin [44] in order to improve the truncated free-free modal representation of a component by including estimates of the residual effects due to the modes higher in frequency than the frequency range of interest. In general, the residual effects are obtained by calculating the component flexibility due to those modes to be retained and then subtracting this from the total flexibility of the respective component. In Rubin's method [44] the first-order response based on MacNeal's approach [40], is used further to estimate residual inertial and dissipative effects of higher order modes. Craig and Chang [47,48] discussed the coupling of substructures represented by Rubin component-modes model. All these works presented a significative improvement to the classical free-interface method, but yet using purely analytical representation of component properties.

Since the free-interface method constitutes the most straightforward approach when the required data must be obtained from testing the components, some authors as Martinez *et al* [49,50] and Coppolino [51] have directed their work in this direction. Although Craig [52] has shown that the residual flexibility and fixed-interface method are equivalent, Klahs and Townley [53] concluded that numerical difficulties may arise in the use of residual flexibility approach.

The mass-loading technique may be classified as an intermediate technique between the fixed-interface method and the free-interface method. As mentioned before, the classical free-interface method is more sensitive to the truncation of the elastic modes used to describe the displacement in the connection region, rather than the fixed-interface method. In an attempt to bring the classical free-interface method (which is the most suitable for experimental purposes but does not offer good accuracy) closer to the fixed-interface method (which leads to better accuracy in the results but is not appropriate for the use of modal testing), the mass-loading technique is an available compromise solution which has been used in some specific fields of research, namely in the spacecraft industry [51].

1.4 SCOPE AND ORGANIZATION OF THIS THESIS

The research project presented in this thesis is concerned with more effective use of structural assembly analysis methods in practice and is mainly formed of four constituent parts as described next.

(i) - Theoretical Basis of Coupling Procedures which is the subject of chapter 2. In this chapter, the mathematical and physical principles inherent to the Impedance and Modal coupling techniques are presented and examined, which are in fact two different approaches to assemble reduced subsystem models. The former one takes advantage, in computational terms, of the reduction performed on the Spatial or Response models of each component whereas the second approach benefits, in the same terms, from the assumption that the subsystem Modal models are reduced in terms of the number of modes included. The limitations associated with the conventional methods to deal with both types of incomplete models are presented at a last stage and are the main basis for the research presented in the subsequent chapters.

(ii) - Refined Impedance and Modal Coupling Methods are presented in chapters 3 and 4, respectively. Chapter 3 is mainly devoted to the refinement of Impedance coupling methods that are able to incorporate the data readily available from measurements. Although a brief examination is carried out on the ways and effects of using reduced theoretical models - Spatial models - attention is principally focused on the use of experimentally-derived Response models which, by nature, are themselves incomplete and prone to measurement errors. The interest in the use of this kind of model is justified by their attractive characteristic which is the valuable information they contain about all the existing modes on the structure. Additionally, since they reflect the 'true' response of the component, they can provide a means of quantifying and qualifying damping and/or non-linear characteristics, which can not be assumed negligible as it is in general. In light of these considerations, the FRF coupling technique is selected to be the suitable mathematical tool which is mostly investigated. Refined algorithms are presented to increase the efficiency of the conventional method presented in chapter 2. The

improvement is achieved by decreasing the number of inversion operations and simultaneously the order of the involved matrices. In doing so, it is also shown that the numerical difficulties arising from inversions carried out on components's ill-conditioned FRF matrices are avoided under certain circumstances and a better prediction of the global structure results can be attained. Central to this work are numerical studies which investigate the sensitivity of the different alternatives under certain simulated practical conditions. One of these undesirable conditions is the existence of linearly dependent responses based on the coordinates located at the connection regions, causing the FRF matrix to be rank-deficient. If it happens that both components possess this characteristic, there is the need to make use of auxiliary mathematical tools which are presented in chapter 5. The second group of techniques - Modal Coupling - is dealt with in chapter 4. In this chapter, a modal coupling technique which also makes use of experimentally-derived data is investigated. Generally designated as free-interface method, since its formulation only requires the component modes to be obtained under a free supported condition at the connection coordinates, it is assumed in this chapter that the necessary modes are those derived from a commonly conducted modal test i.e., none of the coordinates are constrained in any direction. A refined technique is presented whereby the lack of flexibility due to the truncation of the number of modes in each subsystem (in fact, a characteristic of measured data), is compensated by the addition of a 'dummy' flexible system at the interface region. This auxiliary system possesses, in each component, the information of the flexibility associated with its out-of-range unmeasured modes. What the refined technique assumes in fact is a mathematical coupling of both components through those series connected 'dummy' flexible systems which after all are considered as a unique system between the components. The main structure of the computer program is briefly described and the validity and facility of refinement are assessed using case studies.

(iii) - Mathematical and Experimental Tools Used in a Coupling Process constitute the subject of chapters 5 and 6. It has already been stated that subsystem models which are derived from measured data suffer from incompleteness in terms of

coordinates. This may be due to difficulties in accurately measuring certain regions on the structure or due to a lack of ability of conventional transducers to measure certain required coordinates, for instance the rotations. In trying to remedy such inadequacies, one may be tempted to measure as many coordinates as possible, especially at the connection region(s) where a continuous description of the response field is highly desirable in order to attain a closer representation of the actual constraint conditions. However, as shown in chapter 3, such a large number of measured coordinates may well cause some of their responses to be linearly or almost linearly dependent on each other at certain frequency ranges. The result of using models with such a characteristic is a numerical ill-conditioning, especially if the FRF coupling technique is used. In seeking to remedy this undesirable failure, two strategies are proposed in chapter 5. On the one hand, a powerful mathematical technique - the Singular Value Decomposition (SVD) - can be confidently used to invert any matrix even if it is rank-deficient. However, it is shown that this technique should not be used as 'black box' algorithm, since the number of significant singular values is dependent on a specified threshold which is related to the degree of error on the measured data. The second proposed strategy also makes use of the SVD technique, but not this time to be used as an inversion algorithm. It is, instead, used to calculate the rank of a matrix or, in other words, the number of independent responses on a given structure. In addition to this technique, an algorithm which makes use of a QR factorisation is presented to locate those coordinates with dependent responses. If it happens that both components have redundant responses at identical locations, this means that those coordinates can be neglected during the formulation of the constraint equations. This simplification leads to well-conditioned matrices which have a reduced order and which can be inverted quickly using standard algorithms.

In chapter 6, the formulation of constraint conditions is approached from another perspective. It is in fact, the other extreme situation where there is an insufficient number of measurable connection coordinates, due to difficulties inherent to experimental means. The available transducers are well established and are accurate to measure linear responses. However, rotational responses are required in special situations to formulate

proper constraint conditions - particularly when the interface region tends to be localised and a moment is transmitted while the assembled structure is vibrating. A failure to measure rotational responses accurately impairs a realistic formulation of the actual constraint conditions and thus the predicted results have little to do with the actual assembled structure. In this chapter, three techniques are described to estimate rotational responses from measured translational ones. Two of the techniques make use of conventional accelerometers, one of them requiring an additional block attached to the test structure and the other assuming the measurement of two or three closely spaced translational coordinates. Both Response and Modal models are estimated at one end point on each beam possessing one transverse and one rotational coordinate. In both models the residual effect of the out-of-range modes can be included. The third technique makes use of a laser unit which is able to sense the velocity at any point on a vibrating structure. Only recently it has been used in Modal Analysis, particularly to compensate for the lack of measured coordinates with conventional accelerometers. Taking advantage of the ability of the laser system to scan a line or area on a structure, a quasi-continuous definition of the response field can be quickly achieved with such an optical system. One can say that this system allows the user to have an experimental model which can exceed the theoretical one in terms of number of coordinates. Such a large number of measured translational coordinates permits a rigorous approximation with analytical functions and these can subsequently be used to calculate the rotations at any encompassed point during the measurement, since they are the corresponding derivative values. If one assumes that the measurement is undertaken while the structure is vibrating at a natural frequency, the result is the mode shape description in terms of both translational and rotational amplitudes.

(iv) - Experimental Case studies are presented in chapter 7. Central to this chapter, are the results obtained on actual assembled structures. They represent the ultimate test of the validity of the refinements introduced on the conventional coupling techniques and reveal the usefulness of the auxiliary mathematical and experimental tools associated with a coupling procedure.

2 STANDARD COUPLING TECHNIQUES

2.1 INTRODUCTION

This chapter provides an introduction to the generally established coupling techniques. As mentioned in the previous chapter, the main aim of a coupling process is to obtain a model for the assembled structure. The order of the matrices used to formulate the equations of motion of the assembled structure depends on the order of the matrices used to describe each subsystem model, which in turn should be as condensed as possible. How to achieve the required reduction which is undertaken independently on each component, is dependent on the selected format to describe their dynamic characteristics. In fact, the three possible types of subsystem model (Spatial, Modal and Response) are interrelated as shown in chapter 1, but it is important to note that those relations hold strictly for models which are considered complete in terms of both coordinates and modes and so approximations are incurred when incomplete models are used.

The order of the matrices used to formulate the equations of motion of the assembled structure depends *either* on the number of coordinates (connection and interior) *or* on the number of kept modes pertaining to each component model. One can say that two groups of coupling techniques emerge from the large variety of methods which have been used in different fields of research and industry and are classified as,

- Impedance coupling techniques which benefit from the reduction performed on the subsystem models in terms of **coordinates** and,

- Modal coupling techniques which are suitable for the use of reduced models in terms of **modes.**

The former group deals primarily with the coupling of subsystems whose models are described either by their Spatial or by the Response properties. The first of these types of model is used extensively in the Finite Element method but is rarely used in cases which involve experimental modelling. Although Response models can be obtained by theoretical analysis, they mostly constitute the raw data available from modal tests.

The techniques forming the latter group are applied in those situations when the component models are described by their modal properties - Modal models. This type of model is easily generated from an eigensolution, if a theoretical tool such as the Finite Element method is used, or they can be derived from an identification process carried out on measured FRF data.

The following diagram elucidates the different possibilities of performing the coupling using both experimentally- and theoretically-derived subsystem models.

2.2 IMPEDANCE COUPLING TECHNIQUES

2.2.1 INTRODUCTION

The generalised Impedance methods for making vibration analysis of complex structural assemblies are examined in the present section. The subsystems or component models are described by using a Spatial or Response formulation giving rise to the so called **Spatial** or **FRF Coupling** methods which are examined next.

2.2.2 SPATIAL COUPLING METHOD

This is the method mostly used in the Finite Element software packages since each component's properties are themselves derived from a suitable assembling of the analytically-derived element's stiffness and mass matrices, leading to a description of the component's model in terms of their spatially distributed properties. The dynamic characteristics of the overall structure are subsequently obtained using the same assembling technique as used at the component level, but this time the component's spatial matrices playing the role of the matrices to be "added". The straightforward results of this assembling technique are the spatial matrices of the complete structure i.e., mass, stiffness and sometimes damping matrices which, since they are known, can be input to an eigen-solver to obtain the modal properties or they can be used to generate the Response model.

Let us consider two undamped components **A** and **B** described by their spatial properties, the corresponding mass and stiffness matrices being of orders $\mathbf{N_A}$ and $\mathbf{N_B}$ respectively, and each being partitioned according to the selected interior and connection coordinates. The equations of equilibrium for each subsystem, acted on only by interconnecting forces are,

$$\begin{vmatrix} {}_A\mathbf{M}_{ii} & \vdots & {}_A\mathbf{M}_{ic} \\ \cdots & \vdots & \cdots \\ {}_A\mathbf{M}_{ci} & \vdots & {}_A\mathbf{M}_{cc} \end{vmatrix} \begin{Bmatrix} {}_A\ddot{\mathbf{u}}_i \\ \cdots \\ {}_A\ddot{\mathbf{u}}_c \end{Bmatrix} + \begin{bmatrix} {}_A\mathbf{K}_{ii} & \vdots & {}_A\mathbf{K}_{ic} \\ \cdots & \vdots & \cdots \\ {}_A\mathbf{K}_{ci} & \vdots & {}_A\mathbf{K}_{cc} \end{bmatrix} \begin{Bmatrix} {}_A\mathbf{u}_i \\ \cdots \\ {}_A\mathbf{u}_c \end{Bmatrix} = \begin{vmatrix} \mathbf{0} \\ \cdots \\ {}_A\mathbf{f}_c \end{vmatrix} \tag{2.1}$$

$$\begin{vmatrix} {}_B\mathbf{M}_{jj} & \vdots & {}_B\mathbf{M}_{jc} \\ \cdots & \vdots & \cdots \\ {}_B\mathbf{M}_{cj} & \vdots & {}_B\mathbf{M}_{cc} \end{vmatrix} \begin{Bmatrix} {}_B\ddot{\mathbf{u}}_j \\ \cdots \\ {}_B\ddot{\mathbf{u}}_c \end{Bmatrix} + \begin{bmatrix} {}_B\mathbf{K}_{jj} & \vdots & {}_B\mathbf{K}_{jc} \\ \cdots & \vdots & \cdots \\ {}_B\mathbf{K}_{cj} & \vdots & {}_B\mathbf{K}_{cc} \end{bmatrix} \begin{Bmatrix} {}_B\mathbf{u}_j \\ \cdots \\ {}_B\mathbf{u}_c \end{Bmatrix} = \begin{Bmatrix} \mathbf{0} \\ \cdots \\ {}_B\mathbf{f}_c \end{Bmatrix} \tag{2.2}$$

where the index c denotes the $\mathbf{n_C}$ coordinates involved in the physical connection and **i, j** the remaining coordinates for components **A** and **B,** respectively.

The compatibility of displacements and equilibrium of forces between the subsystems undergoing free vibrations are expressed by the following equations:

$$\{{}_A\mathbf{f}_c\} = -\{{}_B\mathbf{f}_c\} = \{\mathbf{f}_c\} \tag{2.3}$$

$$\{{}_A\mathbf{u}_c\} - \{{}_B\mathbf{u}_c\} = \{\mathbf{0}\} \tag{2.4}$$

By invoking these equations, the overall system mass and stiffness matrices $[{}_C\mathbf{M}]_{N_C x N_C}$ and $[{}_C\mathbf{K}]_{N_C x N_C}$ will be of order $N_C = N_A + N_B - n_C$ and are given by,

$$[{}_C\mathbf{M}]_{N_C x N_C} = [{}_A\mathbf{M}]_{N_A x N_A} \oplus [{}_B\mathbf{M}]_{N_B x N_B} \tag{2.5}$$

and

$$[{}_C\mathbf{K}]_{N_C x N_C} = [{}_A\mathbf{K}]_{N_A x N_A} \oplus [{}_B\mathbf{K}]_{N_B x N_B} \tag{2.6}$$

the operation sign $\oplus$ meaning the following **assembly** of the above mentioned sub-matrices,

$$[{}_C\mathbf{M}]_{N_C x N_C} = \begin{vmatrix} {}_A\mathbf{M}_{ii} & \vdots & {}_A\mathbf{M}_{ic} & \vdots & \mathbf{0} \\ \cdots & \vdots & \cdots & \vdots & \cdots \\ {}_A\mathbf{M}_{ci} & \vdots & {}_A\mathbf{M}_{cc} + {}_B\mathbf{M}_{cc} & \vdots & {}_B\mathbf{M}_{cj} \\ \cdots & \vdots & \cdots & \vdots & \cdots \\ \mathbf{0} & \vdots & {}_B\mathbf{M}_{jc} & \vdots & {}_B\mathbf{M}_{jj} \end{vmatrix} \tag{2.7}$$

$$[{}^{C}K]_{N_C x N_C} = \begin{bmatrix} {}^{A}K_{ii} & {}^{A}K_{ic} & 0 \\ {}^{A}K_{ci} & {}^{A}K_{cc}+{}^{B}K_{cc} & {}^{B}K_{cj} \\ 0 & {}^{B}K_{jc} & {}^{B}K_{jj} \end{bmatrix} \qquad (2.8)$$

Since the mass and stiffness matrices $[{}^{C}M]_{N_C x N_C}$ and $[{}^{C}K]_{N_C x N_C}$ are known, a classical eigensolution will give the natural frequencies and mode shape vectors for the global system. This analysis is suitable for the use of theoretically-derived subsystems, but it is not generally used in cases where the data available is obtained from a modal testing.

2.2.3 FRF COUPLING METHOD

In contrast, the FRF **Coupling** analysis method makes use of subsystem models derived directly from FRF data (commonly available from experimental studies but seldom from theoretical modelling). The dynamic properties of those models are synthesised in terms of the FRF **matrix** and generally denoted as [H(o)] (such as Receptance, Mobility or Inertance matrices).

As in the preceding analysis, the coordinates involved in the connection between components A and B should be identified and represented by index c (and similarly **i** and **j** for the remaining ones) leading to the following partitioned FRF matrices:

$$[{}_{A}H(\omega)]_{N_A x N_A} = \begin{bmatrix} {}^{A}H_{ii} & {}^{A}H_{ic} \\ {}^{A}H_{ci} & {}^{A}H_{cc} \end{bmatrix} \qquad (2.9)$$

$$[{}_{B}H(\omega)]_{N_B x N_B} = \begin{bmatrix} {}^{B}H_{ii} & {}^{B}H_{jc} \\ {}^{B}H_{cj} & {}^{B}H_{cc} \end{bmatrix} \qquad (2.10)$$

By invoking the constraint equations (2.3) and (2.4) used in the previously presented Spatial coupling method, the FRF matrix of the coupled structure is provided [1] by a similar “addition” as presented next :

$$[{}_C\mathbf{H}(\omega)]_{N_C x N_C} = \left[[{}_A\mathbf{H}(\omega)]^{-1}_{N_A x N_A} \oplus [{}_B\mathbf{H}(\omega)]^{-1}_{N_B x N_B} \right]^{-1}_{N_C x N_C} \quad (2.11)$$

Denoting by $\mathbf{Z}_{kl}$ the element **k,l** in the generalised Impedance matrix **[Z(o)] = [H(ω)]$^{-1}$**, the operation sign $\oplus$ means the following assembly of the corresponding partitioned Impedance matrices,

$$[{}_C\mathbf{H}(\omega)]_{N_C x N_C} = \begin{bmatrix} {}_A\mathbf{Z}_{ii} & {}_A\mathbf{Z}_{ic} & \mathbf{0} \\ {}_A\mathbf{Z}_{ci} & {}_A\mathbf{Z}_{cc} + {}_B\mathbf{Z}_{cc} & {}_B\mathbf{Z}_{cj} \\ \mathbf{0} & {}_B\mathbf{Z}_{jc} & {}_B\mathbf{Z}_{jj} \end{bmatrix}^{-1} \quad (2.12)$$

The FRF matrices of each substructure (available over a frequency range of interest, which is the same for both structures) are "added" together frequency by frequency until the whole FRF matrix is completely calculated. The equation (2.12) can be generalised to include more than two subsystems without having to perform once again all the frequency by frequency "addition", provided the generalised Impedance matrices of each component are suitably assembled as shown in fig. 2.2 for the case of three components.

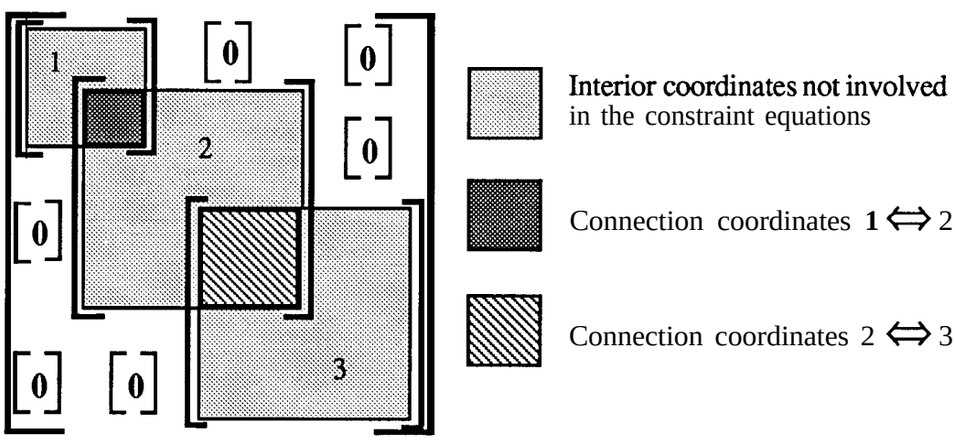

Fig. 2.2 - Assembly of Impedance matrices

As shown in equation (2.11), the whole system FRF matrix is obtained after three matrix inversions, two of them carried out on the subsystem's FRF matrices and another on the assembled Impedance matrix.

A refined version of an algorithm, which reduces the number of inversions to be carried out on matrices having a reduced order, and a detailed analysis of the numerical difficulties which may arise in some particular situations, mainly due to the errors inherent to the measured data and to the redundancy of the connection coordinates, constitutes the ingredients of chapter 3.

2.3 MODAL COUPLING TECHNIQUES

2.3.1 INTRODUCTION

In this section we shall be concerned with the Modal Coupling techniques, also referred to in the related literature as Time Domain or Component Mode Synthesis methods. The basic philosophy is the same as for the previous group i.e., they permit the use of reduced component models in order to achieve a reduced order in the final equation of motion matrices of the assembled structure. However, unlike the Impedance based methods, which take advantage on the reduction of the number of **coordinates, these** methods use a reduction performed on the number of **modes** used to describe each component model while still accounting for **all** the physical DoF. By using a Ritz-type transformation, the reduced number of principal coordinates is related to the number of modes that are taken into account for the modal estimation; generally, the information relating to the higher natural frequency modes is discarded. This feature in the method reduces the computational effort required in the system analysis and parallels the modal information in a real test, since it is only possible to measure some of the existing modes in a structure. The objective is to maintain a specified level of accuracy in the dynamic analysis, while using only the lower order modes for computational efficiency.

Amongst the different available methods, two groups emerge and may be classified as,

- the ***fixed-interface*** and
- the ***free-interface*** methods.

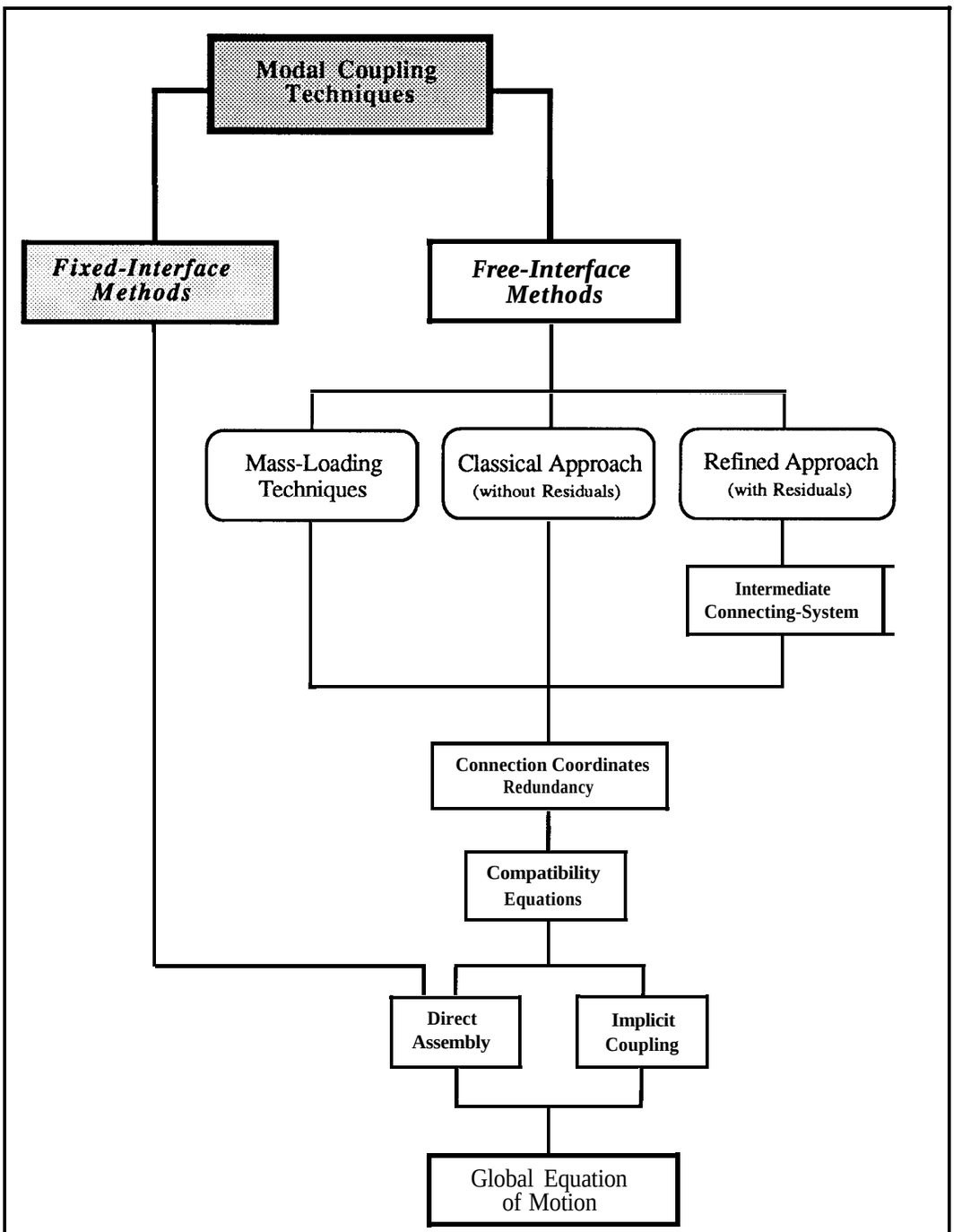

Fig. 2.3 - Modal coupling techniques

In both the methods, the solution of the original model is approximated by a summation of assumed displacements or Ritz vectors, their amplitudes being the generalized coordinates used to reduce the order of the original model. The Ritz vectors are selected in a predetermined fashion based *either* on the dynamic characteristics only or on both the dynamic and static characteristics of the individual subsystems.

Essentially, the methods differ from each other according to the dynamic displacement shapes used to form the truncated set of the natural modes. In the first method, the elastic modes pertaining to a fixed-interface component are retained, whereas in the second method, the modes are obtained by assuming the component to be vibrating in a freely-supported condition at its attachment points.

2.3.2 FIXED-INTERFACE METHODS

2.3.2.1 INTRODUCTION

The basic idea for the fixed-interface methods relies on the philosophy of the static substructuring technique proposed by Przemieniecki in 1963 [29]. This was mainly directed towards the use of the finite element technique with the total displacement for each component coordinate being calculated by a superposition of the displacements obtained with fixed and relaxed interface conditions.

In 1965, Hurty [30] proposed the Normal mode or Component Mode Synthesis method, at this time focusing his work on dynamic structural systems and taking into account both the component's elastic and mass properties.

Later, Craig and Bampton [31] re-formulated Hurty's method by simplifying the choice of the groups of modes for the transformation matrix construction. In the present work we are assuming the standard fixed-interface method to be that re-formulated version, which is summarised in the following section.

2.3.2.2 THEORY

Let us assume at this stage that each component's spatial properties are known. The corresponding equation of motion, according to the selected connecting and interior degrees of freedom (DoF), can be written in the following partitioned form,

$$\begin{bmatrix} \mathbf{M}_{ii} & : & \mathbf{M}_{ic} \\ \cdots & : & \cdots \\ \mathbf{M}_{ci} & : & \mathbf{M}_{cc} \end{bmatrix} \begin{Bmatrix} \ddot{\mathbf{u}}_i \\ \cdots \\ \ddot{\mathbf{u}}_c \end{Bmatrix} + \begin{bmatrix} \mathbf{K}_{ii} & : & \mathbf{K}_{ic} \\ \cdots & : & \cdots \\ \mathbf{K}_{ci} & : & \mathbf{K}_{cc} \end{bmatrix} \begin{Bmatrix} \mathbf{u}_i \\ \cdots \\ \mathbf{u}_c \end{Bmatrix} = \begin{Bmatrix} \mathbf{f}_i \\ \cdots \\ \mathbf{f}_c \end{Bmatrix} \qquad (2.13)$$

where

$\{\mathbf{u}_c\}$ and $\{\mathbf{u}_i\}$ - are the displacements at the n_c connection (primary) and at the n_i interior (secondary) coordinates respectively:

$\{\mathbf{f}_c\}$ and $\{\mathbf{f}_i\}$ - are the forces at the n_c connection (primary) and at the n_i interior (secondary) coordinates respectively.

Assuming now that the n_C connection coordinates are fixed ($\{\mathbf{u}_c\}=\{\ 0\ \}$), and that no external forces are acting at the interior DoF ($\{\mathbf{f}_i\}=\{\ 0\ \}$), the corresponding equation of motion becomes:

$$[\mathbf{M}_{ii}]\{\ddot{\mathbf{u}}_i\} + [\mathbf{K}_{ii}]\{\mathbf{u}_i\} = \{\mathbf{0}\} \qquad (2.14)$$

The assumption of harmonic motion leads to an eigen-solution which consists of $m = n_i$ mass-normalized eigenvectors $[\Phi_{im}]$ and the respective eigenvalues $[\omega^2_{rm}]$. Each interior DoF displacement can now be approximated by a summation of the known **fixed-interface modes** as,

$$\{\mathbf{u}_i\} = [\Phi_{im}]\{\mathbf{p}_m\} \qquad (2.15)$$

The second kind of modes required to approximate the displacements at the interior coordinates are the **constraint or static modes** which are calculated by relaxing each connection coordinate, but now neglecting the mass properties of the interior DoF. This is in fact a Guyan static reduction [54], as described by the following equations:

$$\begin{bmatrix} \mathbf{K}_{ii} & : & \mathbf{K}_{ic} \\ \cdots & : & \cdots \\ \mathbf{K}_{ci} & : & \mathbf{K}_{cc} \end{bmatrix} \begin{Bmatrix} \mathbf{u}_i \\ \cdots \\ \mathbf{u}_c \end{Bmatrix} = \begin{Bmatrix} \mathbf{0} \\ \cdots \\ \mathbf{f}_c \end{Bmatrix} \tag{2.16}$$

which gives the displacements $\{\mathbf{u}_i\}$ in terms of $\{\mathbf{u}_c\}$:

$$\{\mathbf{u}_i\} = -[\mathbf{K}_{ii}]^{-1}[\mathbf{K}_{ic}]\{\mathbf{u}_c\} \tag{2.17}$$

or, assuming that the transformation matrix is $[\Phi^*_{ic}] = -[\mathbf{K}_{ii}]^{-1}[\mathbf{K}_{ic}]$, equation (2.17) is re-written as:

$$\{\mathbf{u}_i\}_{n_i x 1} = [\Phi^*_{ic}]_{n_i x n_c}\{\mathbf{u}_c\}_{n_c x 1} \tag{2.18}$$

The **static or constraint modes** are thus the columns of the Guyan transformation matrix $[\Phi^*_{ic}]$.

A Ritz-type transformation matrix can now be constructed in terms of both elastic (fixed-interface) and static (constraint) modes, as presented next:

$$\begin{Bmatrix} \mathbf{u}_i \\ \cdots \\ \mathbf{u}_c \end{Bmatrix} = \begin{bmatrix} \Phi_{im} & : & \Phi^*_{ic} \\ \cdots & : & \cdots \\ \mathbf{0} & : & \mathbf{I} \end{bmatrix} \begin{Bmatrix} \mathbf{p}_m \\ \cdots \\ \mathbf{u}_c \end{Bmatrix} = [\mathbf{T}] \begin{Bmatrix} \mathbf{p}_m \\ \cdots \\ \mathbf{u}_c \end{Bmatrix} \tag{2.19}$$

The main advantage of this subsystem description is that it is possible to truncate the number of modes or modal coordinates (generally the higher natural frequency modes), while still accounting for **all** the physical DoF. Assuming that only the first m_k of the total m modes are known, equation (2.19) can now be written as:

$$\begin{Bmatrix} \mathbf{u}_i \\ \cdots \\ \mathbf{u}_c \end{Bmatrix} \approx \begin{bmatrix} \Phi_{ik} & : & \Phi^*_{ic} \\ \cdots & : & \cdots \\ \mathbf{0} & : & \mathbf{I} \end{bmatrix} \begin{Bmatrix} \mathbf{p}_k \\ \cdots \\ \mathbf{u}_c \end{Bmatrix} = [\mathbf{T}_k] \begin{Bmatrix} \mathbf{p}_k \\ \cdots \\ \mathbf{u}_c \end{Bmatrix} \tag{2.20}$$

Substituting equation (2.20) into (2.13) (only considering the interconnecting forces) and pre-multiplying by $[\mathbf{T}_k]$ leads to:

$$[\mathbf{T}_k]^T[\mathbf{M}][\mathbf{T}_k] \begin{Bmatrix} \ddot{\mathbf{p}}_k \\ \cdots \\ \ddot{\mathbf{u}}_c \end{Bmatrix} + [\mathbf{T}_k]^T[\mathbf{K}][\mathbf{T}_k] \begin{Bmatrix} \mathbf{p}_k \\ \cdots \\ \mathbf{u}_c \end{Bmatrix} = [\mathbf{T}_k]^T \begin{Bmatrix} \mathbf{0} \\ \cdots \\ \mathbf{f}_c \end{Bmatrix} \tag{2.21}$$

or in a partitioned form,

$$\begin{bmatrix} \tilde{M}_{kk} : \tilde{M}_{kc} \\ \cdots\cdots : \cdots\cdots \\ \tilde{M}_{ck} : \tilde{M}_{cc} \end{bmatrix} \begin{Bmatrix} \ddot{p}_k \\ \cdots \\ \ddot{u}_c \end{Bmatrix} + \begin{bmatrix} \tilde{K}_{kk} : \tilde{K}_{kc} \\ \cdots\cdots : \cdots\cdots \\ \tilde{K}_{ck} : \tilde{K}_{cc} \end{bmatrix} \begin{Bmatrix} p_k \\ \cdots \\ u_c \end{Bmatrix} = [T_k]^T \begin{Bmatrix} 0 \\ \cdots \\ f_c \end{Bmatrix} \qquad (2.22)$$

where

$$[\tilde{M}_{kk}] = [I]$$

$$[\tilde{M}_{kc}] = [\tilde{M}_{ck}]^T = [\Phi_{ik}]^T ([M_{ii}][\Phi^*_{ic}] + [M_{ic}])$$

$$[\tilde{M}_{cc}] = [M_{cc}] + [\Phi^*_{ic}]^T ([M_{ii}][\Phi^*_{ic}] + [M_{ic}]) + [M_{ci}][\Phi^*_{ic}]$$

$$[\tilde{K}_{kk}] = \begin{bmatrix} \ddots & & \\ & \omega_r^2 & \\ & & \ddots \end{bmatrix}$$

$$[\tilde{K}_{kc}] = [\tilde{K}_{ck}]^T = [0]$$

$$[\tilde{K}_{cc}] = [K_{cc}] + [K_{ci}][\Phi^*_{ic}] \qquad (2.23)$$

It is interesting to note that;

(i) the mass and stiffness matrices related only to the connection coordinates ($\{u_c\}$ are the same as the reduced matrices obtained by applying a Guyan reduction to the initial [M] and [K] matrices;

(ii) in the cases when the boundary is statically determinate;

- the constraint mode partition $[\Phi^*_{ic}]$ reduces to a geometric rigid body transformation which is independent of the stiffness properties,
- the boundary mass partition $[\tilde{M}_{cc}]$ is the rigid body mass matrix referenced to boundary motions, and
- the boundary stiffness $[K_{cc}]$ vanishes

(iii) in the case of an intermediate boundary, $\left[\Phi^{*}_{ic}\right]$ is primarily a function of local stiffness properties if the boundary is geometrically localised. However, when the boundary is quite distributed, $\left[\Phi^{*}_{ic}\right]$ is a function of the overall component stiffness.

The next operation is at the system level when all the component matrices are assembled together according to the compatibility and equilibrium equations necessary to describe the physical connections.

Assuming for simplification that $\{{}_A u_c\}$ and $\{{}_B u_c\}$ already represent displacements referred to the original global coordinate system u, the final equation for the coupled structure is now given in a new coordinate system - say p - by;

$$\begin{bmatrix} {}_A I_{kk} & 0 & {}_A\tilde{M}_{kc} \\ 0 & {}_B I_{kk} & {}_B\tilde{M}_{kc} \\ {}_A\tilde{M}_{ck} & {}_B\tilde{M}_{ck} & {}_A\tilde{M}_{cc}+{}_B\tilde{M}_{cc} \end{bmatrix} \begin{Bmatrix} {}_A\ddot{p}_k \\ \cdots \\ {}_B\ddot{p}_k \\ \cdots \\ \ddot{u}_c \end{Bmatrix} + \begin{bmatrix} {}_A\omega_r^2 & 0 & 0 \\ 0 & {}_B\omega_r^2 & 0 \\ 0 & 0 & {}_A\tilde{K}_{cc}+{}_B\tilde{K}_{cc} \end{bmatrix} \begin{Bmatrix} {}_A p_k \\ \cdots \\ {}_B p_k \\ \cdots \\ u_c \end{Bmatrix} = \begin{Bmatrix} 0 \\ \cdots \\ 0 \\ \cdots \\ 0 \end{Bmatrix} \qquad (2.24)$$

The natural frequencies $\left[\omega_r^2\right]$ and mode shapes $[\Psi]$ for the overall system are obtained by solving the eigenproblem associated with equation (2.24). The displacements in the p coordinates may be represented as a transformation of a new coordinate system $\{\xi\}$:

$$\begin{Bmatrix} {}_A p_k \\ \cdots \\ {}_B p_k \\ \cdots \\ u_c \end{Bmatrix} = [\Psi]\{\xi\} \qquad (2.25)$$

Alternatively, the displacements referred to the original system u may be represented as:

$$\begin{Bmatrix} {}^{A}u_i \\ \cdots \\ {}^{B}u_i \\ \cdots \\ u_c \end{Bmatrix} = \begin{bmatrix} {}^{A}\Phi_{ik} & 0 & {}^{A}\Phi^{*}_{ic} \\ \cdots & \cdots & \cdots \\ {}^{B}\Phi_{ik} & 0 & {}^{B}\Phi^{*}_{ic} \\ \cdots & \cdots & \cdots \\ 0 & 0 & I \end{bmatrix} [\Psi] \{\xi\} \qquad (2.26)$$

$$\text{or} \quad \begin{Bmatrix} {}^{A}u_i \\ \cdots \\ {}^{B}u_i \\ \cdots \\ u_c \end{Bmatrix} = [\Gamma] \{\xi\} \qquad (2.27)$$

where $[\Gamma]$ is the matrix of eigenvectors, this time referred to the u coordinate system.

The fixed-interface method is widely applied in the cases when the component dynamic properties are described by their mass and stiffness matrices. In general, this method is expected to be accurate when the final system allows the component of interest to have little motion near the attachment points, or if a flexible component is rigidly linked to a relatively stiff component. The mass associated with the connection DoF is often neglected but in turn the local stiffness is accurately included. The accuracy of the results predicted using the fixed-interface method can be still improved by expanding the transformation matrix given by eq. (2.20) to include other type of 'modes', such as the attatchment modes as presented by Craig and Chang [47].

This group of methods are easy to handle with theoretically defined mass and stiffness component matrices. However, from an experimental point of view they are not recommended, mainly due to two reasons;

- the imposition of a fixed-interface may be easy to implement when we are dealing with theoretical subsystem matrices, but it is very difficult to simulate a perfectly fixed support condition during a modal test,

- some of the matrices necessary to calculate the constraint modes are very difficult and tedious to obtain by static or dynamic testing.

2.3.3 FREE-INTERFACE METHODS

2.3.3.1 INTRODUCTION

This is a group of methods developed with the same basic idea as that outlined in the previous section, but this time using another type of transformation matrix for reduction purposes. In this case, the necessary natural modes incorporated in that matrix are those obtained from a subsystem vibrating either in its free-interface or completely free support condition. This being the most readily simulated condition during a experimental test, it constitutes an attractive technique for the use of combined experimental/theoretical analysis of dynamic structural systems.

One of the early works reporting use of free-interface modes was presented by Hou [34] and possesses some similarities with Goldman's method [33] but uses a less complicated procedure for generating the system transformation matrix. In this thesis, Hou's method will be referred as the classical approach (which assumes the components to be rigidly connected). For convenience of presentation, the free-interface methods will be presented as follows:

- first of all, the free-interface methods will be described according to the type of linkage between subsystems i.e., it may be ***rigid*** or ***flexible***. At this stage, interest is confined to the type of existing physical connection, excluding the effects of the mode set truncation;

- in the last part, a brief description of the mass-loading technique is made. This is an alternative technique which in fact tries to bring the classical free-interface method closer to the fixed-interface method.

2.3.3.2 FREE-INTERFACE METHOD with *Rigid Connection*

Let us consider two undamped subsystems A and B which are described by their spatial properties, the corresponding matrices being partitioned according to the selected interior and connection DoF as represented in fig. 2.4.

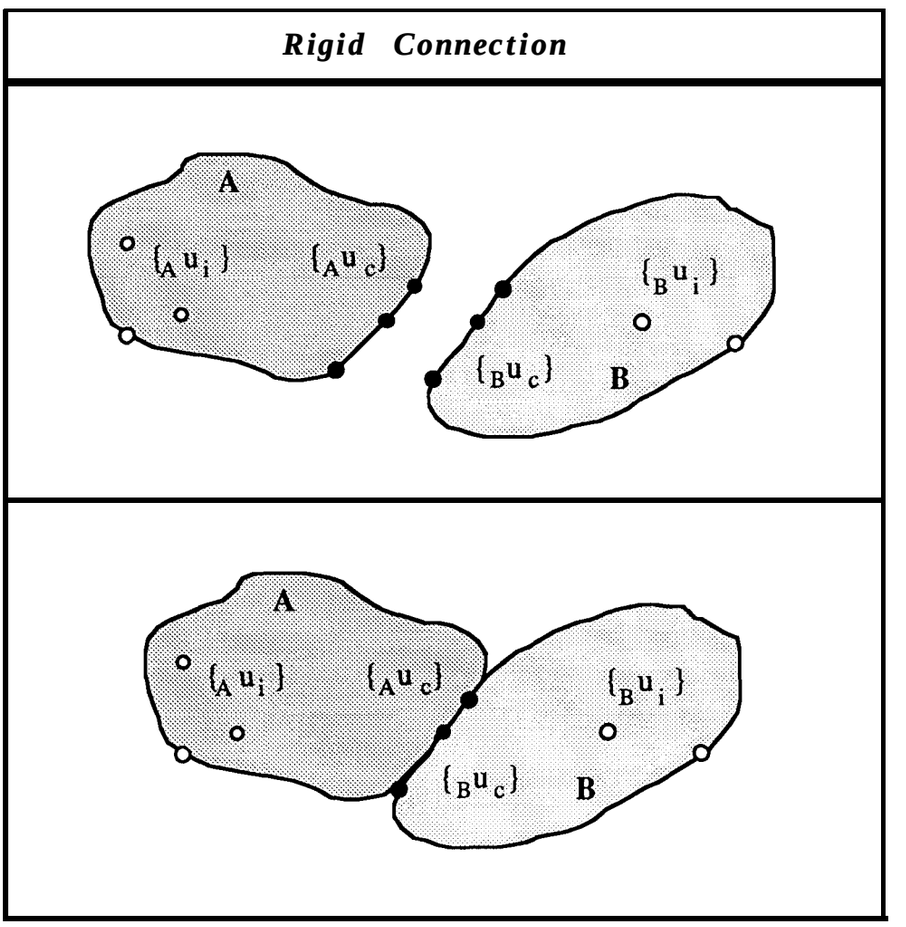

Fig. 2.4 - Rigid connection of two subsystems

As in equation (2.13), the equations of equilibrium for both subsystems acted on only by interconnecting forces are;

$$\begin{bmatrix} {}_A\mathbf{M}_{ii} & \vdots & {}_A\mathbf{M}_{ic} \\ \cdots\cdots & \vdots & \cdots\cdots \\ {}_A\mathbf{M}_{ci} & \vdots & {}_A\mathbf{M}_{cc} \end{bmatrix} \begin{Bmatrix} {}_A\ddot{\mathbf{u}}_i \\ \cdots \\ {}_A\ddot{\mathbf{u}}_c \end{Bmatrix} + \begin{bmatrix} {}_A\mathbf{K}_{ii} & \vdots & {}_A\mathbf{K}_{ic} \\ \cdots\cdots & \vdots & \cdots\cdots \\ {}_A\mathbf{K}_{ci} & \vdots & {}_A\mathbf{K}_{cc} \end{bmatrix} \begin{Bmatrix} {}_A\mathbf{u}_i \\ \cdots \\ {}_A\mathbf{u}_c \end{Bmatrix} = \begin{Bmatrix} \mathbf{0} \\ \cdots \\ {}_A\mathbf{f}_c \end{Bmatrix} \qquad (2.28)$$

$$\begin{bmatrix} {}_B\mathbf{M}_{ii} & \vdots & {}_B\mathbf{M}_{ic} \\ \cdots\cdots & \vdots & \cdots\cdots \\ {}_B\mathbf{M}_{ci} & \vdots & {}_B\mathbf{M}_{cc} \end{bmatrix} \begin{Bmatrix} {}_B\ddot{\mathbf{u}}_i \\ \cdots \\ {}_B\ddot{\mathbf{u}}_c \end{Bmatrix} + \begin{bmatrix} {}_B\mathbf{K}_{ii} & \vdots & {}_B\mathbf{K}_{ic} \\ \cdots\cdots & \vdots & \cdots\cdots \\ {}_B\mathbf{K}_{ci} & \vdots & {}_B\mathbf{K}_{cc} \end{bmatrix} \begin{Bmatrix} {}_B\mathbf{u}_i \\ \cdots \\ {}_B\mathbf{u}_c \end{Bmatrix} = \begin{Bmatrix} \mathbf{0} \\ \cdots \\ {}_B\mathbf{f}_c \end{Bmatrix} \qquad (2.29)$$

For each component individually, the free-interface modes are obtained by setting $\{f_c\} = \{0\}$ and solving the resulting eigenvalue problem,

$$\left(-\omega^2[M] + [K]\right)\{u\} = \{0\} \tag{2.30}$$

leading to the m natural frequencies and mode shapes, which in turn may be mass-normalised as,

$$\left[\Phi_m\right]^T [M] \left[\Phi_m\right] = [I] \tag{2.31}$$

$$\left[\Phi_m\right]^T [K] \left[\Phi_m\right] = \left[\omega_r^2\right] \tag{2.32}$$

For each component the physical displacements $\{u\}$ can now be written as a series expansion of the orthogonal mode shape matrix $[\Phi_m]$, which contains up to six rigid body modes (if the structure is completely unrestrained) plus the elastic free-interface modes:

$$\begin{Bmatrix} u_i \\ \cdots \\ u_c \end{Bmatrix} = \begin{bmatrix} \Phi_{im} \\ \cdots\cdots \\ \Phi_{cm} \end{bmatrix} \{p_m\} = \left[\Phi_m\right] \{p_m\} \tag{2.33}$$

The vector $\{p_m\}$ contains the generalised or modal coordinates as weighting factors of the series expansion or, in other words, the amplitudes of each independent selected pattern (or mode shape). This equation is exact only for the cases when *all the* modes are represented. However, in practical cases only a truncated set of m_k modes is considered or measured, leading to an approximate description of the displacements for each subsystem:

$$\begin{Bmatrix} {}_A u_i \\ \cdots \\ {}_A u_c \end{Bmatrix} \approx \begin{bmatrix} {}_A\Phi_{ik} \\ \cdots\cdots \\ {}_A\Phi_{ck} \end{bmatrix} \{{}_A p_k\} = \left[{}_A\Phi_k\right] \{{}_A p_k\} \tag{2.34}$$

$$\begin{Bmatrix} {}_B u_i \\ \cdots \\ {}_B u_c \end{Bmatrix} \approx \begin{bmatrix} {}_B\Phi_{ik} \\ \cdots\cdots \\ {}_B\Phi_{ck} \end{bmatrix} \{{}_B p_k\} = \left[{}_B\Phi_k\right] \{{}_B p_k\} \tag{2.35}$$

or $$\begin{Bmatrix} {}_A u \\ \cdots \\ {}_B u \end{Bmatrix} \approx \begin{bmatrix} {}_A\Phi_k & \vdots & 0 \\ \cdots & \vdots & \cdots \\ 0 & \vdots & {}_B\Phi_k \end{bmatrix} \begin{Bmatrix} {}_A p_k \\ \cdots \\ {}_B p_k \end{Bmatrix} \qquad \textit{(2.36)}$$

Substituting these displacements into equations (2.28) and (2.29) results in a set of uncoupled equations for the ***disconnected*** components,

$$[I] \begin{Bmatrix} {}_A\ddot{p}_k \\ \cdots \\ {}_B\ddot{p}_k \end{Bmatrix} + \begin{bmatrix} \omega^2_{A\,rk} & \vdots & 0 \\ \cdots & \vdots & \cdots \\ 0 & \vdots & \omega^2_{B\,rk} \end{bmatrix} \begin{Bmatrix} {}_A p_k \\ \cdots \\ {}_B p_k \end{Bmatrix} = \begin{bmatrix} {}_A\Phi^T_{ck} & \vdots & 0 \\ \cdots & \vdots & \cdots \\ 0 & \vdots & {}_B\Phi^T_{ck} \end{bmatrix} \begin{Bmatrix} {}_A f_c \\ \cdots \\ {}_B f_c \end{Bmatrix} \qquad (2.37)$$

These are the equations which can be established ***either*** using the theoretical derivation hitherto presented or using the modal data base available from experimental modal tests.

When both subsystems are connected, undergoing free vibrations together, the only forces acting on them are the equal and opposite forces at the interfaces. This equilibrium is expressed as,

$$\{{}_A f_c\} = -\{{}_B f_c\} \qquad \textit{(2.38)}$$

while the corresponding compatibility equation for the interface displacements is,

$$\{{}_A u_c\} = \{{}_B u_c\} \qquad (2.39)$$

This constraint condition may be reformulated taking into account the approximation assumed in equation (2.36) and is written as,

$$\left[{}_A\Phi_{ck} : -{}_B\Phi_{ck}\right] \begin{Bmatrix} {}_A p_k \\ \cdots \\ {}_B p_k \end{Bmatrix} = [S]\,\{p\} = \{0\} \qquad \textit{(2.40)}$$

The matrix ***[S]*** may be partitioned as

$$\left[S_d \vdots S_i\right] \begin{Bmatrix} p_d \\ \cdots \\ p_i \end{Bmatrix} = \{0\} \qquad (2.41)$$

where $[S_d]$ is a non-singular square matrix and $[S_i]$ is the remaining part of $[S]$. This requires that the total number of modes for both components ($m_{kt} = m_{kA} + m_{kB}$) be greater than the number of connection coordinates n_c. Making use of this partition we have,

$$\{p_d\} = -[S_d]^{-1}[S_i]\{p_i\} \tag{2.42}$$

Then, the following transformation matrix can be constructed,

$$\begin{Bmatrix} {}_A p_k \\ \cdots \\ {}_B p_k \end{Bmatrix} = \begin{vmatrix} p_d \\ \cdots \\ p_i \end{vmatrix} = \begin{bmatrix} -[S_d]^{-1}[S_i] \\ \cdots\cdots\cdots\cdots \\ [I] \end{bmatrix} \{p_i\} \tag{2.43}$$

$$\begin{Bmatrix} {}_A p_k \\ \cdots \\ {}_B p_k \end{Bmatrix} = [T]\{q\} \tag{2.44}$$

To generate the matrix $[T]$, a set of m_i independent vectors $[S_i]$ must be obtained from matrix $[S]$, while a set of m_d dependent vectors $[S_d]$ is retained. This requirement may be difficult to satisfy, especially if some of the connection coordinate responses reveal a near dependency which will cause matrix $[S_d]$ to be ill-conditioned or even singular. A suitable process can be devised by applying the Singular Value Decomposition (SVD) technique [55] to the matrix $[S]$, keeping only the independent vectors that will constitute a matrix of a defined rank which may differ from its order - the number n_c of the attachment DoF. How to handle this numerical difficulty is one of the topics investigated in chapter 5.

Substituting (2.44) into equation (2.37) and pre-multiplying by $[T]^T$ yields,

$$[M_q]\{\ddot{q}\} + [K_q]\{q\} = \{f_q\} \tag{2.45}$$

where

$$[\mathbf{M}_q] = [\mathbf{T}]^T [\mathbf{T}]$$

$$[\mathbf{K}_q] = [\mathbf{T}]^T \begin{bmatrix} {}_A\omega_{rk}^2 & \mathbf{0} \\ \cdots\cdots & \cdots\cdots \\ \mathbf{0} & {}_B\omega_{rk}^2 \end{bmatrix} [\mathbf{T}]$$

$$\{\mathbf{f}_q\} = [\mathbf{T}]^T \begin{bmatrix} {}_A\Phi_{ck}^T \\ \cdots\cdots \\ -{}_B\Phi_{ck}^T \end{bmatrix} \{\mathbf{f}_c\}$$

The second term of equation (2.45) vanishes, since no external forces are acting on the coupled system. Thus, the solution of this equation gives the $(m_{kt} - n_c)$ natural frequencies $\left[\omega_{rk}^2\right]$ and mode shapes $[\Psi]$ for the overall system, but referred to the q coordinates. The mode shapes are then transformed to the original coordinates u according to:

$$[\Phi] = \begin{bmatrix} {}_A\Phi_k & \mathbf{0} \\ \cdots\cdots & \cdots\cdots \\ \mathbf{0} & {}_B\Phi_k \end{bmatrix} [\mathbf{T}] [\Psi] \qquad (2.46)$$

Finally, for use with externally applied forces, equation (2.45) can be transformed into the coupled system modal coordinates ξ by letting,

$$\{\mathbf{q}\} = [\Psi] \{\xi\} \qquad (2.47)$$

which leads to,

$$[\mathbf{M}_\xi] \{\ddot{\xi}\} + [\mathbf{K}_\xi] \{\xi\} = \{\mathbf{f}_\xi\} \qquad (2.48)$$

$$[M_\xi] = [\Psi]^T [T]^T [T] [Y] \tag{2.49}$$

$$[K_\xi] = [\Psi]^T [T]^T \begin{bmatrix} {}_A\omega_{rk}^2 & & \vdots & & 1 \\ \cdots & & \cdots & & \cdots \\ 0 & & \vdots & & {}_B\omega_{rk}^2 \end{bmatrix} [T][\Psi] \tag{2.50}$$

$$\{f_\xi\} = [\Psi]^T [T]^T \begin{bmatrix} {}_A\Phi_{ck}^T \\ \cdots \\ -{}_B\Phi_{ck}^T \end{bmatrix} \{f_c\} \tag{2.5 1}$$

2.3.3.3 FREE-INTERFACE METHOD with *Elastic Connection*

Let us assume now that the previously mentioned subsystems A and B are to be coupled through an intermediate flexible system C as shown in fig. 2.5.

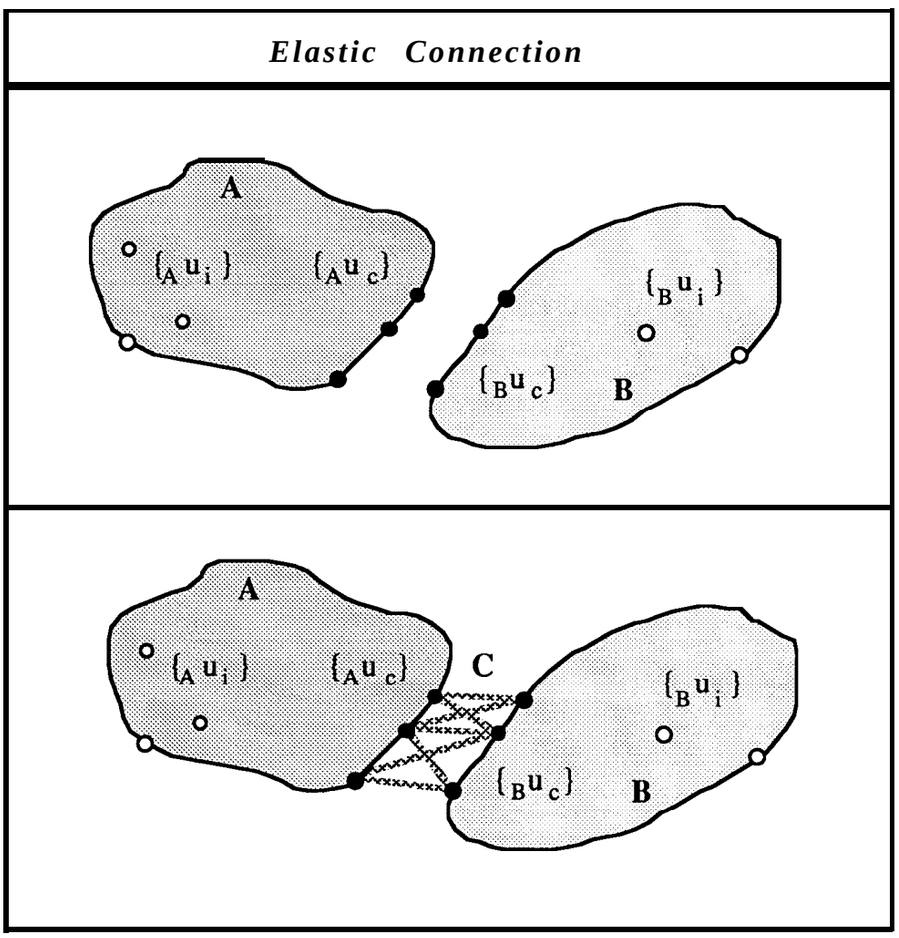

Fig. 2.5 - Elastic connection of two subsystems

In this case we assume that the Modal models for each component are already known, whatever method is used for their derivation. The equations of motion for both disconnected components have already been derived (vide eq. 2.37) and are given as,

$$[\mathbf{I}]\begin{Bmatrix} {}_A\ddot{\mathbf{p}}_k \\ \cdots \\ {}_B\ddot{\mathbf{p}}_k \end{Bmatrix} + \begin{bmatrix} {}_A\omega_{rk}^2 & \vdots & \mathbf{0} \\ \cdots & \vdots & \cdots \\ \mathbf{0} & \vdots & {}_B\omega_{rk}^2 \end{bmatrix}\begin{Bmatrix} {}_A\mathbf{p}_k \\ \cdots \\ {}_B\mathbf{p}_k \end{Bmatrix} = \begin{bmatrix} {}_A\Phi_{ck}^T & \vdots & \mathbf{0} \\ \cdots & \vdots & \cdots \\ \mathbf{0} & \vdots & {}_B\Phi_{ck}^T \end{bmatrix}\begin{Bmatrix} {}_A\mathbf{f}_c \\ \cdots \\ {}_B\mathbf{f}_c \end{Bmatrix} \qquad (2.52)$$

If the two components are now connected via an elastic system, the only constraint equation which expresses that condition is,

$$\{{}_A\mathbf{f}_c\} = -\{{}_B\mathbf{f}_c\} \qquad (2.53)$$

since, in this case, simple compatibility of displacements is not applicable, i.e.:

$$\{{}_A\mathbf{u}_c\} \neq \{{}_B\mathbf{u}_c\} \qquad (2.54)$$

However, the elastic properties of the connecting system can be represented by means of its stiffness matrix $[\mathbf{K}_{cpl}]$ if the mass properties are neglected (although in the case of a more refined approach, these can be assigned to the interface coordinates of each component).

To illustrate the construction of the stiffness coupling matrix, let us assume a simple system connected via two coordinates represented as $\mathbf{u}_{c1}$ and $\mathbf{u}_{c2}$. The forces applied to component A due to the relative motion of both components are given as,

$$\{{}_A\mathbf{f}_c\} = \begin{Bmatrix} {}_Af_{c1} \\ {}_Af_{c2} \end{Bmatrix} = -\left| \begin{bmatrix} K_{11} & K_{12} & \vdots & -K_{11} & -K_{12} \\ K_{21} & K_{22} & \vdots & -K_{21} & -K_{22} \end{bmatrix} \right| \begin{Bmatrix} {}_Au_{c1} \\ {}_Au_{c2} \\ \cdots \\ {}_Bu_{c1} \\ {}_Bu_{c2} \end{Bmatrix}$$

which for a multi-point connection will be written as,

$$\{{}_A\mathbf{f}_c\} = -\left[\mathbf{K}_{cc} \vdots -\mathbf{K}_{cc}\right]\begin{Bmatrix}{}_A\mathbf{u}_c \\ \cdots \\ {}_B\mathbf{u}_c\end{Bmatrix} \tag{2.55}$$

and similarly for the forces acting on B:

$$\{{}_B\mathbf{f}_c\} = -\left[-\mathbf{K}_{cc} \vdots \mathbf{K}_{cc}\right]\begin{Bmatrix}{}_A\mathbf{u}_c \\ \cdots \\ {}_B\mathbf{u}_c\end{Bmatrix} \tag{2.56}$$

Thus,

$$\begin{Bmatrix}{}_A\mathbf{f}_c \\ \cdots \\ {}_B\mathbf{f}_c\end{Bmatrix} = -\left[\begin{array}{c:c} \mathbf{K}_{cc} & -\mathbf{K}_{cc} \\ \cdots & \cdots \\ -\mathbf{K}_{cc} & \mathbf{K}_{cc} \end{array}\right]\begin{Bmatrix}{}_A\mathbf{u}_c \\ \cdots \\ {}_B\mathbf{u}_c\end{Bmatrix} = -\left[\mathbf{K}_{cpl}\right]\begin{Bmatrix}{}_A\mathbf{u}_c \\ \cdots \\ {}_B\mathbf{u}_c\end{Bmatrix} \tag{2.57}$$

but since we have assumed the transformation of coordinates (2.36), equation (2.52) can now be written as,

$$[\mathbf{I}]\begin{Bmatrix}{}_A\ddot{\mathbf{p}}_k \\ \cdots \\ {}_B\ddot{\mathbf{p}}_k\end{Bmatrix} + \left[\begin{array}{c:c} {}_A\omega_{rk}^2 & \mathbf{0} \\ \cdots & \cdots \\ \mathbf{0} & {}_B\omega_{rk}^2 \end{array}\right] +$$

$$\left[\begin{array}{c:c} {}_A\Phi_{ck}^T & \mathbf{0} \\ \cdots & \cdots \\ \mathbf{0} & {}_B\Phi_{ck}^T \end{array}\right]\left[\mathbf{K}_{cpl}\right]\left[\begin{array}{c:c} {}_A\Phi_{ck} & \mathbf{0} \\ \cdots & \cdots \\ \mathbf{0} & {}_B\Phi_{ck} \end{array}\right]\begin{Bmatrix}{}_A\mathbf{p}_k \\ \cdots \\ {}_B\mathbf{p}_k\end{Bmatrix} = \{\mathbf{0}\} \tag{2.58}$$

which is the equation of motion for the final coupled system. This equation differs slightly from the equation derived by Martin and Ghlaim [56,57] since in equation (2.58) the only rows involved in the calculation of the coupling terms are those related to the connection coordinates.

2.3.4 MASS-LOADING TECHNIQUE

2.3.4.1 INTRODUCTION

This may be classified as an intermediate technique between the fixed-interface and the free-interface methods. As mentioned before, the classical free-interface method is more sensitive to truncation of the elastic modes used to describe the displacement in the connection region than is the fixed-interface method. In an attempt to bring the classical free-interface method (which is the most suitable for experimental purposes but does not offer good accuracy) closer to the fixed-interface method (which leads to better accuracy in the results but is not appropriate for the use of modal testing), the mass-loading technique is an available compromise solution which has been used in some specific fields of research, namely in the spacecraft industry [51].

By adding some discrete masses at each of the component connection coordinates, the deformation near the interface is increased and a better estimation for the local flexibility is obtained, provided that the auxiliary masses are connected in such a way that does not affect the local stiffness properties of the component. The appropriate size of the mass to be added is dependent on the characteristics of the component to be tested, rather than on those pertaining to the adjoining subsystem. This fulfills the independency requirement for a substructuring procedure.

From an experimental standpoint this technique offers some advantages as stated by Sekimoto [58] and Gwim [59];

- it is less time consuming to collect data as compared with the free-interface method including residual effects,

- more modes are brought into the frequency range of interest, thus providing better information about the component model,

- if adequate mass blocks are used, a convenient means of measuring rotational responses is provided (although this might be offset by a reduction in the amplitude of such rotations).

2.3.4.2 THEORY

The procedure to couple the components is similar to that presented in Section 2.3.3.2 for the case of the free-interface method with a rigid connection. The main steps involved are the same, but in this case there are three additional steps which are carried out in order to obtain a better description of each subsystem's dynamic properties. All the major steps are presented briefly below:

Step 1 - Definition of the original disconnected substructures.

The equations of motion are the same as those presented in section 2.3.3.2.

Step 2 - Modification of the components by adding some extra masses.

The auxiliary masses are added to the connection coordinates $\{\mathbf{u}_c\}$. The equation of motion for each substructure is now,

$$\left[[\mathbf{M}] + [\mathbf{A}\ \mathbf{M}]\right]\{\ddot{\mathbf{u}}\} + [\mathbf{K}]\{\mathbf{u}\} = \{\mathbf{f}\} \qquad (2.59)$$

or $$\left[\mathbf{M}_{mod}\right]\{\ddot{\mathbf{u}}\} + [\mathbf{K}]\{\mathbf{u}\} = \{\mathbf{f}\} \qquad (2.60)$$

where [AM] is the modification matrix. The modified mass matrix will be

$$\left[\mathbf{M}_{mod}\right] = \begin{bmatrix} \mathbf{M}_{ii} & : & \mathbf{M}_{ic} \\ \cdots & : & \cdots \\ \mathbf{M}_{ci} & : & \mathbf{M}_{cc} \end{bmatrix} + \begin{bmatrix} \mathbf{0} & : & \mathbf{0} \\ \cdots & : & \cdots \\ \mathbf{0} & : & \Delta\mathbf{M}_{cc} \end{bmatrix} \qquad (2.61)$$

The eigensolution will lead to the mass-loaded system eigenvalues $\left[\omega^2_{r_{mod}}\right]$ and associated mass-normalised eigenvectors $\left[\mathbf{p}_{mod}\right]$, constituting the necessary values to define the Modal model for each modified subsystem. The values directly available from a

test conducted on the mass-loaded component are the kept or measured modes $[\Phi_{k_{mod}}]$ and the respective natural frequencies $\left[\omega^2_{rk_{mod}}\right]$.

The equation of motion referred to the modal coordinates is then,

$$[\Phi_{k_{mod}}]^T [M_{mod}][\Phi_{k_{mod}}]\{\ddot{p}_k\} + [\Phi_{k_{mod}}]^T [K][\Phi_{k_{mod}}]\{p_k\} = \{0\} \tag{2.62}$$

or $$[I]\{\ddot{p}_k\} + \left[\omega^2_{rk_{mod}}\right]\{p_k\} = \{0\} \tag{2.63}$$

Step 3 - Mass cancellation

The effects of the additional masses now need to be removed before the coupling process is performed. This is achieved by the following analytical process:

$$[\Phi_{k_{mod}}]^T [M][\Phi_{k_{mod}}] = [I] - [\Phi_{k_{mod}}]^T [\Delta M][\Phi_{k_{mod}}] \tag{2.64}$$

and the equation for each component is given as,

$$\left[[I] - [\Phi_{k_{mod}}]^T [\Delta M][\Phi_{k_{mod}}]\right]\{\ddot{p}_k\} + \left[\omega^2_{rk_{mod}}\right]\{p_k\} = \{0\} \tag{2.65}$$

Step 4- Coupling

The coupling process follows now the same procedure presented for the case of the free-interface method with a rigid connection (vidé section 2.3.3.2).

All the steps are now schematically presented in fig. 2.6.

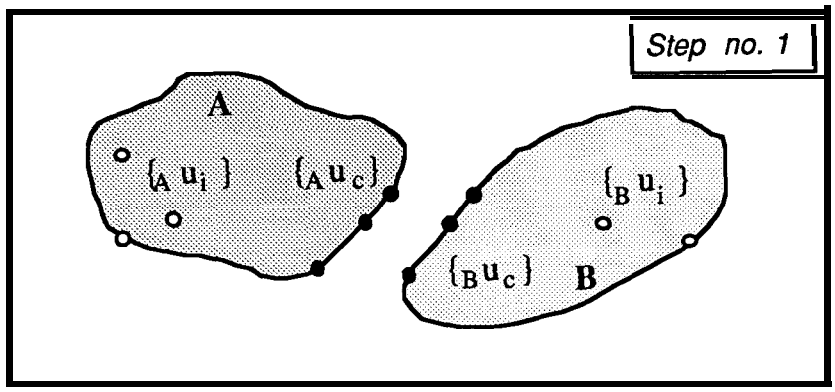

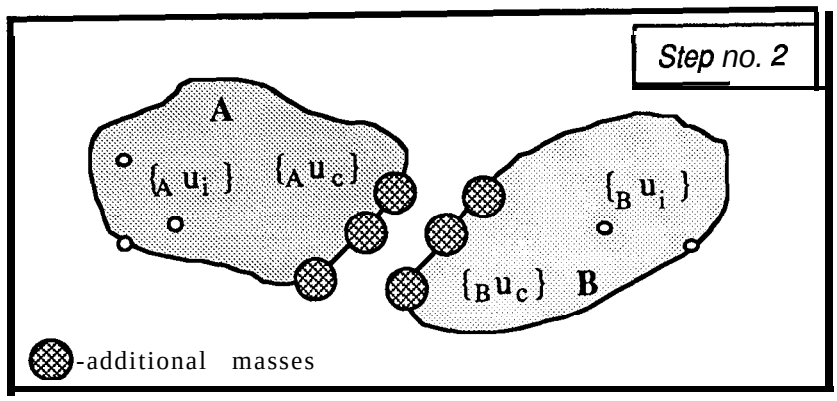

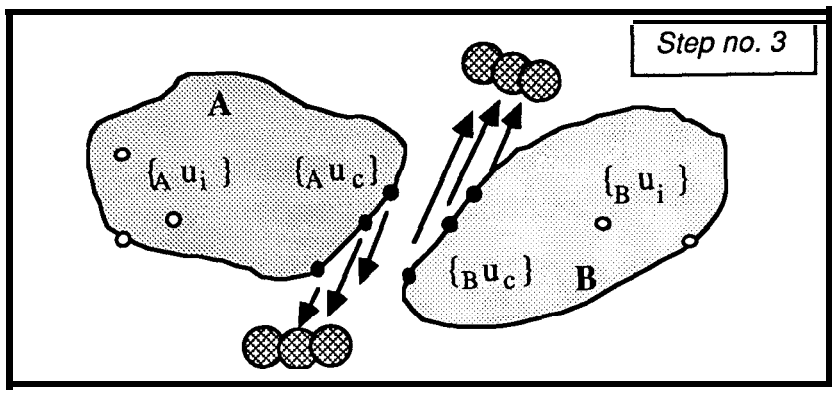

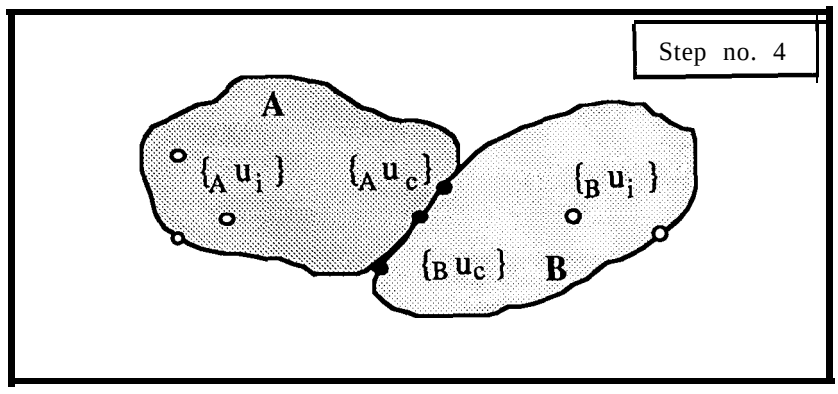

Fig. 2.6 - Steps involved in the mass-loading technique

2.4 LIMITATIONS ON THE TECHNIQUES

The theoretical basis of the standard coupling techniques has been presented. Each has its own limitations in certain circumstances and these constitute the reasons for the following discussion.

Impedance Coupling Techniques

As stated before, Spatial coupling is extensively used in applications of the Finite Element method but is rarely used in cases which involve experimental modelling. Reduction methods have been developed to condense Spatial models to primary (master) coordinates - a process of **coordinate reduction** which inevitably will cause a mode reduction - in order to decrease the computational needs to solve the global problem. However, the selection of those coordinates must be properly made and some attempts to define a criterion are carried out in chapter 3.

In contrast to Spatial coupling, there is the FRF coupling technique which is particularly suitable for use with data measured on the components. It makes use of Response models derived directly from experimental data (but seldom from theoretical modelling). The collected data in terms of **FRFs** defined over a frequency range of interest are used to assemble the FRF matrix which, for every frequency value, expresses the contribution of the in- and out-of-range modes pertaining to each component. One can say that in physical terms the FRF coupling technique is very attractive since it makes use of models whose dynamic characteristics are fully quantified and thus they do not suffer from modal incompleteness. However, there is a numerical aspect associated with this technique which may cause the coupling procedure to fail. As shown in section 2, the required FRF matrix of the coupled structure is obtained after three matrix inversions - two of these carried out before and one after the FRF matrices are assembled. Should one of these matrices be near singular, the results will reflect the numerical errors caused by the inversion and will predict the dynamic behaviour of the overall structure erratically. Unfortunately, when dealing with experimentally-derived FRF matrices, one is mostly restricted to use models that are inaccurate due to the experimental or systematic errors in

the measurement stage, one of these being a slight variation in the resonance frequencies when the model is said to suffer from inconsistency. The FRF matrix then tends to be ill-conditioned, and the inverse is very sensitive to a slight change in one of the FRF matrix elements in the vicinity of every resonance frequency since it will tend to have and order equal to the measured coordinates and to have rank one due to the dominating effect of one single mode (vide chapter 1, section 1.2). This local dominance is even stronger in lightly-damped structures and additional peaks tend to appear on the assembled structure FRFs at frequencies which may be misinterpreted as true resonances of the coupled structure.

Another situation which may lead to near singular matrices is caused by local rigidities at the measured coordinates. Over certain frequency ranges, the response in some coordinates may tend to be nearly dependent and here again, the FRF matrix will tend to be rank-deficient. The ways of tackling these numerical difficulties are addressed in chapters 3 and 5.

Modal Coupling Techniques

Unlike the Impedance-based methods which take advantage on the reduction of the number of **coordinates,** the Modal coupling methods use a reduction performed on the number of **modes** used to describe each component model while still accounting for **all the** physical coordinates. In spite of the fact that fixed-interface methods give better predictions than the free-interface methods, they are generally not suitable to handle data which are available from modal tests - the Modal model whose mode shapes are obtained from a component tested in its simulated free-free support condition. This is the main reason for the development of better procedures to improve the accuracy of results predicted using free-interface methods. One cause of the failure of these methods is the poor description of each subsystem displacements in the interface region due to the reduction performed on the number of modes. Two feasible alternatives to improve the

previously presented mass-loading technique *or* by compensating for the lack of flexibility due to the truncation on the number of modes. This latter approach is investigated in chapter 4, where a refined technique is described to include into the coupling process the information on the residual flexibility associated with the neglected or unmeasured modes of each subsystem model, without having to carry all the steps required by the mass-loading technique.

3 IMPEDANCE COUPLING TECHNIQUES

3.1 INTRODUCTION

The generalised Impedance-based methods for making vibration analysis of complex structural assemblies are examined in the present chapter in order to evaluate their applicability when incomplete subsystem models are used. The subsystems or component models are described by using a Spatial or Response formulation, and special attention is given to the **coordinate incompleteness** of these models.

However, it is assumed that whatever the performed reduction on the number of coordinates in each subsystem model, it will not be extended to the originally defined set of connecting coordinates which are explicitely required for the formulation of the constraint equations between subsystem models. This has a completely different effect in the coupling analysis since by ignoring a connection coordinate we are making the subsystem unable to “pass” some of its dynamic information to another one, when they are acting together. For example, if a rotation coordinate is eliminated (or ignored) at the junction between two components, these are presumed to have relative motion with respect to that coordinate and would thus be pin-jointed. Thus, the set of the retained coordinates - the primary or master coordinates - always contains the originally defined interface one and in the most extreme situation the reduction process is assumed to condense all the dynamic properties only to the connecting coordinates.

Although a brief examination is carried out on the ways and effects of reducing the theoretically-derived models - Spatial models - the attention is mainly focused on the ways and effects of using experimentally-derived models - Response models - which by nature are themselves incomplete in terms of coordinates and prone to errors even though they contain information related to both the in- and out-of-range frequency of interest modes. The attractive and conceptually-simple technique that offers the possibility of dealing directly with measured data is the FRF coupling technique. The numerical difficulties associated with the corresponding algorithm in some particular situations, especially in the presence of measured data, has motivated the investigation of new approaches to tackle this problem.

3.2 INCOMPLETE OR REDUCED SUBSYSTEM MODELS

3.2.1 SPATIAL MODEL INCOMPLETENESS

In many practical situations such those using the Finite Element method, the computational limitations often require the order of the final coupled system to be reduced as much as possible. This is achieved by reducing the order (N) of each subsystem model - or in other words, by confining our interest only to a restricted set of coordinates on each subsystem - say, $n_p < N$ - and/or to only some of the modes $(m_k < N)$. These considerations lead to the formulation of condensed, reduced or incomplete models.

The number of DoF to be retained in the dynamic analysis (at least the DoF involved in the connection with other components) is specified by the user. In the case of Spatial models, a transformation matrix relating the remaining DoF (called secondary or slave coordinates) to those retained (primary or master coordinates) is used to reduce the order of the subsystem. The reduction process [60] is often performed upon a transformation which neglects inertia or static contribuitions for the eliminated DoF, and is then used to derive the spatial matrices of the condensed system, $[M^R]_{n_p x n_p}$ and $[K^R]_{n_p x n_p}$.

The equation of equilibrium for an undamped subsystem acted on only by forces on the primary (master) coordinates can be written in the following partitioned form,

$$\begin{bmatrix} \mathbf{M}_{ss} & : & \mathbf{M}_{sp} \\ \cdots\cdots & : & \cdots\cdots \\ \mathbf{M}_{ps} & : & \mathbf{M}_{pp} \end{bmatrix} \begin{Bmatrix} \ddot{\mathbf{u}}_s \\ \cdots \\ \ddot{\mathbf{u}}_p \end{Bmatrix} + \begin{bmatrix} \mathbf{K}_{ss} & : & \mathbf{K}_{sp} \\ \cdots\cdots & : & \cdots\cdots \\ \mathbf{K}_{ps} & : & \mathbf{K}_{pp} \end{bmatrix} \begin{Bmatrix} \mathbf{u}_s \\ \cdots \\ \mathbf{u}_p \end{Bmatrix} = \begin{Bmatrix} \mathbf{0} \\ \cdots \\ \mathbf{f}_p \end{Bmatrix} \qquad (3.1)$$

secondary DoF ➡ $\{\mathbf{u}_s\}_{n_s x 1}$

Primary DoF • $\{\mathbf{u}\}_{n_p x 1}$

All the coordinates can be related to the primary coordinates by using the following transformation matrix,

$$\begin{Bmatrix} \mathbf{u}_s \\ \cdots \\ \mathbf{u}_p \end{Bmatrix} = \begin{bmatrix} [\mathbf{T}]_{n_s x n_p} \\ \cdots\cdots\cdots \\ [\mathbf{I}]_{n_p x n_p} \end{bmatrix} \{\mathbf{u}_p\} \qquad (3.2)$$

where the matrix **[T]** is given by,

$$[\mathbf{T}]_{n_s x n_p} = (1-\beta)\left[-[\mathbf{K}_{ss}]^{-1}[\mathbf{K}_{sp}]\right] + \beta\left[-[\mathbf{M}_{ss}]^{-1}[\mathbf{M}_{sp}]\right] \qquad (3.3)$$

being β a reduction coefficient whose limits are $\beta=0$ for **static reduction** and $\beta=1$ for **dynamic reduction.**

The matrices describing the **reduced Spatial model** are given as,

$$[\mathbf{M}^R]_{n_p x n_p} = \begin{bmatrix} [\mathbf{T}]^T \\ \vdots \\ [\mathbf{I}] \end{bmatrix}_{n_p x N} \begin{bmatrix} \mathbf{M}_{ss} & : & \mathbf{M}_{sp} \\ \cdots\cdots & : & \cdots\cdots \\ \mathbf{M}_{ps} & : & \mathbf{M}_{pp} \end{bmatrix}_{N x N} \begin{bmatrix} [\mathbf{T}] \\ \cdots\cdots \\ [\mathbf{I}] \end{bmatrix}_{N x n_p} \qquad (3.4)$$

$$[\mathbf{K}^R]_{n_p x n_p} = \begin{bmatrix} [\mathbf{T}]^T \\ \vdots \\ [\mathbf{I}] \end{bmatrix}_{n_p x N} \begin{bmatrix} \mathbf{K}_{ss} & : & \mathbf{K}_{sp} \\ \cdots\cdots & : & \cdots\cdots \\ \mathbf{K}_{ps} & : & \mathbf{K}_{pp} \end{bmatrix}_{N x N} \begin{bmatrix} [\mathbf{T}] \\ \cdots\cdots \\ [\mathbf{I}] \end{bmatrix}_{N x n_p} \qquad (3.5)$$

Whatever value is assumed for the coefficient β, the reduction in the DoF implies a reduction in the available existing modes as well. The validity of the condensed model generally depends on the mass and stiffness values assigned to the secondary coordinates. Generally, the use of frequency-dependent mass matrices improves the

accuracy of the reduced model properties, as shown by Kuhar and Stahle [41] and Imregum [61].

3.2.2 MODAL MODEL INCOMPLETENESS

The incompleteness in the Modal model is generally due to the inherent difficulty in attempting to use experimental data to define a finite model for a continuous subsystem. It is not realistic to undertake measurements either in all the coordinates and/or over a frequency range encompassing all natural frequencies. In the present analysis, however, we shall assume that all the N natural frequencies are known in the frequency range of interest, and the limitation is only concerned with the number of measured coordinates, say $n_p < N$, selected for the FRF measurements.

Let us assume that a subsystem Modal model is described by its (incomplete) modal properties:

$[\Phi^R]_{n_p x N}$ - rectangular modal matrix (mass-normalised eigenvectors $n_p < N$)

$[\omega_r^2]_{NxN}$ - eigenvalues (diagonal matrix)

It is important to note that a Guyan-reduced Spatial model leads to an incomplete Modal model in terms of both coordinates and modes, in spite of the fact that in this case the modal matrix is square.

Depending on the format assumed for the other subsystems dynamic properties description, the Modal model may be converted as described next.

3.2.2.1 MODAL Model → RESPONSE Model

In this case, it is assumed that the Modal model to be converted to Response one which is required by the **FRF Coupling** method. Let us assume that the FRF matrix is the Receptance, which is provided by the equation:

$$[\alpha(\omega)^R]_{n_p x n_p} = [\Phi^R]_{n_p x N} \left[(\omega_r^2 - \omega^2) \right]^{-1}_{N x N} [\Phi^R]^T_{N x n_p} \qquad (3.6)$$

This FRF matrix, although limited to only n_p points of interest on the substructure, contains information on <u>all</u> the N modes and is thus accurate for those coordinates retained. In order to study the effects of this reduction, while the models are described by their modal properties, we shall consider an ideal Modal model which possesses the **complete** information,

$$[\Phi]_{N x N} \qquad \left[\omega_r^2 \right]_{N x N}$$

The deletion of one coordinate - say, the k^{th} - corresponds to the elimination of the k^{th} row in the modal matrix so that we are ignoring the relative amplitude of that DoF in all the modes. This does not mean that the real system no longer has that DoF; only that we are not including information about its motion. In this way we are condensing the information in previously selected coordinates, as sketched in the following figure,

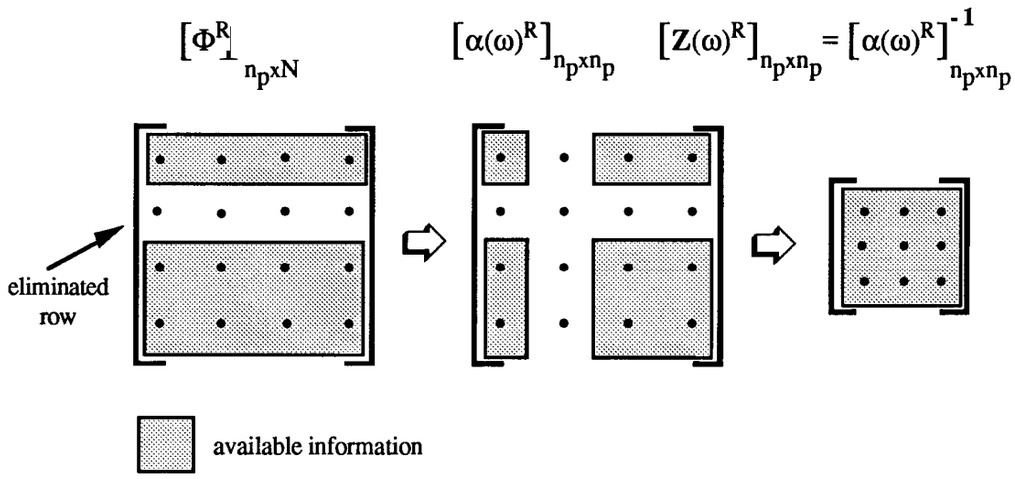

Fig. 3.1 - Modal → Response reduction

Inversion of the matrix $[\alpha(\omega)^R]_{n_p x n_p}$ leads to the reduced Dynamic Stiffness matrix $[Z(\omega)^R]_{n_p x n_p}$. In the limiting case when a zero frequency value ω is assumed, that reduced matrix $[Z(0)^R]_{n_p x n_p}$ corresponds to the well-known Guyan reduced stiffness matrix [54].

3.2.2.2 MODAL Model → SPATIAL Model

Since the reduced modal matrix $[\Phi^R]_{n_p x N}$ is rectangular, the use of a pseudoinverse is required for the calculation of the matrix $\left([\alpha(\omega)]^{-1}\right)^R_{n_p x n_p}$. The Dynamic Stiffness matrix $[Z(\omega)^R]_{n_p x n_p}$ may be calculated as shown by Ewins [1] as,

$$[Z(\omega)^R]_{n_p x n_p} = \left([\alpha(\omega)]^{-1}\right)^R_{n_p x n_p} = [\Phi^+]^T_{n_p x N} \left[(\omega_r^2 - \omega^2)\right]_{NxN} [\Phi^+]_{N x n_p} \quad (3.7)$$

where

$$[\Phi^+]_{N x n_p} = [\Phi^R]^T_{N x n_p} \left[[\Phi^R]_{n_p x N} [\Phi^R]^T_{N x n_p} \right]^{-1}_{n_p x n_p} \quad (3.8)$$

leading to the spatial properties

$$[Z(\omega)^R]_{n_p x n_p} = [D]_{n_p x n_p} - \omega^2 [E]_{n_p x n_p} \quad (3.9)$$

with

$$[D]_{n_p x n_p} = [\Phi^+]^T_{n_p x N} \left[\omega_r^2\right]_{NxN} [\Phi^+]_{N x n_p} \quad (3.10)$$

$$[E]_{n_p x n_p} = [\Phi^+]^T_{n_p x N} [\Phi^+]_{N x n_p} \quad (3.11)$$

The matrices **[D]** and **[E]** may be treated as (pseudo) stiffness and mass matrices for the subsystem.

It would be expected that the results obtained for the response of a coupled structure using those spatial properties i.e., by calculating $\left(\left[\alpha(\omega)\right]^{-1}\right)^{R}_{n_p x n_p}$ should give us the same results as when we use the inverse $-\left[\alpha(\omega)^{R}\right]^{-1}_{n_p x n_p}$ - of the **reduced Response model matrix** $\left[\alpha(\omega)^{R}\right]_{n_p x n_p}$. However, it should be noted that the matrices **[D]** and **[E]** do not represent the true stiffness and mass matrices for the component. The deletion of a coordinate, say **k,** may be done by eliminating the k^{th} row in the modal matrix. As a consequence, the respective k^{th} row and column in the complete Dynamic Stiffness matrix $\left[Z(\omega)\right]_{n_p x n_p}$ **are** also eliminated, but this has a rather different consequence to the previous one. In this case, we are assuming that coordinate to be fixed (grounded),as illustrated in the following figure,

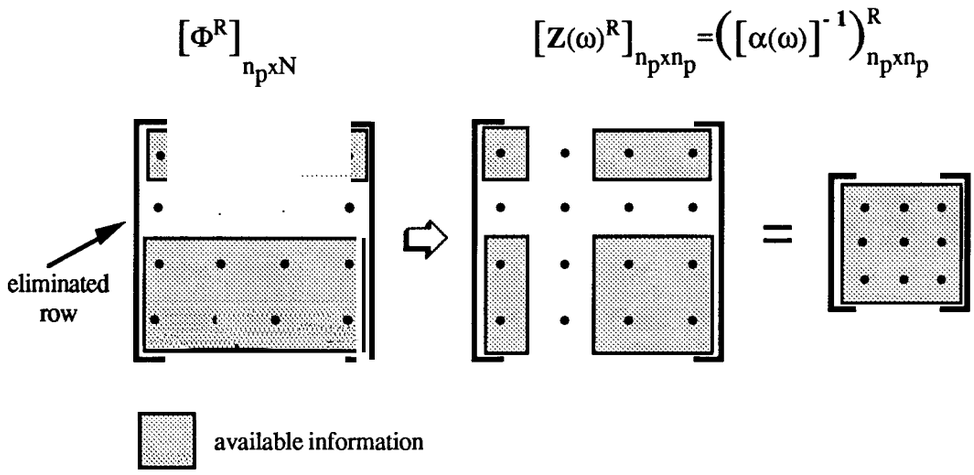

Fig. 3.2 - Modal → Spatial reduction

The available information in $\left[Z(\omega)^R\right]_{n_p x n_p} = \left(\left[\alpha(\omega)\right]^{-1}\right)^R_{n_p x n_p}$ for the **reduced Pseudo-Spatial model** has no natural connection with the actual component, since for $\omega = 0$ it corresponds to a partition of the complete subsystem static stiffness matrix.

3.2.3 PROCEDURES TO REDUCE MODELS

The different possibilities of performing a reduction on the original models are now grouped into four procedures which lead to the final format required to either the Spatial or FRF coupling techniques.

Procedure A using the *Spatial* **Method**

SPATIAL Model → **Guyan** Reduction → *SPATIAL* Model

$[K]_{NxN}$ $[M]_{NxN}$ ⇨ $[K^R]_{n_p x n_p}$ $[M^R]_{n_p x n_p}$

(Reduced Stiffness and Mass matrices)

Procedure B using the *Pseudo Spatial* **Coupling Method**

MODAL Model → *Pseudo SPATIAL* Model

$[\Phi]_{NxN}$ ⇨ $[\Phi^R]_{n_p x N}$ ⇨ $\left([\alpha(\omega)]^{-1}\right)^R_{n_p x n_p}$ ⇨ $[D]_{n_p x n_p}$ $[E]_{n_p x n_p}$

(Reduced pseudo stiffness and mass matrices)

In both previously-mentioned procedures all the subsystems are converted to a final **reduced Spatial model. The** result for the overall structure is then obtained in terms of its mass and stiffness properties.

Procedure C using the *FRF* **Coupling Method**

MODAL Model → *RESPONSE* Model

$[\Phi]_{NXN}$ ⇨ $[\Phi^R]_{n_p x N}$ ⇨ $[\alpha(\omega)^R]_{n_p x n_p}$ ⇨ $[\alpha(\omega)^R]^{-1}_{n_p x n_p}$

Procedure D using the *FRF* **Coupling Method**

MODAL Model → *RESPONSE* Model

$[\Phi]_{NXN}$ ⇨ $[\Phi^R]_{n_p x n_p}$ ⇨ $[\alpha(\omega)^R]_{n_p x n_p}$ ⇨ $[\alpha(\omega)^R]^{-1}_{n_p x n_p}$

In these two last procedures the final format for each component is a **reduced Response model,** herein assumed as the Receptance model.

3.3 COUPLING USING REDUCED MODELS

A computer program available in the Modal Testing group was used to perform the coupling process. One of the facilities offered in this program called MODALP [62] and run in a HP microcomputer series 9000 is the dynamic analysis of assembled structures, from either experimentally or theoretically-derived FRF matrices for each subsystem A and B, and is based on the following equation (vidé chapter 2, section 2.2.3),

$$\left[{}_{C}\mathbf{H}(\omega)\right]_{N_C x N_C} = \left[\left[{}_{A}\mathbf{H}(\omega)\right]^{-1}_{N_A x N_A} \oplus \left[{}_{B}\mathbf{H}(\omega)\right]^{-1}_{N_B x N_B} \right]^{-1}_{N_C x N_C} \qquad (3.12)$$

In the case when experimental data are not available, they may be simulated from the theoretically-derived FRF elements by polluting them with random errors.

3.3.1 NUMERICAL EXAMPLES

Three numerical examples are presented next to assess the validity of the procedures presented in section 3.2.3.

3.3.1.1 SUBSYSTEM DESCRIPTION

Three subsystems are described theoretically in terms of their Spatial and Modal models. They are the components of the different global structures analysed in the present work.

SUBSYSTEM 1A 4 DoF Undamped Spring-Mass System

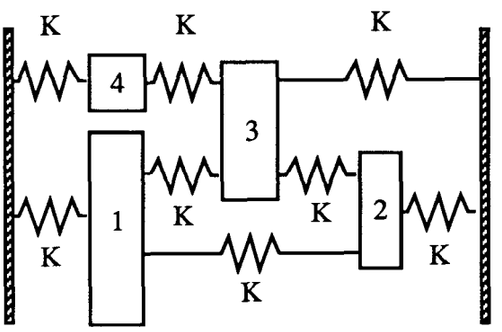

(K = 1000 N/m)

Fig. 3.3 a) - Subsystem 1A - 4 DoF undamped system

SPATIAL Model

$$[M]_{4x4} = \begin{bmatrix} 0.5 & 0 & 0 & 0 \\ 0 & 1.5 & 0 & 0 \\ 0 & 0 & 2.0 & 0 \\ 0 & 0 & 0 & 0.1 \end{bmatrix} \qquad [K]_{4x4} = \begin{bmatrix} 3000 & -1000 & -1000 & 0 \\ -1000 & 3000 & -1000 & 0 \\ -1000 & -1000 & 4000 & -1000 \\ 0 & 0 & -1000 & 2000 \end{bmatrix}$$

MODAL Model

$$[\Phi]_{4x4} = \begin{bmatrix} 0.397 & -0.075 & 1.355 & 0.012 \\ 0.517 & -0.604 & -0.185 & 0.003 \\ 0.506 & 0.470 & -0.121 & -0.086 \\ 0.264 & 0.268 & -0.091 & 3.138 \end{bmatrix}$$

$$[\omega^2]_{4x4} = \text{Diag} \; [\; 8.366E2 \;\; 2.437E3 \;\; 6.452E3 \;\; 2.027E4 \;]$$

SUBSYSTEM 1B -4 DoF Undamped Spring-Mass System

This subsystem has the same physical configuration of subsystem 1A, as shown in Fig. 3.3 b). The only difference between them is the value assumed for the mass m_4, which in this case is equal to 10.

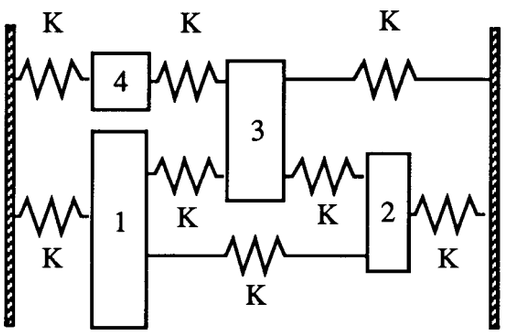

(K = 1000 N/m)

Fig. 3.3 b) - Subsystem 1B - 4 DoF undamped system

SPATIAL Model

$$[M]_{4x4} = \begin{bmatrix} 0.5 & 0 & 0 & 0 \\ 0 & 1.50 & 0 & \\ 0 & 0 & 2.0 & 0 \\ 0 & 0 & 0 & 10 \end{bmatrix} \quad [K]_{4x4} = \begin{bmatrix} 3000 & -1000 & -1000 & 0 \\ -1000 & 3000 & -1000 & 0 \\ -1000 & -1000 & 4000 & -1000 \\ 0 & 0 & -1000 & 2000 \end{bmatrix}$$

MODAL Model

$$[\Phi]_{4x4} = \begin{bmatrix} 0.064 & 0.405 & -0.025 & -1.353 \\ 0.067 & 0.565 & -0.557 & 0.182 \\ 0.121 & 0.451 & 0.515 & 0.131 \\ 0.309 & -0.057 & -0.022 & -0.002 \end{bmatrix}$$

$$\left[\omega^2\right]_{4x4} = \text{Diag} \; [\; 1.614E2 \; 9.889E2 \; 2.586E3 \; 6.464E3 \;]$$

SUBSYSTEM 2 - 2 DoF Undamped Free-free System

This is a simple 2 DoF undamped system which is connected with subsystem 1A and subsystem 1B,

(K = 1000 N/m)

Fig. 3.4 - Subsystem 2 - 2 DoF Free-free system

SPATIAL Model

$$[M]_{2x2} = \begin{bmatrix} 0 & 0 \\ 0 & 1 \end{bmatrix} \qquad [K]_{2x2} = \begin{bmatrix} 1000 & -1000 \\ -1000 & 1000 \end{bmatrix}$$

MODAL Model

$$[\Phi]_{2x2} = \begin{bmatrix} -1 & 0.32E\text{-}3 \\ -1 & -0.32E04 \end{bmatrix} \qquad \left[\omega_r^2\right]_{2x2} = \begin{bmatrix} 0 & 0 \\ 0 & 1E10 \end{bmatrix}$$

3.3.1.2 RESULTS

Four different procedures, as described in 3.2.3 were used for the analyses of the three following theoretical examples ;

EXAMPLE 1 - 5 DoF Undamped System

In this example, coordinate 1 of **subsystem 1A** was connected to coordinate 2 of **subsystem 2** as illustrated in fig. 3.5 and the predicted FRFs (point Receptances) are presented in fig. 3.6 (only one coordinate neglected in subsystem 1A) and in fig. 3.7 (two eliminated coordinates) both using the different procedures.

EXAMPLE 2 - 5 DoF Undamped System

In this example the **subsystem 1B** was connected (coord. 1) to **subsystem 2** (coord. 2) as illustrated in fig. 3.5 and the FRFs (point Receptances) are presented in fig. 3.8 (only one coordinate neglected in subsystem 1A) and in fig. 3.9 (two eliminated coordinates) both using the different procedures. This example was used in order to estimate the aptitude of the reduced model in each method when a mass modification m_4 was made in subsystem 1A.

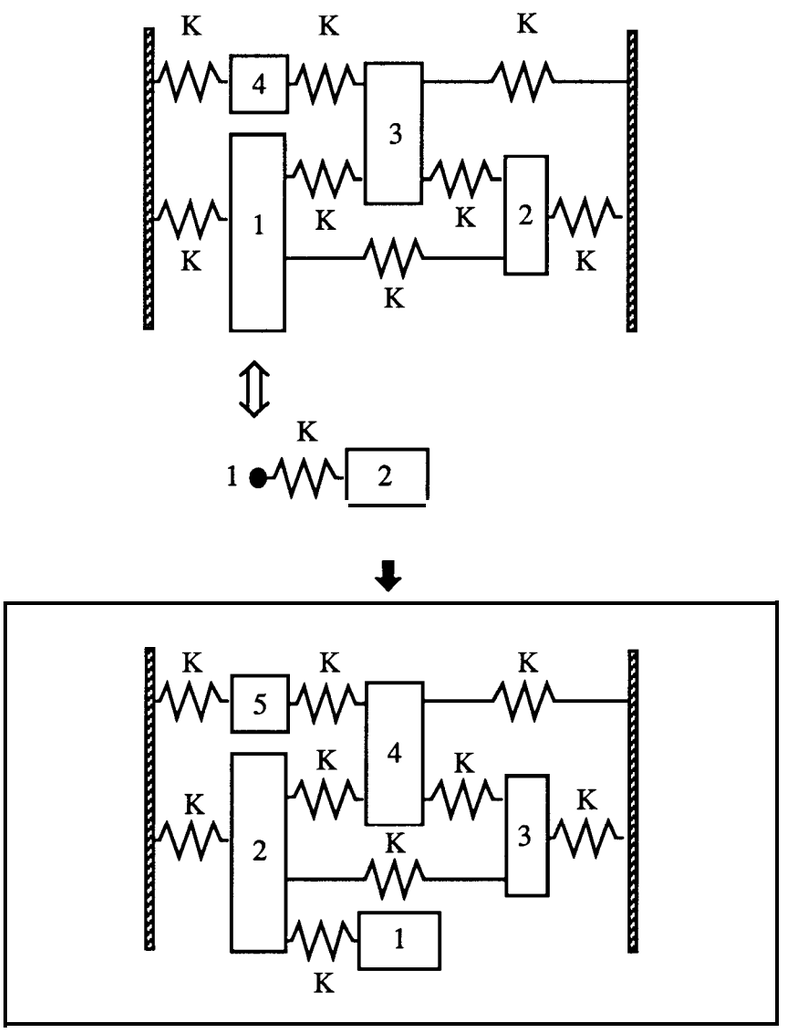

Fig. 3.5 - Subsystem 1A + Subsystem 2

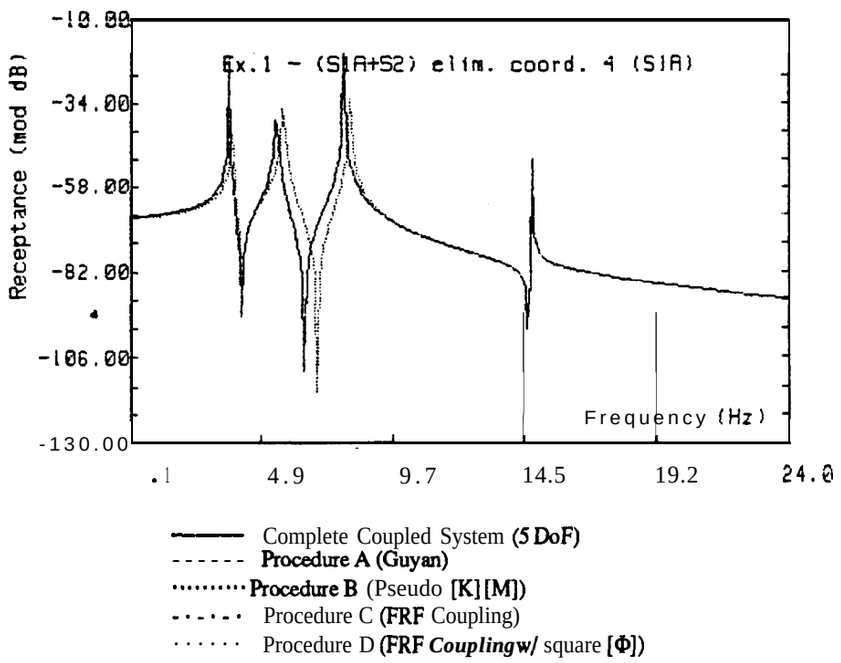

Fig. 3.6 - **Subsystem 1A** (M4=0.1, eliminated coord. 4) + **Subsystem 2**

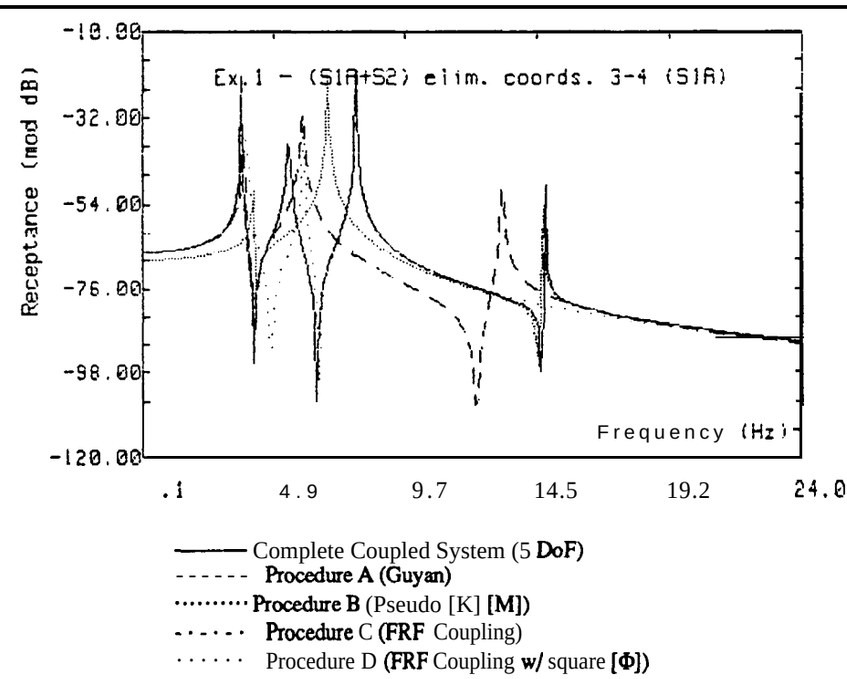

Fig. 3.7 - **Subsystem 1A** (M4=0.1, eliminated coords. 3 and 4) + **Subsystem 2**

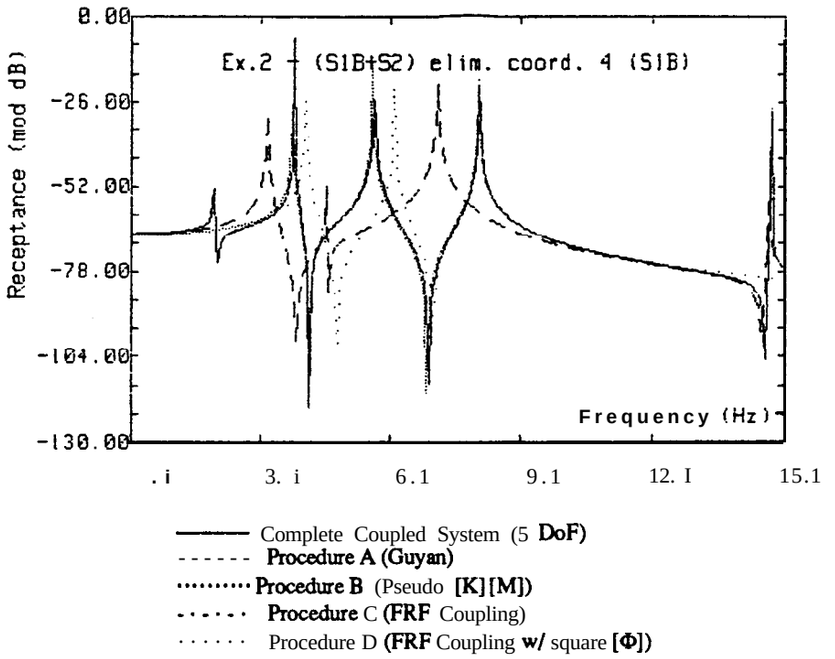

Fig. 3.8 - **Subsystem 1B** (M4=10, eliminated coord. 4) + **Subsystem 2**

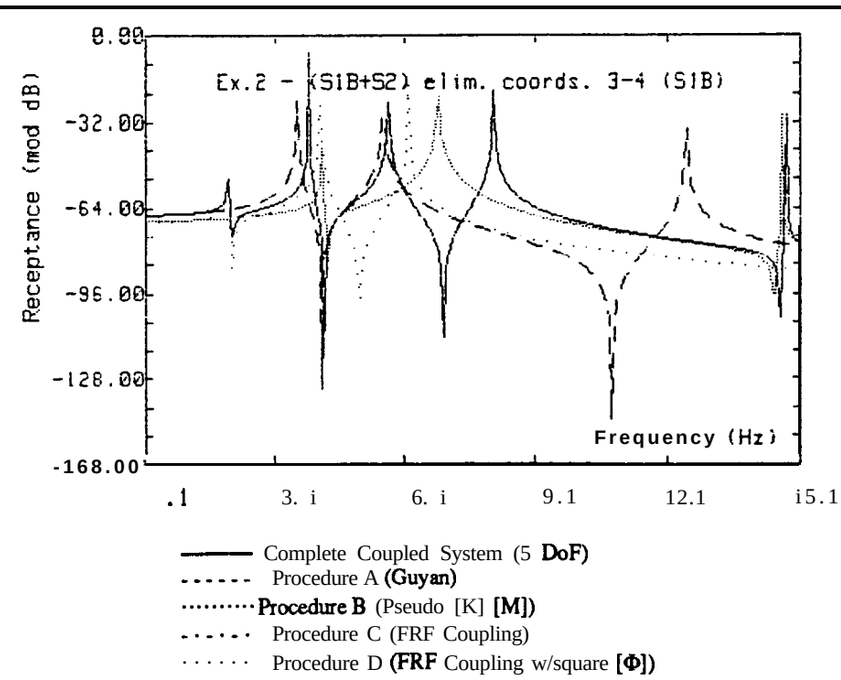

Fig. 3.9 - **Subsystem 1B** (M4=10, eliminated coords. 3 and 4) + **Subsystem 2**

EXAMPLE 3 - 6 DoF Undamped System

In this example the **subsystem 1B** is connected (using coordinates 1,2) to **subsystem 1B** (using coordinates 4,3) as illustrated in fig. 3.10. In this example the FRF coupling technique was used by assuming that the FRF matrix components were polluted by 5% error in order to simulate exprimental data. One of the predicted **FRFs** (a point Receptance) is shown in fig. 3.11.

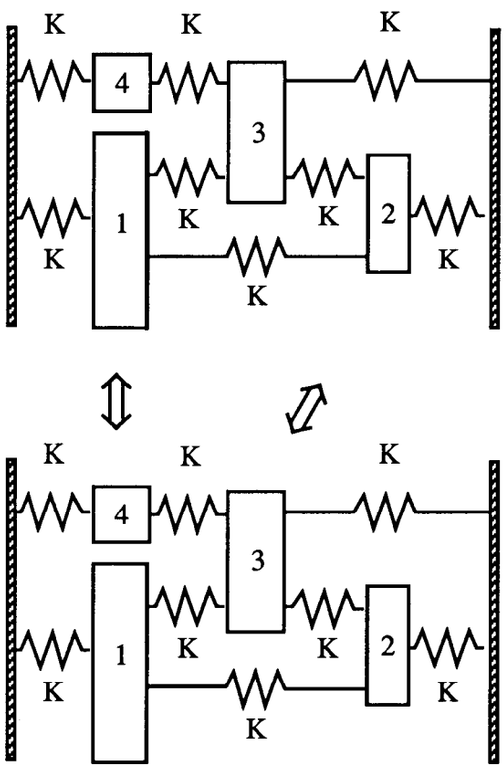

Fig. 3.10 - Subsystem 1B + Subsystem 1B

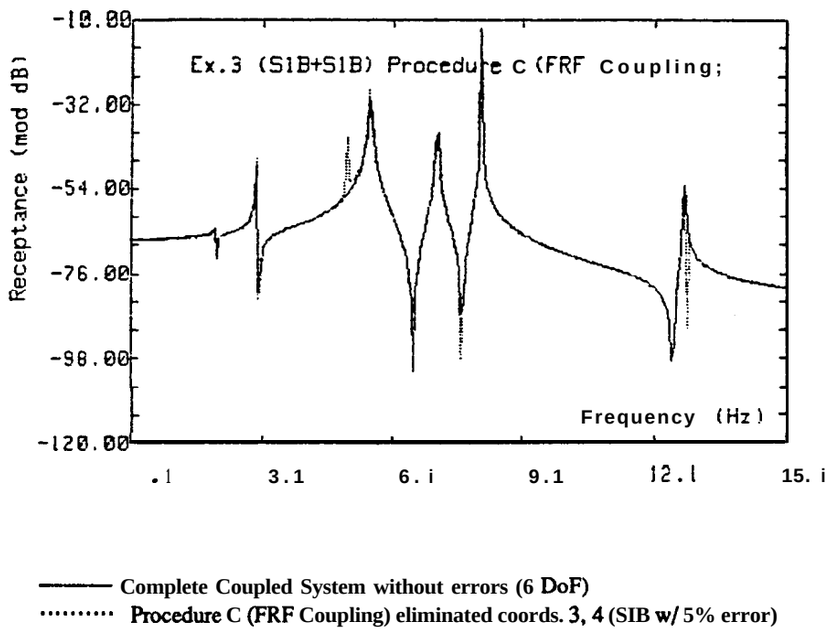

Fig. 3.11 - **Subsystem 1B** (M4=10, eliminated coords. 3 and 4, FRF polluted with 5% error) + **Subsystem 1B**

3.3.1.3 DISCUSSION OF RESULTS

In this work, the subsystem models were chosen as simple spring-mass systems which are not intended to represent the models for an actual structure. However, with these simple systems we can understand how a selected procedure may be applied to a real problem. Since we can know the complete dynamic information for those models, the simulated incompleteness on the number of coordinates was achieved either by using a Spatial model description or by using a Modal one. In the former group (Procedure A) the Guyan reduction was used - a classical static reduction was performed - while in the latter group (Procedures B,C and D), the rows on the complete modal matrix were successively "deleted".

The results obtained for the coupled structures differ essentially for two reasons;

i) the way the incompleteness was assumed,

ii) the method used for the coupling process.

The numerical examples show that:

- different results are predicted for the same assembly when procedures A and B are used to reduce the subsystem models; both procedures resort to the same coupling method. In this case the difference is explained by the reduction performed in subsystem 1 since, when a Guyan reduction is applied, the dynamic properties for the complete system are only preserved in the reduced model if the relative mass value of the eliminated coordinate is neglegible [60]. In contrast, Procedure B is convenient when high relative mass values are to be neglected. However, it is important to note that both procedures lead to the same result if one assumes $\beta=1$ in the transformation matrix [T] (vide eq.(3.3), section 3.2.1) which is used in procedure A. In this particular case both procedures are two equivalent ways of performing a dynamic reduction.

- different results are predicted for the same assembly when procedures B and C are used to reduce the subsystem models; both procedures resort to the same incomplete model. The main reason for this is explained in 3.2.2.1 and 3.2.2.2 and, as mentioned there, the dynamic properties of the structure are preserved (over the frequency range encompassing its natural frequencies) by using procedure C. In this case there is no difference in the response characteristics of the reduced model, whichever coordinate is eliminated (excluding those involved in the physical connection). The existence of some “extra” peaks in the frequency response function of example 3 (see fig.3.11), when experimental data are simulated, is not due to any incompleteness of the subsystem but due to an inherent problem in the FRF coupling process, since at some subsytem resonances the inversion of the polluted receptance matrix may encounter some numerical difficulties.

3.3.2 CONCLUSIONS; USE OF DIFFERENT PROCEDURES

- The use of reduced Spatial models in procedure A **(static reduction)** leads to results whose accuracy depends on the coordinates eliminated - it is a question of mass value dependency, so the choice of the secondary coordinates should be done according to the relative mass values (when a coordinate with a high relative mass value is eliminated the dynamic information of the subsystem is altered and may affect the overall system behaviour).

- In contrast, the reduced pseudo-Spatial model in Procedure B **(dynamic reduction)** only 'preserves' the dynamic properties of the complete system if the eliminated coordinates have high relative mass values. It was also found that this procedure is a particular case of Procedure A (if one assumes $\beta=1$ in equation 3.3), despite of the different ways of arriving at the final reduced subsystem models.

- The only procedure that is 'insensitive' to the degree of incompleteness in terms of coordinates for the subsystem model is Procedure C, which gives accurate results in all the tested cases.

- In Procedure D, which is a particular case of Procedure C, the results obtained are not accurate in all the cases since the residual effects of the neglected modes were not included.

3.4 THE NEED TO USE ALTERNATIVE FRF COUPLING METHODS

The results achieved with the previously presented coupling exercises showed that the incompleteness in terms of coordinates in the component models does not play an important rule in the prediction of the global structure results whenever the FRF coupling method is used. It should be noticed, however, that the incompleteness which is referred to is only related to the interior coordinates. At this stage it is therefore assumed that the

the necessary and sufficient number of connecting coordinates which, unfortunately, is not always obvious, as will be seen later, in chapter 5.

3.4.1 OCCURENCE OF ILL-CONDITIONED FRF MATRICES

The results achieved with the use of the FRF coupling method showed that when experimental simulated data is used to represent each subsystem Response model, the predicted final response possesses some undesired false peaks. The explanation of this phenomenon can be found by regarding the interrelationship between the Response and the Modal models (vide chapter 1). In the vicinity of each subsystem resonance frequency the corresponding FRF matrix is largely dominated by one single term, or in other words, the matrix will have order n (number of primary coordinates) but also tends to have rank 1 (the single dominating mode). This means that every FRF matrix tends to be rank-deficient or nearly singular in the vicinity of each subsystem natural frequency, especially in the case of lightly-damped structures where the local dominance of a single mode is strongest. As far as a purely theoretical FRF matrix is of concern near a resonance frequency, the inversion - although applied to a matrix having a high condition number - leads to a correct dynamic stiffness matrix subsequently used in the assembling process. However, when measured FRF matrices are dealt with, their elements are prone to errors which will cause a pronounced deviation of the inverse matrix from the existing but unknown ideal dynamic stiffness matrix. The result of these perturbed matrices on each single component will show up in the predicted response mainly at the frequencies close to each subsystem natural frequencies as discussed by Larsson [63]. A remedy suggested by Ewins [16] to avoid the existence of these extra peaks is the smoothing of each FRF before it is used to create the FRF matrix. In order to do so, the Response model is converted to a Modal one which is subsequently used to regenerate the smoothed FRF matrix which will behave better in numerical terms, therefore giving a more accurate prediction of the global Response model. This approach, however, withdraws the main

virtue of the FRF coupling technique which is the direct use of what is measured on the actual components without the need of a complementary identification stage.

Besides the occurence of the ill-conditioned matrices near a resonance frequency, presented above, there are other situations when the required coupling algorithms can behave erraticaly, even for other frequencies in the range of interest. It is enough to have any linear dependency or near-dependency among some of the rows (or columns) in a given FRF matrix and the inversion may well fail. Unfortunately, this is a common practical problem when dealing with the subsystem models, mainly due to the following two reasons,

- the FRF matrix has been generated from a set of inadequate modal data. The procedure C presented in 3.2.3 shows that in the case of a modal matrix containing more coordinates (n) than modes (m), the generated FRF matrix will be of order n although having rank of m; in this case the matrix is singular since there exist (n-m) linearly dependent rows (or columns) and it is impossible to calculate the corresponding inverse even though it exists, generally the subsystem dynamic stiffness matrix. To prevent this situation, more modes should be included (up to the number of coordinates) and very likely the undesired singularity will be removed. Should it be impracticable to apply this remedy, other alternatives can be found such as those making use of more sophisticated algorithms enabling the calculation of the closest inverse of a rank-deficient matrix. This is one of the topics considered in chapter 5;

- the FRF matrix has been measured on a structure in which some of the coordinates are situated on locally rigid regions - either interior or interface ones - causing the responses over a certain frequency range to be linearly dependent on each other. In this case the FRF matrix tends to be or is rank deficient. Should at least one of the components behave in this manner, the coupling will fail numerically. A way of circumventing this problem is to detect the redundant coordinates prior to the coupling of the components and, if possible, neglect them or, once again to make use of proper algorithms which are presented after the following section.

3.4.2 MODEL INCONSISTENCY

In chapter 1 it has been shown how a Response model can be fully created over a certain frequency range by measuring either: (i) all the elements in the FRF matrix (or only the upper or lower triangular matrix assuming a symmetric matrix) or (ii) one single row or column of the corresponding matrix enabling the identification of the corresponding Modal model. In the latter case the full set of FRFs can subsequently be generated over the selected frequency range provided the effect of the out-of-range modes can be neglected.

In practical terms the quality of the measured set of FRFs can be checked by comparing the various estimates of the modal parameters with each other. It often happens that a unique set of modal parameters cannot be extracted directly from the same set of FRFs and then the model is said to suffer from self-inconsistency.

3.4.3 ALTERNATIVE FRF COUPLING TECHNIQUES

The FRF coupling technique discussed so far is suitable for cases where the reduced Response models do not lead to numerical failures in the coupling process. Additionally, it was shown that alternative algorithms are necessary to deal with rank-defficient FRF matrices, at least over certain frequency ranges where for instance the local rigidities cause the rows to be dependent. This is an important aspect to be taken into account in the previously presented FRF coupling technique, since the final FRF matrix is obtained after carrying out three inversion processes.

3.4.3.1 FRF COUPLING ALGORITHM 2

A first approach to the numerical difficulties which arise in the coupling process will be in terms of a possible improvement to handle the redundancy in some of the primary coordinates and in someway trying to speed up the required calculation time. Let us

assume that the generalised Impedance matrices of each component are expanded in the following way,

$$\left[{}^{*}_{A}\mathbf{Z}(\omega)\right]_{N_C x N_C} = \begin{bmatrix} {}_{A}\mathbf{Z}_{ii}+{}_{A}\mathbf{D}_{ii} & {}_{A}\mathbf{Z}_{ic} & \mathbf{0} \\ {}_{A}\mathbf{Z}_{ci} & {}_{A}\mathbf{Z}_{cc}+{}_{A}\mathbf{D}_{cc} & 0 \\ 0 & 0 & {}_{B}\mathbf{D}_{ii} \end{bmatrix} \tag{3.13}$$

$$\left[{}^{*}_{B}\mathbf{Z}(\omega)\right]_{N_C x N_C} = \begin{bmatrix} -{}_{A}\mathbf{D}_{ii} & 0 & 0 \\ 0 & {}_{B}\mathbf{Z}_{cc}-{}_{A}\mathbf{D}_{cc} & {}_{B}\mathbf{Z}_{ic} \\ \mathbf{0} & {}_{B}\mathbf{Z}_{ci} & {}_{B}\mathbf{Z}_{cc}-{}_{B}\mathbf{D}_{ii} \end{bmatrix} \tag{3.14}$$

where the matrices [D] are arbitrary. In assuming this, the coupled system matrix $\left[{}_{C}\mathbf{Z}(\omega)\right]_{N_C x N_C}$ can now be obtained as a **simple addition** of the same-order expanded matrices $\left[{}^{*}_{A}\mathbf{Z}(\omega)\right]_{N_C x N_C}$ and $\left[{}^{*}_{B}\mathbf{Z}(\omega)\right]_{N_C x N_C}$ as,

$$\left[{}_{C}\mathbf{Z}(\omega)\right]_{N_C x N_C} = \left[{}^{*}_{A}\mathbf{Z}(\omega)\right]_{N_C x N_C} + \left[{}^{*}_{B}\mathbf{Z}(\omega)\right]_{N_C x N_C} \tag{3.15}$$

The FRF matrix $\left[{}_{C}\mathbf{H}(\omega)\right]_{N_C x N_C}$ is given as

$$\left[{}_{C}\mathbf{H}(\omega)\right]_{N_C x N_C} = \left[\left[{}^{*}_{A}\mathbf{Z}(\omega)\right]_{N_C x N_C} + \left[{}^{*}_{B}\mathbf{Z}(\omega)\right]_{N_C x N_C} \right]^{-1}_{N_C x N_C} \tag{3.16}$$

or $$\left[{}_{C}\mathbf{H}(\omega)\right]_{N_C x N_C} = \left[\left[{}^{*}_{A}\mathbf{H}(\omega)\right]^{-1}_{N_C x N_C} + \left[{}^{*}_{B}\mathbf{H}(\omega)\right]^{-1}_{N_C x N_C} \right]^{-1}_{N_C x N_C} \tag{3.17}$$

where $\left[{}^{*}_{A}\mathbf{H}(\omega)\right]$ and $\left[{}^{*}_{B}\mathbf{H}(\omega)\right]$ are augmented FRF matrices which are derived in the next paragraph. The main virtue of having this addition of same-order matrices is the reformulation of the calculation of the final FRF matrix since in this way the three matrix inversion operations can be replaced by only one inversion [64] as follows,

$$\left[{}_{C}\mathbf{H}(\omega)\right]_{N_C x N_C} = \left[{}^{*}_{B}\mathbf{H}(\omega)\right] \left[\left[{}^{*}_{A}\mathbf{H}(\omega)\right] + \left[{}^{*}_{B}\mathbf{H}(\omega)\right] \right]^{-1} \left[{}^{*}_{A}\mathbf{H}(\omega)\right] \tag{3.18}$$

Calculation of the augmented FRF matrices $[^{*}\mathbf{H}(\omega)]$

For convenience of simplicity in what follows next, the matrices **[D]** will be taken as identity matrices **[I].** Each generalised Impedance matrix is then given as,

$$\left[{}^{*}_{A}\mathbf{Z}(\omega)\right]_{N_C x N_C} = \left[\begin{array}{c:c} {}_{A}\mathbf{Z} + \mathbf{I} & \mathbf{0} \\ \hdashline \mathbf{0} & \mathbf{I} \end{array}\right] = \left[\begin{array}{c:c} {}'_{A}\mathbf{Z} & \mathbf{0} \\ \hdashline \mathbf{0} & \mathbf{I} \end{array}\right] \qquad (3.19)$$

and

$$\left[{}^{*}_{B}\mathbf{Z}(\omega)\right]_{N_C x N_C} = \left[\begin{array}{c:c} -\mathbf{I} & \mathbf{0} \\ \hdashline \mathbf{0} & {}_{B}\mathbf{Z} - \mathbf{I} \end{array}\right] = \left[\begin{array}{c:c} -\mathbf{I} & \mathbf{0} \\ \hdashline \mathbf{0} & {}'_{B}\mathbf{Z} \end{array}\right] \qquad (3.20)$$

The necessary **[*H(o)]** matrices are then formulated as,

$$\left[{}^{*}_{A}\mathbf{H}(\omega)\right]_{N_C x N_C} = \left[\begin{array}{c:c} \left[\left[{}_{A}\mathbf{H}(\omega)\right] + [\mathbf{I}]\right]^{-1}\left[{}_{A}\mathbf{H}(\omega)\right] & \mathbf{0} \\ \hdashline \mathbf{0} & [\mathbf{I}] \end{array}\right] \qquad (3.21)$$

$$\left[{}^{*}_{B}\mathbf{H}(\omega)\right]_{N_C x N_C} = \left[\begin{array}{c:c} -[\mathbf{I}] & \mathbf{0} \\ \hdashline \mathbf{0} & \left[\left[{}_{B}\mathbf{H}(\omega)\right] - [\mathbf{I}]\right]^{-1}\left[{}_{B}\mathbf{H}(\omega)\right] \end{array}\right]$$

Although this approach requires after all three matrix inversions, the addition of the identity matrix to the original FRF matrices before the inverse is calculated may very well avoid the ill-conditioning problem.

3.4.3.2 FRF COUPLING ALGORITHM 3

In respect of numerical failures due to the redundancy of the primary coordinates, the previous approach constitutes an improvement compared to the method presented in chapter **2, section 2.** However, a recent development of the FRF coupling technique by Jetmundsen, Bielawa and Flannelly [65] has reduced the number of required inversions at each frequency from three to one and, additionaly, the size of the matrix for inversion is dictated only by the number of connection coordinates. This refined method, apart from speeding up the calculations, can yet behave better, in numerical terms, than the

conventional one, since it minimises the crucial inversion operations on matrices which have a smaller order. This may play an important role if subsystems possess dependent coordinates. The algorithm can be derived taking into account the relationship between the elements of the global FRF matrix and the elements in each subsystem FRF matrix. The coordinates in the FRF matrix of the coupled structure can be partitioned according to three regions corresponding to,

- the interior coordinates of component A **(pi)** denoted as **a**
- the interior coordinates of component B ($_B\mathbf{n}_i$) denoted as **b**
- **the** common connection coordinates of component A and B ($_A\mathbf{n}_c = {}_B\mathbf{n}_c = \mathbf{n}_c$) denoted as c

The whole FRF matrix can be partitioned as follows,

$$\left[{}_C\mathbf{H}(\omega)\right]_{N_C x N_C} = \begin{bmatrix} \mathbf{H}_{aa} & \mathbf{H}_{ac} & \mathbf{H}_{ab} \\ \mathbf{H}_{ca} & \mathbf{H}_{cc} & \mathbf{H}_{cb} \\ \mathbf{H}_{ba} & \mathbf{H}_{bc} & \mathbf{H}_{bb} \end{bmatrix} \tag{3.23}$$

Each partition of this FRF matrix can now be interrelated with the submatrices composing the FRF matrices of the subsystems, as derived in Appendix I, leading to the following equation,

$$\begin{bmatrix} \mathbf{H}_{aa} & \mathbf{H}_{ac} & \mathbf{H}_{ab} \\ \mathbf{H}_{ca} & \mathbf{H}_{cc} & \mathbf{H}_{cb} \\ \mathbf{H}_{ba} & \mathbf{H}_{bc} & \mathbf{H}_{bb} \end{bmatrix} = \begin{bmatrix} {}_A\mathbf{H}_{ii} & {}_A\mathbf{H}_{ic} & \mathbf{0} \\ {}_A\mathbf{H}_{ci} & {}_A\mathbf{H}_{cc} & \mathbf{0} \\ \mathbf{0} & \mathbf{0} & {}_B\mathbf{H}_{ii} \end{bmatrix} - \begin{bmatrix} {}_A\mathbf{H}_{ic} \\ {}_A\mathbf{H}_{cc} \\ {}_B\mathbf{H}_{ic} \end{bmatrix} \left[\left[{}_A\mathbf{H}_{cc}\right] + \left[{}_B\mathbf{H}_{cc}\right]\right]^{-1} \begin{bmatrix} {}_A\mathbf{H}_{ic} \\ {}_A\mathbf{H}_{cc} \\ {}_B\mathbf{H}_{ic} \end{bmatrix}^T \tag{3.24}$$

As mentioned before, the main advantage of using this formulation over the two previously presented methods is related to the crucial operation of inversion. Herein only one inversion is required and, additionally, it is applied only to the sum of the sub-matrices which order depends only on the number of connection coordinates. More

interior coordinates can then be included in the analysis without affecting significantly the required computational time. The result of this will be a quicker calculation of the required FRF matrix and, as in the latter approach, it will be able to deal with redundancies on the interior coordinates whenever they are present in each component.

3.4.4 NUMERICAL EXAMPLES

In order to test the aptitude of all the three FRF coupling approaches to deal with subsystems possessing simulated local rigidities therefore causing the responses at some coordinates to be linear dependent from each other over a selected frequency range, two subsystems are described next in terms of their Spatial and Modal models. The frequency range of interest in assumed to be from 0 to 15 Hz and the corresponding Response models were generated from the Spatial ones by truncating each element on the FRF matrix up to the sixth significant digit therefore provoking singular FRF matrices for each subsystem.

3.4.4.1 SUBSYSTEM DESCRIPTION

SUBSYSTEM 3

This is a free-free undamped system with 5 DoF and possesses three rigid regions simulated with relatively stiff springs (springs K_2, K_3 and K_4 in fig. 3.12)

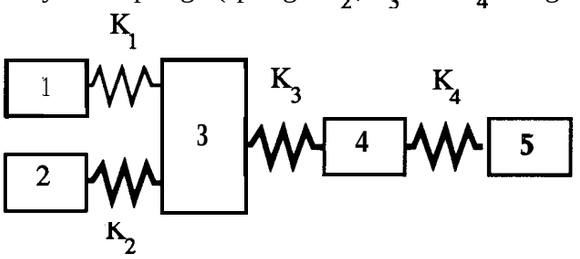

$K_1 = 1\ E3$; $K_2 = 1\ E6$; $K_3 = 1\ E7$; $K_4 = 1\ E5$ (N/m)

$M_1 = 0.5$; $M_2 = 1$; $M_3 = 2$; $M_4 = 1.5$; $M_5 = 0.5$ (Kg)

Fig. 3.12 - Subsystem 3 - 5 DoF Free-free system

SPATIAL Model

$$[M]_{5x5} = \begin{bmatrix} 0.5 & 0 & 0 & 0 & 0 \\ 0 & 10 & 0 & 0 & \\ 0 & 02 & 0 & 0 & \\ 0 & 0 & 0 & 1.5 & 0 \\ 0 & 0 & 0 & 0 & 0.5 \end{bmatrix}$$

$$[K]_{5x5} = \begin{bmatrix} 0 & 1\ E6 & -1.E6 & 0 & 0 \\ -1\ E3 & -1\ E6 & 1.1001E7 & -1\ E7 & 0 \\ 0 & 0 & -1 \quad E7 & 1.01\ E7 & -1\ E5 \\ 1\ E3 & 0 & 0\ -1 \quad E3 & -1\ E5 & 1\ E5 \end{bmatrix}$$

MODAL Model

$$[\Phi]_{5x5} = \begin{bmatrix} 4.2640E\text{-}1 & 1.3484E00 & 1.3176E\text{-}3 & 3.7169E\text{-}4 & 7.9258E\text{-}5 \\ 4.2640E\text{-}1 & -1.3490E\text{-}1 & -1.8399E\text{-}1 & 8.7422E\text{-}1 & 4.3243E\text{-}2 \\ 4.2640E\text{-}1 & -1.3461E\text{-}1 & -1.4354E\text{-}1 & -2.3555E\text{-}1 & -4.7326E\text{-}1 \\ 4.2640E\text{-}1 & -1.3467E\text{-}1 & -1.3319E\text{-}1 & -2.8675E\text{-}1 & 6.0560E\text{-}1 \\ 4.2640E\text{-}1 & -1.3616E\text{-}1 & 1.3404E00 & 5.3626E\text{-}2 & -1.0313E\text{-}2 \end{bmatrix}$$

$$\left[\omega_r^2\right]_{5x5} = \text{diag}(\ 0,\ 2.1997E3, 2.1987E5, 1.2694E6, 1.1944E7)$$

Natural Frequencies 0. 7.464, 74.63, 179.3, 550 Hz

SUBSYSTEM 4

This is a clamped-free undamped system with 5 DoF and possesses one rigid region simulated with one relatively stiff spring (spring K_3 in Fig. 3.13)

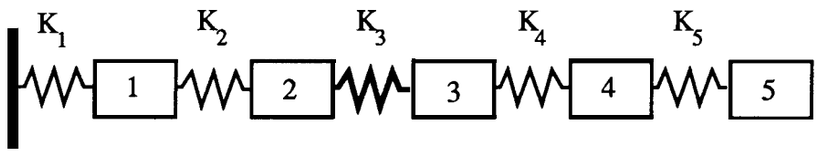

$K_1 = 3\,E3$; $K_2 = K_5 = 1\,E3$; $K_3 = 1\,E7$; $K_4 = 2\,E3$ (N/m)

$M_1 = 1$; $M_2 = 0.5$; $M_3 = 2$; $M_4 = 1.5$; $M_5 = 0.5$ (Kg)

Fig. 3.13 - Subsystem 3 - 5 DoF Clamped-free system

SPATIAL Model

$$[M]_{5x5} = \begin{bmatrix} 0 & 1000 & 0.5 & 0 & 0 \\ 0 & 0 & 2 & 0 & 0 \\ 0 & 0 & 0 & 1.5 & 0 \\ 0 & 0 & 0 & 0 & 0.5 \end{bmatrix}$$

$$[K]_{5x5} = \begin{bmatrix} 4\,E3 & -1\,E3 & 0 & 0 & 0 \\ -1\,E3 & 1.0001E7 & -1\,E7 & 0 & 0 \\ 0 & -1\,E7 & 1.0002E7 & -2\,E3 & 0 \\ 0 & 0 & -2\,E3 & 3\,E3 & -1\,E3 \\ 0 & 0 & 0 & -1E3 & 1\,E3 \end{bmatrix}$$

MODAL Model

$$[\Phi]_{5x5} = \begin{bmatrix} 1.1098E\text{-}1 & -1.6218E\text{-}1 & -2.6013E\text{-}1 & 9.4536E\text{-}1 & -5.0601E\text{-}5 \\ 4.2720E\text{-}1 & -4.0335E\text{-}1 & -1.6605E\text{-}1 & -1.6497E\text{-}1 & 1.2649E00 \\ 4.2723E\text{-}1 & -4.0334E\text{-}1 & -1.6601E\text{-}1 & -1.6505E\text{-}1 & -3.1622E\text{-}1 \\ 5.0486E\text{-}1 & 2.3891E\text{-}1 & 5.7865E\text{-}1 & 1.4094E\text{-}1 & 1.6865E\text{-}5 \\ 5.4600E\text{-}1 & 9.8119E\text{-}1 & -8.4990E\text{-}1 & -1.2963E\text{-}1 & -1.3489E\text{-}9 \end{bmatrix}$$

$$\left[\omega_i^2\right]_{5x5} = \text{diag}(\,1.507E2, 1.513E3, 3.362E3, 4.175E3, 2.501E7\,)$$

Natural Frequencies 1.954. 6.191, 9.228, 10.28, 795.8 Hz

3.4.4.2 RESULTS

The two subsystems are now assumed to be connected through three coordinates. The connection coordinates are selected as 3, 4 and 5 in example I and 2,3 and 4 in the second example. The criteria of selection was established according to the possible redundancy existing on each set of connecting coordinates. In the first example, only subsystem 1 possesses local rigidities in the interfacing region whereas the second example makes use of subsystems both containing localised rigidities in the connecting region.

EXAMPLE I

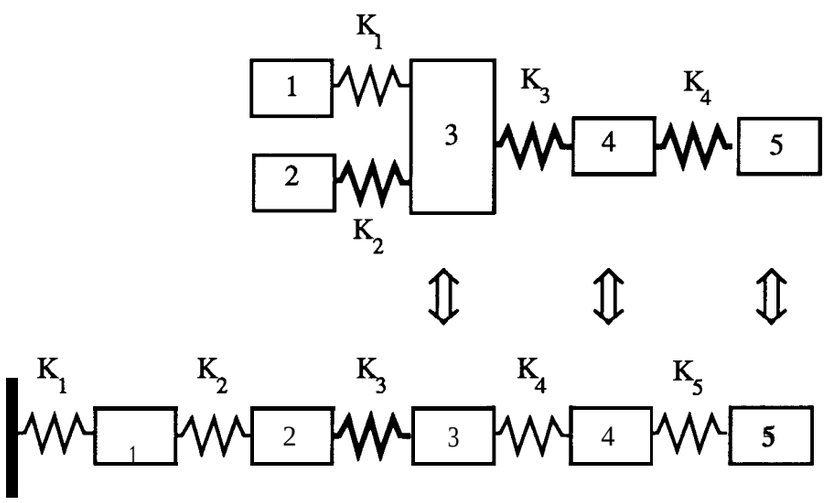

COUPLED STRUCTURE = SUBSYSTEM 3 + SUBSYSTEM 4

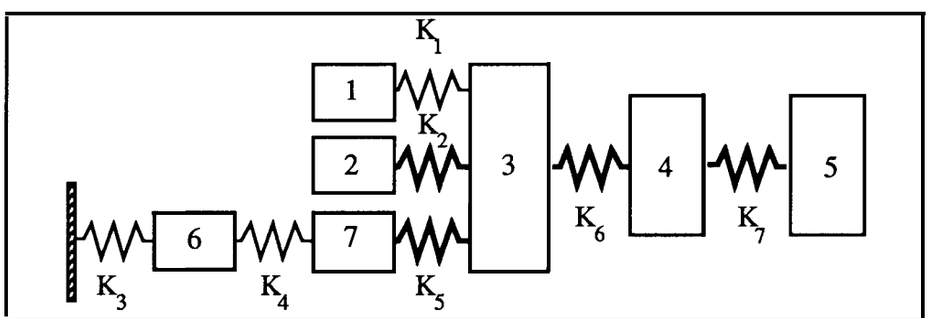

Fig. 3.14 - Subsystem 3 + subsystem 4 (3 connection coordinates)

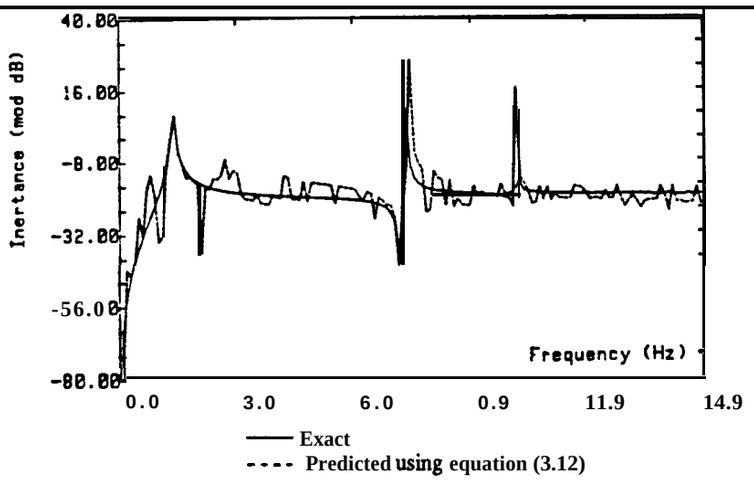

Fig. 3.15 - Predicted FRF (Point Inertance 2,2) using **Algorithm 1**

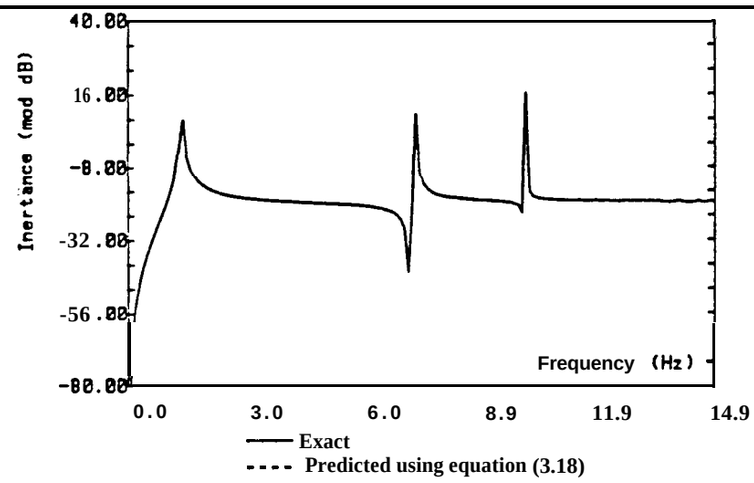

Fig. 3.16 - Predicted FRF (Point Inertance 2,2) using **Algorithm 2**

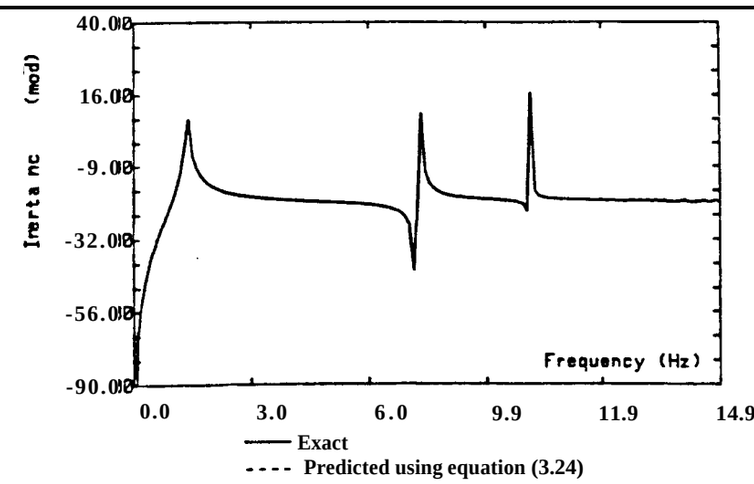

Fig. 3.17 - predicted FRF (Point Inertance 2,2) using **Algorithm 3**

EXAMPLE II

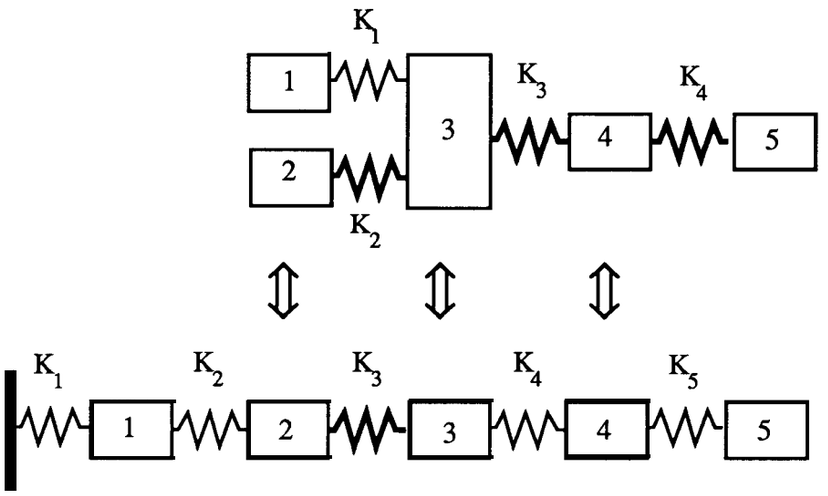

COUPLED STRUCTURE

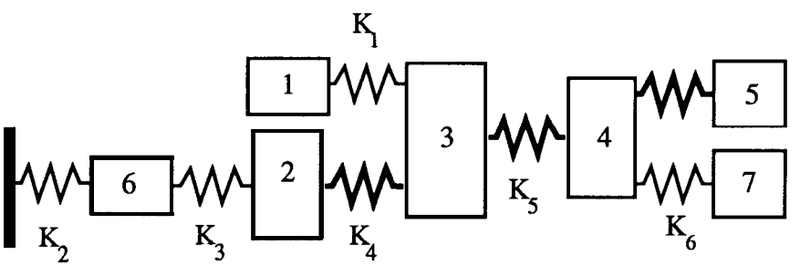

Fig. 3.18 - Subsystem 3 + Subsystem 4 (3 connection coordinates)

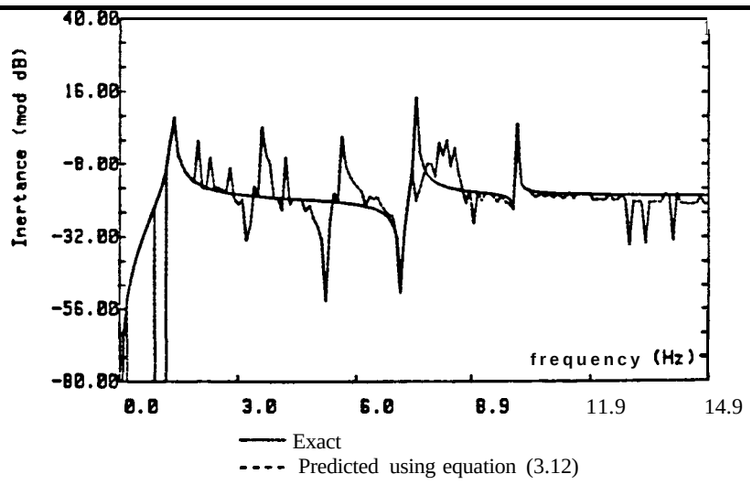

Fig. 3.19 - **Predicted FRF** (Point Inertance **2,2)** using **Algorithm** 1

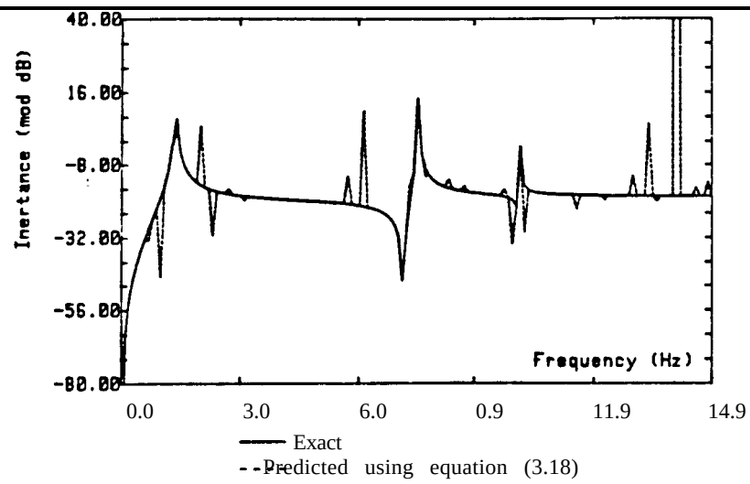

Fig. 3.20 - Predicted FRF (Point Inertance **2,2)** using **Algorithm 2**

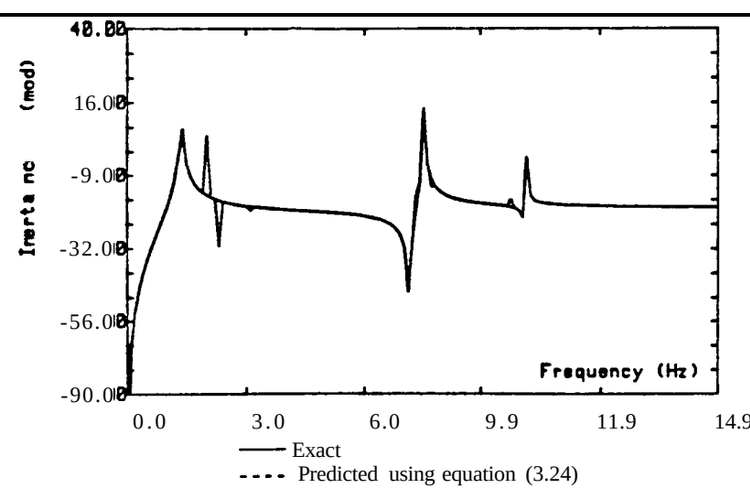

Fig. **3.21 -** Predicted FRF (Point Inertance **2,2)** using **Algorithm 3**

3.4.4.3 DISCUSSION OF RESULTS

The predicted response of the coupled system in both examples I and II show that the approach which makes use of the classical equation (3.12), herein designated as algorithm 1, will experience numerical difficulties whenever any linear dependency exists in a set of coordinates - either interior or connection ones. In example **I** it is assumed that the dependent coordinate belongs to the interior region for one component and to both interior and connecting regions for the other. The approch making use of algorithm 2 (vidé eq. (3.18)) can give accurate estimation of the final coupled response, since it perturbates the initial FRF matrix in a good sense towards the non-singularity. So also does the approach using algorithm 3 (vidé eq. (3.24)) since by adding the two partitions of the FRF matrices corresponding to the coordinates of the interface region the singularity is also removed in spite of the fact that one of the FRF partitions was initially singular.

In example **II** the local rigidities are assumed to be localised in the interior region in one of the components and in the connecting region for **both** components. In this case both approches 2 and 3 fail to give a completely successful prediction. They are still prone to numerical errors in the inversion of the matrices since they are singular.

3.5 CONCLUSIONS

The alternative algorithms making use of inversions carried out on either augmented FRF matrices (algorithm 2 - eq. (3.18)) or partitioned FRF matrices (algorithm 3 - eq. (3.24)) can resolve many of the numerical difficulties encountered during the coupling process using the classical algorithm (algorithm 1 - eq. (3.12)). Whenever locally-rigid regions are confined to the interior coordinates of each component or to only one of the subsystem's connecting coordinates. In such a situation, the approach making use of algorithm 3 presents a remarkable advantage over the other two, since the inversion

operation is only required once and even then is applied to a matrix whose order depends only on the number of connecting coordinates.

For the other most extreme situation when the rigidities are localised in both interface regions, other alternatives are required. For instance, if it is possible to know a priori the number of redundant coordinates - or, in other words, the rank for each subsystem FRF at each frequency in the range of interest - the analyst can make a judgement about the possible exclusion of some of the connection coordinates without affecting the constraint formulation of the actual physical connection. This topic will be discussed further in chapter 5.

4 MODAL COUPLING TECHNIQUES

4.1 INTRODUCTION

In chapter 2 a review of the different standard coupling techniques was presented. Among these there is one which makes use of the Modal models and which takes advantage of a **reduction of the number of modes** or modal coordinates (generally, the higher natural frequency modes), while still accounting for all the physical DoF in each subsystem model before a coupling process is performed. It is interesting to note that this approach to the coupling problem relies on a different philosophy for reducing the subsystem order when compared with the Impedance coupling approach which is based instead on a **reduction of the number of coordinates.**

It has been stated in some survey papers [35-39] that using the free-interface methods like Hou's [34] and Goldman's [33] procedures, very poor accuracy may be obtained for the overall system natural frequencies and mode shapes as compared with that attained by the fixed-interface methods. However, it has since been recognised that the free-interface methods could take advantage of using the directly available data from substructure tests as an input into the coupling process, and this has led to an improvement in the existing methods by developing a great variety of approaches. Some of the improved methods were primarily based on a purely analytical description and determination of the component characteristics [40-44], in other words they are quite adequate if one chooses the theoretical route, while others tried to explore the use of experimentally-derived modal properties as a basis for the formulation of each subsystem's equations of motion. In this

latter approach, one important early work is Klosterman's thesis [45] which provides a comprehensive study of the experimental determination of modal representations of components including the use of these models in the substructure coupling.

The structural definition of components from modal tests has been accomplished and successfully used for design purposes with relatively stiff structures connected with flexible elements such as an automobile frame and body connected by isolation mounts [10,461. For this situation, the subsystems can be tested with free boundaries to obtain a free-free modal data base which is sufficient for use in system synthesis. However, in the case where the components are rigidly connected, the use of a set of truncated modes to establish the compatibility equations sometimes leads to unacceptable errors in the prediction of the assembled system responses. Thus, for rigidly connected subsystems a more accurate definition is necessary either by including more modes or, if these represent an unreasonable number, by providing some information about the effects of the neglected modes. Two possible ways may be used to improve the structural definition of each component; one, by using additional masses attached to the connection points in an attempt to generate a more realistic condition for the component when it is vibrating together with the remaining parts (the localised flexibility properties near the connection area are better represented, since more modes are brought to the frequency range of interest) or two, by seeking to compensate for the lack of flexibility due to the truncation of the set of natural modes by using additional and important information concerning the flexibility effects of the out-of-range modes.

In this chapter, interest is confined to the latter approach whereby a refined method developed by the author [66,67] permits the inclusion of the residual flexibility effects of the neglected or unmeasured modes. This refined approach is presented and compared next with another similar alternative developed by Martinez *et al* [49].

4.2 FREE-INTERFACE METHODS WITH RESIDUAL FLEXIBILITY EFFECT

4.2.1 PREAMBLE

Early work reporting the use of free-interface methods was presented by MacNeal [40] and Rubin [44] in order to improve the truncated free-free modal representation of a component by including estimates of the residual effects due to the modes higher in frequency than the frequency range of interest. In a theoretical standpoint, the residual effects are generally obtained by calculating the component flexibility due to those modes to be retained and then subtracting this from the total known flexibility of the respective component as presented by Craig [68] and Hansteen [69]. All these works provided a significant improvement to the classical free-interface method presented in chapter 2, although using purely analytical representation of component properties.

The free-interface method constitutes the most suitable approach for incorporating experimentally-derived Modal models. Consequently, the author has directed his work based on a free-interface methodology by developing a refined approach which can include the residual flexibility effects of the unmeasured modes. This method is presented next and compared with another one developed by Martinez et *al* [49].

4.2.2 A REFINED APPROACH

Returning to the classical free-interface method (Hou's approach [10]) presented in chapter 2, our attention is now focussed on the thus-presented equation (2.34), which is here re-written as,

$$\{u\} \approx \left[\Phi_k\right] \{p_k\} \qquad (4.1)$$

Equation (4.1) expresses an approximation for the representation of each coordinate displacement in a component whose equation of motion is expressed as,

$$\begin{bmatrix} M_{ii} & : & M_{ic} \\ \cdots & : & \cdots \\ M_{ci} & : & M_{cc} \end{bmatrix} \begin{Bmatrix} \ddot{u}_i \\ \cdots \\ \ddot{u}_c \end{Bmatrix} + \begin{bmatrix} K_{ii} & : & K_{ic} \\ \cdots & : & \cdots \\ K_{ci} & : & K_{cc} \end{bmatrix} \begin{Bmatrix} u_i \\ \cdots \\ u_c \end{Bmatrix} = \begin{Bmatrix} 0 \\ \cdots \\ f_c \end{Bmatrix} \qquad (4.2)$$

This simplification is made in order to reduce the order of the final matrix equation. However, this reduction results in a change of the description of each component stiffness characteristics, since in doing so we are assuming that each component is too stiff. In fact, there is a residual flexibility effect that is not taken into account. The exact description of the displacements is expressed as:

$$\{u\} = \left[\Phi_m\right] \{p_m\} \qquad (4.3)$$

where m is the total number of existing modes. These modes can be separated into two groups; the kept or measured modes $\left[\Phi_k\right]$ and the eliminated or unmeasured modes $\left[\Phi_e\right]$, as represented in the partitioned form:

$$\{u\} = \left[\Phi_k\right]\{p_k\} + \left[\Phi_e\right]\{p_e\} = \left[\Phi_k : \Phi_e\right] \begin{Bmatrix} p_k \\ \cdots \\ p_e \end{Bmatrix} \qquad (4.4)$$

or

$$\begin{Bmatrix} u_i \\ \cdots \\ u_c \end{Bmatrix} = \begin{bmatrix} \Phi_{ik} & : & \Phi_{ie} \\ \cdots & : & \cdots \\ \Phi_{ck} & : & \Phi_{ce} \end{bmatrix} \begin{Bmatrix} p_k \\ \cdots \\ p_e \end{Bmatrix} \qquad (4.5)$$

Substituting this equation into (4.2) results in two uncoupled equations in terms of the principal coordinates (kept and eliminated modes) as follows,

$$[I]\left\{\ddot{p}_k\right\} + \left[\omega_{rk}^2\right]\{p_k\} = \left[\Phi_{ck}\right]^T \{f_c\} \qquad (4.6)$$

and

$$[I]\left\{\ddot{p}_e\right\} + \left[\omega_{re}^2\right]\{p_e\} = \left[\Phi_{ce}\right]^T \{f_c\} \qquad (4.7)$$

By assuming that the out-of-range natural frequencies are $\omega_{re}^2 >> \omega_r^2$, an approximation can be made for the response of those modes i.e., we can say that they respond in a quasi-static manner so that the inertial term can be ignored. Thus, equation (4.7) may be simplified and written as:

$$\left[\omega_{re}^2\right]\{p_e\} = \left[\Phi_{ce}\right]^T \{f_c\} \qquad (4.8)$$

By assuming at this stage that both components are still *disconnected, the* equilibrium equations are;

$$[I]\begin{Bmatrix} {}_A\ddot{p}_k \\ \cdots \\ {}_B\ddot{p}_k \end{Bmatrix} + \left[\begin{array}{c:c} {}_A\omega_{rk}^2 & 0 \\ \hdashline 0 & {}_B\omega_{rk}^2 \end{array}\right]\begin{Bmatrix} {}_Ap_k \\ \cdots \\ {}_Bp_k \end{Bmatrix} = \left[\begin{array}{c:c} {}_A\Phi_{ck}^T & 0 \\ \hdashline 0 & {}_B\Phi_{ck}^T \end{array}\right]\begin{Bmatrix} {}_Af_c \\ \cdots \\ {}_Bf_c \end{Bmatrix} \qquad (4.9)$$

and

$$\left[\begin{array}{c:c} {}_A\omega_{re}^2 & 0 \\ \hdashline 0 & {}_B\omega_{re}^2 \end{array}\right]\begin{Bmatrix} {}_Ap_e \\ \cdots \\ {}_Bp_e \end{Bmatrix} = \left[\begin{array}{c:c} {}_A\Phi_{ce}^T & 0 \\ \hdashline 0 & {}_B\Phi_{ce}^T \end{array}\right]\begin{Bmatrix} {}_Af_c \\ \cdots \\ {}_Bf_c \end{Bmatrix} \qquad (4.10)$$

The constraint equations for both subsystems undergoing free vibrations, are formulated by enforcing compatibility between displacements and equilibrium between forces in the connecting region as follows;

$$\{{}_Au_c\} = \{{}_Bu_c\} \qquad (4.11)$$

$$\{{}_Af_c\} = -\{{}_Bf_c\} = \{f_c\} \qquad (4.12)$$

or, according to the modal description, as:

$$\left[{}_A\Phi_{ck} : -{}_B\Phi_{ck}\right]\begin{Bmatrix} {}_Ap_k \\ \cdots \\ {}_Bp_k \end{Bmatrix} + \left[{}_A\Phi_{ce} : -{}_B\Phi_{ce}\right]\begin{Bmatrix} {}_Ap_e \\ \cdots \\ {}_Bp_e \end{Bmatrix} = \{0\} \qquad (4.13)$$

From equation (4.10) the values for the coordinates p_e can be extracted and substituted in equation (4.13) leading to,

$$\left[{}_A\Phi_{ck} : -{}_B\Phi_{ck} \right] \begin{Bmatrix} {}_A p_k \\ \cdots \\ {}_B p_k \end{Bmatrix} +$$

$$\left[{}_A\Phi_{ce} : -{}_B\Phi_{ce} \right] \begin{bmatrix} {}_A\omega^2_{re} & \vdots & 0 \\ \cdots & \vdots & \cdots \\ 0 & \vdots & {}_B\omega^2_{re} \end{bmatrix}^{-1} \begin{bmatrix} {}_A\Phi^T_{ce} \\ \cdots \\ -{}_B\Phi^T_{ce} \end{bmatrix} \{ f_c \} = \{ 0 \} \quad (4.14)$$

or, making $$\left[{}_A R_{cc} \right] = \left[{}_A\Phi_{ce} \right] \left[{}_A\omega^2_{re} \right]^{-1} \left[{}_A\Phi_{ce} \right]^T \quad (4.15)$$

and $$\left[{}_B R_{cc} \right] = \left[{}_B\Phi_{ce} \right] \left[{}_B\omega^2_{re} \right]^{-1} \left[{}_B\Phi_{ce} \right]^T \quad (4.16)$$

both of these expressing the approximation for the residual flexibility of the eliminated modes in component A and B respectively, the interconnecting force vector $\{ f_c \}$ can now be expressed as,

$$\{ f_c \} = -\left[R^*_{cc} \right]^{-1} \left[{}_A\Phi_{ck} : -{}_B\Phi_{ck} \right] \begin{Bmatrix} {}_A p_k \\ \cdots \\ {}_B p_k \end{Bmatrix} \quad (4.17)$$

where

$$\left[R^*_{cc} \right]^{-1} = \left[{}_A R_{cc} + {}_B R_{cc} \right]^{-1} \quad (4.18)$$

If equation (4.17) is substituted into (4.9), the final equation for the overall system is,

$$[I] \begin{Bmatrix} {}_A \ddot{p}_k \\ \cdots \\ {}_B \ddot{p}_k \end{Bmatrix} + \left[\begin{bmatrix} {}_A\omega^2_{rk} & \vdots & 0 \\ \cdots & \vdots & \cdots \\ 0 & \vdots & {}_B\omega^2_{rk} \end{bmatrix} + \right.$$

$$\left. \begin{bmatrix} {}_A\Phi^T_{ck} & \vdots & 0 \\ \cdots & \vdots & \cdots \\ 0 & \vdots & {}_B\Phi^T_{ck} \end{bmatrix} [K_{cpl}] \begin{bmatrix} {}_A\Phi_{ck} & \vdots & 0 \\ \cdots & \vdots & \cdots \\ 0 & \vdots & {}_B\Phi_{ck} \end{bmatrix} \right] \begin{Bmatrix} {}_A p_k \\ \cdots \\ {}_B p_k \end{Bmatrix} = \{ 0 \} \quad (4.19)$$

where the coupling matrix $[K_{cpl}]$ is formed from the residual flexibility properties of both components as follows;

$$[K_{cpl}] = \begin{bmatrix} [R_{cc}^*]^{-1} & -[R_{cc}^*]^{-1} \\ -[R_{cc}^*]^{-1} & [R_{cc}^*]^{-1} \end{bmatrix} \qquad (4.20)$$

It is interesting to note that this equation is identical to that presented in chapter 2 (eq. 2.58) for the case of two components coupled using a intermediate flexible system. This similarity may be explained as follows;

- the displacement in each connection coordinate is given as:

$$\{u_c\} = [\Phi_{ck}]\{p_k\} + [\Phi_e]\{p_e\}$$

or

$$\{u_c\} = [\Phi_{ck}]\{p_k\} + [R_{cc}]\{f_c\} = \{u_c'\} + \{\Delta u_c\} \qquad (4.21)$$

where $\{u_c'\}$ is the underestimated displacement in the boundary coordinates (component is to stiff) and $\{\Delta u_c\}$ is the displacement due to the "additional" spring located in the boundary region to compensate for the lack of flexibility (associated with the out-of-range modes). The compatibility of displacements between the two components A and B requires that:

$$\{{}_A u_c'\} + \{{}_A \Delta u_c\} = \{{}_B u_c'\} + \{{}_B \Delta u_c\} \qquad (4.22)$$

which expresses the connection between the two subsystems through and intermediate connecting flexible system, as visualised in figs. 4.1 and 4.2

Therefore, it is possible to use the same formulation given for the elastic coupling, provided the stiffness matrix for the intermediate spring-system is constructed as shown in equation (4.20).

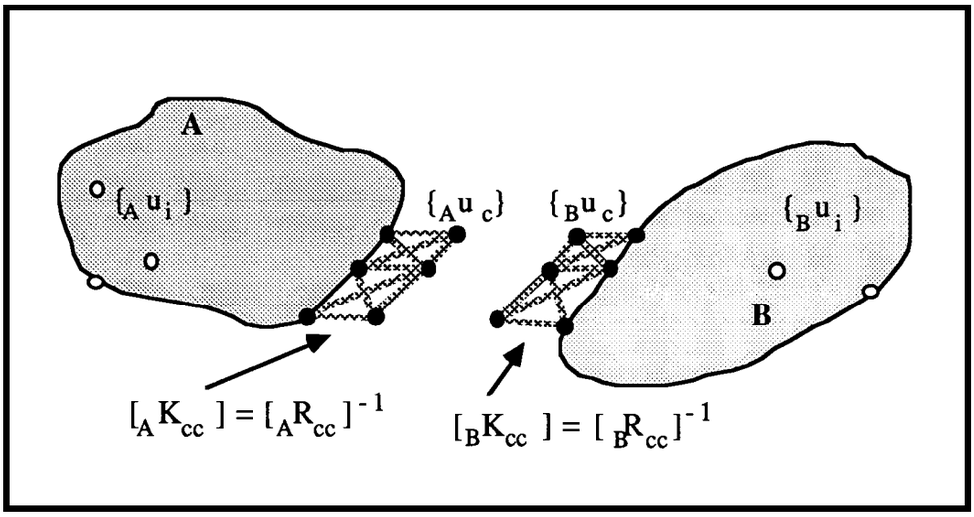

Fig. 4.1 - Auxiliary flexible systems used to represent the flexibility contribuition of the out-of-range eliminated modes in each separated component

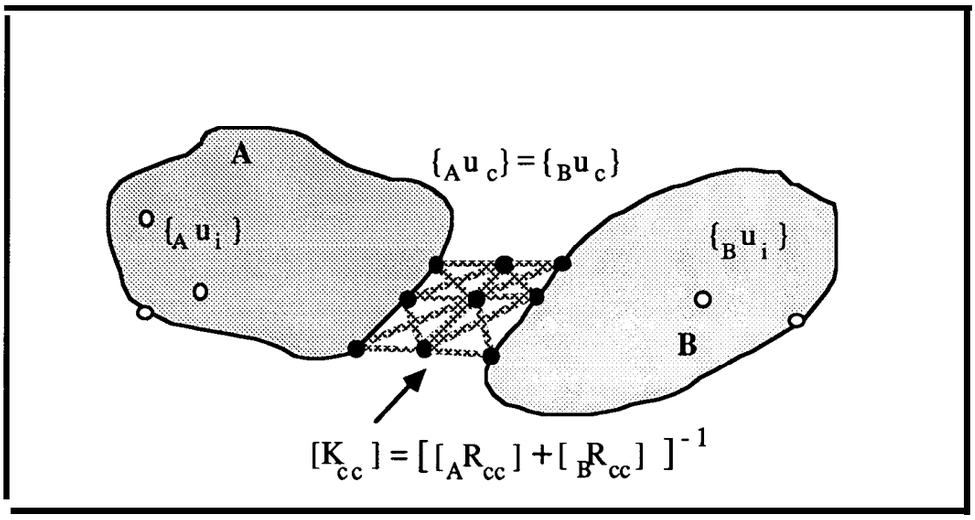

Fig. 4.2 - Two auxiliary flexible systems are connected in series to form the "dummy" interconnecting system.

4.2.3 COMPARISON WITH A PREVIOUS APPROACH

An alternative approach developed by Martinez et *al* [49], and which also takes into account the residual flexibility effect of the out-of-range modes, is now briefly presented. In this case the subsystem displacements are represented as,

$$\{u\} = \left[\Phi_k\right]\{p_k\} + \left[R_c\right]\{p_c\} = \left[\Phi_k : R_c\right]\begin{Bmatrix} p_k \\ \cdots \\ p_c \end{Bmatrix} \tag{4.23}$$

where $[R_c]$ is an appropriate partition of the (theoretical) residual flexibility matrix $[R]$ as shown below,

$$[R] = \left[\begin{array}{c:c} R_{ii} & R_{ci} \\ \hdashline R_{ic} & R_{cc} \end{array}\right] = \left[R_i : R_c\right] \tag{4.24}$$

$$[R_c] = \begin{bmatrix} R_{ic} \\ \cdots \\ R_{cc} \end{bmatrix} \tag{4.25}$$

Substituting equation (4.23) into the general equation of motion (4.2), the following equation is obtained,

$$[M_p]\begin{Bmatrix} \ddot{p} \end{Bmatrix} + [K_p]\{p\} = \{f_p\} \tag{4.26}$$

where

$$[M_p] = \left[\begin{array}{c:c} I_{kk} & 0 \\ \hdashline 0 & H_{cc} \end{array}\right] \tag{4.27}$$

$$[K_p] = \left[\begin{array}{c:c} \omega_{rk}^2 & 0 \\ \hdashline 0 & R_{cc} \end{array}\right] \tag{4.28}$$

$$[f_p] = \begin{bmatrix} \Phi_{ck}^T \\ \cdots \\ R_{cc}^T \end{bmatrix}[f_c] \tag{4.29}$$

$$\text{with } [H_{cc}] = [R_c]^T [M] [R_c] \qquad (4.30)$$

In order to permit a simple and direct matrix assembly for the subsystem matrices it is convenient to obtain an alternative formulation for the component equations. From equation (4.23) we have,

$$\{p_c\} = [R_{cc}]^{-1} \left\{ \{u_c\} - [\Phi_{ck}] \{p_k\} \right\} \qquad (4.31)$$

or, assuming a transformation of coordinates such as,

$$\begin{Bmatrix} p_k \\ \cdots \\ p_c \end{Bmatrix} = \left[\begin{array}{c:c} I_{kk} & 0 \\ \hdashline -[R_{cc}]^{-1}[\Phi_{ck}] & [R_{cc}]^{-1} \end{array}\right] \begin{Bmatrix} p_k \\ \cdots \\ u_c \end{Bmatrix} \qquad (4.32)$$

$$\begin{Bmatrix} p_k \\ - \\ p_c \end{Bmatrix} = [T] \{\zeta\}$$

The new subsystem equation will be

$$[M_\zeta] \{\ddot{\zeta}\} + [K_\zeta] \{\zeta\} = \{f_\zeta\} \qquad (4.33)$$

with

$$[M_\zeta] = \left[\begin{array}{c:c} I_{kk} + \Phi_{ck}^T J_{cc} \Phi_{ck} & -\Phi_{ck}^T J_{cc} \\ \hdashline -J_{cc} \Phi_{ck} & J_{cc} \end{array}\right] \qquad (4.34)$$

$$[K_\zeta] = \left[\begin{array}{c:c} \omega_{rk}^2 + \Phi_{ck}^T R_{cc}^{-1} \Phi_{ck} & -\Phi_{ck}^T R_{cc}^{-1} \\ \hdashline -R_{cc}^{-1} \Phi_{ck} & -R_{cc}^{-1} \end{array}\right] \qquad (4.35)$$

$$\text{with } [J_{cc}] = [T^*]^T [H_{cc}] [T^*] \text{ where } [T^*] = [R_c] [R_{cc}]^{-1}$$

As noted by Craig and Chang [47] and by Martinez and Gregory [50] the MacNeal's approach [40] leads to a different generalised mass matrix which is,

$$[M_\zeta] = \begin{bmatrix} I_{kk} & \vdots & \\ \cdots & \cdots & \\ 0 & \vdots & 1 \end{bmatrix} \qquad (4.36)$$

From an experimental standpoint this matrix is more realistic, since the matrix presented in (4.34) requires the calculation of $[J_{cc}]$ and this is only possible by knowing the component mass matrix. Then, assuming that the data are entirely obtained from test, the final equation for the coupled structure is obtained by a **direct assembly** procedure:

$$\begin{bmatrix} {}_AI_{kk} & 0 & 0 \\ \cdots & \cdots & \cdots \\ 0 & {}_BI_{kk} & 0 \\ \cdots & \cdots & \cdots \\ 0 & 0 & 0 \end{bmatrix} \begin{Bmatrix} {}_A\ddot{p}_k \\ \cdots \\ {}_B\ddot{p}_k \\ \cdots \\ \ddot{u}_c \end{Bmatrix} +$$

$$\left[\begin{array}{ccc} {}_A\omega_{rk}^2 + {}_A\Phi_{ck}^T\, {}_AR_{cc}^{-1}\, {}_A\Phi_{ck} & 0 & -{}_A\Phi_{ck}^T\, {}_AR_{cc}^{-1} \\ \cdots & \cdots & \cdots \\ 0 & {}_B\omega_{rk}^2 + {}_B\Phi_{ck}^T\, {}_BR_{cc}^{-1}\, {}_B\Phi_{ck} & -{}_B\Phi_{ck}^T\, {}_BR_{cc}^{-1} \\ \cdots & \cdots & \cdots \\ -{}_A\Phi_{ck}^T\, {}_AR_{cc}^{-1} & -{}_B\Phi_{ck}^T\, {}_BR_{cc}^{-1} & {}_AR_{cc}^{-1} + {}_BR_{cc}^{-1} \end{array}\right] \begin{Bmatrix} {}_Ap_k \\ \cdots \\ {}_Bp_k \\ \cdots \\ u_c \end{Bmatrix} = \{0\}$$

(4.37)

Discussion of both approaches

In physical terms, Martinez et *al* [49] approach should give the same results as the previously presented author's approach, since the residual flexibility effects are taken into account. Although Craig [52] has shown that the residual flexibility and fixed-interface

method are equivalent, Klahs and Townley [53] concluded that "problems may arise in the use of residual flexibility; the residual flexibility matrix for each component must be invertible and the associated mass matrix i.e., the final mass matrix coefficients related to the boundary points may be singular". In fact, the requirement of the residual flexibility matrix of each subsystem to be invertible is a drawback of Martinez *et al* [49] approach when compared to the author's refined one since this require instead the inversion of the summation of both residual flexibility matrices which is less susceptible to be singular. For instance, should a residual flexibility matrix of a component be calculated using more connecting coordinates than eliminated modes, it will become rank-deficient. Thus, the corresponding inverse is impossible to calculate, although in physical terms it exists.

Moreover, the order of the final assembled equation of motion in Martinez et *al* [49] approach is dependent on the number of connection coordinates, which in the refined one are implicitly defined in the final equation of motion, therefore requiring a less time-consuming eigensolution, especially in multi-point connected structures where the number of connection coordinates may be much greater than the number of kept modes; in this case, the main gain achieved with the reduction in terms of modes - which is the underlying philosophy of Modal coupling techniques - is lost due to the necessary inclusion of the interface coordinate displacements in the final equation of motion.

4.3 COMPUTER PROGRAM

A computer program has been written to implement the method detailed in section 4.22. The component models can be either experimentally- or theoretically-derived and the coupling procedure is performed each time for two components. The main structure of the computer program is presented in figures 4.3 to 4.5. Preceding the coupling stage, and depending on the type of modelling used for each component, there is a pre-processing stage whereby the data is prepared so as to obtain a formatted modal model which is then supplied to the coupling program. Thus, if the theoretical route is of interest, the main steps to obtain the formatted modal model are shown in fig. 4.3. On the other hand, the

alternative experimental route may be chosen for the subsystem modelling, and in this case, the important steps are shown in fig. 4.4. Whichever route is used, the derived modal model data related to the in- and out-of-range modes are stored in a suitable format for subsequent use in the modal coupling process, as described in fig. 4.5.

Associated with this program, there are some extra subroutines for the necessary manipulation and plotting of data. The type of properties used to describe the model can be transformed according to different available options namely, Spatial → Modal (Eigensolution), Spatial → Response, Modal → Spatial and Modal → Response. In order to process data before the modal model is input into the coupling program, there is an additional subroutine to read standard Modal models resulting either from modal testing or an eigensolution. An option is available to read a partition of the corresponding modal matrix containing only the selected connection coordinates and kept modes and subsequently storing the model with a new format containing the information relative to the selected in-range and out-of-range modes and the interior and connection coordinates.

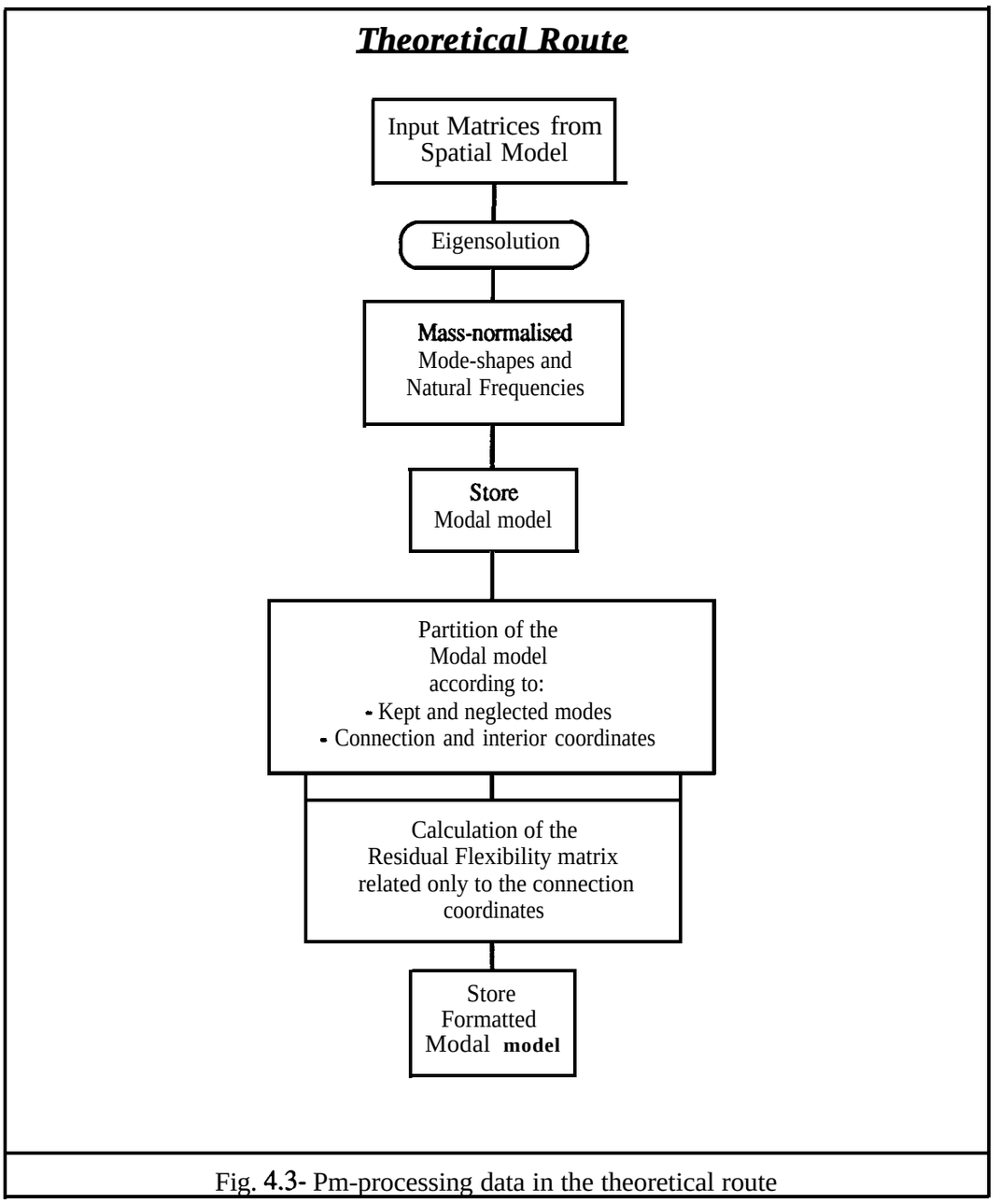

Fig. 4.3- Pm-processing data in the theoretical route

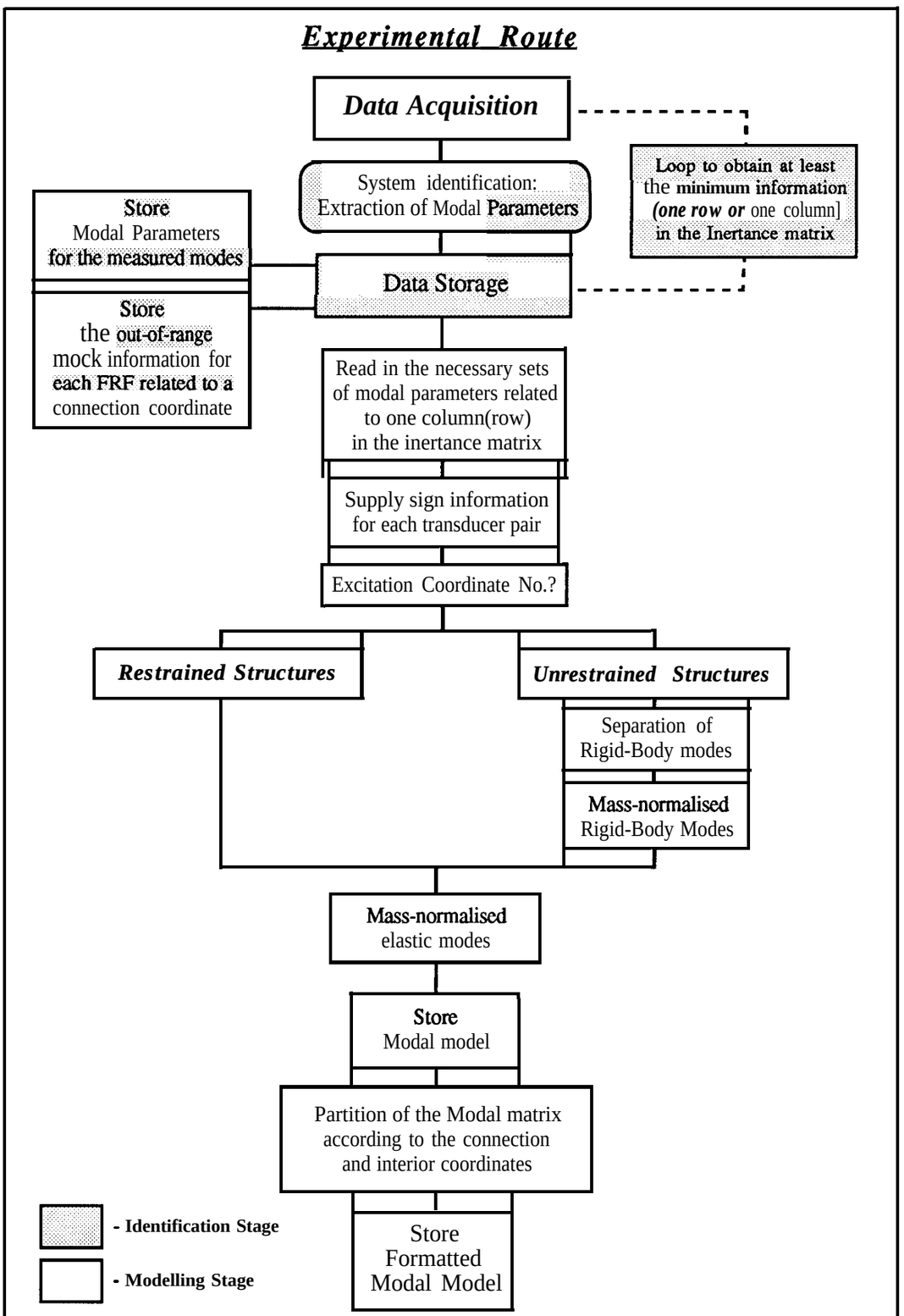

Fig. 4.4 - Pre-processing data in the experimental route

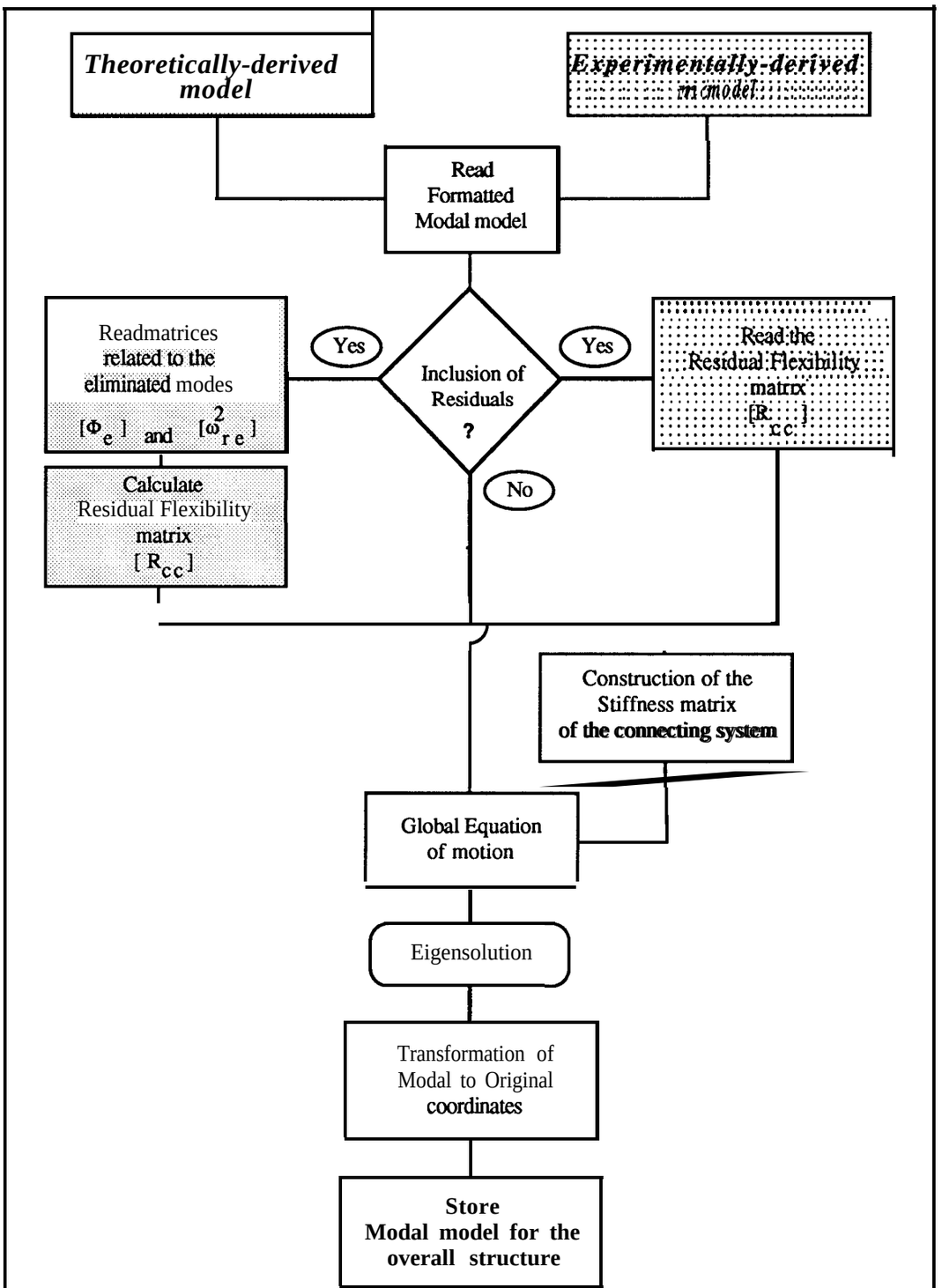

Fig. 4.5 - Structure of the Modal coupling program

The main program was written for the simple case of the coupling of two substructures. However, it can be used to predict the response of a more general structure formed of several components, providing they are connected as presented in fig. 4.6.

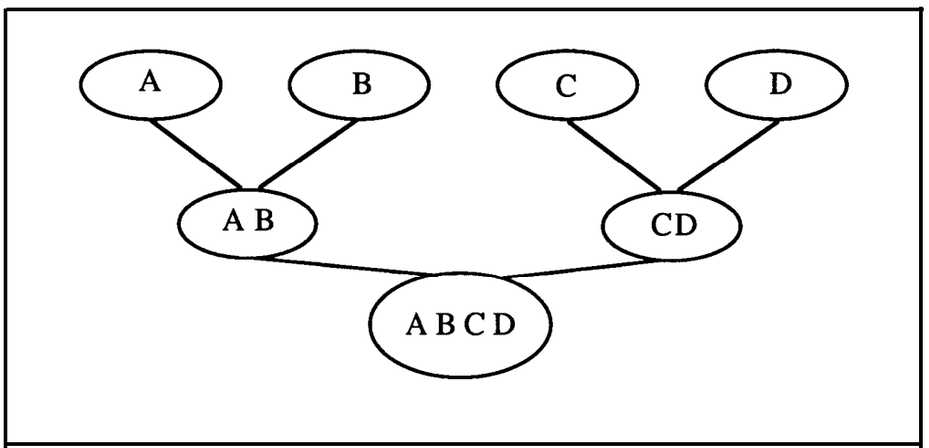

Fig. 4.6 - Assembling of global system ABCD

The different database containing the information for each component's formatted modal model should be created and linked according to the possibility of a subsequent structural modification. For instance, if it is anticipated that component D may be subjected to further modifications after the coupling stage, then it is suggested that the various components be connected in the sequence shown in fig. 4.7, leading to a less time-consuming reanalysis procedure each time the dynamic characteristics of component D are changed.

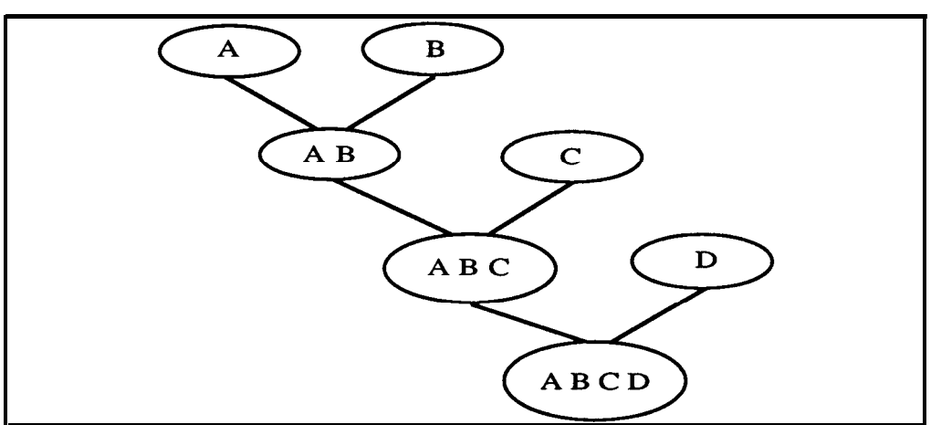

Fig. 4.7 - Assembling global system ABCD (anticipating a modification in component D)

4.4 THEORETICAL CASE STUDY

This case was used to check the working of the Modal Coupling computer program, since it is possible to compare the predicted response with the exact response of the coupled structure. Although in this example only theoretical data are available, it was assumed that one of the subsystem residual flexibility matrices was obtained by following the steps that would be employed in an experimental study. The two subsystems consist of a straight beam (A) and a rigid block (B), the Spatial models of which constitute the initial available data. An eigensolution routine is used to derive both the complete substructure Modal models. However, one of the components - the beam - is assumed to possess different degrees of incompleteness in the number of modes used to describe its properties. The effects of this incompleteness on the predicted dynamic properties of the coupled structure are investigated using both the Modal coupling techniques - the classical free-interface method and the refined approach which includes the residual flexibility effects of the neglected modes.

4.4.1 DESCRIPTION OF COMPONENT A - FREE-FREE BEAM

Component A is a rectangular cross-section straight beam modelled by eight undamped Timoshenko beam elements. The Spatial and Modal models for this component were obtained by using the general-purpose computer program for the vibration analysis of complex structures, COUPLE [70], and only one in-plane flexural response was considered i.e., each node is supposed to have only one translational and one rotational degree of freedom.The connection coordinates are selected as the tip DoF numbers 1 and 2, being the interior coordinates formed of half of the remaining ones - number 3 to 10. All the selected coordinates and the characteristics of the beam are shown in fig. 4.8.

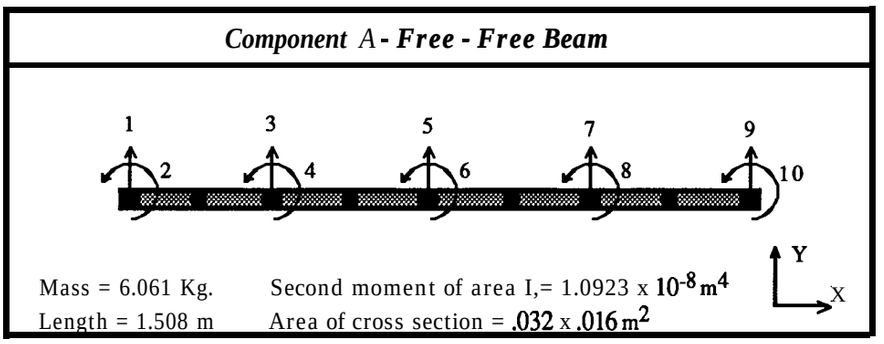

Fig. 4.8 - Beam theoretical model (8 beam elements)

The mass-normalised modal matrix and the corresponding eigenvalues, together forming the **complete Modal model of the beam, are** presented next:

-.244	.786	-.817	-.818	-.820	-.824	.830	-.832	-.765	-.781
.674	-.653	2.518	4.259	5.972	7.724	-9.544	11.397	12.186	15.199
.030	.540	.081	.478	.510	.211	.236	-.566	-.556	-.207
.674	-.653	2.015	1.456	-1.423	-4.917	6.099	-2.836	3.503	12.144
.284	.293	.497	0.000	-.584	0.000	-.592	0.000	-.619	0.000
.674	-.653	0.000	-2.924	0.000	5.450	0.000	-7.856	0.000	13.608
.539	.047	.081	-.478	.510	-.211	.236	.566	-.556	.207
.674	-.653	-2.015	1.456	1.423	-4.917	-6.099	-2.836	-3.503	12.144
.793	-.199	-.817	.818	-.820	.824	.830	.832	-.765	.781
.674	-.653	-2.518	4.259	-5.972	7.724	9.544	11.397	-12.186	15.199

Eigenvalues	Natural Frequencies (Hz)
1.92E-08	0.00
5.59E-08	0.00
5.51E+04	37.35
4.18E+05	102.93
1.61E+06	201.91
4.42E+06	334.45
9.93E+06	501.62
1.96E+07	704.09
3.43E+07	931.80
6.78E+07	1310.41

The frequency range encompassing **all the** natural frequencies is assumed to be:

0 -1500 Hz **10** modes included - (all the available modes)

In order to study the effects of incompleteness in the number of modes in this component, various alternative frequency ranges of interest were selected as:

0 - 600 Hz 7 modes included - (2 rigid-body + first 5 elastic modes)

0 - 250 Hz 5 modes included - (2 rigid-body + **first** 3 elastic modes)

0 - 50 Hz 3 modes included - (2 rigid-body + first elastic mode)

Since different sets of truncated modes are assumed, the residual flexibility matrix related to the effect of the neglected modes - in this case referred only to the connection coordinates - must be calculated afresh for each case. This can be done in two ways, using either the theoretical or the experimental route, as presented in Appendix II, both having been used in the present work.

The different conditions of assumed incompleteness of the component A are summarised in the following table 4.1:

Table 4.1 - Incompleteness of component A

Component A : Free-free Beam

Case	Modalmodel	**No.** kent modes	Residual
1	Complete	10	
2A	Incomplete	7	No
2B	Incomplete	**7**	**Theoret.** Complete [R_{cc}]
3A	Incomplete	5	No
3B	Incomplete	**5**	**Theoret. Complete** [R_{cc}]
3c	Incomplete	5	**Theoret.** Diagonal [R_{cc}]
3D	Incomplete	**5**	Experim. Complete [R_{cc}]
3E	Incomplete	5	Experirn. Diagonal [R_{cc}]
4A	Incomplete	3	No
4B	Incomplete	3	**Theoret.** Complete [R_{cc}]

In cases 2B and **4B,** the residual flexibility matrix $[R_{cc}]$ referred to the connecting coordinates is calculated following the **theoretical route.**

Case 2B - Frequency range 0 - 600 Hz (7 kept modes)

$$[R_{cc}] = \begin{bmatrix} 6.148\ E\text{-}g & -9.318\ E\text{-}7 \\ -9.318\ E\text{-}7 & 1.437\ E\text{-}5 \end{bmatrix} \Rightarrow [K_{cc}] = [R_{cc}]^{-1} = \begin{bmatrix} 9.274\ E8 & 6.011\ E7 \\ 6.011\ E7 & 3.966\ E6 \end{bmatrix}$$

Case 4B - Freauency range 0 - 50 Hz (3 kept modes)

$$[R_{cc}] = \begin{bmatrix} 2.302\ E\text{-}6 & -1.454\ E\text{-}5 \\ -1.454\ E\text{-}5 & 1.026\ E\text{-}4 \end{bmatrix} \Rightarrow [K_{cc}] = [R_{cc}]^{-1} = \begin{bmatrix} 4.164\ E8 & 5.895\ E5 \\ 5.895\ E5 & 9.342\ E4 \end{bmatrix}$$

In case 3, both of the possible routes have been tried. In order to create a simulated experimental route, the response model of the beam was calculated, the FRFs (Inertance) referred to connection coordinates (1,2) being presented in fig. 4.9 a) to 4.9 c).

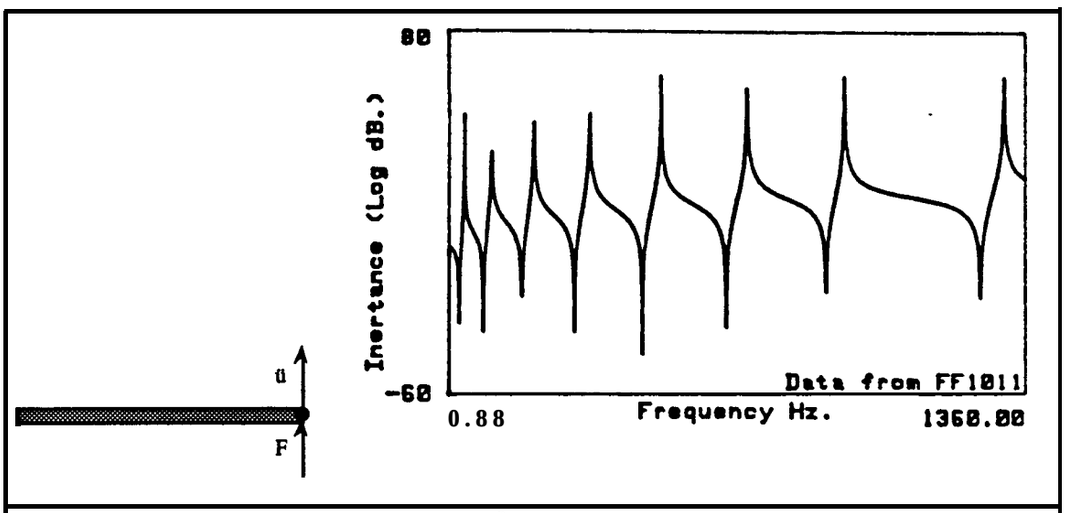

Fig. 4.9 a) - Generated $\frac{\ddot{u}}{F}$ FRF at one one end of the Beam

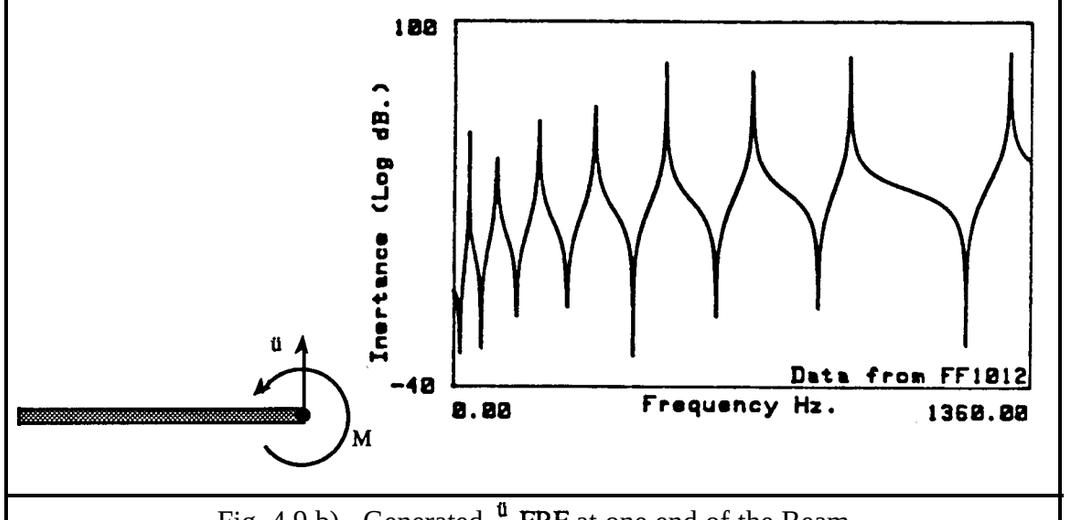

Fig. 4.9 b) - Generated $\frac{\ddot{u}}{M}$ FRF at one end of the Beam

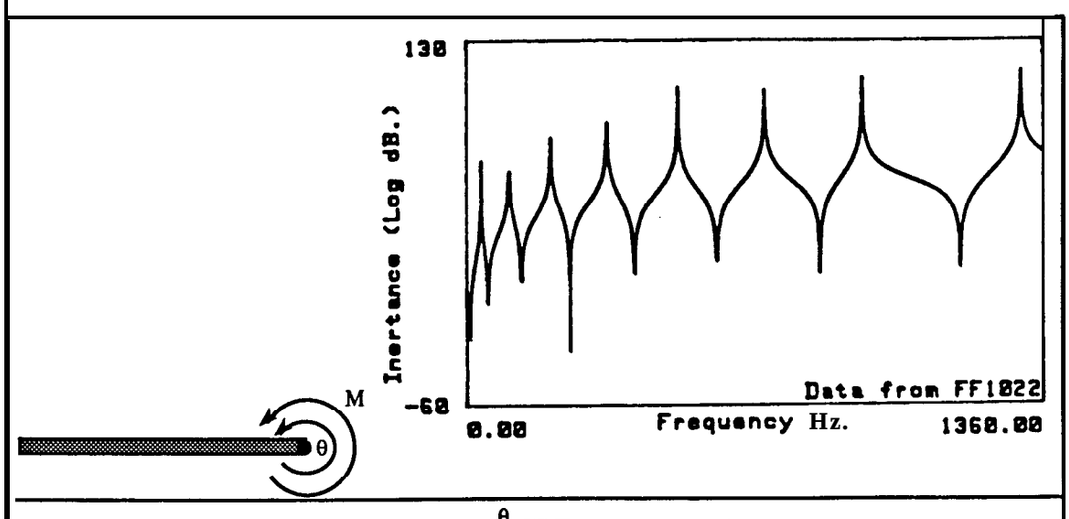

Fig. 4.9 c) - Generated $\frac{\theta}{M}$ FRF at one end of the Beam

In the particular frequency range selected, O-250 Hz, the three curves were analysed by using an appropriate modal analysis program AUTOIDENT [71], which employs a MDOF identification routine applicable for lightly damped structures. For each of the FRF curves, two sets of modal parameters were extracted; the first group containing information on the in-range modes and the second group referring to one or more fictitious modes which are used to determine the residual flexibility matrix which represents the effect of the out-of-range modes. Cases 3B to 3E differ from each other in the kind of stiffness properties derived for the interconnecting system; they are theoretically- or "experimentally''-derived and for each, two types of stiffness matrix were assumed; for one, the connecting matrices were diagonal and constructed only with the connection point direct response residuals while for the other the full connecting matrix was constructed with all the possible response residuals associated with the connection DoF;

Case 3B - Frequency range 0 - 250 Hz (5 kept modes)

$$[R_{cc}] = \begin{bmatrix} 2.845\ E\text{-}7 & -3.172\ E6 \\ -3.172\ E6 & 3.706\ E\text{-}5 \end{bmatrix} \Rightarrow [K_{cc}] = [R_{cc}]^{-1} = \begin{bmatrix} 7.521\ E7 & \\ 6.434\ E6 & 6.434\ E5 \end{bmatrix}$$

Case 3C - Frequency range 0 - 250 Hz (5 kept modes)

$$[R_{cc}] = \begin{bmatrix} 2.845\ E\text{-}7 & 0 \\ 0 & 3.706\ E\text{-}5 \end{bmatrix} \Rightarrow [K_{cc}] = [R_{cc}]^{-1} = \begin{bmatrix} 3.514\ E6 & 0 \\ 0 & 2.698\ E4 \end{bmatrix}$$

In the following cases, 3D and 3E, the residual flexibility matrices are derived using an experimental route. The identified extra modes are,

FRF i,j	Frequency (Hz)	Modal Constant
1,1	450	2.91
1,2	500	-37.93
2,2	500	404.30

and the matrices containing the approximated residual flexibility values are:

Case 3D - Freouency range *0 - 2.50* Hz (5 kept modes)

$$[R_{cc}] = \begin{bmatrix} 3.640\ E\text{-}7 & -3.843\ E\text{-}6 \\ -3.843\ E\text{-}6 & 4.096\ E\text{-}5 \end{bmatrix} \Rightarrow [K_{cc}] = [R_{cc}]^{-1} = \begin{bmatrix} 2.891\ E8 & 2.713\ E7 \\ 2.713\ E7 & 2.569\ E6 \end{bmatrix}$$

Case 3E - Freouency range *0 - 250* Hz (5 kept modes)

$$[R_{cc}] = \begin{bmatrix} 3.640\ E\text{-}7 & 0 \\ 0 & 4.096\ E\text{-}5 \end{bmatrix} \Rightarrow [K_{cc}] = [R_{cc}]^{-1} = \begin{bmatrix} 2.747\ E6 & 0 \\ 0 & 2.441\ E4 \end{bmatrix}$$

4.4.2 DESCRIPTION OF COMPONENT B - RIGID BLOCK

Component B is a rigid block with known mass properties. This component is used to apply a structural modification to the beam, thereby seeking to attain a nearly-clamped condition at one of its ends. The inertia properties of the block are referred to just one plane (Oxy) as shown in fig. 4.10,

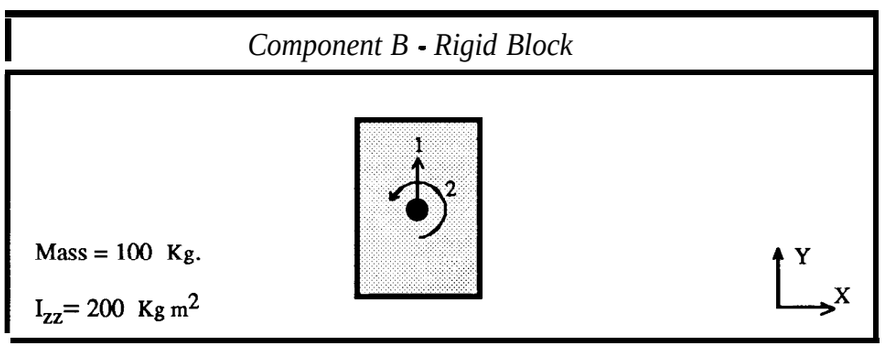

Fig. 4.10 - Rigid block

The Modal model is:

$$[\Phi] = \begin{bmatrix} 0 & 0.1 \\ 0.0707 & 0 \end{bmatrix} \text{ and } \begin{bmatrix} \omega_r^2 \end{bmatrix} = \begin{bmatrix} 0 & 0 \\ 0 & 0 \end{bmatrix}$$

4.4.3 RESULTS

Both substructures were then coupled as shown in fig. 4.11,

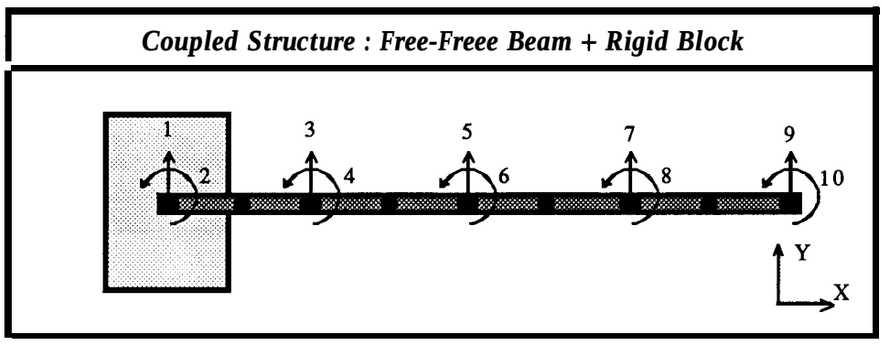

Fig. 4.11 - Free-free beam + Rigid block

The coupling between two components was performed by each of the two different approaches, the beam being assumed to be the only incomplete subsystem. The refined approach which takes into account the residual flexibility effect of the out-of-range modes (vidé section 4.2.2) was applied to the various cases previously described in table 4.1.

The predicted natural frequencies are shown in Table 4.2 for all the cases.

Table 4.2 - **Natural Frequencies of the Coupled Structure**

Case	R.Body		Elastic Modes							
1	0	0	6.6245	40.76	114.09	224.49	373.93	565.74	805.69	1122.
2A	0.	0.	6.94	42.98	121.12	240.68	408.33	---	__	___
2B	0.	0.	6.6245	40.77	114.2	225.34	379.16	642.75	6244.7	----
3A	0.	0.	7.51	47.26	136.8	--	--	---	---	-----
3B	0.	0.	6.6246	40.79	114.8	233.87	1541.1	---	---	-----
3C	0.	0.	6.497	37.75	99.29	184.93	536.73	---	---	-----
3D	0.	0.	6.56	40.6	114.84	235.42	2894.1	---	---	-----
3E	0.	0.	6.41	37.11	97.33	181.65	483.25	---	---	-----
4A	0.	0.	9.8	_	_	_	_	__	__	___
4B	0.	0.	6.628	41.28	278.07	--	--	---	__	-----

The relative errors of the predicted natural frequencies are shown in graph of fig 4.12:

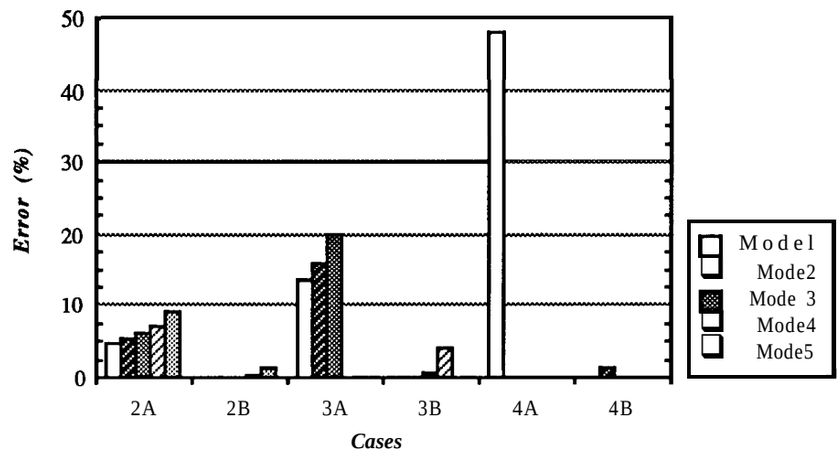

Fig. 4.12 - Natural frequency error (%) relative to the complete system

The predicted FRFs for the various cases of the coupled system are then compared with the corresponding exact response calculated for the whole structure. Plots of the Inertance calculated at the free end of the coupled structure i.e., using the translational (9) and rotational coordinates (10), are shown in the graphs of figures 4.13 to 4.17.

The first three groups of FRFs shown in figures - 4.13, 4.14 and 4.15 - illustrate the difference between the two approaches used to predict the dynamic response of the whole structure when truncated sets of 7, 5 and 3 modes respectively are used to describe the beam connecting displacements in the coupling process. The next two groups of plots represented in figures 4.16 and 4.17, show that the way the residual flexibility matrix is calculated - theoretically or experimentally-simulated - does not have a significant influence on the predicted response.

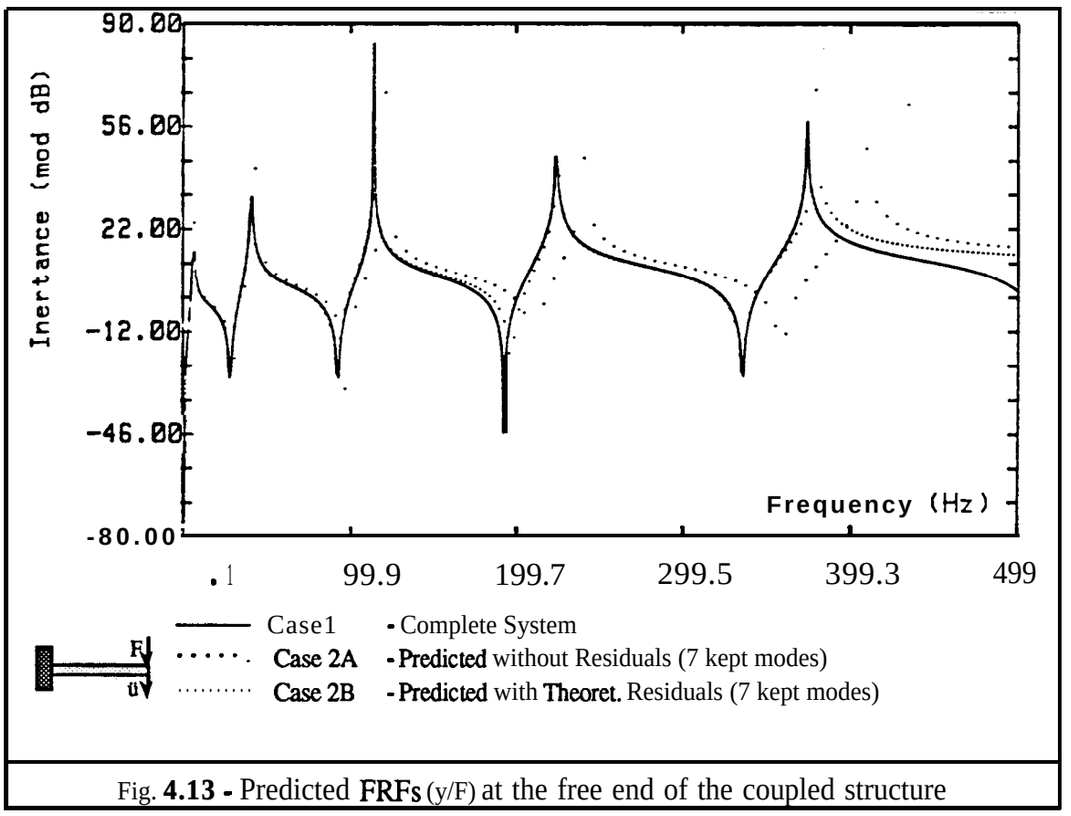

Fig. **4.13** - Predicted FRFs (y/F) at the free end of the coupled structure

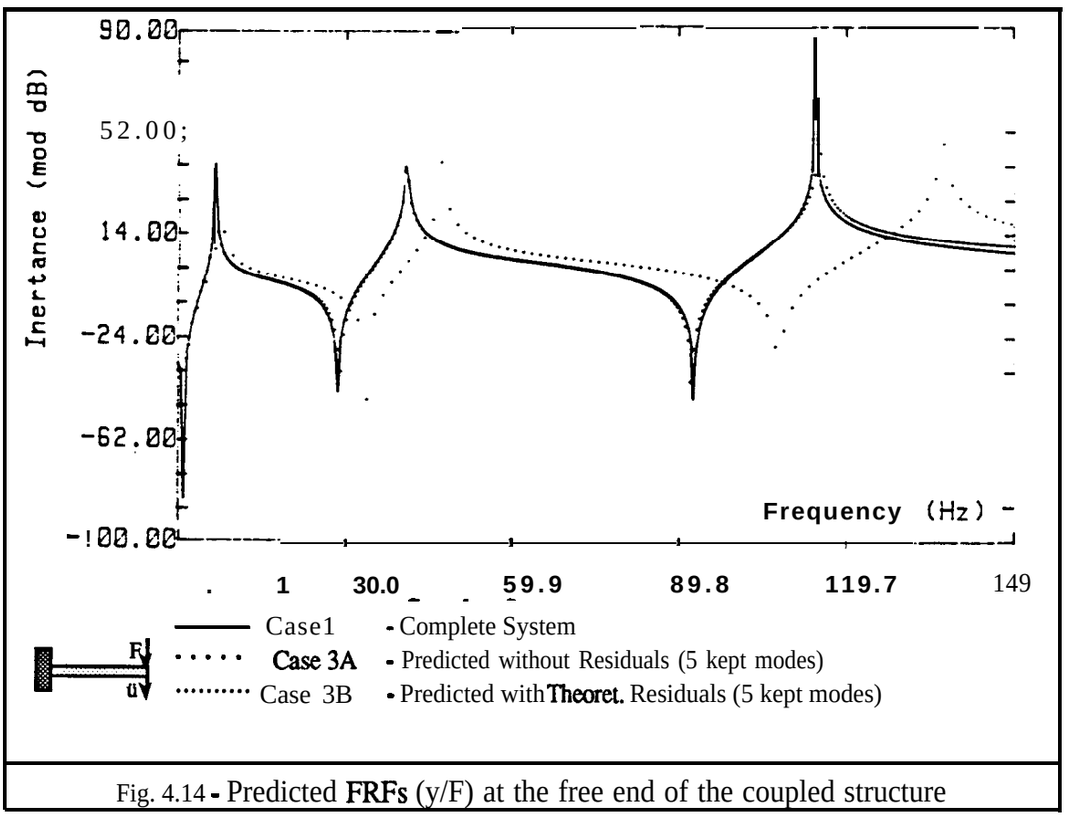

Fig. 4.14 - Predicted FRFs (y/F) at the free end of the coupled structure

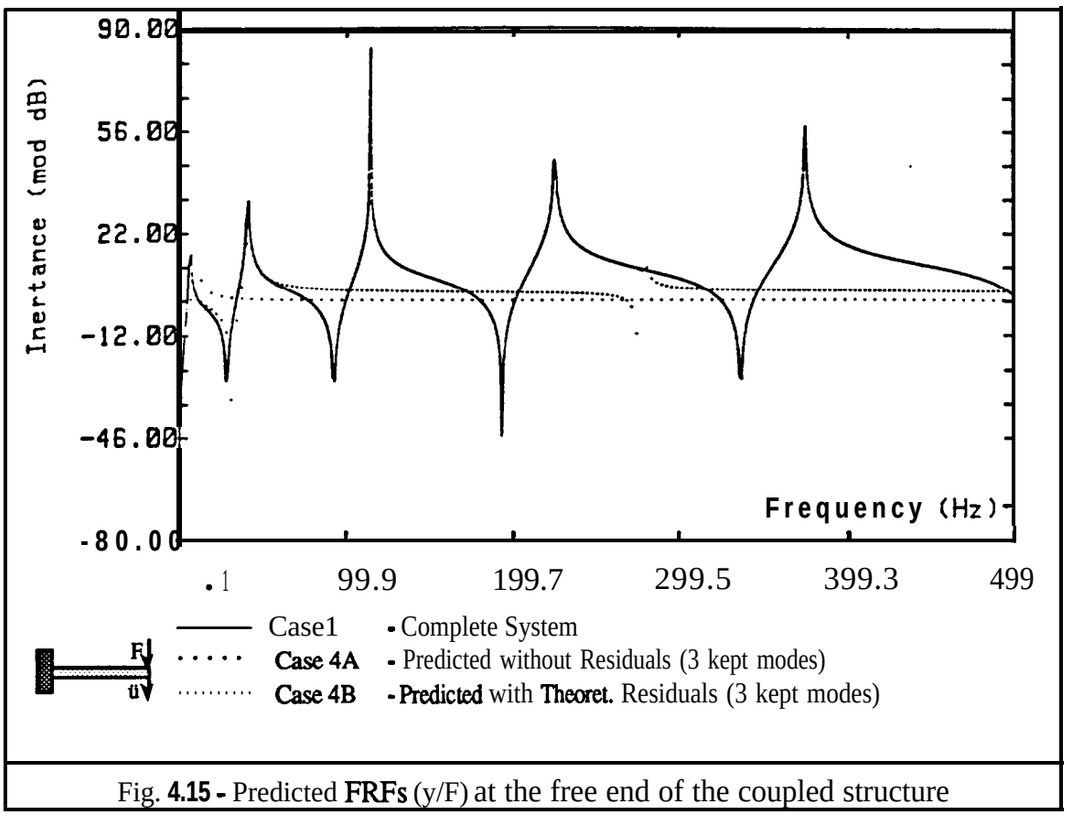

Fig. 4.15 - Predicted FRFs (y/F) at the free end of the coupled structure

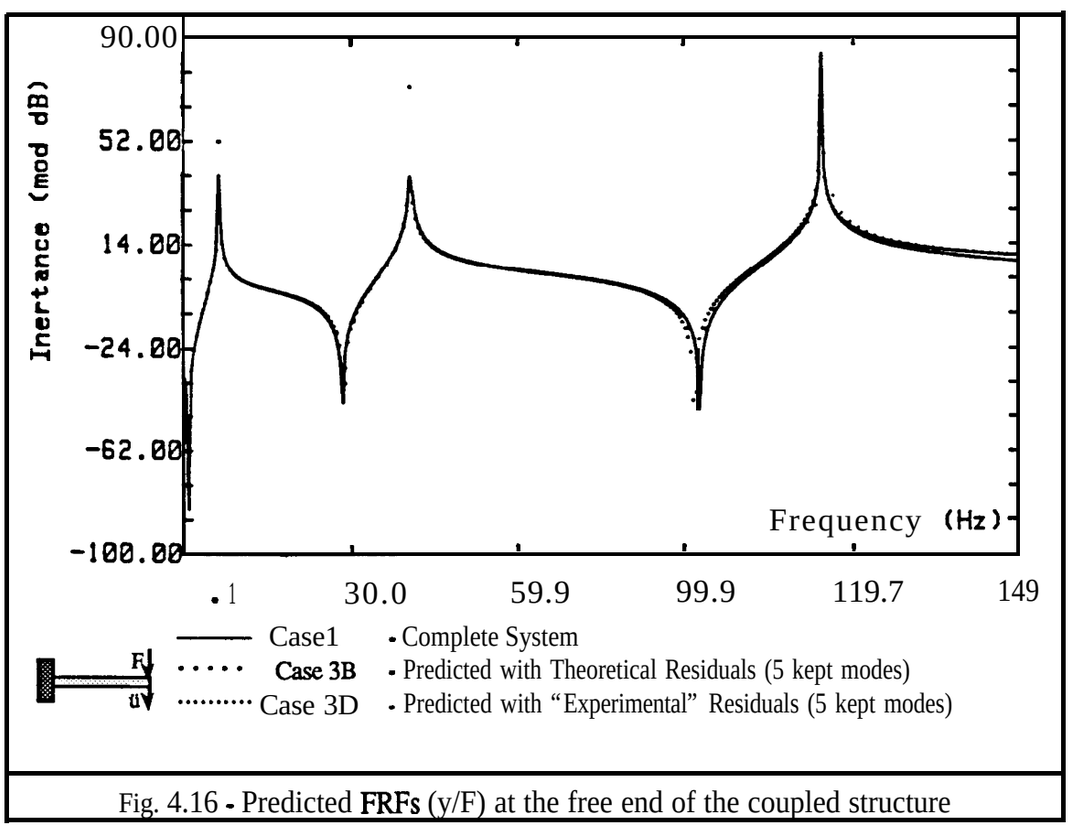

Fig. 4.16 - Predicted FRFs (y/F) at the free end of the coupled structure

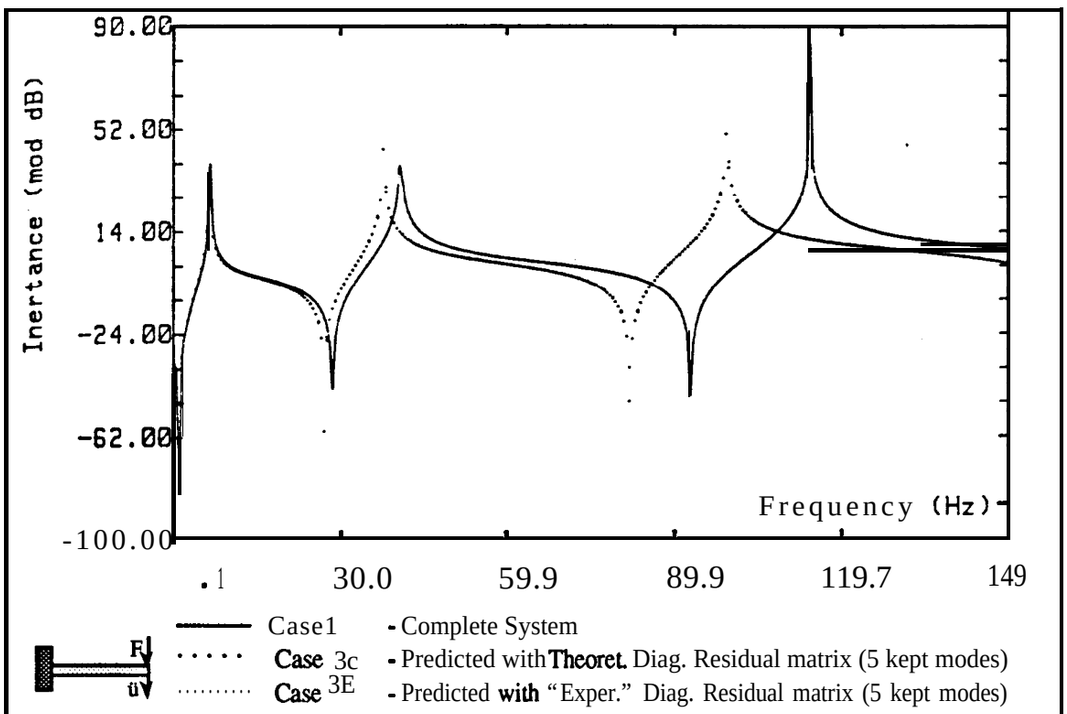

Fig. 4.17 - Predicted FRFs (y/F) at the free end of the coupled structure

4.4.4 DISCUSSION OF RESULTS

It is clear from this theoretical example that the classical free-interface method fails to give accurate predictions of the dynamic properties of the coupled structure, whenever at least one of the component modal matrix is assumed to be incomplete in terms of the available modes; it is also shown that the FRFs predicted under this condition reveal an overestimation of the stiffness properties of the assembled structure which is more evident for the higher natural frequencies of the combined system and as the number of neglected modes is increased. Inclusion of the residual effects of the out-of-range modes by using the refined approach compensates that overestimation, thus giving a more accurate prediction of the final results.

The residual effect of the out-of-range modes in the particular case 3, which assumes only 5 kept modes for component A (beam), was calculated both theoretically, by using the known flexibility matrix of the beam, and experimentally, by identifying one out-of-range

5 SELECTION OF VALID CONNECTION COORDINATES

5.1 INTRODUCTION

The work presented in this chapter was motivated by the numerical difficulties encountered during the coupling algorithms presented so far, which at some stage require the inversion of certain matrices. Those difficulties arise every time the inverse of a singular or near-singular matrix is required which may cause the predicted dynamic properties of the coupled structure to be meaningless. It has been shown that the crucial set of coordinates which require a good formulation in the sense that they should not contain redundancies is the set referred to the interface region. Most of the interface regions are physically connected in a continuous way therefore it is expected that a natural solution to the formulation of the mathematical constraints should involve as many coordinates as it is possible to handle with the computational means available. However, this may very well cause an undesired redundancy in terms of coordinate information, especially for the lower frequency ranges, and which will be even more accentuated if some localised rigid regions exist on the substructures. In fact, the degree of local stiffness will depend on the selected frequency range and it is natural to expect the stiffness of those regions being more considerable for the lower frequencies.

In seeking to remedy the undesirable numerical failures one may attack the problem from two different perspectives. On the one hand, an inspection may be made of the set of

4.5 CONCLUSIONS

A refined Modal coupling technique using free-interface modes was presented in this chapter. The main achievement by this refinement was the inclusion of the residual flexibilty effects which compensate for the truncation in the number of kept or measured modes in each component. The lack of flexibility associated with the description of each component displacement in the connection region has caused the classical free-interface methods to predict results with poor accuracy when compared to the fixed-interface methods - in fact, the components were assumed to be stiffer than they were actually supposed to be. With the inclusion of the residual flexibility information - in fact an approximation when experimental derived models are dealt with - by using a “dummy” interconnecting flexible system, the two main components are mathematically coupled using the best available information provided by data measured over the frequency range in each component. The results obtained in the theoretical case study permit the additional conclusions:

- the refined approach improves the prediction of the dynamic response of the coupled structure when compared with the classical free-interface method; the valid predicted modes may be taken as the number of kept modes in the incomplete subsystem plus one;

- the selected route for the calculation of the residual flexibility matrix does not affect the predicted dynamic response of the overall structure.

fictitious mode. The predicted FRFs using both the calculated residuals do not show any clear difference. However, the flexibility matrix of the interconnecting system should be as complete as possible i.e., the off-diagonal terms representing the cross-flexibilities between the connection coordinates should be calculated whenever it is possible since their exclusion can affect the overall dynamic properties, as shown in the graph of fig. 4.17.

connection coordinates before the subsystems are coupled mathematically and a warning about redundancy is very useful, especially if throughout that inspection the analyst can know what coordinates are responsible for the dependent responses. Thus, a careful analysis of the constraint problem may lead to the elimination of some of those coordinates which, besides removing possibly the redundancy, will additionally decrease the order of the matrices involved. Not surprisingly, this approach might not succeed since only particular cases allow the elimination of some connection coordinates without affecting the meaning of the actual physical connection and other alternatives to solve the problem must be devised. To this end, a powerful numerical algorithm is required to invert any matrix be it singular or not singular. One important mathematical tool which has been used in the statistical and system control research world and which offers the possibility of confident inversion of any matrix is the Singular Value Decomposition. In this work it will be made use of not only to calculate the rank of a given matrix but also to carry out its inversion.

5.2 REDUNDANCY IN THE MODAL AND RESPONSE MODELS

Without loss of generality, the linear dependency herein will be assumed among the coordinates pertaining to the connecting region of each subsystem, since as it was shown in chapter 3 and 4 they form the corresponding sub-matrices involved in the inversion stage of both the FRF and Modal coupling methods.

Let us assume that the Modal matrix has been derived for a given component which includes the mode shape vectors corresponding to the m_k modes existing in the measured frequency range. The partitioned Modal matrix according to the interior and connection coordinates is given as,

$$\begin{Bmatrix} \mathbf{u}_i \\ \cdots \\ \mathbf{u}_c \end{Bmatrix} = \begin{bmatrix} \Phi_{ik} \\ \cdots \\ \Phi_{ck} \end{bmatrix} \{ \mathbf{p}_k \} \qquad (5.1)$$

It may happen that some of the rows in this matrix are nearly dependent on each other in the measured frequency range. Let us assume that rows 1 to 3 of the submatrix $[\Phi_{ck}]$ exhibit some linear dependency.

$$\{u_c\} = \begin{Bmatrix} u_1 \\ u_2 \\ u_3 \\ u_4 \\ \vdots \\ u_{n_c} \end{Bmatrix} = \begin{bmatrix} \begin{bmatrix} \Phi_{11}\Phi_{12}\Phi_{13}\cdots\Phi_{1k} \\ \Phi_{21}\Phi_{22}\Phi_{23}\cdots\Phi_{2k} \\ \Phi_{31}\Phi_{32}\Phi_{33}\cdots\Phi_{3k} \end{bmatrix} \\ \Phi_{41}\ \Phi_{42}\ \Phi_{43}\cdots\Phi_{4k} \\ \vdots\ \ \vdots\ \ \vdots\ \ \vdots\ \ \vdots \\ \Phi_{n_c1}\Phi_{n_c2}\Phi_{n_c3}\cdots\Phi_{n_ck} \end{bmatrix} \begin{Bmatrix} p_1 \\ p_2 \\ p_3 \\ \vdots \\ p_k \end{Bmatrix} \qquad (5.2)$$

They will tend to be even more dependent as the number of kept modes is decreased, for instance to 3. Thus, it is necessary to have a mathematical tool that can detect this characteristic before the matrix is utilised in the coupling algorithm. As was shown in chapter 2 (section 2.3), the classical Modal coupling technique requires the inversion of one partition of the corresponding modal matrix and it is crucial to have an indication of its rank deficiency before this procedure is undertaken.

If the Response model is generated from a Modal model possessing the previously mentioned characteristics, it will exhibit the same ill-conditioning problem at each frequency during a FRF coupling procedure. However, if the FRF matrix is entirely measured instead of being generated from the above mentioned Modal model, the errors on the data will generally serve to make the matrix invertible. Nonetheless, the proximity of the FRF matrix to one of defective rank will often cause it to behave erratically when it is subjected to numerical algorithms.

5.3 THE RANK AND INVERSE OF A MATRIX

5.3.1 THE SINGULAR VALUE DECOMPOSITION

The Singular Value Decomposition (SVD) is an interesting mathematical tool which has proven to be very helpful in the control engineering world. Here that tool will be used to provide quantitative information about the location of redundant coordinates and/or to calculate the inverse of a rank-deficient matrix. It can be applied either to an existing substructure or during the design phase to help detect the inadvertent use of connection coordinates before the information is input to the coupling process.

A review of the SVD of a matrix was given in Golub and Kahan [72] which included a bibliography dealing with applications and algorithms, and some work towards a new algorithm. An improved version of the algorithm is given by Golub and Reinsch in Wilkinson and Reinsch [73]. This algorithm is a special adaptation of the QR algorithn due to Francis [74] for computing the eigenvalues and eigenvectors of a symmetric matrix. As stated by Lawson and Hanson [75] one is most likely to apply Singular Value analysis to matrices where m $\geq$ n; however, the case m $\leq$ n can be converted to this case by adjoining n-m rows of zeros to the matrix [A] or by applying the analysis to the transpose matrix $[A]^T$.

The SVD is a numerical algorithm developed to minimise computational errors involving large matrix operations. The SVD of a **real** matrix [A] results in three component matrices as follows,

$$[A]_{mxn} = [U]_{mxm} \left[\begin{bmatrix} \Sigma \\ 0 \end{bmatrix} \right]_{mxn} [V]^T_{nxn} \qquad (5.3)$$

with the component matrices described as,

$[U]_{mxm}$ orthonormal real matrix formed of the **left singular vectors**

$[\Sigma]_{nxn} = \begin{bmatrix} \sigma_1 & & 0 \\ & \sigma_2 & \\ & & \ddots \\ 0 & & \sigma_n \end{bmatrix}$ diagonal matrix of scalars called the **singular values** which may be organised such that $\sigma_1 \geq \sigma_2 \geq \ldots \geq \sigma_n \geq 0$

$[V]_{nxn}$ orthonormal real matrix formed of the **right singular vectors**

Both [U] and [V] are ideally conditioned matrices where each column vector has unit length and is orthogonal to all other vectors in the matrix set. In terms of matrix operations, both [U] and [V] represent a simple coordinate rotation. They are interrelated as,

$$[U]^T[U] = [U][U]^T = [I]_{mxm} \tag{5.4-a}$$

$$[V]^T[V] = [V][V]^T = [I]_{nxn} \tag{5.4-b}$$

The SVD of a **complex** matrix [A] results also in three component matrices as follows,

$$[A]_{mxn} = [U]_{mxm}\begin{bmatrix}[\Sigma] \\ 0\end{bmatrix}_{mxn}[V]^H_{nxn} \tag{5.5}$$

The component matrices [U] and [V] ($[V]^H$ being the complex conjugate transpose of [VJ) are complex unitary matrices but the Singular Values are still real. In this case the following interrelationship exists,

$$[U]^H[U] = [U][U]^H = [I]_{mxm} \tag{5.6-a}$$

$$[V]^H[V] = [V][V]^H = [I]_{nxn} \tag{5.6-b}$$

The singular values of [A] are the positive square roots of the eigenvalues of $[A]^T[A]$ (or $[A]^H[A]$). The columns of [U] - the left singular vectors - are the orthonormal eigenvectors of $[A][A]^T$ (or $[A][A]^H$) while the columns of [V] - the right singular vectors

- are the orthonormal eigenvectors of $[A]^T[A]$ (or $[A]^H[A]$), also called the principal components.

The SVD is designed to determine the rank and the condition of a matrix and to map geometrically the strengths and weaknesses of a set of equations. The computation of the SVD of a matrix has been studied by numerical analysts for some time and can be performed with great accuracy. It is discussed in many textbooks [76-80] and the software is readily available through a number of standard numerical programs as shown in Lawson and Hanson's book [75], Forsythe's book [79] and Glolub and Reinsch [81]. The attractive aspect of SVD in terms of coupling processes is that when applied to a matrix which describes the transfer function characteristics of a given subsystem, the singular vectors and the singular values all have a strong physical interpretation, as was pointed out by Moore [82] in the control systems theory. Let us assume a substructure FRF and Modal matrices which relate the responses at the coordinates with the forces and modes respectively, as shown,

$$\{x\}_{mx1} = [\alpha]_{mxn} \{F\}_{nx1} \quad (m = n) \tag{5.7}$$

$$\{x\}_{mx1} = [\Phi]_{mxn} \{p\}_{nx1} \tag{5.8}$$

By applying the SVD to either a FRF or a Modal matrix, the components [U] and [V] have the following properties;

$[U]_{mxm}$ - The left singular vectors provide the most appropriate coordinate system for viewing the responses. This coordinate system is such that the first singular vector $\{u_1\}$ indicates the easiest direction in which the system can be changed; the second one $\{u_2\}$ is the next easiest direction and so on . . .

$[V]_{nxn}$ - The right singular vectors provide the most appropriate coordinate system for viewing the forces (or modes). The first singular vector $\{v_1\}$ indicates the combination of forces (or modes) which has the most effect on the system; the second one $\{v_2\}$ is the combination which has the next strongest effect and so on...

5.3.2 RANK DEGENERACY

The rank of a matrix is the number of linearly independent rows (and columns) in the given matrix. It is generally acknowledged that the SVD is the only reliable method of determining rank numerically. The usual mathematical notion of rank is not very useful when the matrices in question are not known exactly. For example, suppose that $[A]_{mxn}$ was originally of rank $r<n$ but whose elements have been perturbed by some small errors (e.g. rounding or measurement errors); it is extremely unlikely that these errors will conspire to keep rank of [A] exactly equal to r; indeed what is most likely is that the perturbed matrix will have full rank n. Nonetheless, the nearness of [A] to a matrix of defective rank will often cause it to behave erratically when it is subjected to numerical algorithms. One way to circumventing the difficulties of the mathematical definition of rank is to specify a tolerance and say that [A] is numerically defective in rank if within that tolerance it is near a defective matrix.

The mere observation of small singular values does not solve the ill-conditioned problem for we must still decide upon a value for rank(A). One approach to this deficient problem is to have a parameter $\delta>0$ and a convention that A has numerical rank r if the σ_i satisfy

$$\sigma_1 \geq \sigma_2 \geq \ldots \geq \sigma_r > \delta \geq \sigma_{r+1} \geq \ldots \geq \sigma_n \qquad (5.9)$$

The key quantity in rank determination is obviously the value σ_r. The parameter δ should be consistent with the machine precision E, e.g. $\delta = \varepsilon \| A \|_\infty$. However, if the general level of relative error in the data is larger than ε, then δ should be correspondingly bigger e.g. $\delta = 10^{-2} \| A \|_\infty$, as suggested by Golub and Van Loan [80]. This criterion is useful especially when there is no clear split of the singular values into a set of large values and another set of small values.

If rank(A) = **r** then [A] has **r** linearly independent rows and **r** linearly independent columns. The rank indicates only how many are linearly independent and not where they are located in the matrix. Some rank properties of a matrix are presented in Appendix III.

5.3.3 CONDITION OF A MATRIX AND ITS INVERSE

The SVD is one of the most elegant algorithms for exposing quantitative information about the structure of a linear system problem [A] (x) = (b) . One aim is to examine how perturbations in [A] and (b) can affect the solution {x). By applying the SVD to the matrix [A] one obtains,

$$[A]_{mxn} = \sum_{i=1}^{n} \sigma_i u_i v_i^T = [U]_{mxm} \left[\begin{bmatrix} \Sigma \\ 0 \end{bmatrix} \right]_{mxn} [V]_{nxn}^T \qquad (5.10)$$

Then {x} = [A]+{ b} with

$$[A]^+ = [[U]_{mxm} \left[\begin{bmatrix} \Sigma \\ 0 \end{bmatrix} \right]_{mxn} [V]_{nxn}^T \Big]^{-1} \qquad (5.11)$$

or $$[A]_{nxm}^+ = [V]_{nxn} \left[\Sigma \right]_{nxn}^{-1} [U]_{nxm}^T \qquad (5.12)$$

$$x = \sum_{i=1}^{n} \frac{u_i^T b}{\sigma_i} v_i \qquad (5.13)$$

This expansion shows that small changes in [A] or (b) can induce relatively large changes in $\{x\}$ if σ_n is small. The condition number k(A) of a matrix $[A]_{mxn}$ with singular values $\sigma_1 \geq \sigma_2 \geq \cdots \geq \sigma_n$ depends on the underlying norm. For the particular case of the 2-norm, the condition number is given as,

$$k_2(A) = \text{II A}\|_2 \| \text{A-' II} , = \text{o,(A)} / \sigma_n(A) \qquad (5.14)$$

However, if σ_r is chosen such that

$$\sigma_1 \geq \sigma_2 \geq \cdots \geq \sigma_r \geq \sigma_{r+1} = 0 = \cdots = \sigma_n \qquad (5.15)$$

whereby the singular values $\sigma_{r+1}, \ldots, \sigma_n$ are effectively considered to be zero, the condition number of matrix [A] with rank(A)= r is σ_1 / σ_r. In this case, the matrix [A] can

be approximated to a matrix $[A_r]$ with rank r and the best candidate solution to the linear problemis {x) = $[A_r]^+\{b\}$.

The condition number of [A] quantifies the sensitivity of the [A] { x)=(b) problem, since the relative error in $\{x\}$ can be k(A) times the relative error in [A]. Additionally, it gives a measure of the "nearness" of [A] to singularity. If k(A) is large, then [A] is said to be ill-conditioned or conversely if it is small it is said to be well-conditioned. It is natural to consider how well a determinant size measures ill-conditioning. Unfortunately, there is little correlation between det(A) and the condition number of [A] {x} = {b} . For example, the matrices [B,] defined by,

$$[B_n] = \begin{bmatrix} 1 & -1 & -1 & \dots & -1 \\ 0 & 1 & -1 & \dots & -1 \\ 0 & 0 & 1 & \dots & -1 \\ \cdot & \cdot & \cdot & \cdot & \cdot \\ 0 & 0 & 0 & 0 & 1 \end{bmatrix} \qquad (5.16)$$

always have $|B_n| = 1$ although they tend to be rank-deficient as the order increases. On the other hand, a very well-conditioned matrix can have a very small determinant. For example,

$$[D_n] = \text{diag}\,(10^{-1}, 10^{-1}, \dots, 10^{-1}) \qquad (5.17)$$

satisfies $k(D_n) = 1$ although $|D_n| = 10^{-n}$ which illustrates the fact that the value of a determinant is worthless as an indication of singularity.

By assuming that a certain value σ_r is chosen, the calculation of the pseudo-inverse $[A_r]^+$ only requires the r significant singular values as well as the corresponding vectors of matrices [U] and [VJ. Let us consider these matrices to be partitioned according to the r significant columns such as,

$$[U]_{mxm} = \left[[U_1]_{mxr} \vdots [U_2]_{mx(m-r)} \right] \tag{5.18}$$

$$[V]_{nxn} = \left[[V_1]_{nxr} \vdots [V_2]_{nx(n-r)} \right] \tag{5.19}$$

$$[\hat{\Sigma}]_{nxn} = \begin{bmatrix} [\hat{\Sigma}_1]_{rxr} & [0] \\ [0] & [0] \end{bmatrix} \tag{5.20}$$

The approximated matrix $[A_r]$ will be given as,

$$[A_r]_{mxn} = [U_1]_{mxr} [\hat{\Sigma}_1]_{rxr} [V_1]^T_{rxn} \tag{5.21}$$

and the corresponding pseudo-inverse $[A_r]^+$ is,

$$[A_r]^+_{nxm} = [V_1]_{nxr} [\hat{\Sigma}_1]^{-1}_{rxr} [U_1]^T_{rxm} \tag{5.22}$$

Having calculated the pseudo-inverse it is interesting to note that,

$$[[A_r][A_r]^+]_{mxm} = [U_1][U_1]^T \tag{5.23}$$

$$[[A_r]^+ [A_r]]_{nxn} = [V_1][V_1]^T \tag{5.24}$$

$$[[I] - [A_r][A_r]^+]_{mxm} = [U_2][U_2]^T \tag{5.25}$$

$$[[I] - [A_r]^+ [A_r]]_{nxn} = [V_2][V_2]^T \tag{5.26}$$

which correspond to four fundamental orthogonal projections of $[A_r]$ as stated by Klema and Golub [83].

5.4 SELECTION OF INDEPENDENT COORDINATES

In mathematical terms we shall be concerned with the following problem: given a matrix [A]_ $(m \geq n)$ which is near a matrix $[A_r]_{mxn}$ whose rank is less than n, is it possible to find a set of linearly independent columns of [A] that span a good approximation to the column space of $[A_r]$?. The ideas underlying the approach are the use of singular values of [A] to detect degeneracy and the singular vectors of [A] to rectify it.

Replacing $[A]_{mxn}$ by $[A_r]_{mxn}$ amounts to filtering out the small singular values and can make a great deal of sense in those situations where [A] is derived from noisy data. In other applications however, the rank deficiency implies redundancy among the columns that compose the matrix. For example, if the problem at hand is to approximate a vector of responses {b} , the procedure sketched above will express the approximation as a linear combination of all the columns of [A], even though some of them are clearly redundant. What is needed is a device for selecting a set of linearly independent columns of [A]. In this case one should be interested on using only the independent columns to approximate the observation vector b. How to pick these columns is the problem of subset selection.

The QR factorisation with column pivoting is one method of subset selection which was purposed by Golub, Klema and Stewart [84]. The main steps involved in this selection are,

a) - compute the SVD of [A] and use it to determine the rank r

b) - Partition of matrix [V] into $\begin{bmatrix} V_{11} & V_{12} \\ V_{21} & V_{22} \end{bmatrix} \begin{matrix} (r) \\ (n-r) \end{matrix}$ (5.27)

c) - Use QR algorithm with column pivoting to compute

$$[Q]^T \begin{bmatrix} V^T_{11} & V^T_{21} \end{bmatrix} [P] = \begin{bmatrix} R_{11} & R_{12} \end{bmatrix} \quad (5.28)$$

The permutation matrix [P] is finally used to re-sequence all the columns in

$$[A]\,[P] = \begin{bmatrix} B_1 & B_2 \end{bmatrix} \quad (5.29)$$

such as the columns of $[B_1]$ are sufficiently independent.

This method was applied to some numerical examples and the results were not always successful. For instance the matrix

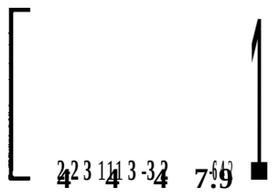

is nearly rank-deficient. After applying the SVD, the rank value was assumed to be **3. The** QR **factorisation** was then undertaken on component V giving the pivot (which is used to create the permutation matrix) ordered as **-** 4, 3, 1, 2 **-** suggesting the elimination of column No. 2 which is not one of the dependent columns **(3,4).**

However, as suggested by Klema and Laub **[83]** the elements of the component matrix **[V]** can be inspected to reveal dependencies or near dependencies among the columns of matrix [A] whereas the columns of [U] can reveal dependencies among the rows of [A]. If the algorithm is applied instead, to the projections $[U_1][U_1]^T$ and $[V_1][V_1]^T$ presented in (5.23 and **5.24),** a better result is found for the selection of the independent rows and columns, respectively.

This alternative method was applied to the above presented matrix, **either** to detect dependency on the rows **or** on the columns; the pivot is now ordered as **-2, 3, 4, 1-** for the rows which indicates the row 1 to be eliminated and for the columns the pivot was ordered as **-** 1, 2, 4, 3 **-** which suggests the elimination of column 3. In fact, this corresponds to the row and column which were introduced on purpose to be linearly dependent. Another test was carried out on the same matrix but changing the order of its columns and the same result was found.

5.5 NUMERICAL EXAMPLES

5.5.1 INTRODUCTION

The mathematical tool we have been concerned with so far - the SVD - will now be used in various coupling exercises. These are performed under conditions which are supposed to simulate practical problems although the subsystems are purely theoretically-derived. One of those practical problems the analyst can be faced with is related to the numerical failures of certain algorithms due to the existence of redundant information or in other terms due to the dependency or near-dependency of the coordinate responses over a selected frequency range.

In respect of the FRF **coupling** technique it was found in chapter 3 that none of the alternative techniques could numerically resolve the difficulty encountered when two subsystems were connected through regions both possessing some linearly dependent coordinates. This caused the corresponding partition of the FRF matrices, at some frequency values, to be rank-deficient and thus impossible to calculate the inversion with usual algorithms.

As suggested there, one possible way of avoiding the dependency is just by eliminating the redundant coordinates and keeping only the set of coordinates which are independent. What may happen however, is that the result of this analysis leads to two sets in which the number of independent coordinates do not match together, either because the quantity is different or the location is not the same; such an elimination would cause the constraints to be altered, which is not the main objective. This solution would only work when the selected independent coordinates for both subsystems match together in terms of quantity and location.

A second alternative to cope with redundancy is by making use of the SVD technique at every frequency where the necessary inversion has to be carried out on the corresponding rank-deficient matrix. This is recommendable in situations where the previously

mentioned alternative does not work, since the inversion using the SVD may be more time consuming than the usual inversion algorithms.

In respect of the **Modal coupling** techniques it is shown in chapter 2 that the classical technique, which does not account for the effects of the out-of-range modes, may suffer from numerical failures whenever the necessary inversion is carried out on a square partition of the modal matrix related to the connecting coordinates. Since this inversion is only required once, the SVD algorithm is highly recommendable, without a previous analysis to select the independent coordinates.

The numerical examples which are presented in this section make use of the FRF coupling techniques applied to four theoretical subsystems. These exhibit a dependency on some coordinate responses due to the existence of localised rigid regions created by using relatively stiff springs to connect some of the discrete masses and then truncating, up to the first six significant digits, the elements in the generated FRF matrix. The frequency range of interest was selected to be O-15 Hz for all four subsystems used.

The following figs. 5.1 to 5.4 represent the discrete masses and springs forming each component and the corresponding Spatial and Modal models. In all of them, there are some **bold springs** connecting discrete masses in order to highlight the localised rigid regions on the structures. These rigidities are extended to the interior and connection coordinates making the corresponding coordinates to be linearly dependent.

5.5.2 SUBSYSTEM DESCRIPTION

Subsystem 1 - 5 DoF undamped Free-Free system

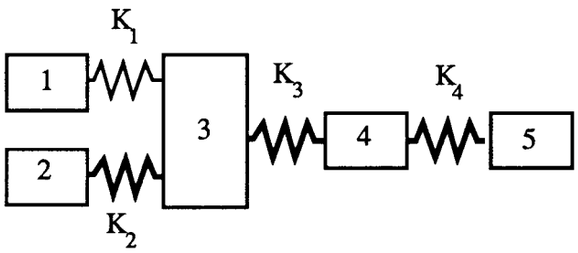

$K_1 = 1\ E3\ ;\ K_2 = 1\ E6\ ;\ K_3 = 1\ E7\ ;\ K_4 = 1\ E5$ (N/m)

$M_1 = 0.5\ ;\ M_2 = 1\ ;\ M_3 = 2\ ;\ M_4 = 1.5\ ;\ M_5 = 0.5$ (Kg)

Fig. 5.1 - Subsystem 1 - 5 DoF Free-free system

SPATIAL Model

$$[M]_{5x5} = \begin{bmatrix} 0.5000 & 0 & 0 & 0 & 0 \\ 0 & 1 & 0 & 0 & 0 \\ 0 & 0 & 2 & 0 & 0 \\ 0 & 0 & 0 & 1.5 & 0 \\ 0 & 0 & 0 & 0 & 0.5 \end{bmatrix}$$

$$[K]_{5x5} = \begin{bmatrix} 1\ E3 & 0 & -1\ E3 & 0 & 0 \\ 0 & 1\ E6 & -1.E6 & 0 & 0 \\ -1\ E3 & -1\ E6 & 1.1001E7 & -1\ E7 & 0 \\ 0 & 0 & -1\ E7 & 1.01\ E7 & -1\ E5 \\ 0 & 0 & 0 & -1\ E5 & 1\ E5 \end{bmatrix}$$

MODAL Model

$$[\Phi]_{5x5} = \begin{bmatrix} 4.2640E\text{-}1 & 1.3484E00 & 1.3176E\text{-}3 & 3.7169E\text{-}4 & 7.9258E\text{-}5 \\ 4.2640E\text{-}1 & -1.3490E\text{-}1 & -1.8399E\text{-}1 & 8.7422E\text{-}1 & 4.3243E\text{-}2 \\ 4.2640E\text{-}1 & -1.3461E\text{-}1 & -1.4354E\text{-}11 & -2.3555E\text{-}1 & -4.7326E\text{-}1 \\ 4.2640E\text{-}1 & -1.3467E\text{-}1 & -1.3319E\text{-}1 & -2.8675E\text{-}1 & 6.0560E\text{-}1 \\ 4.2640E\text{-}1 & -1.3616E\text{-}1 & 1.3404E00 & 5.3626E\text{-}2 & -1.0313E\text{-}2 \end{bmatrix}$$

$$\left[\omega_r^2\right]_{5x5} = [\ 0 \quad 2.1997E3 \quad 2.1987E5 \quad 1.2694E6 \quad 1.1944E7\ ]$$

Natural Frequencies 0, 7.464, 74.63, 179.3, 550 Hz

Subsystem 2 - 5 DoF undamped Clamped-Free system

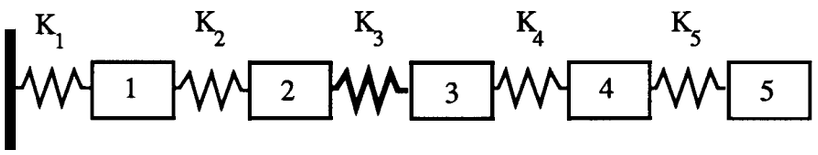

$K_1 = 3\,E3$; $K_2 = K_5 = 1\,E3$; $K_3 = 1\,E7$; $K_4 = 2\,E3$ (N/m)

$M_1 = 1$; $M_2 = 0.5$; $M_3 = 2$; $M_4 = 1.5$; $M_5 = 0.5$ (Kg)

Fig. 5.2 - Subsystem 2 - 5 DoF Clamped-free system

SPATIAL Model

$$[M]_{5x5} = \begin{bmatrix} 1 & 0 & 0 & 0 & 0 \\ 0 & 0.5 & 0 & 0 & 0 \\ 0 & 0 & 2 & 0 & 0 \\ 0 & 0 & 0 & 1.5 & 0 \\ 0 & 0 & 0 & 0 & 0.5 \end{bmatrix}$$

$$[K]_{5x5} = \begin{bmatrix} -1\,E3 & 1.0001E7 & -1\,E7 & 0 & 0 \\ 0 & -1\,E7 & 1.0002E7 & -2\,E3 & 0 \\ 0 & 0 & -2\,E3 & 3\,E3 & -1\,E3 \\ 4\,E3 & -1\,E3 & 0 & -1\,E3 & 1\,E3 \end{bmatrix}$$

MODAL Mode

$$[\Phi]_{5x5} = \begin{bmatrix} 1.1098E\text{-}1 & -1.6218E\text{-}1 & -2.6013E\text{-}1 & 9.4536E\text{-}1 & -5.0601E\text{-}5 \\ 4.2720E\text{-}1 & -4.0335E\text{-}1 & -1.6605E\text{-}1 & -1.6497E\text{-}1 & 1.2649E00 \\ 4.2723E\text{-}1 & -4.0334E\text{-}1 & -1.6601E\text{-}1 & -1.6505E\text{-}1 & -3.1622E\text{-}1 \\ 5.0486E\text{-}1 & 2.3891E\text{-}1 & 5.7865E\text{-}1 & 1.4094E\text{-}1 & 1.6865E\text{-}5 \\ 5.4600E\text{-}1 & 9.8119E\text{-}1 & -8.4990E\text{-}1 & -1.2963E\text{-}1 & -1.3489E\text{-}9 \end{bmatrix}$$

$$\left[\omega_r^2\right]_{5x5} = \text{diag}\,[\,1.507E2 \quad 1.513E3 \quad 3.362E3 \quad 4.175E3 \quad 2.501E7\,]$$

Natural Frequencies 1.954, 6.191, 9.228, 10.28. 795.8 Hz

Subsystem 3 - 7 DoF undamped Clamped-Free system

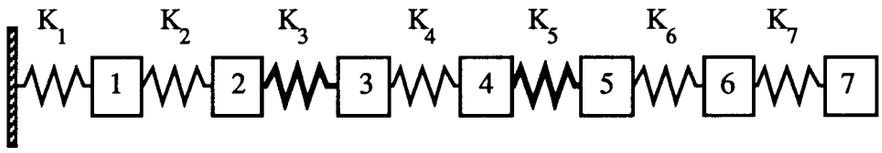

$K_1 = K_4 = 2\,E3$; $K_2 = K_6 = 1\,E3$; $K_3 = K_5 = 1\,E9$; $K_7 = 3\,E3$ (N/m)

$M_1 = M_2 = M_4 = M_5 = 1$; $M_3 = 0.5$; $M_6 = 1.5$; $M_7 = 2$ (Kg)

Fig. 5.3 - Subsystem 3 - 7 DoF Clamped-free system

SPATIAL Model

$$[M]_{7x7} = \text{diag}[\ 1 \quad 1 \quad 0.5 \quad 1 \quad 1 \quad 1.5 \quad 2\ ]$$

$$[K]_{7x7} = \begin{bmatrix} 3E3 & -1E3 & 0 & 0 & 0 & 0 & 0 \\ -1E3 & 1.000001\,E9 & -1E9 & 0 & 0 & 0 & 0 \\ 0 & -1\,E9 & 1.000002E9 & -2E3 & 0 & 0 & 0 \\ 0 & 0 & -2E3 & 1.000002E9 & -1E9 & 0 & 0 \\ 0 & 0 & 0 & -1E9 & 1.000001\,E9 & -1E3 & 0 \\ 0 & 0 & 0 & 0 & -1E3 & 4E3 & -3\,E3 \\ 0 & 0 & 0 & 0 & 0 & -3E3 & 3\,E3 \end{bmatrix}$$

MODAL Model

$$[\Phi]_{7x7} = \begin{bmatrix} 8.733E\text{-}2 & -1.940E\text{-}1 & 6.173E\text{-}1 & 7.373E\text{-}1 & -1.732E\text{-}1 & -4.031E\text{-}11 & 1.924E\text{-}7 \\ 2.563E\text{-}1 & -4.671E\text{-}1 & 3.943E\text{-}1 & -4.407E\text{-}1 & 1.819E\text{-}1 & -4.715E\text{-}7 & -5.773E\text{-}1 \\ 2.563E\text{-}1 & -4.671E\text{-}1 & 3.943E\text{-}1 & -4.407E\text{-}1 & 1.819E\text{-}1 & -4.715E\text{-}7 & 1.155E00 \\ 3.282E\text{-}1 & -3.962E\text{-}1 & -4.155E\text{-}1 & 1.593E\text{-}1 & -1.931E\text{-}1 & 7.071E\text{-}1 & -3.849E\text{-}7 \\ 3.282E\text{-}1 & -3.962E\text{-}1 & -4.155E\text{-}1 & 1.593E\text{-}1 & -1.931E\text{-}1 & 7.071E\text{-}1 & -3.849E\text{-}7 \\ 4.290E\text{-}1 & 2.148E\text{-}1 & -7.310E\text{-}2 & 2.128E\text{-}1 & 6.212E\text{-}1 & 2.357E\text{-}7 & 1.218E\text{-}12 \\ 4.486E\text{-}1 & 3.549E\text{-}1 & 1.273E\text{-}1 & -1.522E\text{-}1 & -3.654E\text{-}1 & -2.236E\text{-}11 & -1.945E\text{-}12 \end{bmatrix}$$

$$\left[\omega_r^2\right]_{5x5} = \text{diag}\ [\ 6.55E1 \quad 5.92E2 \quad 2.36E3 \quad 3.60E3 \quad 4.05E3 \quad 2.00E9 \quad 3.00E9\ ]$$

Natural Frequencies 1.288, 3.873, 7.734, 9.546, 10.13, 7118, 8717 Hz

Subsystem 4 - 7 DoF undamped Free-Free system

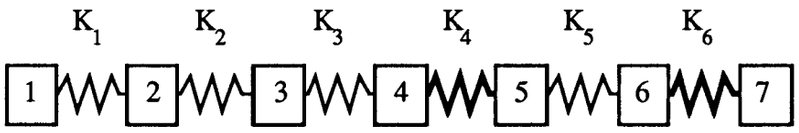

$K_1 = 3\,E3 ; K_2 = K_3 = 1\,E3 ; K_4 = K_6 = 1\,E9 ; K_5 = 2\,E3$ (N/m)

$M_1 = 2 ; M_2 = M_3 = M_5 = M_7 = 1 ; M_4 = M_6 = 0.5$ (Kg)

Fig. 5.4 - Subsystem 4 - 7 DoF Free-free system

SPATIAL Model

$$[M]_{7x7} = \text{diag}[\ 2 \quad 1 \quad 1 \quad 0.5 \quad 1 \quad 0.5 \quad 1\ ]$$

$$[K]_{7x7} = \begin{bmatrix} 3E3 & -3E3 & 0 & 0 & 0 & 0 & 0 \\ -3E3 & 4E3 & -1E3 & 0 & 0 & 0 & 0 \\ 0 & -1E3 & 2E3 & -1E3 & 0 & 0 & 0 \\ 0 & 0 & -1E3 & 1.000001E9 & -1E9 & 0 & 0 \\ 0 & 0 & 0 & -1E9 & 1.000002E9 & -2E3 & 0 \\ 0 & 0 & 0 & 0 & -2E3 & 1.000002E9 & -1E9 \\ 0 & 0 & 0 & 0 & 0 & -1E9 & 1E9 \end{bmatrix}$$

MODAL Model

$$[\Phi]_{7x7} = \begin{bmatrix} 3.780E\text{-}1 & -4.345E\text{-}1 & 2.349E\text{-}1 & 9.865E\text{-}2 & -3.219E\text{-}1 & 1.455E\text{-}14 & 9.152E\text{-}11 \\ 3.780E\text{-}1 & -3.506E\text{-}1 & -4.445E\text{-}2 & -1.190E\text{-}1 & 8.475E\text{-}1 & 1.060E\text{-}13 & 7.384E\text{-}11 \\ 3.780E\text{-}1 & 2.928E\text{-}3 & -8.033E\text{-}1 & -3.781E\text{-}1 & -2.625E\text{-}1 & -3.849E\text{-}7 & -2.721E\text{-}13 \\ 3.780E\text{-}1 & 3.556E\text{-}1 & -1.288E\text{-}1 & 6.142E\text{-}1 & 5.800E\text{-}2 & 1.155E00 & -5.133E\text{-}7 \\ 3.780E\text{-}1 & 3.556E\text{-}1 & -1.288E\text{-}1 & 6.142E\text{-}1 & 5.800E\text{-}2 & -5.773E\text{-}1 & -5.133E\text{-}7 \\ 3.780E\text{-}1 & 4.545E\text{-}1 & 3.808E\text{-}1 & -4.143E\text{-}1 & -1.879E\text{-}2 & 2.566E\text{-}7 & 1.155E00 \\ 3.780E\text{-}1 & 4.545E\text{-}1 & 3.808E\text{-}1 & -4.143E\text{-}1 & -1.879E\text{-}2 & 2.566E\text{-}7 & -5.773E\text{-}1 \end{bmatrix}$$

$$\left[\omega_r^2\right]_{5x5} = \text{diag}\ [\ 0 \quad 2.902E2 \quad 1.784E3 \quad 3.31E3 \quad 5.45E3 \quad 3.0E9 \quad 3.0E9\ ]$$

Natural Frequencies 0, 2.711, 6.723, 9.156, 11.75, 8717, 8717 Hz

5.5.3 RESULTS

5.5.3.1 COORDINATE REDUNDANCY

The algorithm suggested in section **5.4** will be applied to each subsystem model. It can be applied to either a FRF matrix or to a Modal matrix. The first matrix varies with the frequency, thus it is not recommended to carry out the analysis in such a matrix for all the frequencies of interest. It is preferable to analyse the Modal matrix instead, since this may reveal any linear dependency on the coordinates. It may happen that, after inspecting the Modal matrix and taking into account all the modes, the rows of this matrix are found to be independent. However, this does not mean that the FRF matrix cannot exhibit any linear dependency in a particular range. It is realistic to assume that some of the coordinate amplitudes have a similar value in the first three out of ten modes for instance, thus provoking the FRF matrix to be singular or near-singular, mainly for the frequency range encompassing those three modes where there is only a slight contribution of the remaining ones.

5.5.3.2 COUPLED SYSTEMS

The Singular Value Decomposition technique is presented in this chapter as a mathematical tool to resolve the numerical difficulties related to the inversion of some particular matrices during a coupling process. Here the interest in mainly focused on the FRF coupling, since this technique is more sensitive to this numerical problems. The subsystems are coupled using an ‘excessive’ number of connection coordinates, this meaning that although in physical terms the subsystems can be coupled using whatever the number of coordinates it is not true in numerical terms. The algorithms presented in chapter 3 (vide section 3.4 equations (3.12) and (3.24)) are used in two different perspectives;

- firstly, the subsystems are coupled through the selected coordinates where nothing is known about their possible dependency and making use of the approaches and algorithms above mentioned; the computer built-in subroutine is used to invert matrices with a warning about the determinant value,

- secondly, the coordinate dependency is inspected on each subsystem; whenever possible the connection coordinates are reduced and the first step is carried out again.

- as a last alternative, the SVD algorithm is used to carry out the necessary inversion at each frequency.

In **example** I the two subsystems **1** and 2 are coupled using 4 coordinates as shown in fig. 5.5, some of which are redundant and pertain to both interior and connection coordinate sets. This is a similar problem used in chapter 3 (vide 3.4.4) in which the alternative coupling techniques could not solve the problem due to the numerical failures using the computer built-in routine to invert matrices. In this chapter, a further step is taken by using the SVD technique to invert the matrices which are used according to the most refined coupling algorithm presented in chapter 3 (algorithm 3 based on equation (3.24)). This algorithm requires the inversion of a matrix which order is dictated only by the number of connection coordinates.

In **example** II the same subsystems **1** and 2 are coupled using at this time a **reduced set** of 3 interface coordinates, as shown in fig. 5.9. The reduction on the number of these coordinates was performed after a check on the possible redundancy among the connection coordinates in both components. This was possible by making use of the SVD and QR factorisation applied to the connecting partition of the Modal matrix and as a result coordinates Nos. 2,3 and 4 were found to be redundant in subsystem 1 and coordinate No. 2 was redundant in subsystem 2. By virtue of having coordinate No.2 as a redundant coordinate in both components, it was possible to leave out this coordinate for connection purposes without affecting the formulation of physical constraints between the two components. Thus the normal built-in computer routine was used to invert a matrix which, by the mentioned simplification, was reduced and converted to non-singular.

In **example III** the subsystems 3 and 4 are connected using a set of 6 connection coordinates, as shown in fig. 5.12, and identically some of them are supposed to be redundant. A coupling exercise, similar to the one used in example I, is undertaken here.

In **example IV,** subsystems 3 and 4 are connected via a reduced set of 5 coordinates, as presented in fig. 5.18. An inspection on redundancy carried out on the set of connecting coordinates of subsystem 3 led to conclusion that coordinates Nos. 2 and 4 were the dependent ones. An identical inspection on subsystem 4 found coordinates 4 and 7 to be redundant. Similarly to example II, coordinate 4 was neglected in the formulation of the constraint conditions and as a result a non-singular reduced matrix was used during the coupling process, leading to an accurate prediction of the coupled system response.

EXAMPLE I - Subsystem 1 + Subsystem 2 (4 Connection Coordinates)

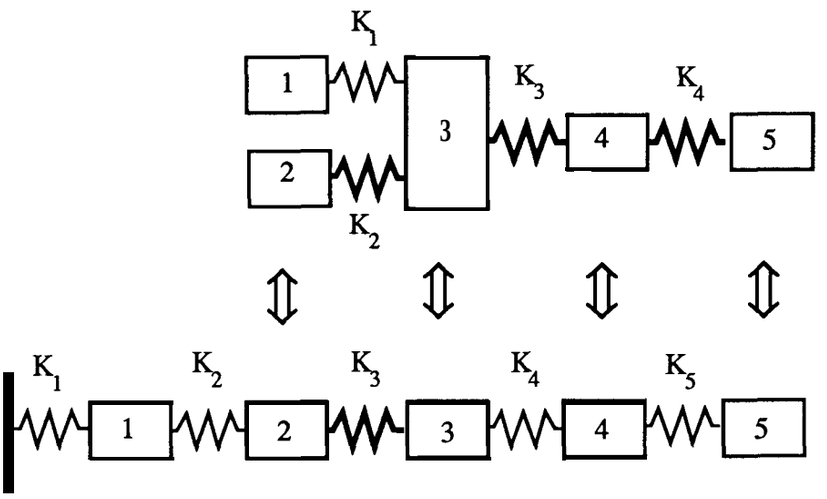

COUPLED STRUCTURE

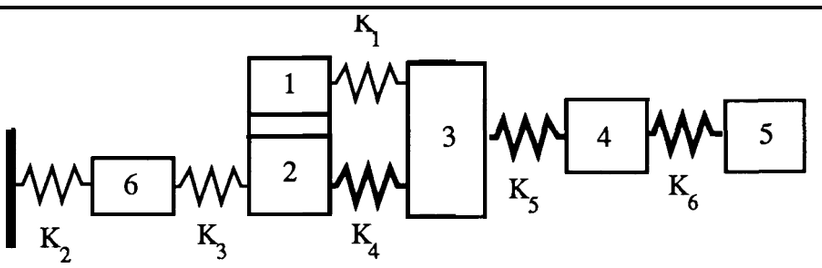

Fig. 5.5 - Subsystem 1 + Subsystem 2 (4 connection coordinates)

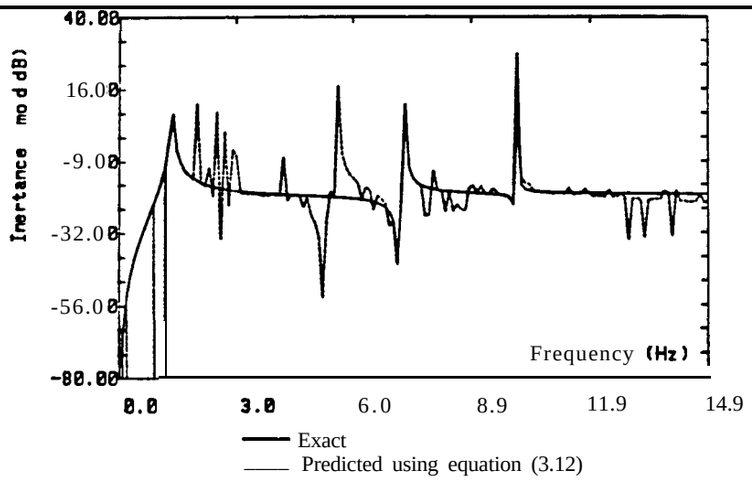

Fig. 5.6 - Predicted FRF (Point Inertance 2,2) using **Algorithm 1**

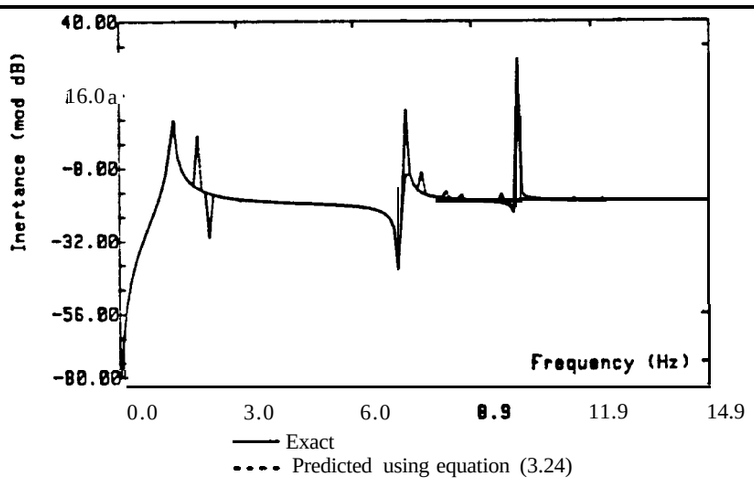

Fig. 5.7 - Predicted FRF (Point Inertance 2,2) using **Algorithm 3**

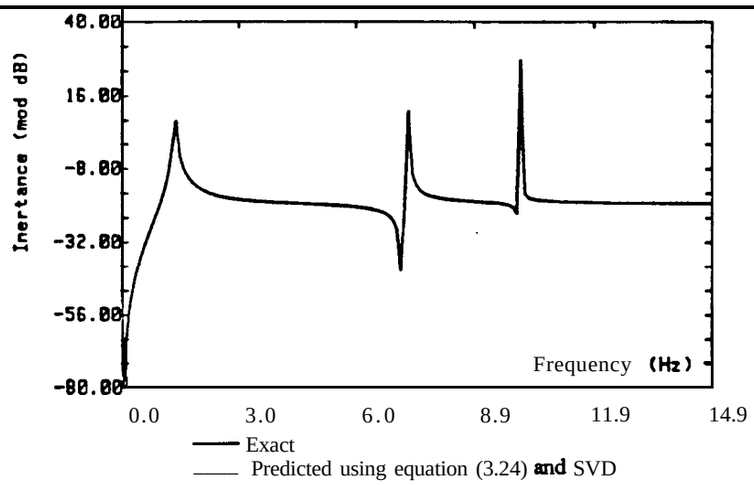

Fig. 5.8 - Predicted FRF (Point Inertance 2,2) using **SVD**

EXAMPLE II - Subsystem 1 + Subsystem 2 (3 Connection Coordinates)

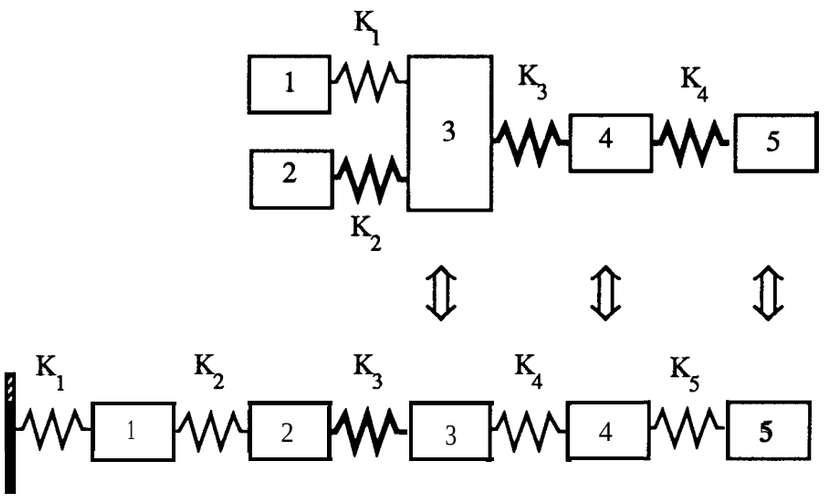

COUPLED STRUCTURE

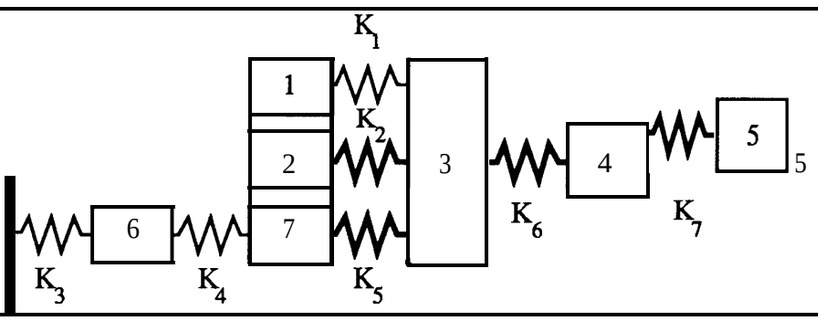

Fig. 5.9 - Subsystem 1 + Subsystem 2 (3 connection coordinates)

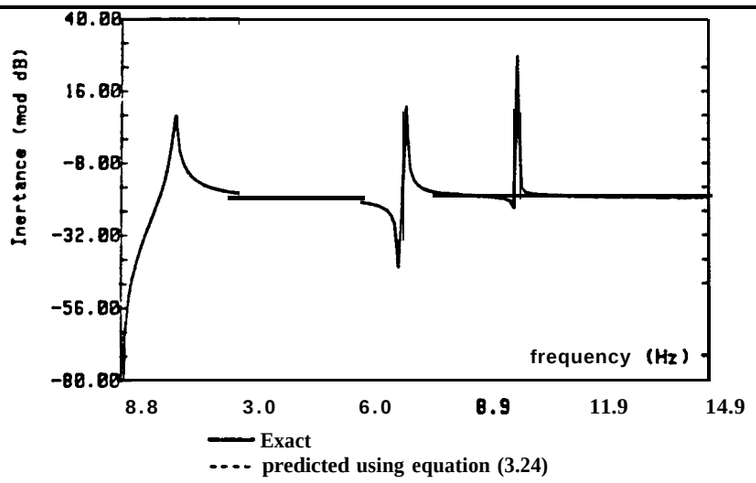

Fig. 5.10 - Predicted FRF (Point Inertance 2.2) using **Algorithm 3**

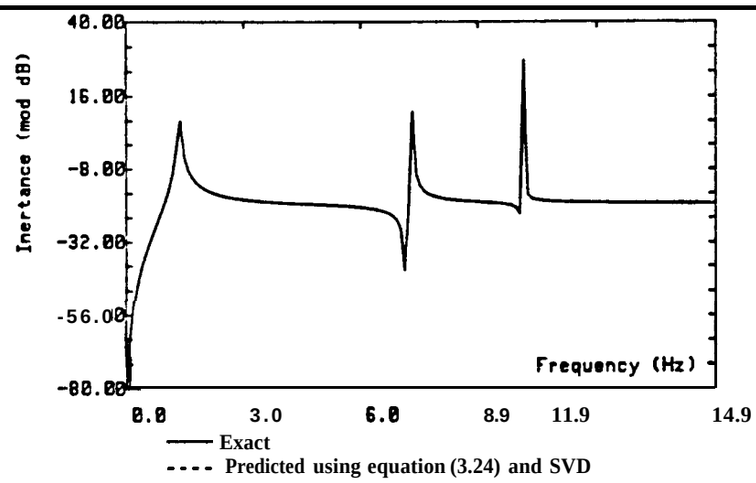

Fig. 5.11 - Predicted FRF (Point Inertance 2,2) using **SVD**

EXAMPLE III - Subsystem 3 + Subsystem 4 (6 **Connection Coordinates)**

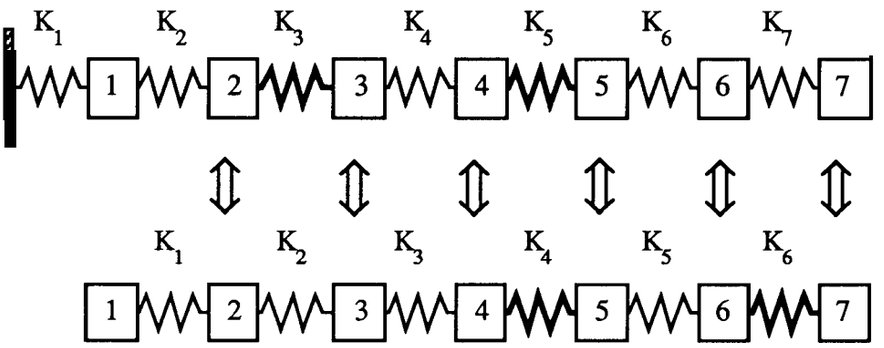

COUPLED STRUCTURE

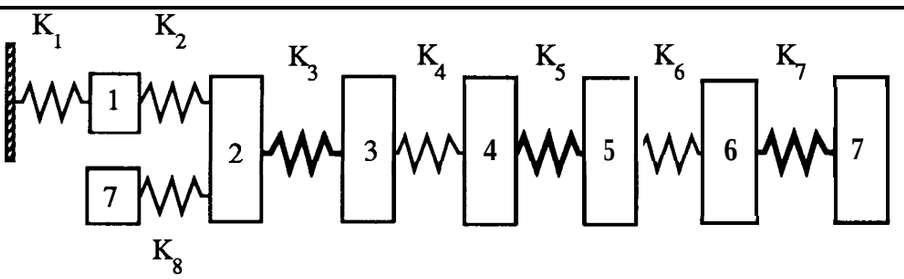

Fig. 5.12 - Subsystem **3** + Subsystem 4 **(6** connection coordinates)

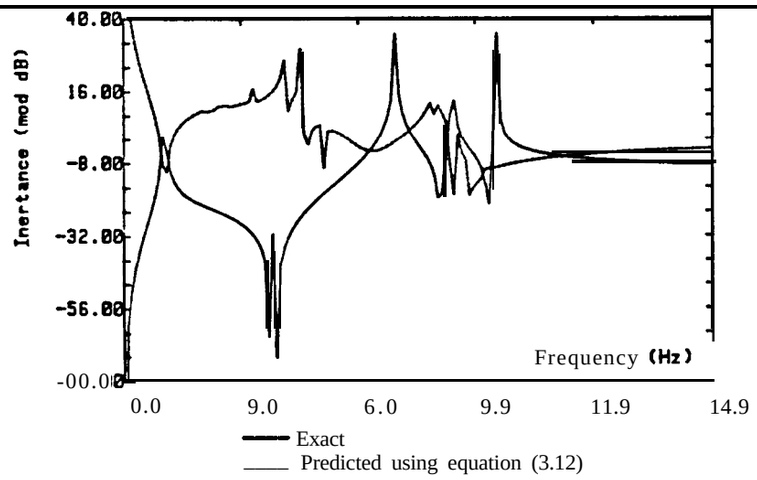

Fig. 5.13 - Predicted FRF (Point Inertance 5,5) using Algorithm 1

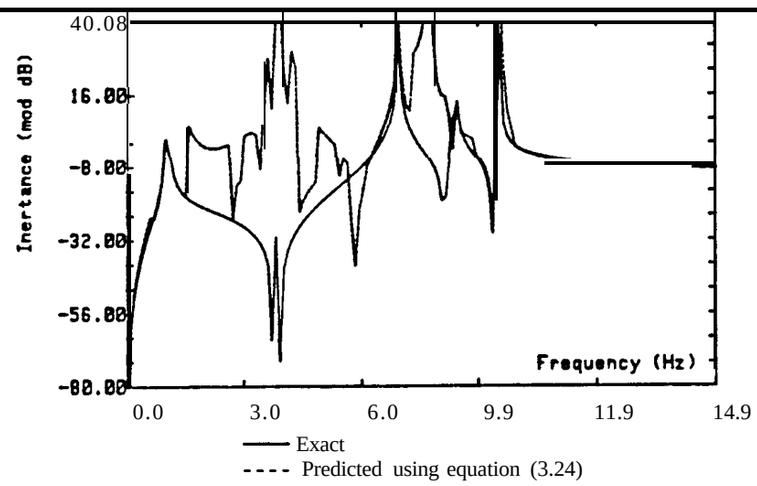

Fie. 5.14 - Predicted FRF Point Inertance 5.5) using Algorithm 3

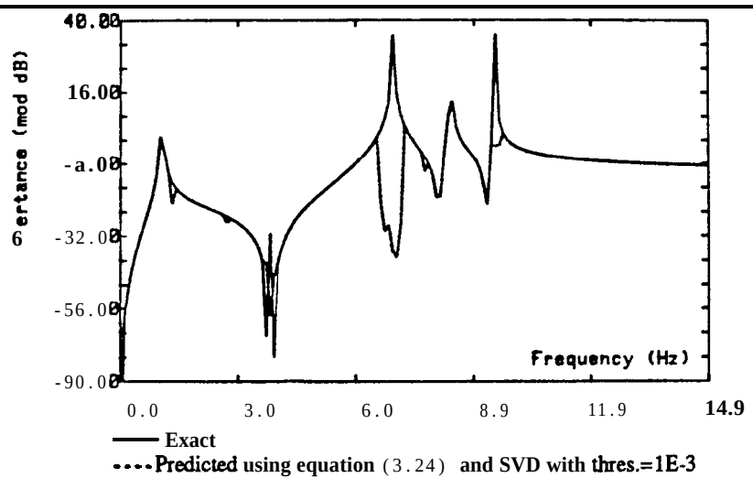

Fig. 5.15 - Predicted FRF (Point Inertance 5,5) using SVD

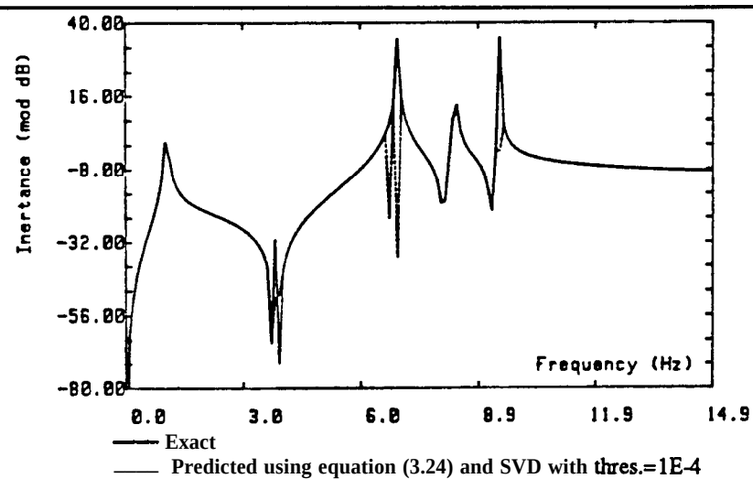

Fig. 5.16 - Predicted FRF (Point Inertance 5,5) using SVD

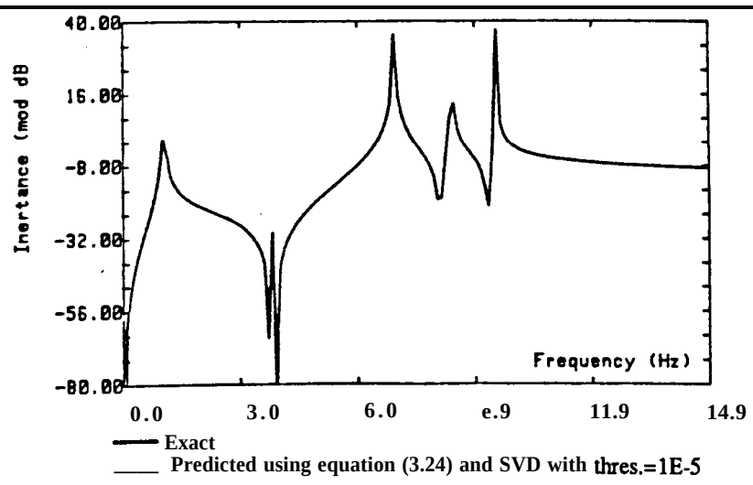

Fig. 5.17 - Predicted FRF (Point Inertance 5,5) using SVD

EXAMPLE IV - Subsystem 3 + Subsystem 4 (5 Connection Coordinates)

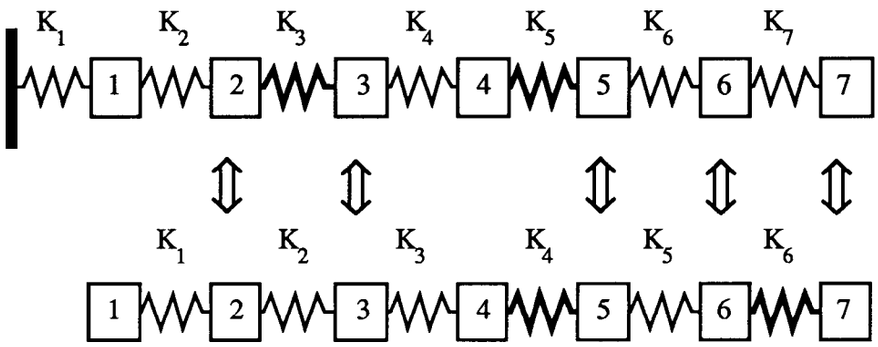

COUPLED **STRUCTURE**

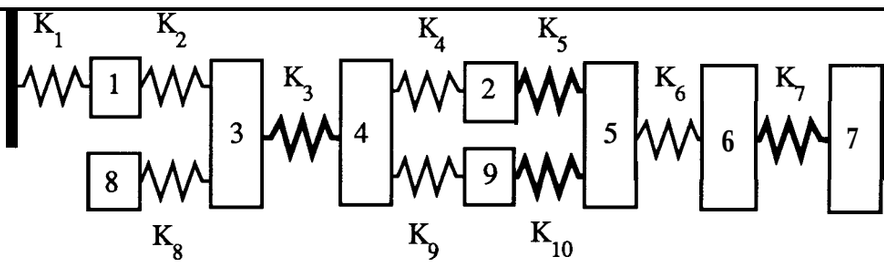

Fig. 5.18 - Subsystem 3 + Subsystem 4 (5 connection coordinates)

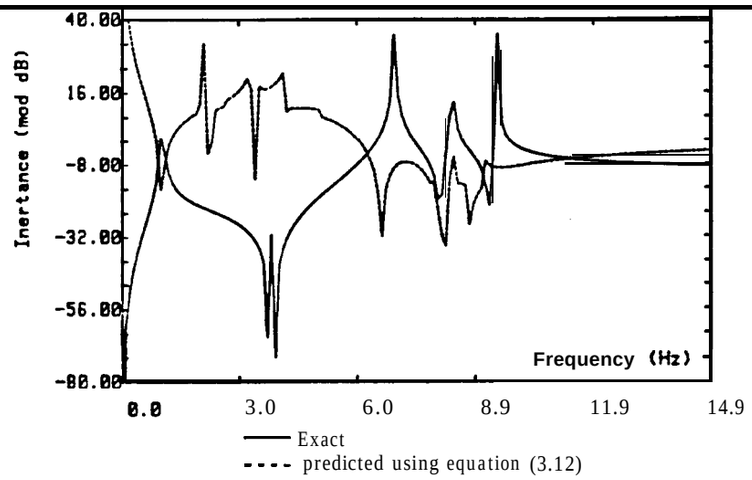

Fig. 5.19 - Predicted FRF (Point Inertance 2,2) using **Algorithm 1**

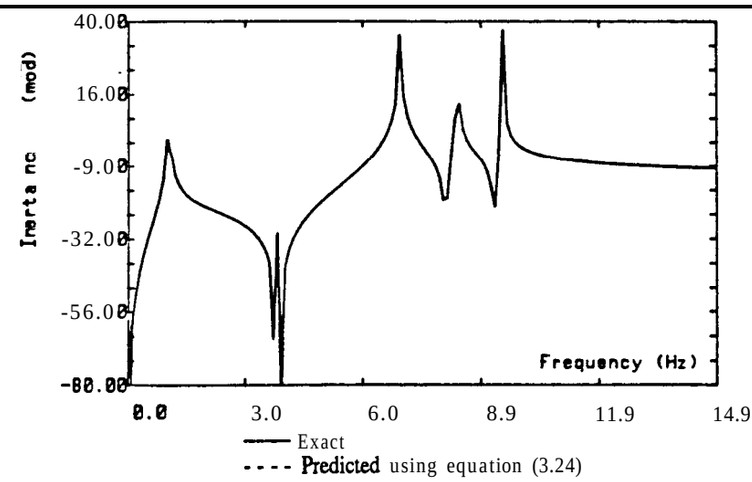

Fig. 5.20 - Predicted FRF (Point Inertance 2,2) using **Algorithm 3**

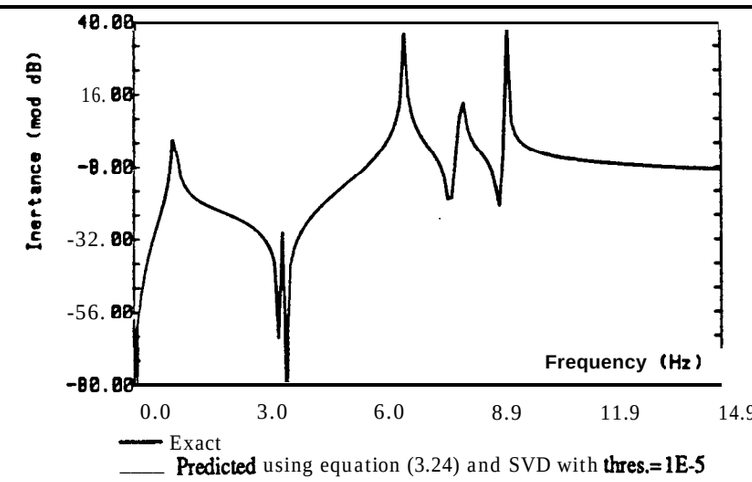

Fig. 5.21 - Predicted FRF (Point Inertance 2,2) using **SVD (SE-5)**

5.5.2 DISCUSSION OF RESULTS

The predicted FRFs of the coupled structures, used in examples I to IV, show that two possible alternatives are available to resolve the numerical difficulties associated with the inversion of singular or near-singular matrices caused by the existence of redundant coordinates at the interface region. It is also shown that the SVD technique must be used with care in terms of selecting the threshold to define the rank of a matrix which in most of the cases is associated with the error inherent to the data. In example III, a value of 10E-3 was initially assumed for u in terms of which δ is calculated (the threshold necessary to define the rank of a matrix as presented in equation (5.9)). The result was a poor prediction for the FRF of the coupled structure in the vicinity of each resonace frequency. When u was decreased to 10E-5, the accuracy of the predicted FRF was notably improved and in good agreement with the known exact FRF of the assembled structure. Similar results were obtained without using the SVD, provided the redundancy was adequately eliminated in the set of interface coordinates as shown in example IV - fig. 5.20.

5.6 CONCLUSIONS

The SVD technique proved to be a useful mathematical tool to be used during a coupling process involving subsystems both of which possessing redundant information (in terms of coordinates) at the interface region.

Additionally, it is shown that common inversion algorithms can still be used provided the redundancy in the connecting region is eliminated. For this purpose, a suitable algorithm

was devised to detect how many and which coordinates are redundant. This may be useful when a large degree of redundancy is present in a multi-point connected system. In such a case, the reduction operated in the initially specified connection matrix may be substantial. Hence, a less time-consuming coupling process is required, simultaneously preserving the accuracy of the final result.

6 EXPERIMENTAL DETERMINATION OF ROTATIONAL RESPONSES

6.1 INTRODUCTION

The dynamic analysis of a complex structure using the substructuring technique, requires knowledge of the dynamic characteristics of the constituent components. For some of these it is not feasible to make a theoretical model, and so their dynamic properties are often obtained using an experimental approach. Although in the case of theoretical modelling it is a common practice to consider the six possible coordinates at each point of interest on the model - three translations and three rotations - the limitations imposed by the currently available measurement techniques makes the consideration of all the six coordinates a very difficult task in practical situations. One of these is concerned to the measurement of the connection coordinates, since the inclusion or exclusion of one of those coordinates in the subsystem model will usually lead to erroneous predictions of the results for the assembled system. In the case of one or more component models being experimentally-derived, the validity of the coupling technique can be distorted by requiring the use of what **can be** measured, rather than what **ought** to be measured.

When the components are undergoing vibrations together in the assembly the mathematically-imposed constraint equations, which make use of the interface coordinates, should reflect as closely as possible the actual physical connections among all the components forming the whole structure.

Representation of the transmission of a moment between two components requires *either* the use of a set of two-connection points with a translational coordinate at each point *or* a single-connection point with only a rotational coordinate. The use of either of these coordinate sets depends mainly on the geometric and stiffness properties in the vicinity of the connecting region.

In spite of the fact that techniques for measuring translational responses are well established with the use of reliable and accurate transducers such as linear accelerometers, this is not the case for rotational responses. Although special angular transducers have been developed to sense rotations, they are not as accessible in terms of price and as accurate as the former ones. Additionally, in cases where the measurement of the FRF matrix elements requires both force and moment excitations, another difficulty is encountered since it is not easy to apply a pure moment excitation in practice. These considerations make hard the task of judging whether it is worth making the effort required for a precise measurement of rotational quantities, bearing in mind the errors introduced when they are neglected. Several investigators have faced the problem of measuring or calculating rotational responses and it is possible to say that two main approaches have been made to obtain the necessary information either direct or indirectly.

Recent work by Licht [25] and Rorrer et *al* [26] present results directly measured on the structures by making use of rotational transducers. The main drawbacks in this approach are the cost and corresponding accuracy associated with these transducers. The cross-sensitivity inherent to all piezoelectric transducers makes the rotational measurements being as accurate as pure is the rotation at a certain point on a structure, since they are sensitive to the simultaneous translational and rotational motions.

In the more classical approach, investigators have focused their attention on the estimation of the rotational information by making use of the translational data available from conventional accelerometers. Some of the related works by O'Callahan et al [85,86] and Smiley and Brinkman [87] made use of both analytical and experimental models to derive rotations by using expansion methods. However, in this thesis we shall assume that no

theoretical model is available and only the data measured on the structure can be used to determine the rotations. Following this route one main distinguish three main techniques.

i) - The exciting block technique.

This is also referred as mass additive technique and it is based on the measurement of accelerometer responses properly placed on an additional block which is attached as close as possible to the point (area) of interest on the test structure; the block is assumed to behave rigidly over the frequency range of interest (and, in the cases of quite heavy structures, to have negligible inertia effects). The relevant works presented by Smith [22], Sainsbury [23], Silva [88] and Ewins and Gleeson [24] have shown that it is possible to estimate accurate rotational response/force parameters, which the more susceptible functions to erroneous estimations are those related to moment excitations.

ii - The use of translational data from closely-spaced accelerometers.

This approach presents an advantage over the previous one, especially in the cases of slender or like beam components, since the mass and stiffness properties are not altered in the measurement region. This technique has been used by Sattinger [28] and Chen and Cherng [27] and suggests a practical alternative to the exciting block technique. It is based on the estimation of the rotational properties from spatial derivatives of the translational data which in turn are gathered from accelerometers placed on the structure at convenient distances from each other. By using a finite difference technique the necessary Response and Modal models can be generated from linear accelerations and force excitations only.

iii) - the use of translational data from a quasi-continuous line measurement.

With the advent of sophisticated scanning optical transducers, such those making use of laser beams, it is nowadays possible to measure rapidly the velocity response at different points along a line or over an area on the surface of a structure in a quasi-continuous way. This quasi-continuous definition of the displacement field for each mode, near a point of interest on the structure, permits a more precise calculation of the spatial derivatives, and

thus a better estimation of the rotational responses necessary to construct the required model to be used in a coupling process.

6.2 OBJECTIVE

The main objective in this chapter is the comparison of the rotational properties estimated from all the three aforementioned experimental techniques with those derived from theoretical models. Since two different coupling methods are of interest in this work - the Impedance and the Modal Coupling techniques - the comparison is made in terms of the corresponding subsystem model formats i.e., Response and Modal models.

In the first experimental case study they are all compared based on the derived or measured mode shapes i.e., only in terms of their Modal models. This is due to the fact that the laser measurement has been undertaken by exciting the structure (at the exciting block) with a shaker at each resonance, thus measuring the mode shapes. In the second experimental case study the sensitivity study is only focused on the techniques which make use of accelerometer measurements. This is the most likely situation encountered in industry and in the research laboratory, since sophisticated equipment such as the laser unit are not widely available due to its high cost. The two techniques (i) and (ii) are used in order to assess both Modal and Response models estimated from accelerometers suitably placed on two structures with those derived from the corresponding theoretical models. In these case-studies the gathered data are the FRFs related to the different measuring and hammer excitation points.

6.3 MEASUREMENT WITH ACCELEROMETERS

6.3.1 MEASUREMENT USING AN EXCITING BLOCK

The point Inertance matrix involving translational and rotational responses can be measured by attaching an exciting block equipped with two accelerometers. The exciting block technique is based on the work undertaken by Sainsbury [23] who developed different types of exciting blocks for both single and twin shaker excitations. Relying on the main conclusions of the multi-directional measurements in Sainsbury's work, the single-shaker technique was selected in the present work which requires a simpler set-up (when compared with the twin-shaker technique) yet gives fairly accurate results. The main disadvantage is that the data must be processed in order to obtain all the required point Inertances, but the same is true of the twin-shaker approach when the results are to be fully corrected for the exciting block inertia and impure excitation. Further studies in this area were undertaken by Gleeson [17] who used a single-shaker excitation technique, investigating the effects of accelerometer cross-sensitivity and the errors arising from base strain effects. The results predicted for a two-beam assembly showed that the errors in θ/M_θ mobilities caused the process to be very sensitive and inaccurate in the vicinity of the component resonance frequencies. Moreover, in the case of highly resonant beams, Ewins and Gleeson [24] concluded that it is preferable to derive two of the elements in the 4^{th} order point mobility matrix from the measurement of the remaining two, which are y/F_y and θ/F_y.

In the present work, vibration is confined to a single plane. Thus, only three of the six coordinates at each point are of concern - two translations and one rotation - and these, in turn, can be further reduced to one translation and one rotation if only flexural vibrations are of concern. Thus, the FRF matrix to be estimated which relates the responses to the excitations at point P, shown in figs. 6.1a-b, is

$$\begin{Bmatrix} y \\ \theta \end{Bmatrix} = [H]_{est} \begin{Bmatrix} F_y \\ M_\theta \end{Bmatrix} \quad \text{with} \quad [H]_{est} = \begin{bmatrix} H_{yy} & H_{y\theta} \\ H_{\theta y} & H_{\theta\theta} \end{bmatrix} \qquad (6.1)$$

Let us consider the two independent excitations which are applied to the beam (in two separate tests), as shown in figs. 6.1a and 6.1b,

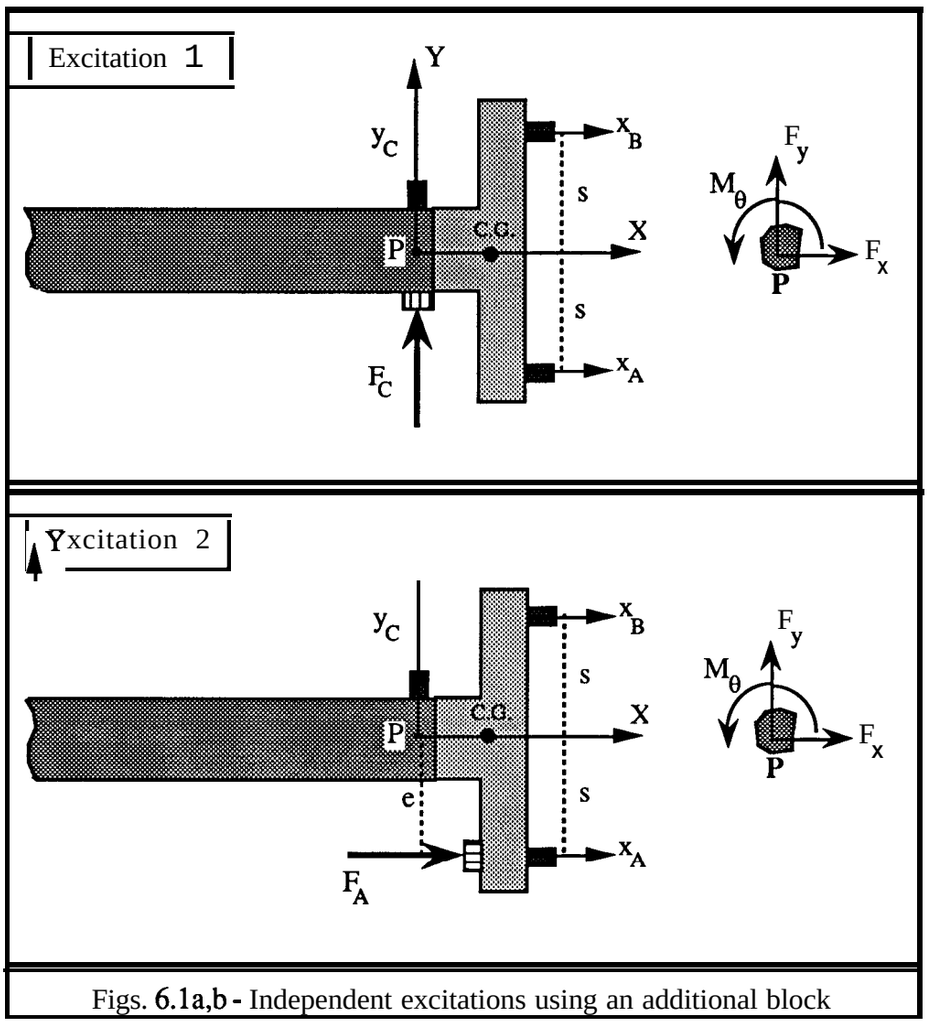

Figs. 6.1a,b - Independent excitations using an additional block

The kinematic relationships between the set of measured translational coordinates and the final set including a point translational and rotational coordinate are as follows,

$$\ddot{x}_A = \ddot{x}_{AT} + \ddot{x}_{AR} = \ddot{x}_{AT} + s\,\ddot{\theta}$$

$$\ddot{x}_B = \ddot{x}_{BT} + \ddot{x}_{BR} = \ddot{x}_{BT} - s\,\ddot{\theta}$$

.....

$$\ddot{x}_P = \frac{\ddot{x}_A + \ddot{x}_B}{2}$$

$$\ddot{y}_P = \ddot{y}_C \qquad (6.2)$$

$$\ddot{\theta}_P = \frac{\ddot{x}_A - \ddot{x}_B}{2s}$$

Since we are interested only in the transverse motion of the beam, the transformation matrix relating the measured and estimated responses is given as,

$$\begin{Bmatrix} \ddot{y}_P \\ \ddot{\theta}_P \end{Bmatrix} = [P] \begin{Bmatrix} \ddot{y}_C \\ \ddot{x}_A \\ \ddot{x}_B \end{Bmatrix} \quad \text{with} \quad [P] = \begin{bmatrix} 1 & 0 & 0 \\ 0 & \frac{1}{2s} & -\frac{1}{2s} \end{bmatrix} \tag{6.3}$$

The force and moment transmitted to point P due to the both excitation cases, provided the inertia properties of the block are neglected, is given as:

$$\begin{Bmatrix} F_y \\ M_\theta \end{Bmatrix} = [T] \begin{Bmatrix} F_C \\ F_A \end{Bmatrix} \quad \text{with} \quad [T] = \begin{bmatrix} 1 & 0 \\ 0 & e \end{bmatrix} \tag{6.4}$$

Should the inertia properties of the exciting block be taken into account, the transmitted forces are related to the applied forces as,

$$\begin{Bmatrix} F_y \\ M_\theta \end{Bmatrix} = [T] \begin{Bmatrix} F_C \\ F_A \end{Bmatrix} - [M][P] \begin{Bmatrix} \ddot{y}_C \\ \ddot{x}_A \\ \ddot{x}_B \end{Bmatrix} \quad \text{with} \quad [M] = \begin{bmatrix} m & mx_G \\ mx_G & J_p \end{bmatrix} \tag{6.5}$$

where the matrix $[M]$ reflects the inertia properties of the additional body.

The FRF matrix [HI,,,,, which is directly measured on the structure, possesses two columns each being obtained for one excitation case;

$$[H]_{meas} = \begin{bmatrix} \frac{\ddot{y}_C}{F_C} & \frac{\ddot{y}_C}{F_A} \\ \frac{\ddot{x}_A}{F_C} & \frac{\ddot{x}_A}{F_A} \\ \frac{\ddot{x}_B}{F_C} & \frac{\ddot{x}_B}{F_A} \end{bmatrix} \tag{6.6}$$

The FRF matrix to be derived $[H]_{est}$ is related to the measured FRF according to the following relationship:

$$[H]_{est} = [P][H]_{meas} \left[[T] - [M][P][H]_{meas} \right]^{-1} \tag{6.7}$$

The quantity $H_{\theta\theta}$ is difficult to estimate accurately, not least because of the problem of producing an input moment M_θ at point P. In such a case it is often preferable to derive the modal constants of that FRF ($H_{\theta\theta}$) from those of H_{yy} and $H_{\theta y}$, which are amenable to reasonably accurate measurement, as suggested by Ewins and Gleeson [24], although there is no possibility of including the residual flexibility effects of the out-of-range modes.

6.3.2 MEASUREMENT WITHOUT AN EXCITING BLOCK

In this case, two or three accelerometers are placed on the structure, one being attached as close as possible to the point P where the rotation is to be estimated, as shown in fig.6.2.

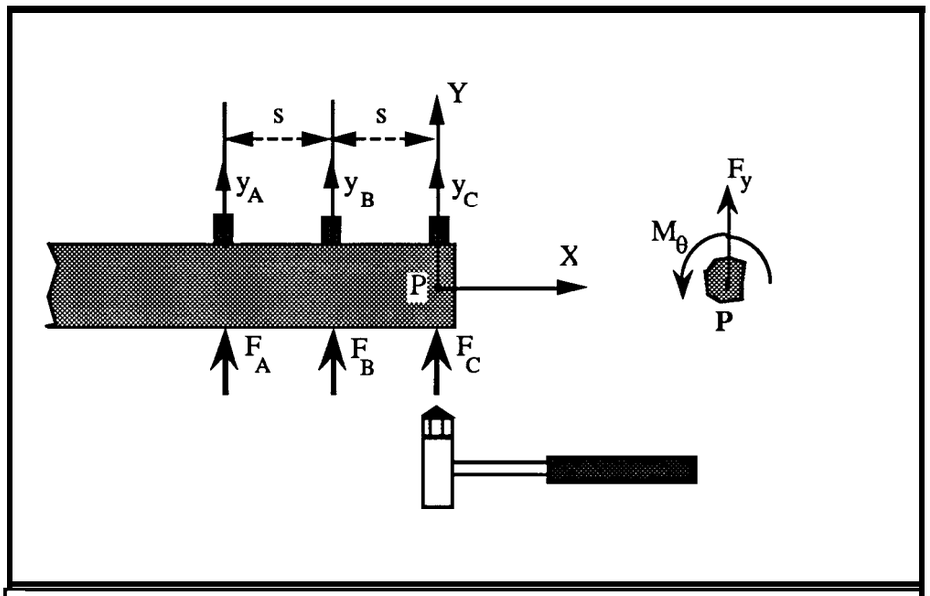

Fig. 6.2 - Set-up using three closely-spaced accelerometers

By measuring a set of translational quantities at a limited number of points only, it is possible to express approximately the rotational responses in terms of those translations, as presented by Chen and Chemg [27] and Sattinger [28].

In the case where a FRF coupling technique is proposed, calculation of the rotational

may result since differences between quantities are considered which are very much smaller than the quantities themselves and the small relative errors in the measured data may result in a large error in the estimated response. However, an alternative way is presented in this work whereby the explicit calculation of the rotational FRFs is not necessary, should a Modal coupling technique be used. In this case, the estimated Modal model is calculated from the Modal model referred to the measured coordinates.The two possible estimations - the first and second order - are presented next for both Response and Modal models.

6.3.2.1 First Order Approximation - two-point measurement

a) The Response Model estimation

The set of FRFs necessary to construct the measured Response model are;

$$[H]_{meas} = \begin{bmatrix} \frac{\ddot{y}_B}{F_B} & \frac{\ddot{y}_B}{F_C} \\ \frac{\ddot{y}_C}{F_B} & \frac{\ddot{y}_C}{F_C} \end{bmatrix} = \begin{bmatrix} H_{BB} & H_{BC} \\ H_{CB} & H_{CC} \end{bmatrix} \qquad (6.8)$$

At the connection point P the responses and excitations are related as,

$$\begin{Bmatrix} y \\ \theta \end{Bmatrix} = [H]_{est} \begin{Bmatrix} F_y \\ M_\theta \end{Bmatrix} \quad \text{with} \quad [H]_{est} = \begin{bmatrix} H_{yy} & H_{y\theta} \\ H_{\theta y} & H_{\theta\theta} \end{bmatrix} \qquad (6.9)$$

The applied forces and measured responses should be equivalent to the set of forces and coordinates that is assumed to exist at point P, which implies that;

$$[H]_{est} = [T]\ [H]_{meas}\ [T]^T \quad \text{with} \quad [T] = \begin{bmatrix} 0 & 1 \\ -\frac{1}{s} & \frac{1}{s} \end{bmatrix} \qquad (6.10)$$

which gives the estimated FRFs necessary to construct the Response model as follows,

$$\begin{aligned} H_{YY} &= H_{CC} \\ H_{y\theta} &= \frac{1}{s}(H_{CC} - H_{CB}) \\ H_{\theta y} &= \frac{1}{s}(H_{CC} - H_{BC}) \\ H_{\theta\theta} &= \frac{1}{s^2}(H_{CC} + H_{BB} - H_{CB} - H_{BC}) \end{aligned} \qquad (6.11)$$

b) The Modal Model estimation

As presented in the introduction chapter, the Response model is related to the Modal model as follows,

$$[H] = [\Phi]\,[\Lambda]^{-1}\,[\Phi]^{T} \qquad (6.12)$$

The Modal model referred to the measured coordinates can be derived from a row (or column) of the measured FRF matrix over a selected frequency range encompassing m_k modes. The information related to the effects of the out-of-range modes can be synthesised in a Residual matrix $[H_{Resid.}]$. By assuming this, the measured Response and Modal models are related by,

$$[H]_{meas} = [\Phi_k]_{meas}\,[\Lambda_k]^{-1}\,[\Phi_k]^{T}_{meas} + [H_{Resid.}]_{meas} \qquad (6.13)$$

with

$$[\Phi_k]_{meas} = \begin{bmatrix} \Phi_{Bk} \\ \Phi_{Ck} \end{bmatrix} \quad \text{and}$$

$$[H_{Resid.}]_{meas} = \begin{bmatrix} [H_{BB}]_{Resid} & [H_{BC}]_{Resid} \\ [H_{CB}]_{Resid} & [H_{CC}]_{Resid} \end{bmatrix}$$

The estimated Modal model and Residual Flexibility matrix can be related to the corresponding measured Modal model and Residual Flexibility by using the transformation matrix (6.10),

$$[\Phi_k]_{est.} = \begin{bmatrix} \Phi_{y} \\ \Phi_{\theta} \end{bmatrix} = [T]\,[\Phi_k]_{meas} \qquad (6.15)$$

$$[H_{Resid}]_{est.} = \begin{bmatrix} [H_{yy}]_{Resid} & [H_{y\theta}]_{Resid} \\ [H_{\theta y}]_{Resid} & [H_{\theta\theta}]_{Resid} \end{bmatrix} = [T]\,[H_{Resid.}]_{meas}\,[T]^{T} \qquad (6.16)$$

6.3.2.2 Second Order Approximation - three-point measurement

a) The Response Model estimation

In this case three points are used and it is necessary to measure at least six FRFs (this corresponding to the assumption that the measured matrix is symmetric), as presented next:

$$[H]_{meas} = \begin{bmatrix} \frac{\ddot{y}_A}{F_A} & sym & sym \\ \frac{\ddot{y}_B}{F_A} & \frac{\ddot{y}_B}{F_B} & sym \\ \frac{\ddot{y}_C}{F_A} & \frac{\ddot{y}_C}{F_B} & \frac{\ddot{y}_C}{F_C} \end{bmatrix} = \begin{bmatrix} H_{AA} & sym & sym \\ H_{BA} & H_{BB} & sym \\ H_{CA} & H_{CB} & H_{CC} \end{bmatrix} \qquad (6.17)$$

and the corresponding estimated matrix is,

$$\begin{bmatrix} H_{YY} & H_{y\theta} \\ H_{\theta y} & H_{\theta\theta} \end{bmatrix} = [T]\,[H]_{meas}\,[T]^T \text{ with } [T] = \begin{bmatrix} 0 & 0 & 1 \\ \frac{1}{2s} & \frac{4}{-2s} & \frac{3}{2s} \end{bmatrix} \qquad (6.18)$$

The final values corresponding to the estimated FRFs are given as,

$$\begin{aligned} H_{YY} &= H_{CC} \\ H_{y\theta} = H_{\theta y} &= \frac{1}{2s}(3H_{CC} - 4H_{CB} + H_{CA}) \\ H_{\theta\theta} &= \frac{1}{4s^2}(9H_{CC} - 24H_{CB} + 6H_{CA} - 16H_{BB} - 8H_{BA} + H_{AA}) \end{aligned} \qquad (6.19)$$

b) The Modal Model estimation

The Modal model referred to the translational and rotational coordinates at point P can be estimated by using the same procedure presented for the first order approximation, but this time requiring the second order transformation matrix [T] (vide eq. 6.18).

6.4 MEASUREMENT USING A SCANNING LASER SYSTEM

6.4.1 INTRODUCTION

An optical technique is described for measuring the dynamic response of a structure undergoing harmonic vibrations. It is essentially a laser Doppler velocimeter which is a non-contacting optical sensing device for accurately measuring point velocities [89]. The non-contact nature of the instrument makes it particularly attractive for the use on either light-weight structures where the measurement interaction must be minimised and it is possible to measure the extent to which the vibrating properties of a structure are affected by the physical contact of the accelerometers, or whenever it is impracticable to attach any transducer to the structure, for instance in the case of hot surfaces. In addition to this advantage over accelerometers, it is possible to measure a quasi-continuous line or area on the structure, thus reducing the degree of incompleteness in terms of coordinates, which sometimes is a disadvantage of experimentally-derived models when compared with the theoretical ones.

6.4.2 BASIC PRINCIPLES OF LASER DOPPLER VELOCIMETRY

The laser Doppler velocimeter is based on the measurement of the Doppler shift of the frequency of a laser light beam reflected by a moving object. When a beam of light strikes a moving surface, the reflected beam is frequency shifted with reference to the incident one by an amount that is proportional to the velocity of the reflective surface. This frequency shift is called the Doppler shift and depends on the wavelength of the the incident light as well as the positioning of the laser source, the scattering surface and the observer. The ratio of the Doppler shift to the incident light frequency is of the order of the ratio of the velocity of the moving surface to the velocity of the light. Thus, for velocities of the order of few meters per second, the change in frequency of the light is only a few parts per billion. This change, which is the difference in frequency between

6.4 MEASUREMENT USING A SCANNING LASER SYSTEM

6.4.1 INTRODUCTION

An optical technique is described for measuring the dynamic response of a structure undergoing harmonic vibrations. It is essentially a laser Doppler velocimeter which is a non-contacting optical sensing device for accurately measuring point velocities [89]. The non-contact nature of the instrument makes it particularly attractive for the use on either light-weight structures where the measurement interaction must be minimised and it is possible to measure the extent to which the vibrating properties of a structure are affected by the physical contact of the accelerometers, or whenever it is impracticable to attach any transducer to the structure, for instance in the case of hot surfaces. In addition to this advantage over accelerometers, it is possible to measure a quasi-continuous line or area on the structure, thus reducing the degree of incompleteness in terms of coordinates, which sometimes is a disadvantage of experimentally-derived models when compared with the theoretical ones.

6.4.2 BASIC PRINCIPLES OF LASER DOPPLER VELOCIMETRY

The laser Doppler velocimeter is based on the measurement of the Doppler shift of the frequency of a laser light beam reflected by a moving object. When a beam of light strikes a moving surface, the reflected beam is frequency shifted with reference to the incident one by an amount that is proportional to the velocity of the reflective surface. This frequency shift is called the Doppler shift and depends on the wavelength of the the incident light as well as the positioning of the laser source, the scattering surface and the observer. The ratio of the Doppler shift to the incident light frequency is of the order of the ratio of the velocity of the moving surface to the velocity of the light. Thus, for velocities of the order of few meters per second, the change in frequency of the light is only a few parts per billion. This change, which is the difference in frequency between

the incident and scattered signals, can be measured by optically combining them to produce an easily measured difference signal at the Doppler frequency.

The vibration imager shown schematically in fig. 6.3 was developed by Ometron Plc. and is based on the Michelson interferometer [90]. The signal and reference beams are recombined in such a way that they can constructively or destructively interfere with one another depending upon the difference between their optical path lengths. The laser beam reflected back along the same path re-enters the optical unit: if the test part moves at a constant velocity, the intensity of the recombined beam oscillates at a uniform frequency, one cycle corresponding to a surface movement of $\lambda/2$, where λ is 0.633 x 10^{-6} m, equivalent to the wavelength of the laser. The relationship between the surface velocity v along the line of sight and the frequency Fd of the oscillation is v = Fd $\lambda/2$ = 0.3164 x 10-6 m/s.

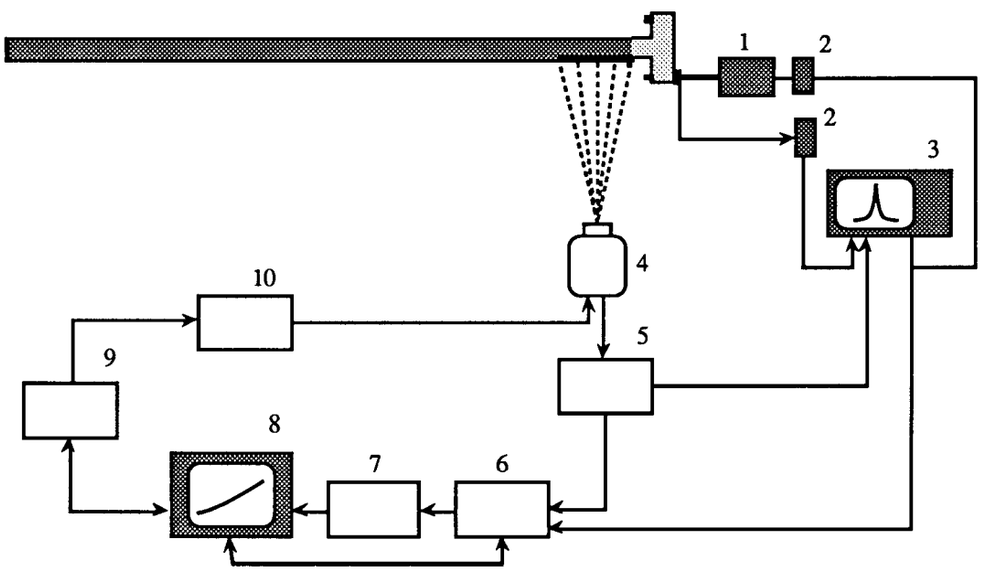

1 - Shaker
2 - Amplifier
3 - F.F.T. Analyser
4 - Scan + Optical unit
5 - Analogue processor
6 - Lock-in amplifier
7 - A/D converter
8 - Post-processing and computer display
9 - Scan control - computer
10 - D/A converter

Fig. 6.3 - Experimental set-up for the laser measurement

6.4.3 OPERATION

The velocity signal from the analog processor passes directly into the lock-in amplifier. An electronic reference signal is taken from the signal generator driving the vibrating structure. This reference signal at the vibration frequency is correlated with the velocity signal by a lock-in amplifier, resulting in information on the phase and amplitude of vibration of interest.

The operator can select either a single-point or a scan measurement mode. In the former, the operator can measure the velocity at different points on the structure; these are chosen by moving via a mouse or handset the laser spot across the surface of interest by virtue of computer controlled mirrors placed in the laser path. The vibration imager can therefore be used as if it was a movable non-contact transducer and in this particular mode of operation, the scattered signal can be intercepted prior to entering the lock-in amplifier and input to an F.F.T. analyser permitting the measurement of a FRF over a certain frequency range. In the second mode of operation - the scanning mode, which is carried out upon the same frequency of the reference signal - the operator can choose to measure and display any of the following outputs from the lock-in amplifier:

i) - the in-phase RMS vibration amplitude (X)

ii) - the quadrature RMS vibration amplitude (Y)

iii) - the absolute RMS magnitude $R = \sqrt{X^2+Y^2}$

iv) - the phase angle variations between the reference and velocity signals

Data are presented on a monitor in various formats; colour-filled grids, colour-filled contours, isometric plots and line plots. An interrogating cursor moves over the screen synchronously with the laser spot in order to identify locations on the structure of interesting features on the display.

6.4.4 DATA ANALYSIS

The data analysis technique is based on a curve-fitting algorithm, especially developed during this work, which makes use of the instantaneous velocity measured at specific points on the structure. By fitting the measured data with a polynomial function, the rotational quantity is easily calculated by differentiating the corresponding function at any measured point.

6.5 EXPERIMENTAL CASE STUDY I

6.51 STRUCTURE No. 1 - Long Beam + Exciting Block

The test structure used consists of a steel straight beam with an uniform rectangular cross-section shown in fig. 6.4.

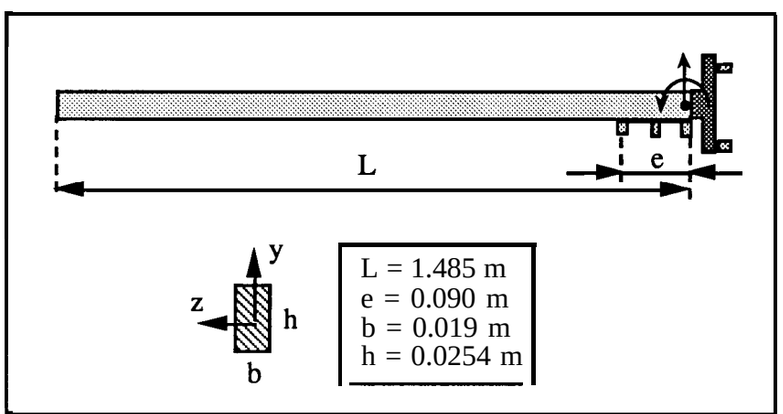

Fig. 6.4 - Beam + exciting block + 3 closely-spaced accel.

The point rotational response of interest is at one end of the beam, which is supposed to be subsequently connected to another component. An aluminium block is attached to the end of the beam, thereby providing the means for measuring rotational responses using accelerometers as well as for applying the necessary torque excitation. In order to make possible a comparison of all the results obtained under the same conditions in all the measuring techniques involved in this work, the test structure is assumed to be formed by the beam and the exciting block together. The main reason for this assumption is due to the fact that for the specific case of the laser measurement the structure was excited

through the aluminium block, at the corresponding composite structure's resonance frequencies.

6.5.2 MEASUREMENT - SHAKER TEST

The last 90 mm close to one of the ends of the beam was taken as the total length for the scanning laser line measurement (as shown in fig. 6.4). A light-weight B&K accelerometer type 4393 was placed at one of the line ends to provide a means of normalising the measured velocities with the laser, thus enabling a correct comparison between laser and accelerometer quantities.The structure was initially excited with a shaker via the exciting block over a frequency range O-800 Hz using a pseudo-random signal and the response signals were measured either with the accelerometer or with the laser focused on it, being the FRF processed with a B&K 2034 analyser. The two curves are plotted together in fig. 6.5 after a differentiation of the laser measured FRF to yield Inertance

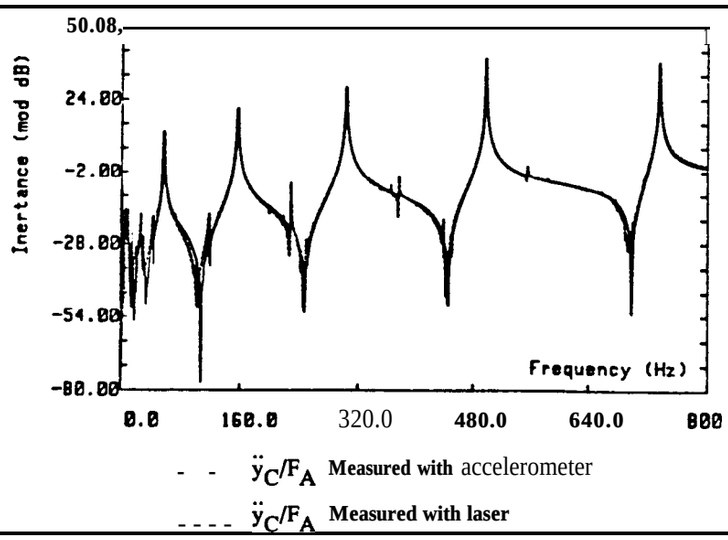

Fig. 6.5 - Measured FRFs using accelerometer and laser

This introductory test has provided a FRF from which five natural frequencies could be identified. At each of these frequencies, a sinusoidal excitation was applied to the structure, and the laser beam was scanned over the entire line. At a second stage, in order to gather data with accelerometers, pseudo-random excitations were applied to the test

component and for each of them the FRFs were measured for different positions of the accelerometer.

6.5.3 ESTIMATION OF MODAL MODELS

The velocity pattern for each of the modes was measured directly with the laser equipment. However, the use of three accelerometers equi-spaced over the entire line of measurement allows the derivation of the modal model only referred to the three equi-spaced coordinates. The mode shapes were also derived from the theoretical model, shown in fig. 6.6, constructed by using 30 undamped Timoshenko beam elements and a rigid mass simulating the inertia properties of the exciting block, this being one of the facilities available in the computer program COUPLE [70].

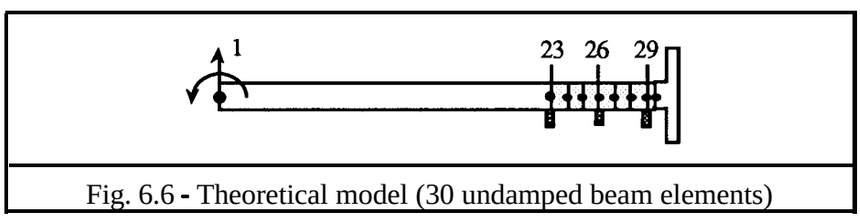

Fig. 6.6 - Theoretical model (30 undamped beam elements)

The pattern of each mode normalised to the maximum amplitude and obtained using the three different procedures are presented in figs. 6.7 a-e).

Each of the line data measured with the laser system has to be subsequently fitted with a polynomial function, the degree depending on the curvature of each mode shape. In the first mode occurring at 57 Hz the measured curve presented some ‘drop-outs’ which could hardly be avoided using different values for the sample time and time constant in the lock-in amplifier (this seems to be an important limitation of the equipment in the low frequency range). The corresponding bad measured points were then rejected during the curve-fitting process, since those responses are not expected on a continuous vibrating structure. Two of the fitted curves for mode nos. 1 and 5 are presented in fig. 6.8.

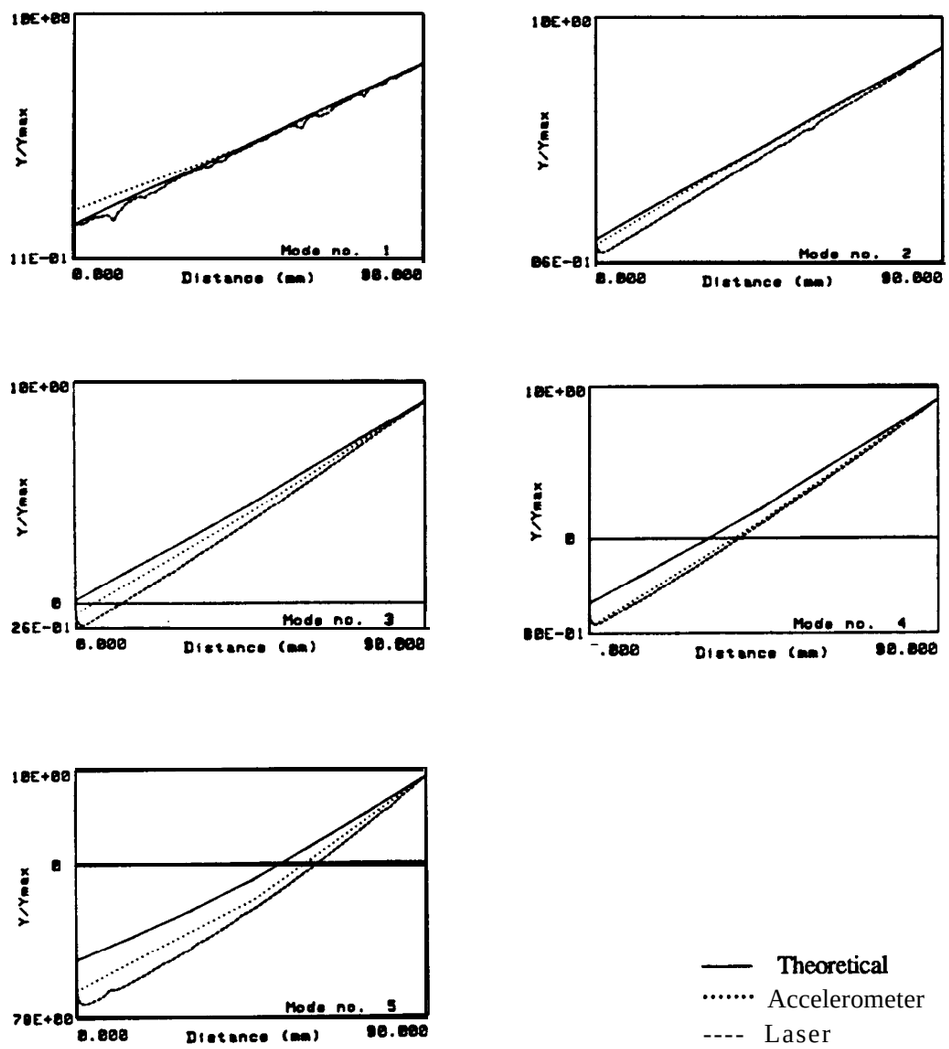

Fig. 6.7 - Mode shapes (90mm at the end of beam) **measured with** accelerometer and laser and derived **from** the **theoretical** model

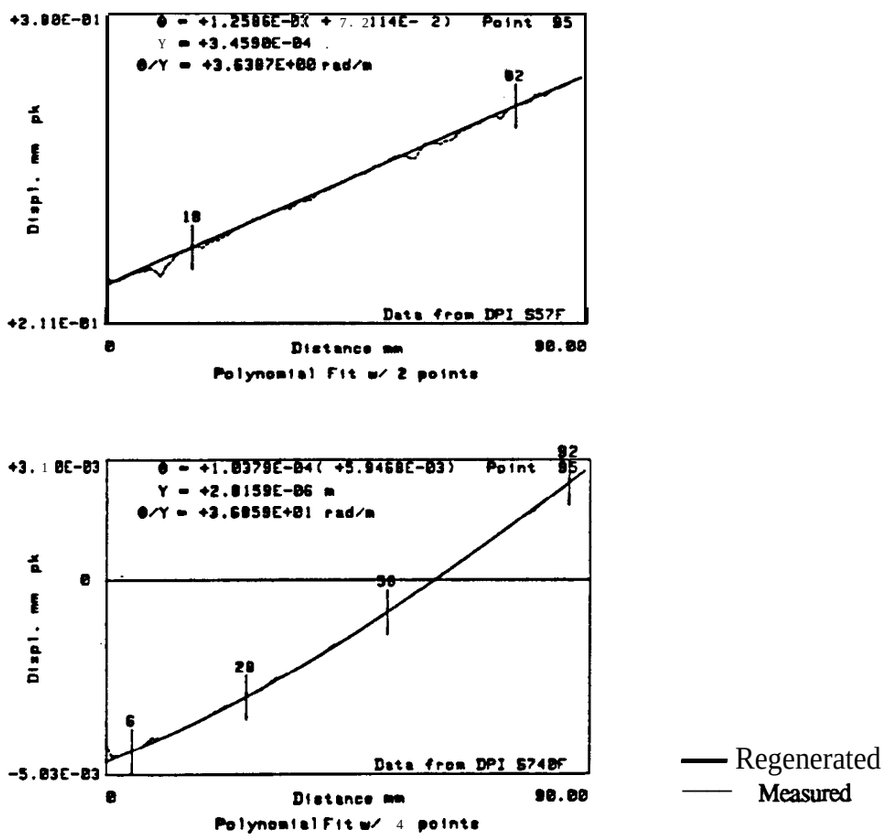

Fig. **6.8** - Curve-fitting of mode **1** (degree 1 polyn.) and 5 (degree **3** polyn.)

In the procedures using accelerometer data (linear **FRFs),** the rotational **FRFs** need to be explicitly calculated and the modes identified in order to obtain the rotational amplitudes of the mode shapes referred to the end coordinates. The rotational **FRFs** related to $\frac{y}{M}$ and $\frac{\theta}{M}$ are calculated using the block and three accelerometer approaches, as shown next in fig. 6.9 and fig. 6.10, respectively.

The amplitudes of the rotations derived from all the procedures are presented in table 6.1 and the relative errors in graph of fig. 6.11.

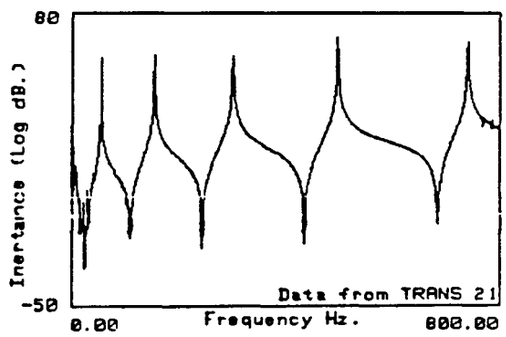

Fig. 6.9 - $\frac{y}{M}$FRF using three accelerometers

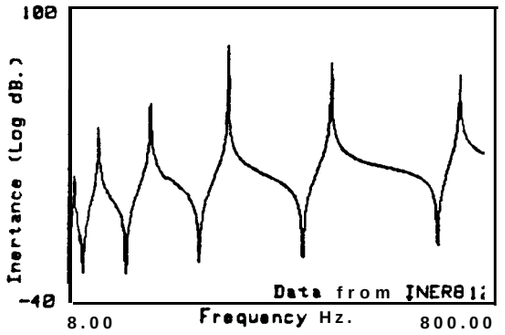

Fig. 6.10 a) - $\frac{y}{M}$FRF using exciting block

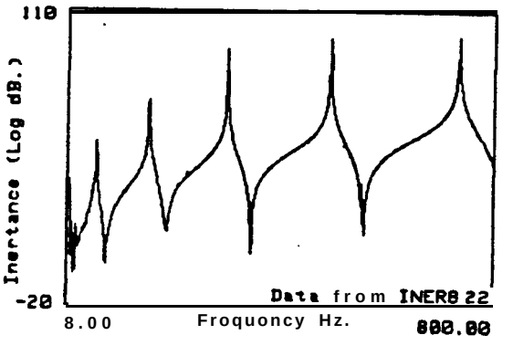

Fig. 6.10 b) - $\frac{\theta}{M}$FRF using exciting block

Table 6.1 - Mass normalised rotational amplitudes of the first 5 flexural modes

Modes	Freq.(Hz)	Theory	Laser	Trans.	Block
1	57	2.529	2.451	2.550	2.409
2	156	4.267	4.303	4.297	4.380
3	304	5.983	6.387	6.028	6.052
4	500	7.775	8.486	7.556	8.122
5	741	9.621	10.808	9.159	10.060

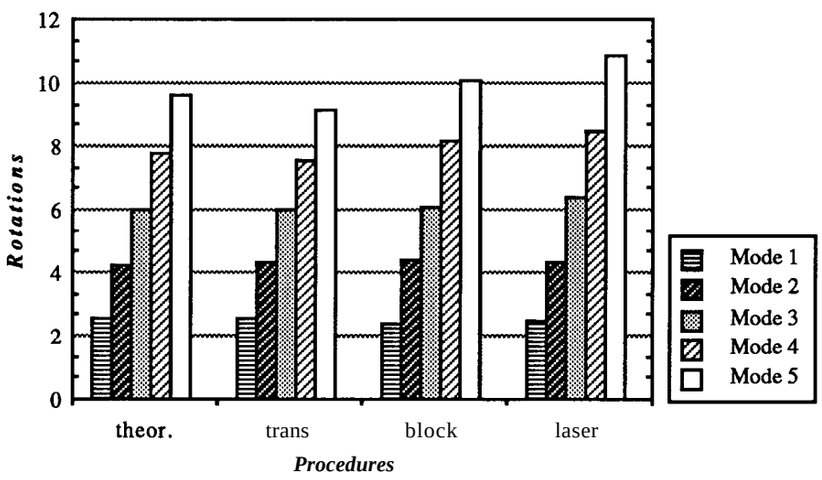

Fig. 6.11- Mass normalised rotational amplitudes of mode shapes

6.6 EXPERIMENTAL CASE STUDY II

6.6.1 STRUCTURES No. 2 and 3 - Long Beam (LB) and Short Beam (SB)

The test structures consist of two straight steel beams shown in fig. 6.12 with a uniform rectangular cross-section. The point rotational response of interest for each beam is selected to be at one of the ends, which is supposed to be subsequently connected to the other one. An aluminium block has been attached at the end of each beam to provide one of the means for measuring the rotational responses using accelerometers, as well as to apply the necessary torque excitation.

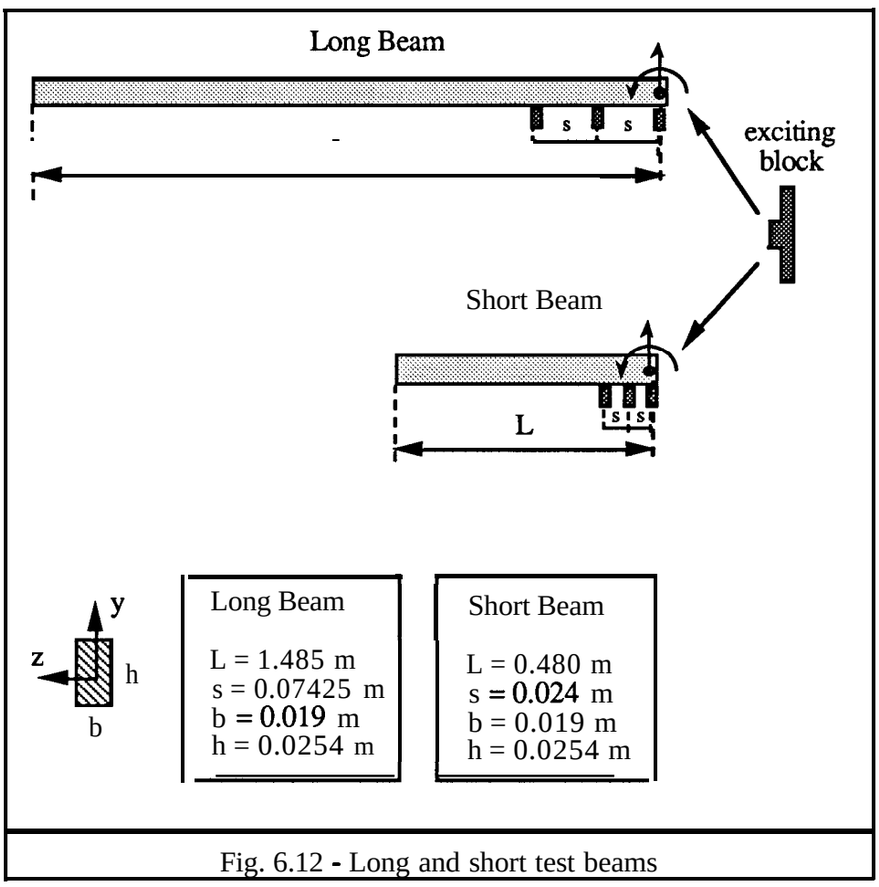

Fig. 6.12 - Long and short test beams

6.6.2 MEASUREMENT - HAMMER TEST

In this case study a hammer excitation was selected in an attempt to obtain as consistent a model as possible, seeking to overcome the effects of moving the additional mass of the force transducer. The possible inconsistency is only due to the different places where the light-weight accelerometer is attached, mainly for the higher modes. Both techniques (i) and (ii) previously described in 6.3.1 and 6.3.2 are of interest, and at this time the exciting-block technique was applied with the subsequent cancellation of the added mass. The frequency ranges for each beam were selected as,

Long Beam - (O-800 Hz) encompassing 5 in-plane flexural modes

Short Beam - (O-3200 Hz) encompassing 3 in-plane flexural modes

In order to perform a sensitivity study (mainly for technique (ii)), the first and second order approximations to estimate the rotational properties were applied by using the translational data from the accelerometers placed apart from each other by a distance s, which quantity was varied between 5% to 20% of the total length of the two beams.

A section corresponding to the end 20% of the total length of a free-free beam is presented next in fig. 6.13, showing the corresponding segment of the first five ideal mode shapes derived from an analytical solution presented by Bishop and Johnson [4],

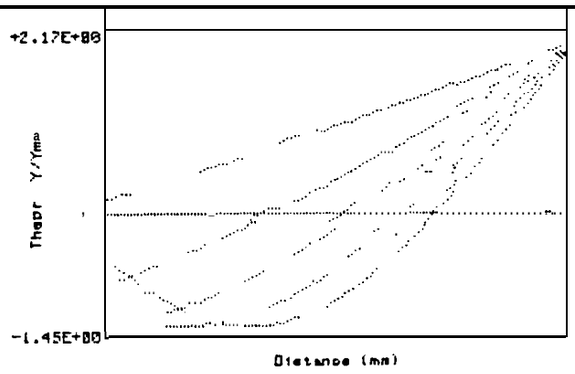

Fig. 6.13 - First 5 flexural modes of a free-free beam (segment corresponding to the end 20% of total length)

6.6.3 ESTIMATION OF MODAL AND RESPONSE MODELS

The first- and second-order estimations of the Response and Modal models were undertaken according to five procedures named and summarised in the following table;

Table 6.2 - Procedures to estimate Response and Modal models

Procedure	Name	No. Points	Distance (d)	d/L
1	3PS	3	S	0.05
2	3P2S	3	2s	0.1
3	2PS	2	S	0.05
4	2P2S	2	2s	0.1
5	2P4S	2	4S	0.2

One can consider two main routes to achieve the desired model whose properties are referred to the connecting coordinates. These two routes will lead either to a Response model to be used in a FRF coupling technique, or to a Modal model which is the required format subsystem data for Modal coupling techniques. From the measurement viewpoint, the possible routes are sketched in the following diagram,

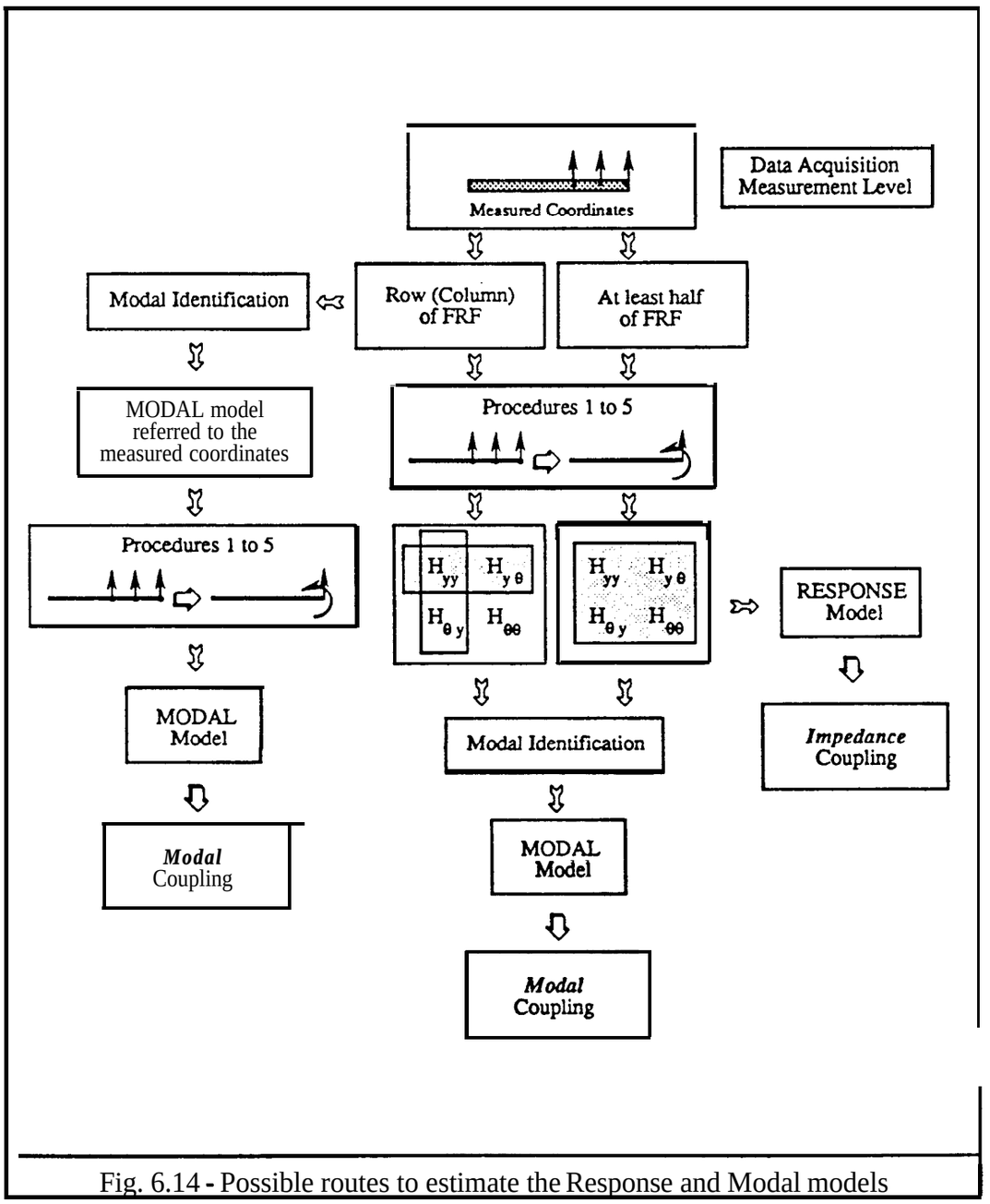

Fig. 6.14 - Possible routes to estimate the Response and Modal models

Estimation of Response Models - the Impedance route

As shown in sections 6.3.2.1 and 6.3.2.2, it is possible to estimate both $H_{y\theta}$ and $H_{\theta\theta}$ from the measured translational data (which includes H_{yy}). By using the block approach and the procedures presented in table 6.2 the Response model of each beam has been estimated, whose $\frac{Y}{M}$ and $\frac{\theta}{M}$ FRFs are shown in figs. 6.15 to 6.17.

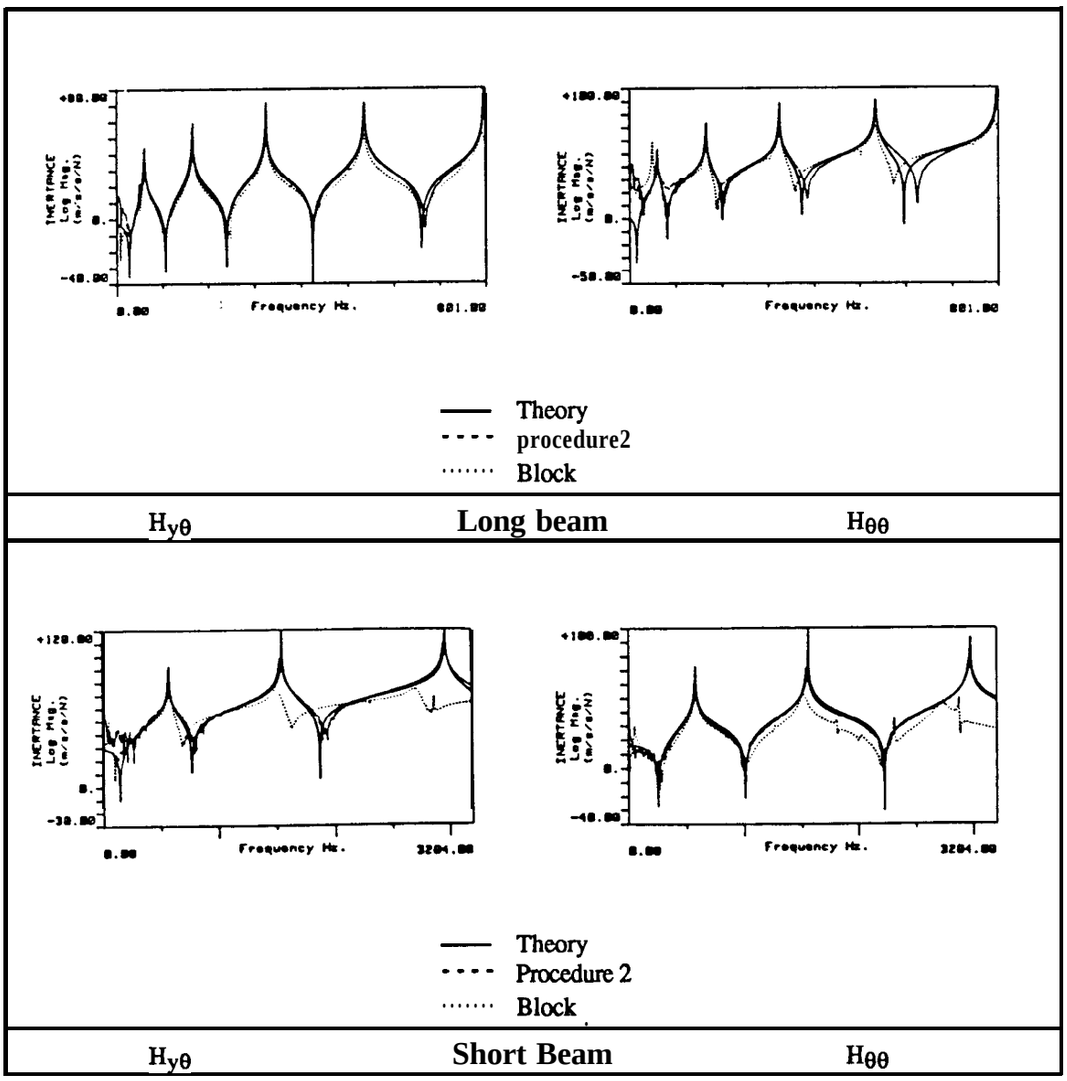

Fig. 6.15 - Theoretical versus estimated using procedure 2 and exciting block

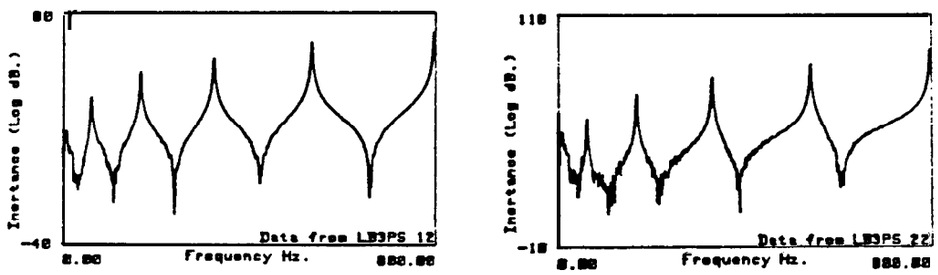

$H_{y\theta}$ **Procedure 1** - 3 accel. dist.= 5% of L $H_{\theta\theta}$

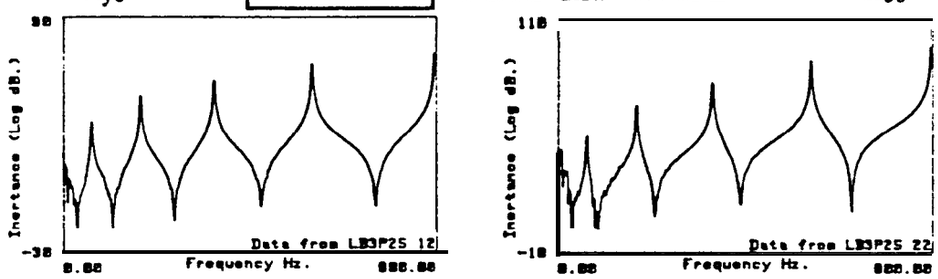

$H_{y\theta}$ **Procedure 2** - 3 accel. dist.= 10% of L $H_{\theta\theta}$

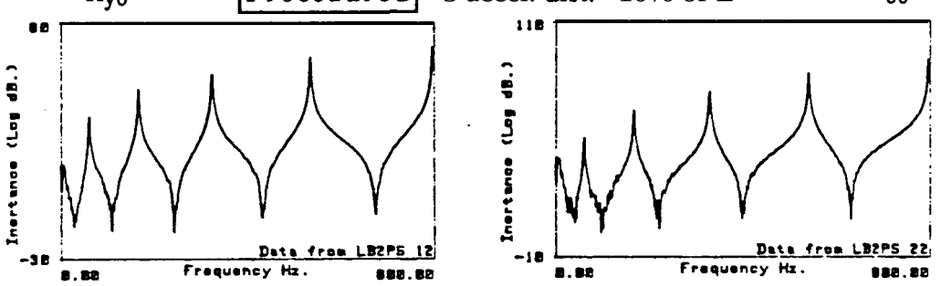

$H_{y\theta}$ **Procedure 3** - 2 accel. dist.= 5% of L $H_{\theta\theta}$

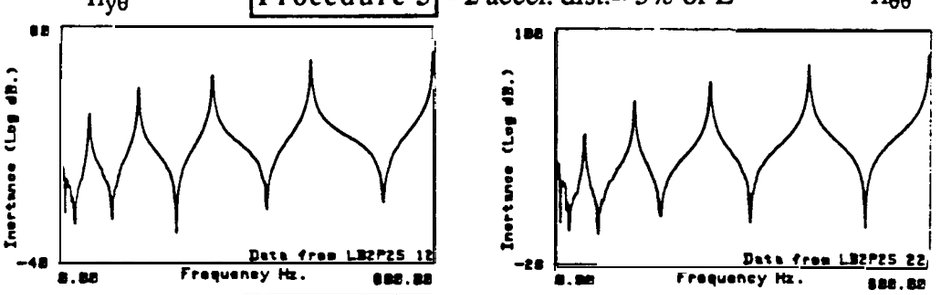

$H_{y\theta}$ **Procedure 4** - 2 accel. dist.= 10% of L $H_{\theta\theta}$

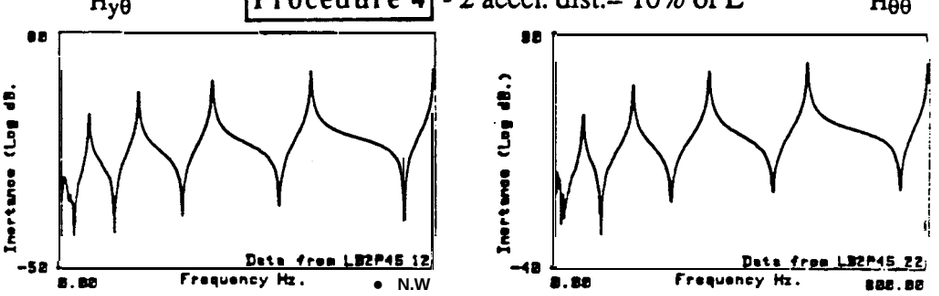

$H_{y\theta}$ **Procedure 5** - 2 accel. dist.= 20% of L $H_{\theta\theta}$

Fig. 6.16 Long Beam estimated FRFs using closely spaced accelerometers

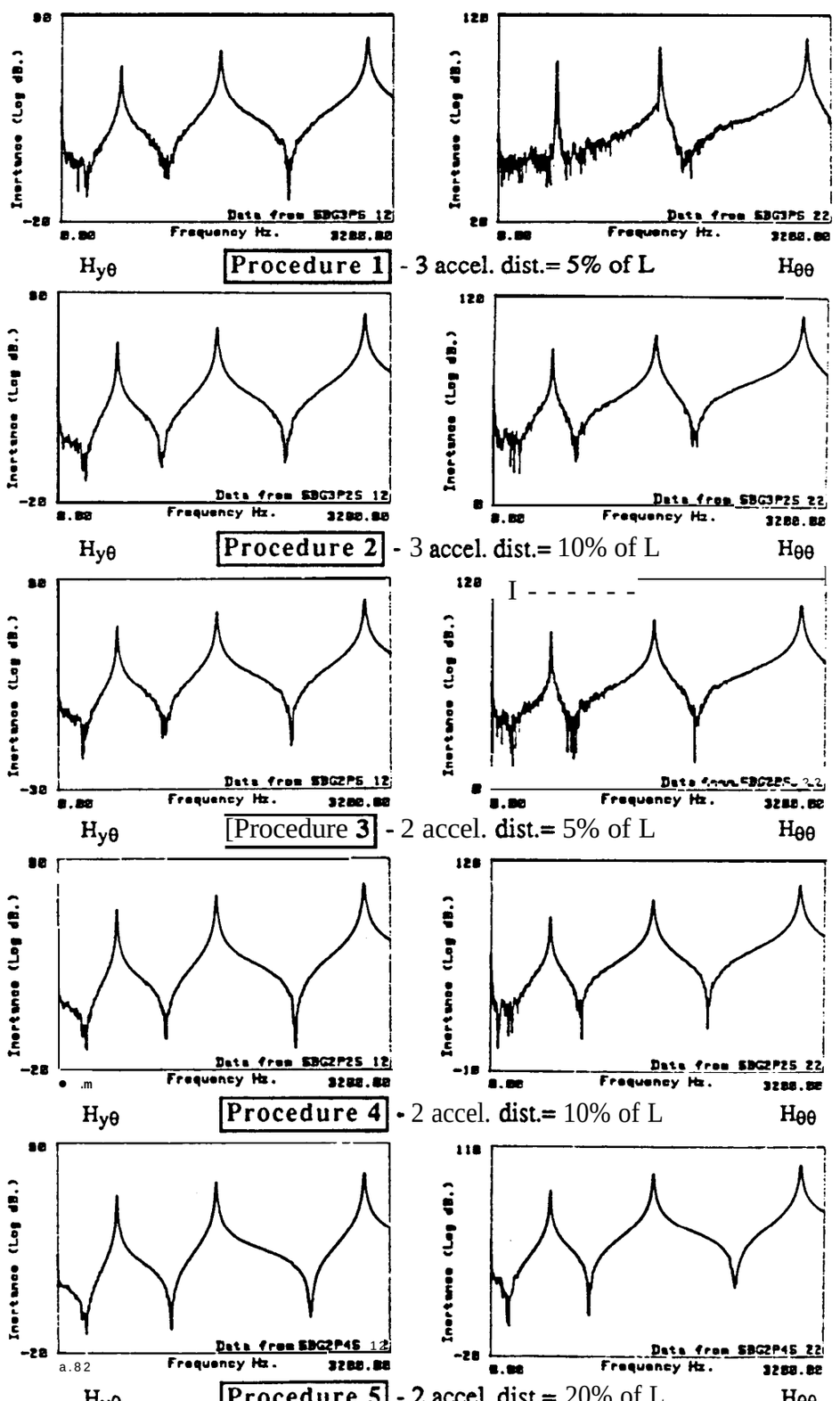

Fig. 6.17 - Short Beam estimated FRFs using closely-spaced accelerometers

Having achieved the estimation of the Response model via the previously-mentioned procedures, the Impedance route is terminated. Each of the models is now ready for input into an FRF coupling process. However, a further step was taken in this work whereby the FRFs corresponding to $H_{y\theta}$ and $H_{\theta\theta}$ were identified in order to obtain the amplitudes of the mode shape rotational coordinate. The justification for this step relies on the need to compare all the models in terms of the same data format. Two approaches are of interest as described next:

a) modal identification is carried out directly on the estimated $H_{\theta\theta}$. This approach implies the measurement of at least half the FRF matrix and, additionally it provides the way to calculate the residual flexibility effects of the out-of-range modes. Alternatively,

b) only one row (or column) of the FRF matrix is measured, thus giving the estimation of $H_{y\theta}$ (or $H_{\theta y}$). This curve must be converted to modal form before that for $H_{\theta\theta}$ can be derived. This approach is suggested by Gleeson [17] to prevent the calculation and use of the most likely error contaminated FRF - the $H_{\theta\theta}$, whenever lightly-damped structures are dealt with. The impossibility of calculating the residual effects of the out-of-range modes on $H_{\theta\theta}$ is the main drawback for the subsequent use of the modal data.

The error relative to the theoretically calculated rotations are presented in figs. 6.19 and 6.20 for the long beam and figs. 6.22 and 6.23 for the short beam.

Estimation of Modal Models - the Modal route

In this second route, the target is assumed to be the estimation of the Modal models referred to the end coordinates of the beam. The set of FRFs that need to be measured and converted to modal data are those pertaining to one row (or column) of the FRF matrix in terms of the measuring translational coordinates. Since those are identified, it is possible to construct the Modal model in terms of those coordinates. Procedures 1 to 5, which are described in section 6.6.3, allow the estimation of the final Modal models referred to the

connecting coordinates, as well as the corresponding residual flexibility matrices corresponding to the FRFs H_{yy}, $H_{y\theta}$ and $H_{\theta\theta}$ which are presented in fig. 6.18.

The Modal models are compared in terms of the errors of the rotational values for each mode relative to the analytical ones, as it is presented in fig. 6.21 for the long beam and fig. 6.24 for the short beam. The errors relative to the theoretical value of the rigid body rotational amplitude are separately presented in graph of fig. 6.25; the estimated values were derived from the translational measured ones, shown in figs. 6.26 and 6.27, by using the same previously mentioned procedures.

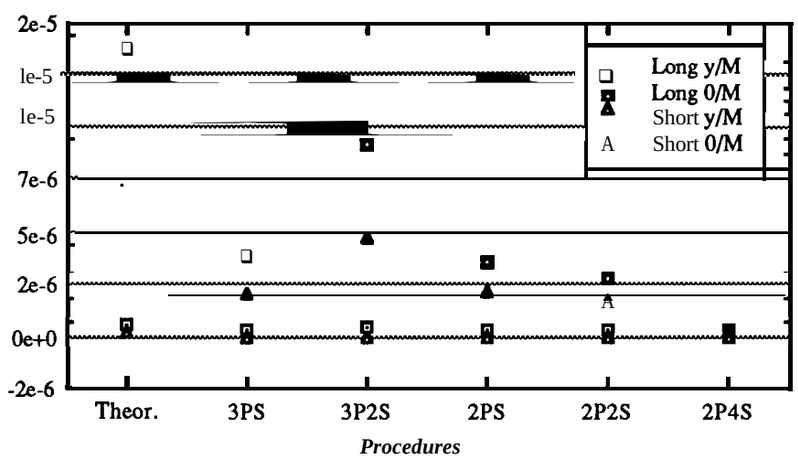

Fin. 6.18 - Estimated residual flexibilitv values for $H_{y\theta}$ and $H_{\theta\theta}$

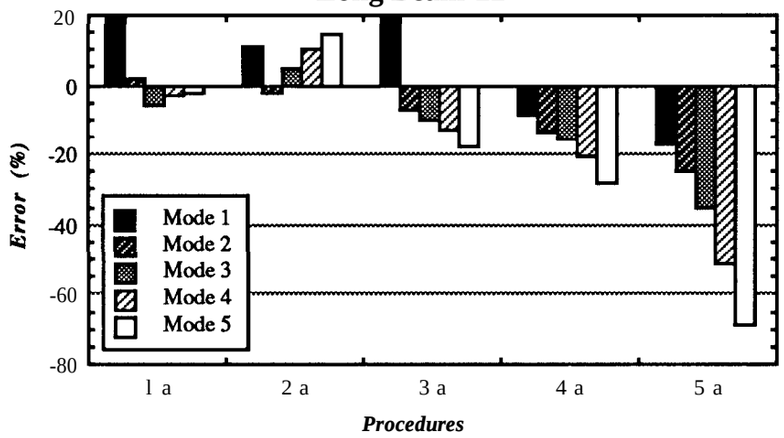

Fig. 6.19 - Rotations extracted from $H_{\theta\theta}$ - **Impedance route**

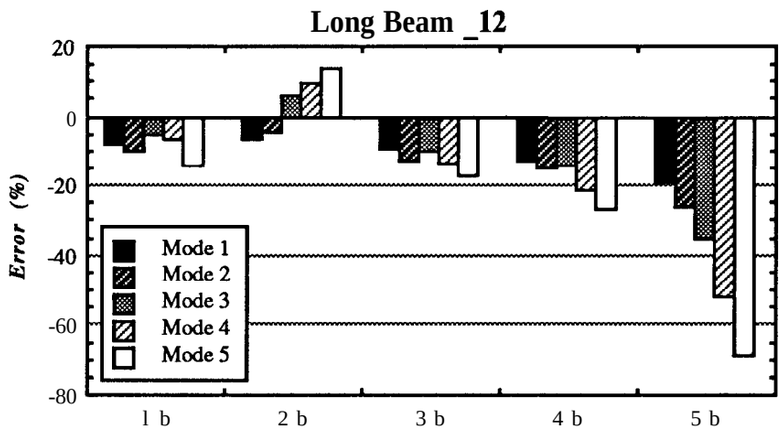

Fig. 6.20 - Rotations derived from $H_{y\theta}$ - **Impedance route**

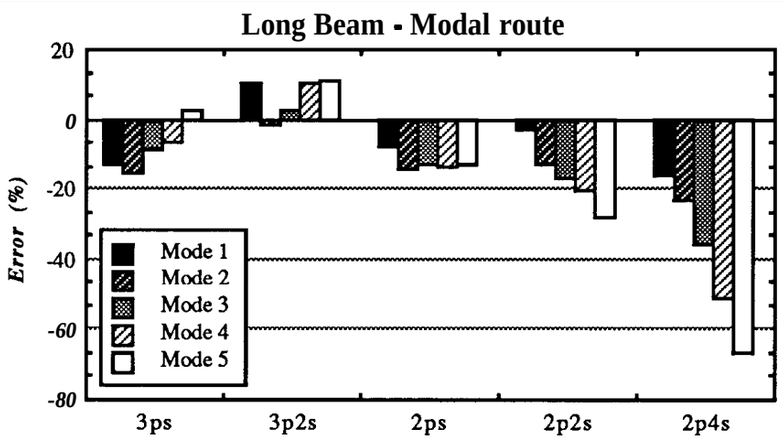

Fig. 6.21 - Rotations derived from modal models - **Modal route**

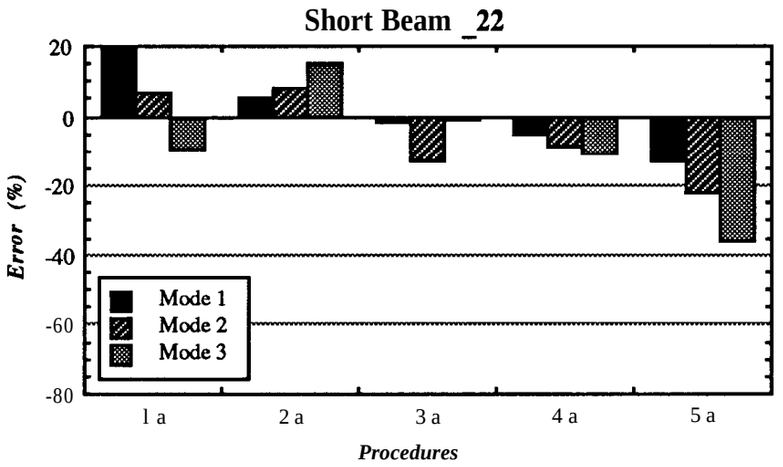

Fig. 6.22 - Rotations extracted from $H_{\theta\theta}$ - **Impedance route**

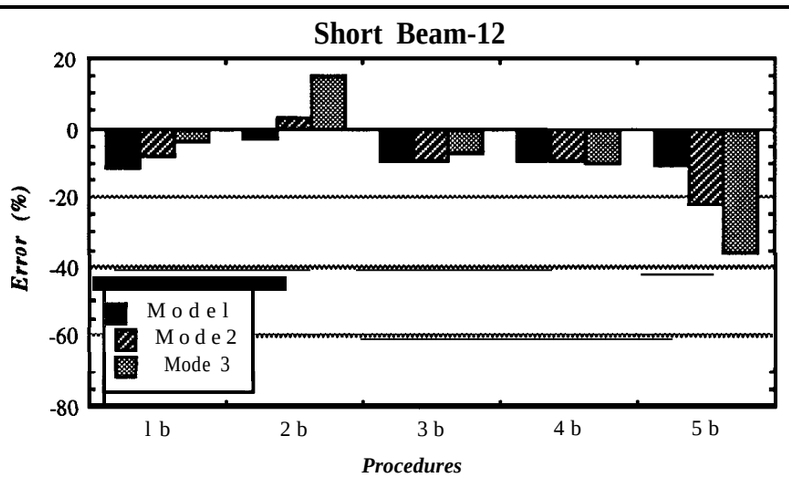

Fig. 6.23 - Rotations derived from $H_{y\theta}$ - **Impedance route**

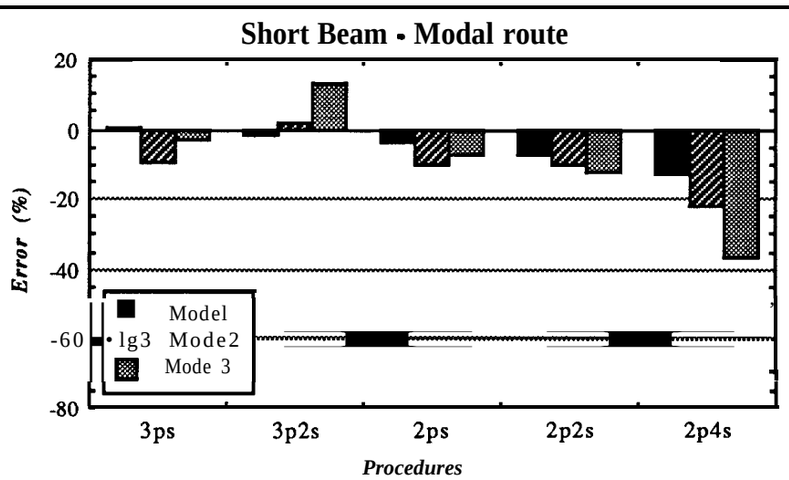

Fig. 6.24 - Rotations derived from modal models - **Modal route**

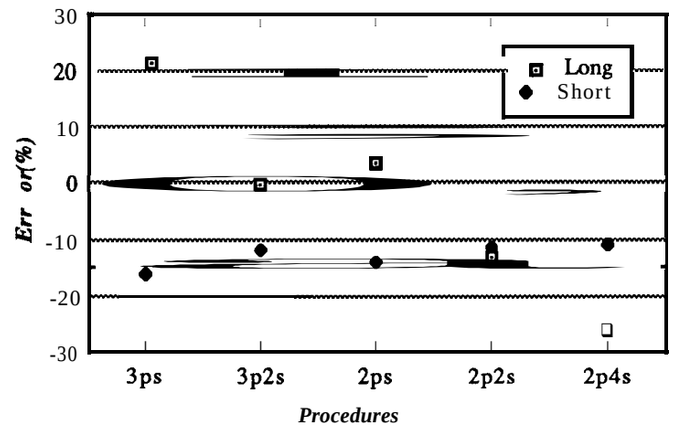

Fig. 6.25 - Errors relative to the theoretical rotational rigid body amplitude $(1/\sqrt{I_z})$

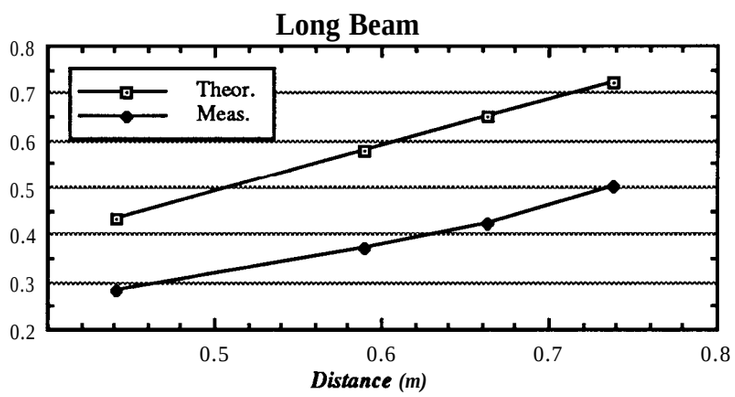

Fig. 6.26 - Translational rigid body response

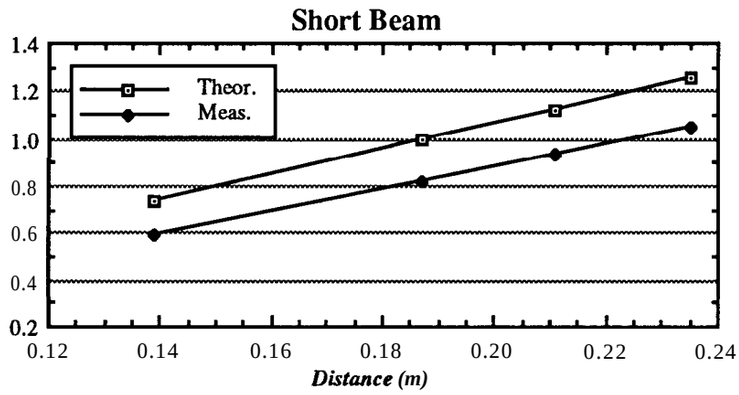

Fig. 6.27 - Translational rigid body response

6.7 DISCUSSION OF RESULTS

Case-Study I

Tests have been carried out using an additional block at one end of the beam. However, the laser measurement does not require such a block in general since there is neither the need to apply an exciting moment nor the need to estimate the rotations from translational responses measured on an extra block. This alleviates the task of estimating the rotational mode shapes when compared to the exciting block technique which requires the cancellation of the extra mass effects.

The measured segment on the beam is about 6% of its total length and only the first five flexural modes were measured. The associated curvature for each mode makes the polynomial curve-fitting algorithm adequate to the corresponding segment even for the higher frequency range. That would not be the case for a longer segment which would require a more general curve-fitting algorithm.

The possibility of using an optical means to measure the FRFs has also been tested; this has resulted in measured FRFs whose accuracy was of the same order as the ones using accelerometers, nevertheless exhibiting a high sensitivity to any occurring responses as shown in fig.6.5 (some spikes occurred at the natural frequencies corresponding to the out-of-plane motion). The FRF measurement was achieved by using the laser spot fixed at one particular location on the structure and then feeding the velocity signal to the analyser prior to enter the lock-in amplifier. This particular measurement has required an extreme care when focussing the laser spot on the structure which therefore was vibrating with a low amplitude.

Case-Study II

The Response models have been derived only from the measurement of translational responses. By converting both $H_{y\theta}$ and $H_{\theta\theta}$ to the modal form it is difficult to get accurate modal parameters, especially for the lower range modes. It is preferable to identify $H_{y\theta}$ curve and then calculate the corresponding rotational parameters as has been presented by Ewins and Gleeson [24] but this cannot be extended to the identification of the out-of-range modes. The rotational mode shapes obtained by following the presented modal route are of the same magnitude of error as for the previous approach yet providing a way to derive the rotational residual flexibility values pertaining to the out-of-range modes.

A visual inspection of the estimated FRFs $H_{y\theta}$ and $H_{\theta\theta}$ reveals some common features for both beams;

- The $H_{y\theta}$ FRFs are less noisy than the FRFs for $H_{\theta\theta}$,
- The noise on both types of FRFs tends to decrease as the frequency increases i.e., for the higher modes the FRFs are cleaner than for the lower frequency ranges,
- As the distance s decreases, the antiresonances in the high frequency region are closer to the ideal values; conversely, those in the low frequency range are not well defined. These become well defined as the distance s increases, but this has the effect of shifting up the higher antiresonances.
- It appears that there exists an optimum solution for the pair - distance s and order of approximation - which, in both of the free-free beams, is the distance s taken as 10% of the total length and using a second order estimation. The main features of the quality of the estimated FRFs are outlined in the following table,

	Quality of estimated FRFs	
	Low-frequency	High-frequency
Distances ↑	↑	↓
↓	↓	t
Order ↑	↓	↑
↓	↑	↓

6.8 CONCLUSIONS

Case-Study I

The laser measurement technique can estimate very easily the rotational mode shapes when compared to the techniques using accelerometers. Additionally, since it is possible to measure in a quasi-continuous way the mode shape patterns over a specified length or area on a structure, it allows more accurate calculations of the spatial derivatives, mainly for the higher modes. This constitutes the main drawback to the data measured with closely-spaced accelerometers since it is impracticable to obtain a precise description of the displacement field near the connection region.

Although the results are only concerned to a very simple case study, it is believed that in more complex structures involving tridimensional measurements, the laser technique will offer the best capability - if the cost of the equipment is affordable.

There are, however, some drawbacks associated with the measurements carried out with the laser technique. On the one hand, by estimating the rotational responses from the displacement pattern of each mode in the frequency range of interest, there is no possibility of calculating the residual flexibility due to the out-of-range modes; generally, this knowledge is important whenever the modal models are used and therefore more modes must be measured. On the other hand, the optically-based system may be unable to reach some important areas or points on the structure; for instance, should a shaker be placed near the region of interest it can obstruct the directed laser beam path, or in other cases, the point of measurement can be located at an inaccessible interior surface.

Case-Study II

The use of two or three closely-spaced accelerometers near the point of interest constitutes a practicable alternative to the exciting-block approach which in turn, is prone to errors when the frequency increases and the canceled mass is large compared to the mass of the structure. It constitutes an ideal technique in the cases where the Modal models have to be

derived, since it requires the modal identification of the measured curves rather than the estimated ones and additionally it allows estimation of the residual effects of the out-of-range modes. However, the first approach is very sensitive to the measurement and excitation locations as well as to the order of the interpolation and it appears that there is no optimum balance between those parameters over all the frequency range. Nevertheless, there are some ideal combinations of those parameters for the low and high frequency ranges.

7 EXPERIMENTAL CASE STUDIES

7.1 INTRODUCTION

In this chapter, both the Impedance and Modal coupling techniques will be applied to a number of case studies. Not only the coupling techniques themselves are of concern but also the auxiliary mathematical and experimental tools which were discussed and presented in chapter 5 and 6.

The first part of this chapter is devoted mainly to the application of the refined Modal coupling technique presented in chapter 4, which enables the residual flexibility values to be included in the coupling process, to an experimental case study. This first case study deals with a real structure formed of two components and assesses the refined technique in the presence of a real practical problem where measured data are used to derive both subsystem models showing the significance and facility of the refinement. The experimentally-derived derived models of each component also give evidence of the critical problem of numerical failure caused by redundancy in terms of the connection coordinates, mainly when the classical approach is used, demonstrating the usefulness of the mathematical tools presented in chapter 5. Additionally, the mathematical formulation of the constraint equations using the connection displacements (and rotations) and forces (and moments) requires the measurement of rotational quantities in most cases. This example shows that in some situations there is no need to calculate those values explicitly, provided the interface region exhibits a reasonable stiffness over the frequency range of

interest and at least two points can be chosen a considerable distance apart from each other.

The need to calculate rotational responses in certain beam-like structures in order to fulfil the proper constraint conditions at the connecting region, is revealed by the second case study where an assembly of two straight beams is dealt with. These components have already been investigated in chapter 6 where different procedures were used to estimate the necessary rotational quantities. These rotational data are used in the present chapter in order to construct a variety of Response and Modal models for both beam components which are subsequently input either to a FRF or to a Modal coupling procedure. The final results for the assembled beam predicted by both coupling techniques are then compared with each other.

7.2. EXPERIMENTAL CASE STUDY I

7.2.1 INTRODUCTION

A real structure was taken at this stage in order to test the ability of the refined approach when only measured data are available to derive the Modal models for each component. At the time each modal model is derived for a component, additional information is linked to it - the residual flexibility of the out-of-range modes - and this is expressed as a matrix whose elements are referred to the connection coordinates. The dynamic response of the assembled structure is predicted using both of the two approaches: the classical free-interface method and the refined approach which includes the residual information via an interconnecting elastic system (chapter 4, vidé section 4.2.2).

7.2.2 TEST STRUCTURE

The complete structure for which dynamic properties are to be predicted is formed of the two components shown in figures 7.1 and 7.2 - a curved frame and an I-section beam.

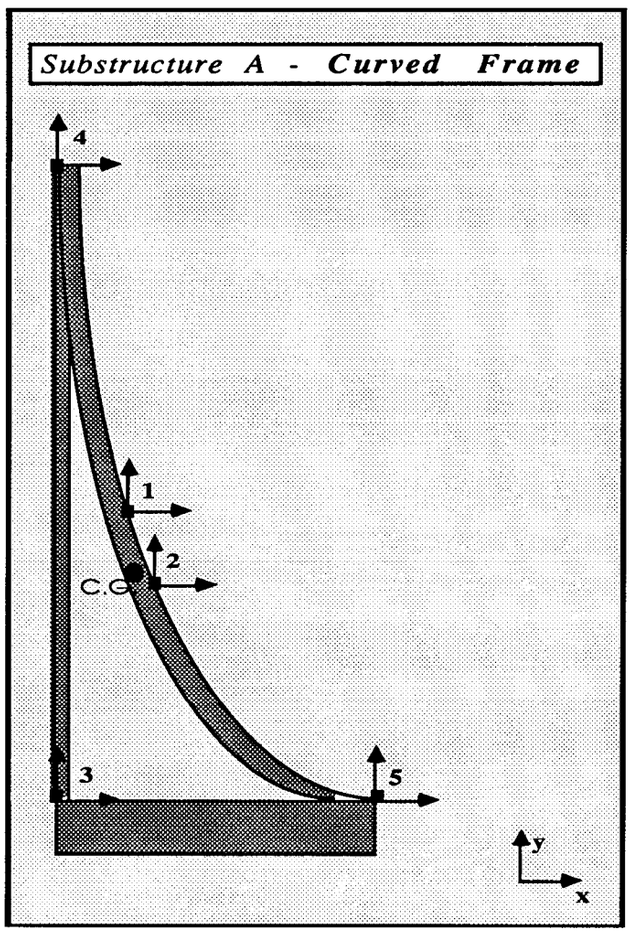

Fig. 7.1 - Curved frame

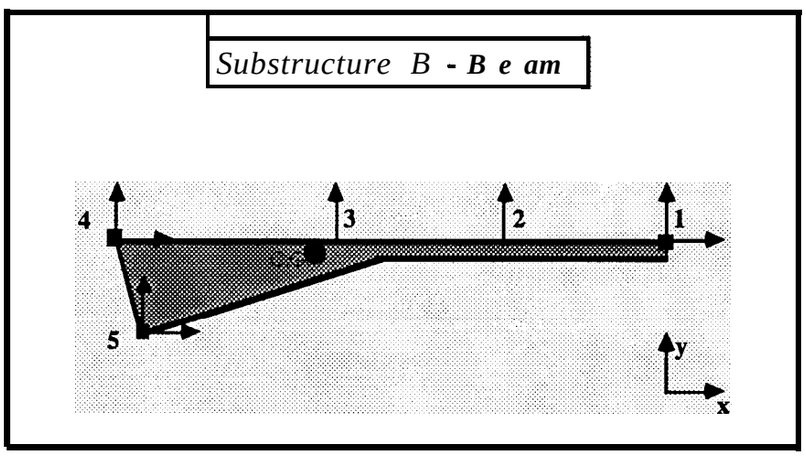

Fig. 7.2 - I-section beam

Component A is a physical representation of a curved frame, to which an I-section beam - designated here as component B - is attached to form the complete structure C represented in fig. 7.3.

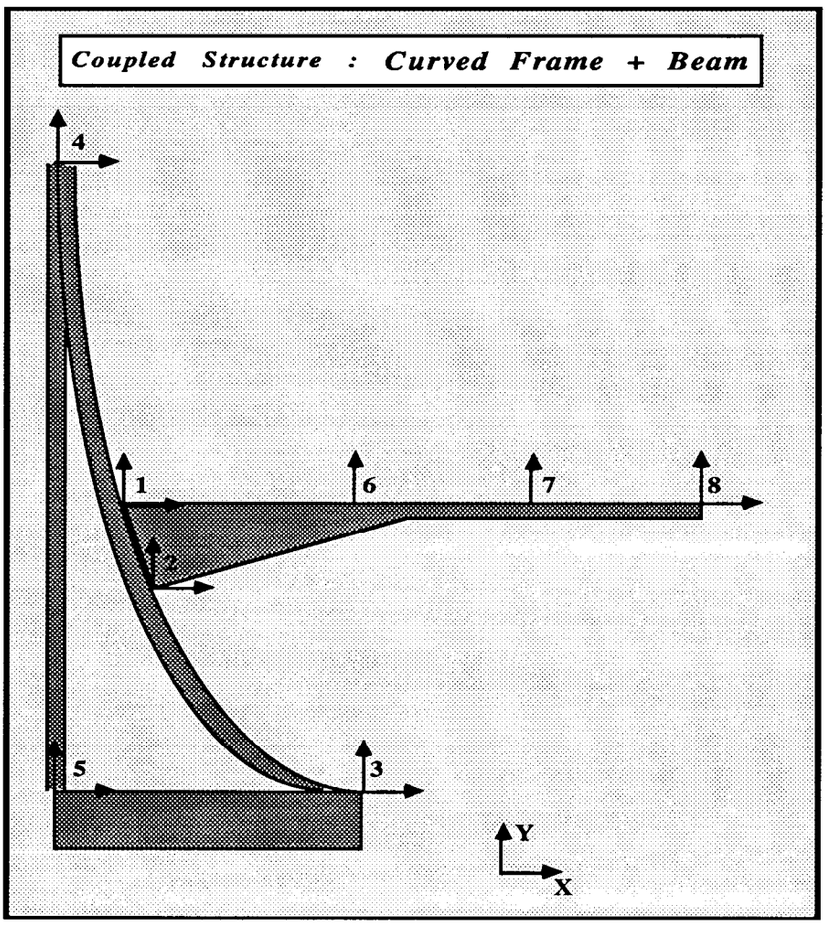

Fig. 7.3 - Coupled structure

This structure C has already been tested in an earlier investigation into the Receptance coupling methods [90,91]. At that time, the assumed set of connection coordinates between the two physical models was referred to just one point possessing three degrees of freedom (only the in-plane of symmetry response was considered) - two linear coordinates and a rotational coordinate. The Impedance Coupling method was used by assembling the respective measured FRFs for each component [62,70].

An alternative set of connection coordinates is used in the present work, constituting a statically determinate set of **linear** coordinates **-** 2 coordinates at the lower connection points (point 2 in component A and point 5 in component B) and **1** coordinate at the upper connection points (point 1 in component A and point 4 in component B).

The particular geometry configuration in the connecting region for both components necessarily led to the use of small aluminium cubes for measuring each point linear response in the two perpendicular directions. These blocks were attached to the measuring connecting points of both subsystems in such a way that made both subsystem coordinate systems coincide with each other and thus with the global coordinate system. This simple assumption taken at this stage results in less time-consuming subsequent matrix operations in the input data for the coupling process.

7.2.3 **MEASUREMENT CONSIDERATIONS**

Both substructures possess planes of symmetry which coincide when the two components are linked together as intended. Thus, the whole structure still possesses a plane of symmetry and its dynamic response may be classified as:

- in-plane vibrations excited by in-plane force excitation;
- out-of-plane vibrations for all other cases.

Some introductory tests were carried out on both freely-simulated supported substructures in order to gain a general insight into their dynamic responses. As a consequence, two main simplifications were made for the subsequent work:

(i) both substructures exhibit a dynamic behaviour which can be assumed to resulting from linear and lightly-damped structures. The damping effect can then be neglected in the identification and modelling stages;

(ii) only the in-plane dynamic response needs to be investigated. The modal density in the frequency range of interest for each component is smaller than for the out-of-plane case and the in-plane modes are well separated. The selected frequency ranges for each component are:

Component A - Curved *Frame* *0- 800* Hz encompassing 9 in-plane modes
(3 rigid-body modes + 6 flexural modes)

Component B - *Beam* 0- 1600 Hz encompassing 5 in-plane modes
(3 rigid-body modes + 2 flexural modes)

7.2.4 EXPERIMENTAL SET-UP

The response (acceleration) at the selected points and directions of each component was measured using B&K (type 4393) lightweight piezoelectric accelerometers which were attached to the structure by using beeswax. According to the standard rules provided by the manufacturer this type of accelerometer can be assumed as having a negligible mass-loading effect on the structures and the method of attachment was reasonable for the frequency range of interest of each component [92].

Each substructure was excited in two different ways:

(i) in the introductory tests, an impulse excitation was applied by using a hammer; and

(ii) in order to measure more accurate data for the identification stage of each subsystem, a pseudo-random excitation was chosen to drive a shaker in each selected frequency range; the shaker was connected via a push-rod to a B&K type 8200 force transducer attached to the measuring point on the structure. The command signal was supplied by a B&K 2034 analyser which also performed the FFT to each measured ratio acceleration/force.

All the measured FRFs were stored using an HP series 900 microcomputer, this also being used to run the identification program AUTOIDENT [71], which is a modal parameter estimation algorithm appropriate for the responses of lightly-damped structures.

7.2.5 MEASUREMENT AND MODELLING

Both substructures have a plane of symmetry (Oxy), this being the only plane of measurement for the responses and excitation forces.

7.2.5.1 RIGID-BODY PROPERTIES

Both components are supported in a simulated freely-supported condition. The necessary rigid-body properties - namely, the mass and the principal moment of inertia I,, - were first estimated before the modal test took place. The first estimation of the location of the centre of gravity was made by supporting each subsystem twice from two different points located on the plane of symmetry. The cross point between the two vertical lines passing through each suspension point gives the location of the centre of gravity.

The compound pendulum technique was used to determine an approximate value for the principal moment of inertia, I,. By hanging each structure in such a way that only makes possible the rigid-body rotational motion along its plane of symmetry, the measured natural frequency of such a single DoF system is related to the value of its principal moment of inertia. The geometric characteristics and the theoretical rigid-body modes (calculated according to the theory presented in Appendix IV) are presented in tables 7.1 and 7.2 for the curved frame and in tables 7.3 and 7.4 for the I-section beam.

Component A - *Curved Frame*

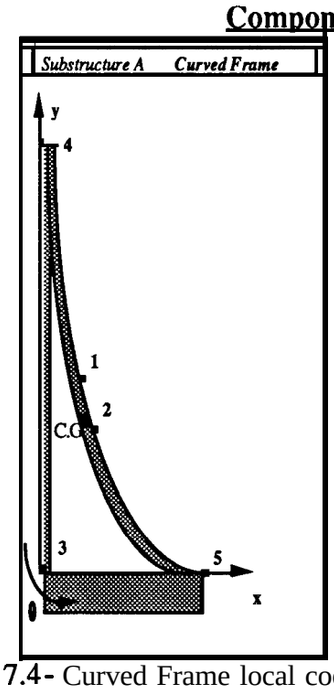

Fig. 7.4- Curved Frame local coordinate system

Table 7.1 - Geometric and Inertia characteristics of Curved Frame

Point	Coord. X	Coord. Y
1	0.086	0.380
2	0.125	0.289
C.G.	0.090	0.296
3	0	0
4	0	0.846
5	0.338	0
Mass = 38.41 Kg.	I_{zz}= 3.46 Kg m^2	

Mass Normalised Rigid-Body Modes

Table 7.2 - Curved Frame Rigid-Body mode shapes

Coord.	Transl. x	Transl. y	Rotation θ
1X	0.161	0	-0.04516
1Y	0	0.161	-0.00215
2X	0.161	0	0.00376
2Y	0	0.161	0.01892
3X	0.161	0	0.1591
3Y	0	0.161	-0.04838
4X	0.161	0	-0.2957
4Y	0	0.161	-0.04838
5X	0.161	0	0.1591
5Y	0	0.161	0.1333

Component B - *I Section Beam*

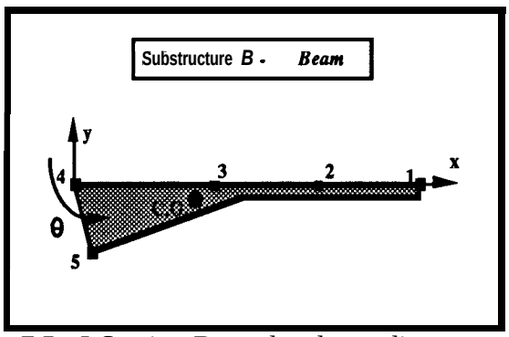

Fig. 7.5 - I-Section Beam local coordinate system

Table 7.3 - Geometric and Inertia characteristics of Beam

Point	Coord. X	Coord. Y
1	0.685	-0.005
2	0.493	0
3	0.330	0
C.G.	0.323	-0.021
4	0	0
5	0.023	-0.09
Mass = 2.2 Kg.		I_{zz}= 0.09 Kg m^2

Mass Normalised Rigid-Body Modes

Table 7.4 - I-section Beam Rigid-Body mode shapes

Coord.	Transl. x	Transl. x	Rotation θ
1x	0.674	0	-0.05
1Y	0	0.674	1.207
2X	0.674	0	-0.067
2Y	0	0.674	-0.577
3X	0.674	0	-0.067
3Y	0	0.674	-0.023
4X	0.674	0	-0.067
4Y	0	0.674	-1.077
5X	0.674	0	0.233
5Y	0	0.674	-1.000

7.2.5.2 SUBSYSTEM MODELLING

Two groups of coordinates have been selected for each component: the first group contains all the connection coordinates and the second group consists of the remaining or interior ones. The size of this latter group depends on the definition required for the system mode shapes, while the number of connection coordinates depends on the local connecting area and the associated stiffness properties in each component.

For the modelling stage of each component i.e., the construction of the respective Modal models, an excitation is generally applied at one of the coordinates while all the necessary FRFs sharing the same excitation point are measured, in order to obtain one column in the Inertance matrix [1]. In this particular case study, the substructure's Modal models will be further used in the coupling stage with different approaches, one of which requires knowledge of the residual effects of the higher unmeasured modes. For this purpose, the excitation also needs to be applied at all the connection coordinates in order to measure the corresponding FRFs (in fact, the pairs of values referred to the connection coordinate response / connection excitation) which, after an identification procedure, will give the necessary residual information of the unmeasured modes. Since this extra excitation had to be applied to each component, it was decided to take advantage of this by measuring not only the FRFs related to connection coordinates, but also those related to the interior ones. In doing so, extra Modal models could be derived (in fact other columns in Inertance matrix are used) and there was a possibility of correlating different models in order to check their consistency and validity.

7.2.5.2.1 CURVED FRAME MODELLING

Fig. 7.6 shows the different cases for the pseudo-random excitation applied to the curved frame and the respective measured responses at various stations with the associated sign for each transducer and the related pair of response / excitation.

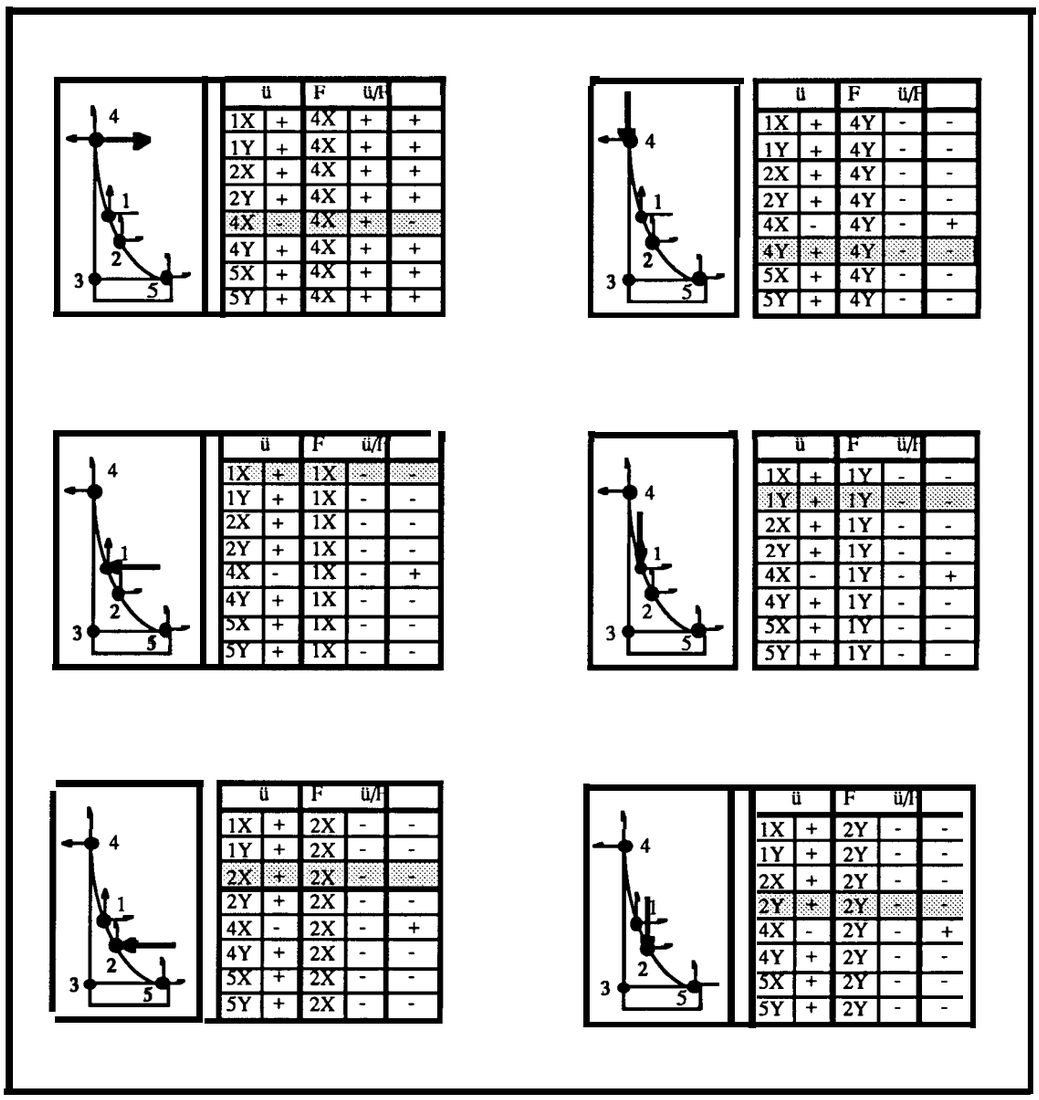

Fig. 7.6 - Curved frame excitation and measurement locations

Figs. 7.7 a,b,c) show some measured FRFs on the curved frame over the frequency range O-800 Hz, which encompasses natural frequencies corresponding to the first six elastic in-plane modes. The particular FRF presented in fig. 7.7 a) will be mentioned later as the FRF of the unmodified curved frame when a comparison is made with the predicted FRF of the curved frame with the beam attached to it.

The Modal model presented in table 7.5 is derived from the identified modal parameters pertaining to the measured FRFs sharing a common excitation point (coordinate 5). As mentioned earlier, the excitation has also been applied to the two connecting points (3 coordinates), thus measuring 5 FRFs which were subsequently subjected to a modal identification stage with a suitable computer program [71], mainly to extract the modal parameters related to the out-of-range modes. These five modal parameters were then used, as presented in Appendix II, to construct half the residual flexibility matrix which simulates the dummy flexible system at the interface coordinates and is assumed to be symmetric ;

Experimental Residuals - Curved Frame

$$[R_{cc}] = \begin{bmatrix} 2.7244E\text{-}09 & 4.0108E\text{-}10 & 2.3027E\text{-}10 \\ 4.0108E\text{-}10 & 2.7858E\text{-}09 & 0 \\ 2.3027E\text{-}10 & 0 & 5.2771E\text{-}10 \end{bmatrix}$$

Stiffness matrix of the dummy connecting system - Curved frame

$$[K_{cc}] = [R_{cc}]^{-1} = \begin{bmatrix} 3.8969E08 & -5.6105E07 & -1.7005E08 \\ -5.6105E07 & 3.6704E08 & 2.4482E07 \\ -1.7005E08 & 2.4482E07 & 1.9692E09 \end{bmatrix}$$

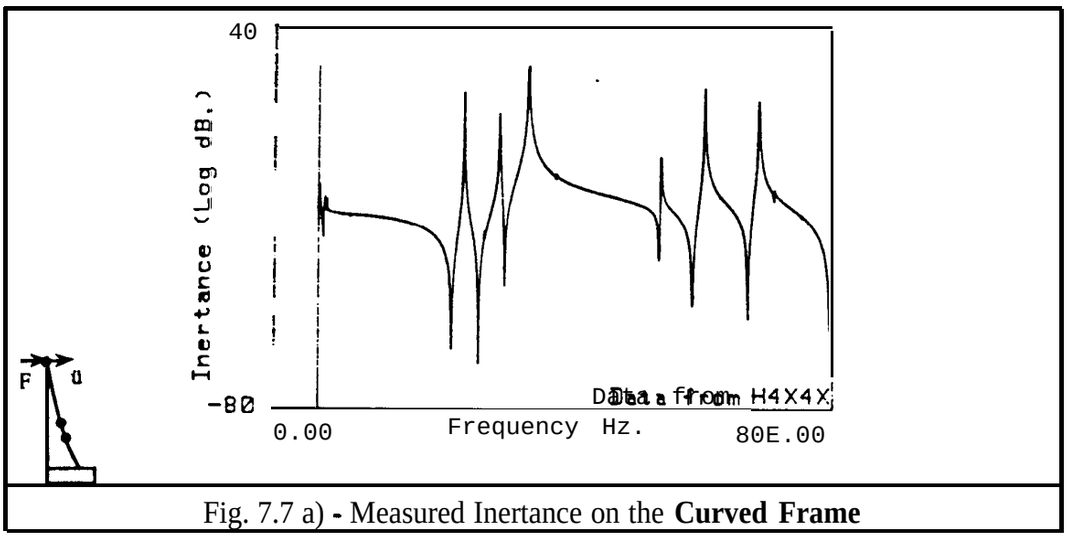

Fig. 7.7 a) - Measured Inertance on the **Curved Frame**

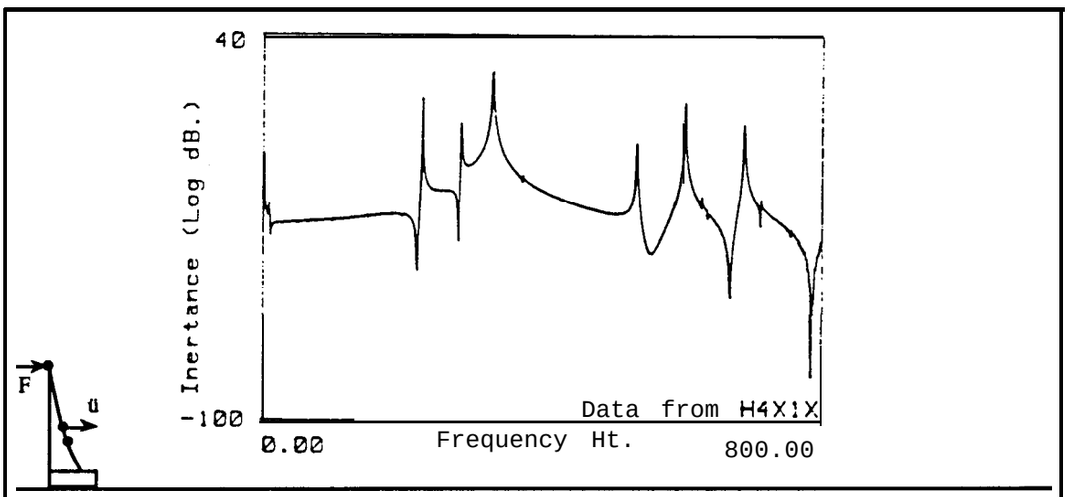

Fig. 7.7 b) - Measured Inertance on the **Curved Frame**

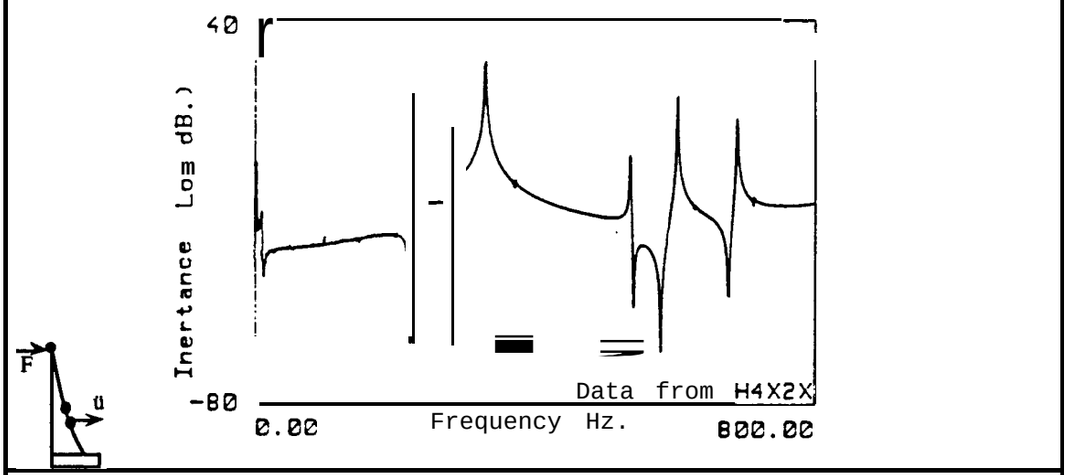

Fig. 7.7 c) - Measured Inertance on the **Curved Frame**

```
T I T L E  -->> H4X1X H4X1Y H4X2X H4X2Y H4X4X H4X4Y H4X5X H4X5Y Rig.Body Mode
s = 3
FILE Name -->> MDU_HULL4X:,700,1
Coord. =  8 Modes =  9
```

	1	2	3	4	5	6	7	8	9
1	+1.6135E-01	+0.0000E+00	+4.6684E-02	+7.4957E-02	+6.6660E-02	-2.5576E-01	+4.4189E-02	-5.6829E-02	-3.0481E-02
2	+0.0000E+00	+1.6135E-01	-1.4374E-02	-6.3547E-03	+8.2987E-03	-5.4069E-02	+2.5836E-02	-4.5021E-02	-1.0441E-02
3	+1.6135E-01	+0.0000E+00	-2.9422E-03	+6.5042E-02	+4.5018E-02	-2.5380E-01	+2.4268E-02	-5.7497E-02	-3.9896E-02
4	+0.0000E+00	+1.6135E-01	-1.7065E-02	-2.3757E-03	+1.1042E-02	-4.5664E-02	+2.3877E-02	-4.4445E-02	-7.8362E-03
5	+1.6135E-01	+0.0000E+00	+2.8828E-01	+8.3555E-02	+1.0034E-01	+2.7008E-01	+3.5040E-02	+9.7129E-02	+9.0400E-02
6	+0.0000E+00	+1.6135E-01	+7.9434E-02	+9.8318E-03	+2.8631E-02	+4.9377E-03	+3.9589E-02	-2.5145E-03	+2.9172E-02
7	+1.6135E-01	+0.0000E+00	-1.4798E-01	+3.1666E-02	+2.8469E-02	+4.5528E-02	-3.3105E-03	-5.3637E-03	-2.2985E-02
8	+0.0000E+00	+1.6135E-01	-1.2306E-01	-3.0876E-02	+5.6457E-01	+3.9231E-03	-8.1219E-02	+1.2892E-03	-6.3673E-01

Eigenvalues	Natural Frequencies
1.000E-08	1.592E-05 Hz
1.000E-06	1.592E-04 Hz
3.948E-07	1.000E-04 Hz
2.107E+06	2.310E+02 Hz
3.229E+06	2.860E+02 Hz
4.351E+06	3.320E+02 Hz
1.138E+07	5.370E+02 Hz
1.450E+07	6.060E+02 Hz
1.874E+07	6.890E+02 Hz

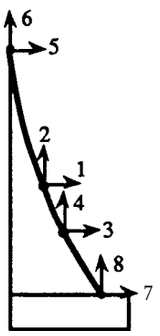

Table 7.5 - **Experimentally-derived Curved Frame** Modal Model

7.2.5.2.2 BEAM MODELLING

In fig. 7.8, the different cases for the pseudo-random excitation applied to the beam are shown together with the respective measured responses at various stations with the associated sign for each transducer and the related pair of response / excitation.

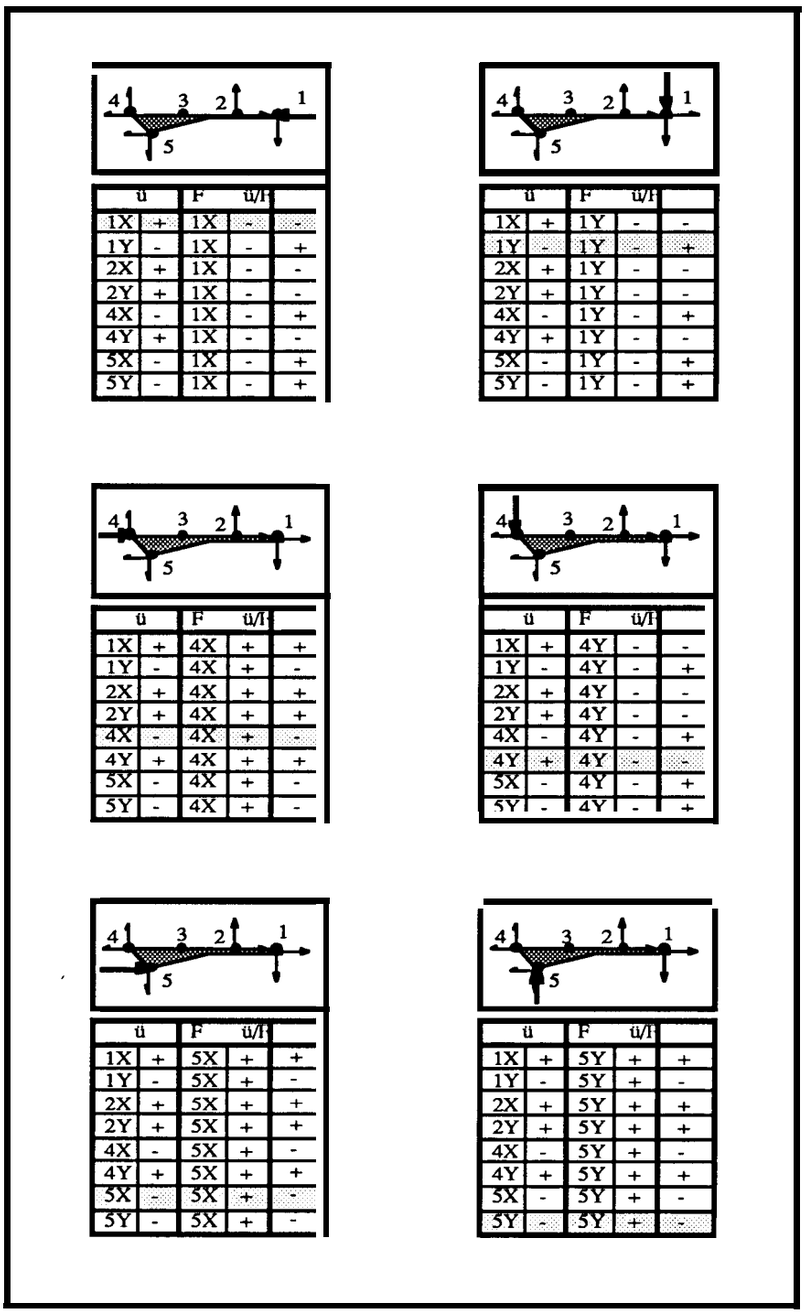

Fig. 7.8 - Beam excitations and measurement locations

Figs. 7.9 a,b,c) show some of the measured FRFs on the beam over the frequency range O-1600 Hz, which encompasses the natural frequencies corresponding to the fiit two in-plane bending modes. The particular FRF presented in fig. 7.9 a) will be mentioned later as the FRF of the unmodified beam when a comparison is made with the predicted FRF of the beam with the curved frame attached to it.

The Modal model presented in table 7.6 is derived from the identified modal parameters pertaining to the measured FRFs sharing a same excitation point (coordinate 6). Identically to the curved frame, the out-of-range modes were also identified in order to construct the corresponding residual flexibility matrix presented next;

Experimental Residuals - Beam

$$[R_{cc}] = \begin{bmatrix} 4.4053E\text{-}9 & 0 & 0 \\ 0 & 5.8985E\text{-}9 & 0 \\ 0 & 0 & 1.0214E\text{-}8 \end{bmatrix}$$

Stiffness matrix of the dummy connecting system - Beam

$$[K_{cc}] = [R_{cc}]^{-1} = \begin{bmatrix} 2.2700E08 & 0 & 0 \\ 0 & 1.6953E08 & 0 \\ 0 & 0 & 9.7903E07 \end{bmatrix}$$

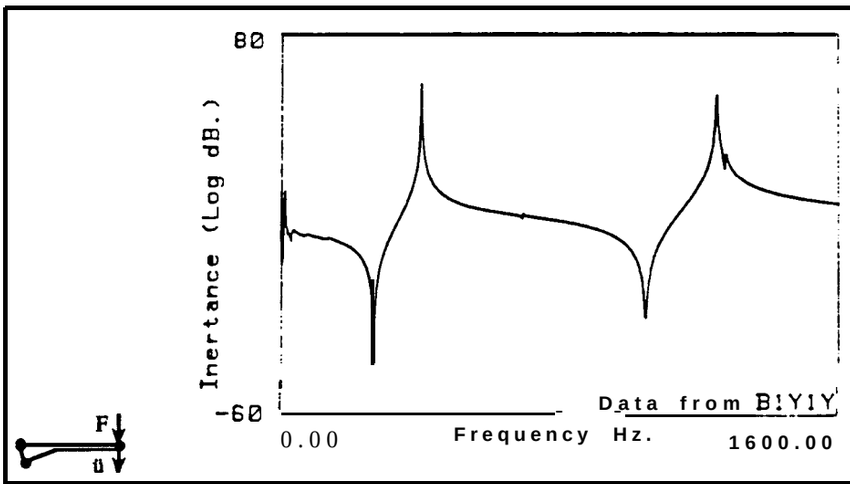

Fig. 7.9 a) - Measured Inertance on the **Beam**

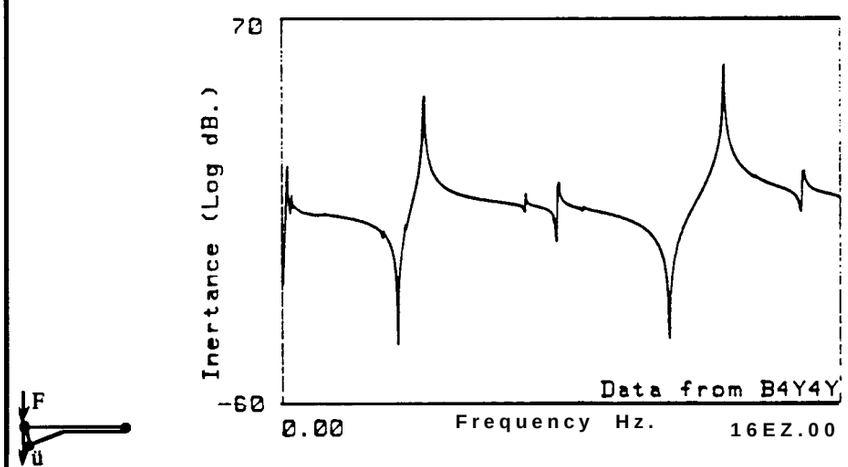

Fig. 7.9 b) - Measured Inertance on the **Beam**

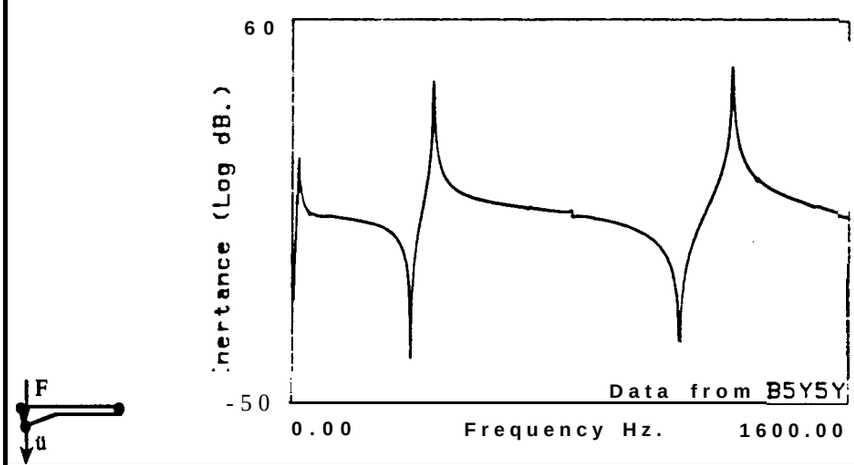

Fig. 7.9 c) - Measured Inertance on the **Beam**

TITLE -->> B1Y4X B1Y4Y B1Y5X B1Y5Y B1Y1X B1Y1Y B1Y1X B1Y2Y B1Y1X B1YCG
Rig.Body Modes = 3
FILE Name -->> MDU_BEAM1Y:,700,1
Coord. = 10 Modes = 5

	1	2	3	4	5
1	+6.7420E-01	+0.0000E+00	-7.2536E-02	+1.0079E-01	-1.7597E-01
2	+0.0000E+00	+6.7420E-01	-1.0581E+00	+8.6837E-01	-7.2826E-01
3	+6.7420E-01	+0.0000E+00	+2.2565E-01	-3.7401E-01	+4.1095E-01
4	+0.0000E+00	+6.7420E-01	-9.9127E-01	+7.6243E-01	-6.1402E-01
5	+6.7420E-01	+0.0000E+00	-7.3701E-02	-1.6923E-03	-4.9722E-02
6	+0.0000E+00	+6.7420E-01	+1.2019E+00	+1.5073E+00	+1.3128E+00
7	+6.7420E-01	+0.0000E+00	-7.3701E-02	-1.6923E-03	-4.9722E-02
8	+0.0000E+00	+6.7420E-01	+4.1181E-01	-8.0720E-01	-5.3387E-01
9	+6.7420E-01	+0.0000E+00	-7.3701E-02	-1.6923E-03	-4.9722E-02
10	+0.0000E+00	+6.7420E-01	+2.4991E-03	-7.2056E-01	+6.5777E-01

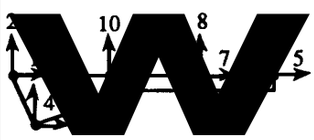

Eigenvalues	Natural Frequencies
1.000E-08	1.592E-05 Hz
1.000E-06	1.592E-04 Hz
3.948E-07	1.000E-04 Hz
6.572E+06	4.080E+02 Hz
6.268E+07	1.260E+03 Hz

Table 7.6 - Experimentally-derived **Beam** Modal Model

7.2.6 RESULTS

The actual substructures are connected together to form the complete assembly. From an experimental standpoint, the complete structure was tested following the same steps as those utilized during the subsystem identification and modelling stages. The final result of these tests is a description of the dynamic properties based on either a Modal or Response model. These dynamic properties will be taken as the reference values for the purposes of comparison with the predicted dynamic behaviour resulting from the use of the classical and the refined coupling approaches.

Both these approaches are applied in the present case study for each of two different situations. First, a statically determinate set of connection coordinates is used to formulate the constraint conditions in the interface region - 1 vertical and 2 horizontal coordinates as described in section 7.2.2. Next, another vertical coordinate is added to the previous set making the subsystems constrained in the X and Y direction at both connecting points (areas). Some of the measured FRFs are compared with the predicted responses as shown in figs. 7.11 ab) ab to 7.14 ab). The experimentally-derived modal model is shown in table 7.14 and the corresponding mode shapes are sketched in figs. 7.10 a) and b).

The degree of importance of each subsystem's residual flexibility effects on the dynamic properties of the assembled structure may be seen in figs. 7.14 ab) to 7.16 ab). Starting from the omission of the residual flexibility effect for both the components (in fact, utilizing the classical free-interface method with rigid connections between the substructures), the residual flexibility is then gradually taken into account up to the maximum of 100%. This could be visualised as though the components had been connected through a intermediate elastic system which at the begining was very stiff and then was made progressively more compliant. For each percentage value for the residual, the Modal model of the global structure is calculated and then the mode shapes may be animated by using an appropriate computer program [94] and some of the corresponding sketches are shown in figs. 7.18 to 7.21. These mode shapes are presented mainly to show the evolution of the predicted natural frequencies and mode shapes of the assembled

structure when the flexibility of the dummy interconnecting system varies from zero to the full correct value.

The refined approach allows the inclusion of any percentage of residual effects. If this value is too small, the predicted results ought to be similar to those obtained by using the classical free-interface method. Tables 7.11 and 7.12 show the natural frequencies predicted by the different approaches and making use of both sets of interface coordinates.

7.2.7 **DISCUSSION OF RESULTS**

Two sets of connecting coordinates and two coupling approaches were used to predict the dynamic behaviour of the assembled structure which is formed of two components connected (glued with a hard adhesive) by a small area - the tip cross-section of the beam. The first attempt to model this connecting area, which behaves almost rigidly over the measured frequency range O-1600 Hz, was undertaken by assuming only two connecting points, separated by a distance equal the height of the corresponding cross-section of the beam. Two coordinates were selected at the top point and only one horizontal coordinate was assumed for the lower point. This set was believed to express the transmission of horizontal and vertical forces and a moment between the two components. In fact, as seen in figs. 7.11 b) and 7.12 b), the predicted results using the refined approach are in good agreement with the measured ones apart from a small discrepancy in the natural frequency of the fifth flexural mode. A careful analysis of the mode shapes of the assembled structure obtained from measured data, shown in figs. 7.10 a) and b), reveals that the first and fifth flexural mode shapes correspond to two extra natural frequencies added to the curved frame when the beam is attached to it, whereas the original natural frequencies are virtually unchanged due to being 17.5 times heavier than the beam (see original and modified FRFs of curved frame in fig. 7.22). At these extra natural frequencies, the beam behaves in a nearly-clamped condition: thus, they correspond closely to the first and second bending modes and the curved frame is acting as if it was a rigid body attached to

the beam. Since the clamping conditions of a vibrating beam play an important role on its dynamic properties, it was decided to improve the formulation of the connection conditions between the curved frame and the beam. This was achieved by introducing an extra vertical constraint between the two lower connection points, thus using 4 connection coordinates. Surprisingly, the classical Modal coupling approach (vide chapter 2, section 2.3.3.2) predicted unrealistic results, as shown in figs. 7.13 a) and 7.14 a), and the refined approach (vide chapter 4, section 4.2.2) predicted similar results, as shown in figs. 7.13 b) and 7.14 b), to those obtained by the previously used connecting conditions. Naturally, there was a reason for that failure and a first attempt to explain it was linked to any numerical failure of the coupling algorithm, since in physical terms the constraint conditions should have provided a closer representation of those existing in the assembled structure. The mathematical tools presented in chapter 5 were used to detect any redundancy in the interface region which could have caused a failure in the required inversion of a square partition of the modal matrix for one of the components. The results of this analysis are presented in table 7.7 and 7.8 and it is shown that there is a local rigidity between the vertical coordinates in both components, especially for the beam. In such a case, the SVD technique (vide chapter 5) should be used to avoid numerical failure of the inversion of the selected matrix or, alternatively, another partition containing most of the higher mode shapes can be chosen since the dependency is less likely to happen. However, upon the use of redundant connecting coordinates and as mentioned before, the refined approach has not caused any numerical failure mainly due to the fact that the inversion required at some stage is applied to a matrix obtained by adding in series the two dummy flexible components containing the out-of-range information and this is less susceptible to be singular.

the beam. Since the clamping conditions of a vibrating beam play an important role on its dynamic properties, it was decided to improve the formulation of the connection conditions between the curved frame and the beam. This was achieved by introducing an extra vertical constraint between the two lower connection points, thus using 4 connection coordinates. Surprisingly, the classical Modal coupling approach (vide chapter 2, section 2.3.3.2) predicted unrealistic results, as shown in figs. 7.13 a) and 7.14 a), and the refined approach (vide chapter 4, section 4.2.2) predicted similar results, as shown in figs. 7.13 b) and 7.14 b), to those obtained by the previously used connecting conditions. Naturally, there was a reason for that failure and a first attempt to explain it was linked to any numerical failure of the coupling algorithm, since in physical terms the constraint conditions should have provided a closer representation of those existing in the assembled structure. The mathematical tools presented in chapter 5 were used to detect any redundancy in the interface region which could have caused a failure in the required inversion of a square partition of the modal matrix for one of the components. The results of this analysis are presented in table 7.7 and 7.8 and it is shown that there is a local rigidity between the vertical coordinates in both components, especially for the beam. In such a case, the SVD technique (vide chapter 5) should be used to avoid numerical failure of the inversion of the selected matrix or, alternatively, another partition containing most of the higher mode shapes can be chosen since the dependency is less likely to happen. However, upon the use of redundant connecting coordinates and as mentioned before, the refined approach has not caused any numerical failure mainly due to the fact that the inversion required at some stage is applied to a matrix obtained by adding in series the two dummy flexible components containing the out-of-range information and this is less susceptible to be singular.

7.2.8 CONCLUSIONS

The residual flexibility effects of the out-of-range modes associated with each component play an important role in the prediction of the dynamic response of a coupled structure.

The results from the case study show that the degree of importance of each residual flexibility effect is associated with the relative mass of each component - the lighter the component the more important becomes its residual flexibility.

In the present case study, one of the components - the curved frame - possesses a mass some 17.5 times greater the other (the beam). The natural frequencies of the coupled structure in the selected frequency range (O-800 Hz) are mainly formed of those pertaining to the original curved frame but, additionally, two other modes are seen. These two modes are related to the dynamic behaviour of the beam as if it was assumed nearly clamped at the connection end. One can say that the curved frame has drastically modified the dynamic characteristics of the beam whereas this component only has slightly affected the curved frame properties.

The use of a redundant set of connecting coordinates needs a careful analysis of the possible numerical difficulties during the coupling process, especially in the classical free-interface method.

Table 7.7 - SVD technique on partition of modal matrix of **Curved Frame**

$[\Phi]_{4x9} =$

1.614E-1	0.000E00	4.668E-2	7.496E-2	6.666E-2	-2.558E-1	4.419E-2	-5.683E-2	-3.048E-2
0.000E00	1.614E-1	-1.437E-2	-6.355E-3	8.299E-3	-5.407E-2	2.584E-2	-4.502E-2	-1.044E-2
1.614E-1	0.000E00	-2.942E-3	6.504E-2	4.502E-2	-2.538E-1	2.427E-2	-5.750E-2	-3.990E-2
0.000E00	1.614E-1	-1.706E-2	-2.376E-3	1.104E-2	-4.566E-2	2.388E-2	-4.444E-2	-7.836E-3

Matrices [U] and [V] from SVD on matrix $[\Phi]^T$

$$[U]_{9x4} = \begin{bmatrix} -4.788E\text{-}1 & 1.991E\text{-}1 & 1.127E\text{-}1 & -3.323E\text{-}1 \\ -1.015E\text{-}1 & -9.411E\text{-}1 & -7.224E\text{-}2 & -1.036E\text{-}1 \\ -5.635E\text{-}2 & 1.212E\text{-}1 & -8.333E\text{-}1 & 2.789E\text{-}1 \\ -2.052E\text{-}1 & 1.124E\text{-}1 & -1.202E\text{-}1 & -6.011E\text{-}1 \\ -1.723E\text{-}1 & 1.362E\text{-}2 & -3.385E\text{-}1 & -4.374E\text{-}1 \\ 7.876E\text{-}1 & -2.370E\text{-}2 & -1.218E\text{-}1 & -4.156E\text{-}1 \\ -1.178E\text{-}1 & -1.017E\text{-}1 & -3.307E\text{-}1 & 1.411E\text{-}1 \\ 1.978E\text{-}1 & 1.904E\text{-}1 & -3.141E\text{-}2 & 7.977E\text{-}2 \\ 1.100E\text{-}1 & 1.035E\text{-}2 & -1.829E\text{-}1 & -2.224E\text{-}1 \end{bmatrix}$$

$$[V]_{4x4} = \begin{bmatrix} -7.037E\text{-}1 & 1.583E\text{-}1 & -6.926E\text{-}1 & -5.969E\text{-}3 \\ -1.531E\text{-}1 & -6.923E\text{-}1 & -8.750E\text{-}3 & 7.051E\text{-}1 \\ -6.795E\text{-}1 & 1.344E\text{-}1 & 7.212E\text{-}1 & -6.621E\text{-}3 \\ -1.400E\text{-}1 & -6.911E\text{-}1 & -9.606E\text{-}3 & -7.090E\text{-}1 \end{bmatrix}$$

Singular values..... 4.661E-1, 2.372E-1, 4.100E-2, 6.113E-3

Condition Number..... 76.244

Horizontal norm..... 0.609

Vertical norm..... 0.737

Threshold..... 10E-2 x Vertical norm = **0.00737**

Rank..... 4

Check on dependency gives columns ordered as 3,1, 4, 2

Table 7.8 - SVD technique applied on partition of modal matrix of **Beam**

$$[\Phi]_{4x5} = \begin{bmatrix} 6.742E\text{-}1 & 0.000E00 & -7.254E\text{-}2 & 1.008E\text{-}1 & -1.760E\text{-}1 \\ 0.000E00 & 6.742E\text{-}1 & -1.058E00 & 8.684E\text{-}1 & -7.283E\text{-}1 \\ 6.742E\text{-}1 & 0.000E00 & 2.257E\text{-}1 & -3.740E\text{-}1 & 4.110E\text{-}1 \\ 0.000E00 & 6.742E\text{-}1 & -9.913E\text{-}1 & 7.624E\text{-}1 & -6.140E\text{-}1 \end{bmatrix}$$

Matrices [U] and [V] from SVD on matrix $[\Phi]^T$

$$[U]_{5x4} = \begin{bmatrix} 4.923E\text{-}2 & 9.856E\text{-}1 & -1.552E\text{-}1 & 4.382E\text{-}2 \\ -3.926E\text{-}1 & 1.290E\text{-}1 & 6.170E\text{-}1 & -4.061E\text{-}1 \\ 6.216E\text{-}1 & -7.853E\text{-}2 & -2.918E\text{-}1 & -1.391E\text{-}1 \\ -5.156E\text{-}1 & -5.268E\text{-}2 & -2.788E\text{-}1 & 6.638E\text{-}1 \\ 4.372E\text{-}1 & 5.441E\text{-}2 & 6.576E\text{-}1 & 6.110E\text{-}1 \end{bmatrix}$$

$$[V]_{4x4} = \begin{bmatrix} -5.978E\text{-}2 & 6.834E\text{-}1 & -7.145E\text{-}1 & -1.372E\text{-}1 \\ -7.169E\text{-}1 & 8.835E\text{-}2 & 1.172E\text{-}2 & 6.915E\text{-}1 \\ 2.318E\text{-}1 & 7.184E\text{-}1 & 6.413E\text{-}1 & 1.376E\text{-}1 \\ -6.548E\text{-}1 & 9.518E\text{-}2 & 2.794E\text{-}1 & -6.958E\text{-}1 \end{bmatrix}$$

Singular values..... .2.356, 9.589E-1, 3.181E-1, 7.082E-3

Condition Number.. ..... .332.606

Horizontal norm.. ..... .2.347

Vertical norm.. ..... .3.329

Threshold ..... 10E-2 x Vertical norm = 0.03329

Rank 3

Check on dependency gives columns ordered as 1, 3, 2, 4

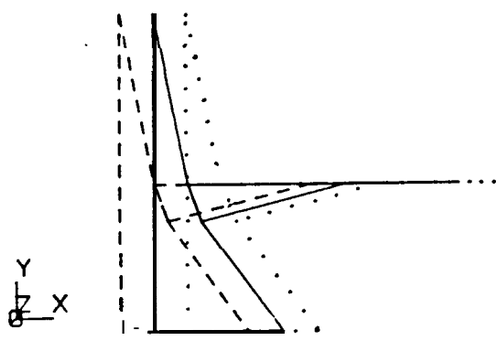

Mode Number 1
Frequency = 0.00 Hz.

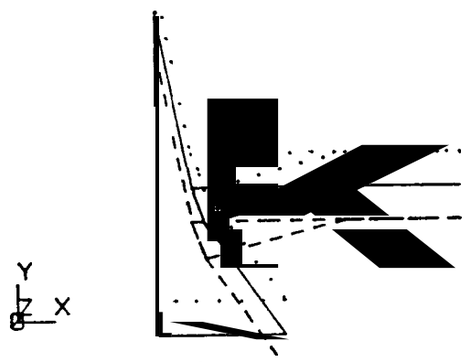

Mode Number' 2
Frequency = 0.00 HZ.

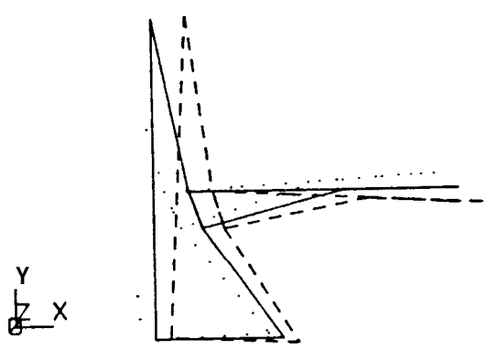

Mode Number 3
Frequency = 0.00 Hz.

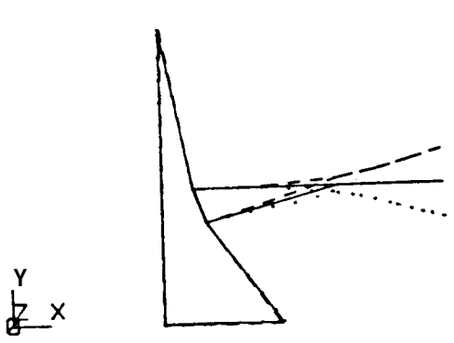

Mode Number 4
Frequency = 149.00 Hr.

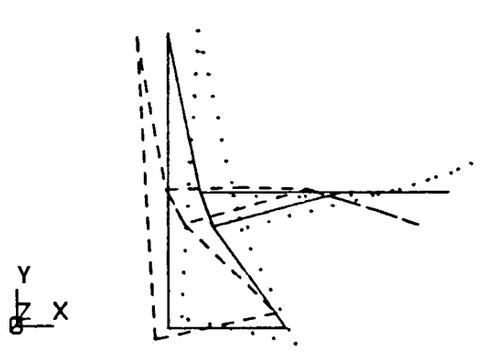

Mode Number 5
Frequency = 231.00 Hz.

Fig. 7.10 a) - **"Curved Frame + Beam" -** Rigid-Body and fiit 2 Elastic Mode Shapes

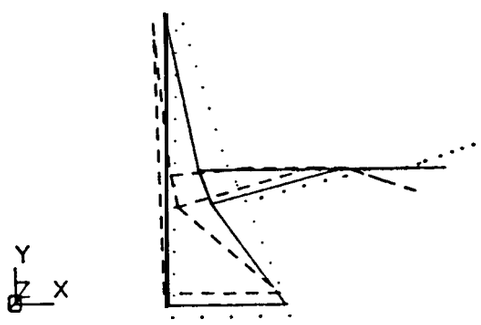

Mode Number 6
Frequency = 286.00 Hz.

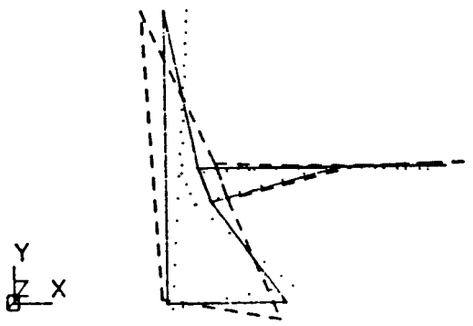

Mode Number 7
Frequency = 313.00 Hz.

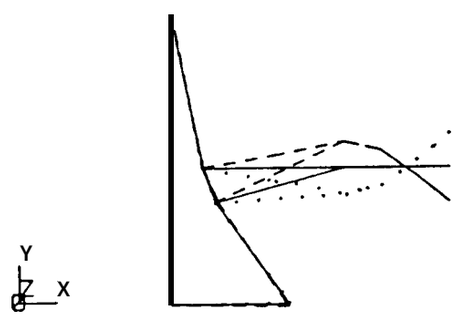

Mode Number 8
Frequency = 512.00 Hz.

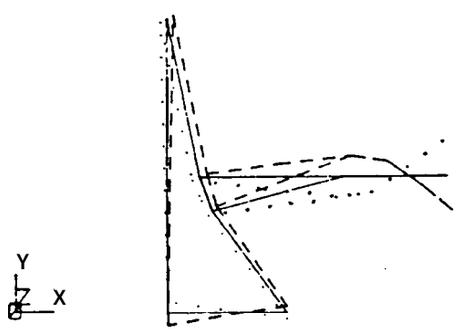

Mode Number 9
Frequency = 537.00 Hz.

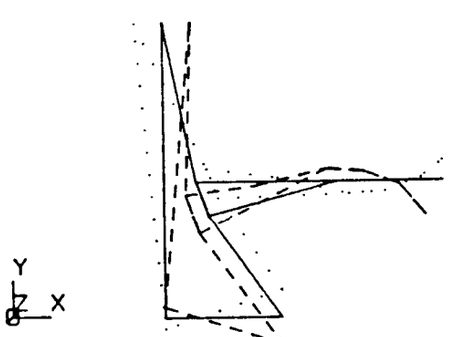

Mode Number 10
Frequency = 603.00 Hz.

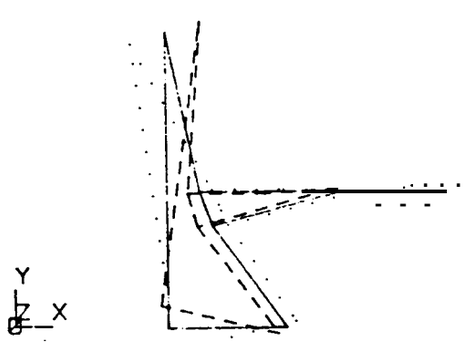

Mode Number 11
Frequency = 688.00 Hz.

Fig. 7.10 b) - **"Curved Frame + Beam"** Elastic Mode Shapes

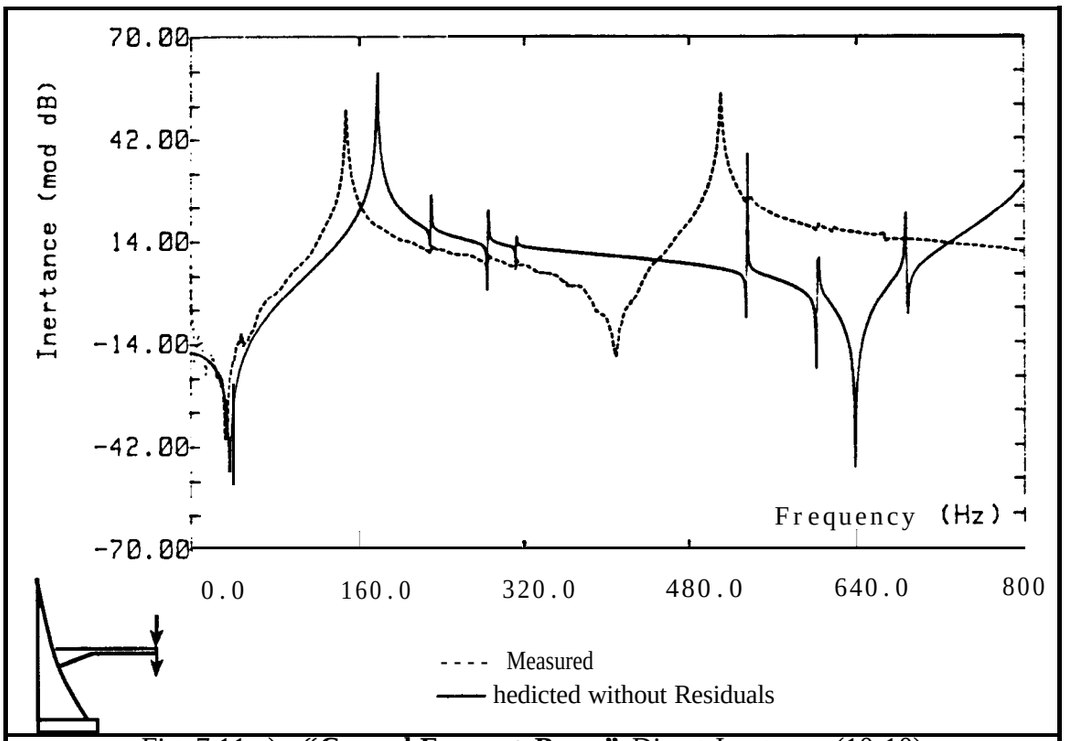

Fig. 7.11 a) - **"Curved Frame + Beam"** Direct Inertance (10-10)
(3 *connection coordinates)*

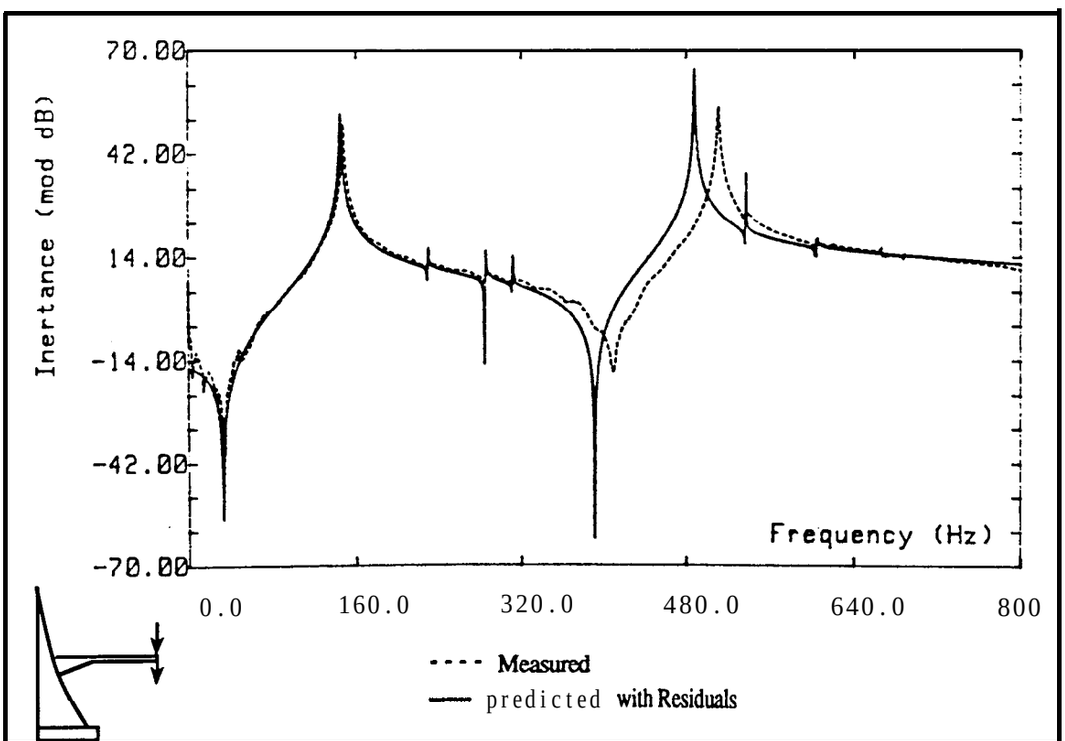

Fig. 7.11b) - "Curved Frame + Beam" Direct Inertance (10-10)
(3 *connection coordinates)*

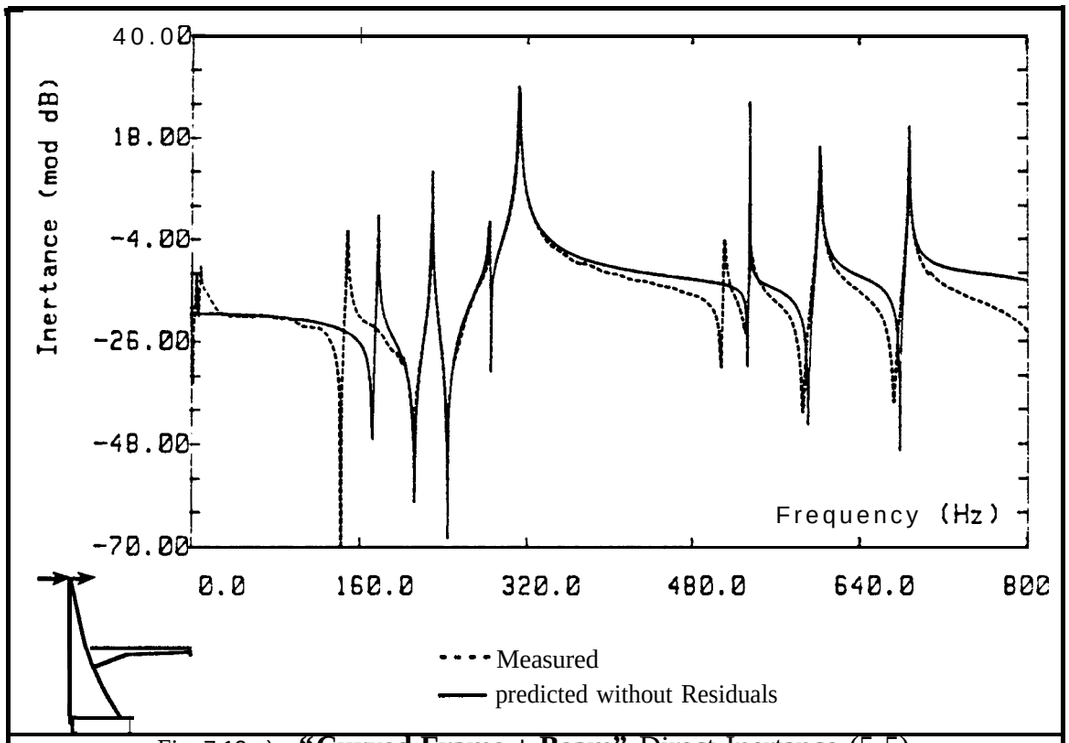

Fig. 7.12 a) - **"Curved Frame + Beam"** Direct Inertance (5-5)
(3 *connection coordinates)*

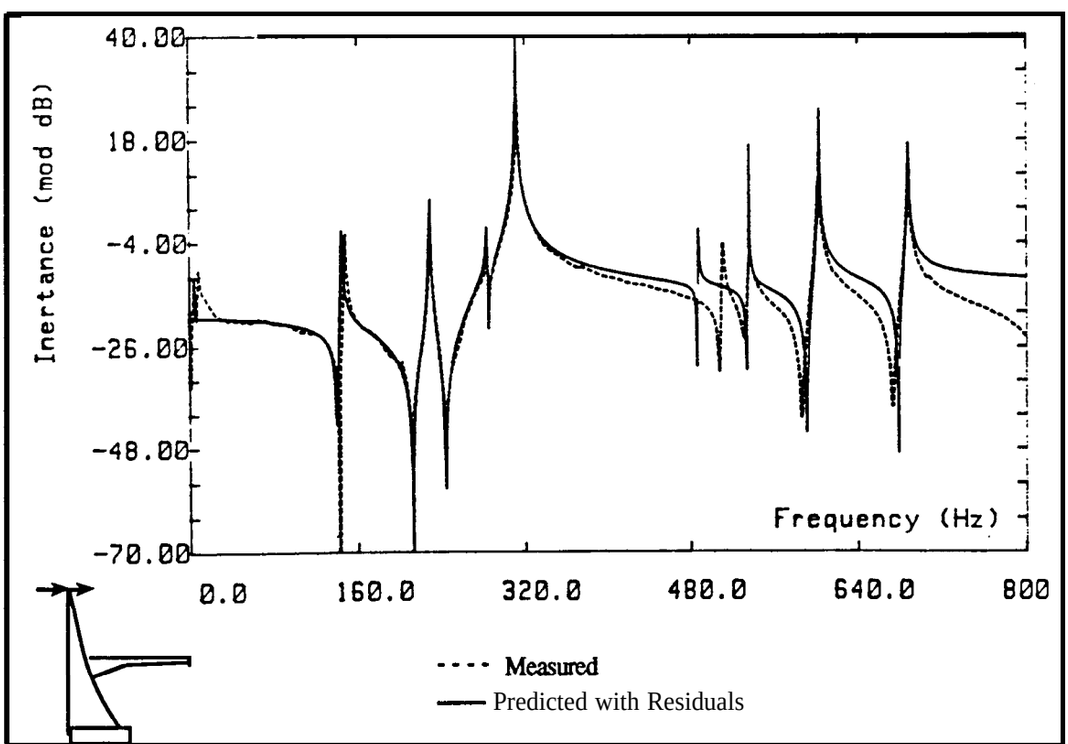

Fig. 7.12 b) - **"Curved Frame + Beam"** Direct Inertance (5-5)
(3 *connection coordinates)*

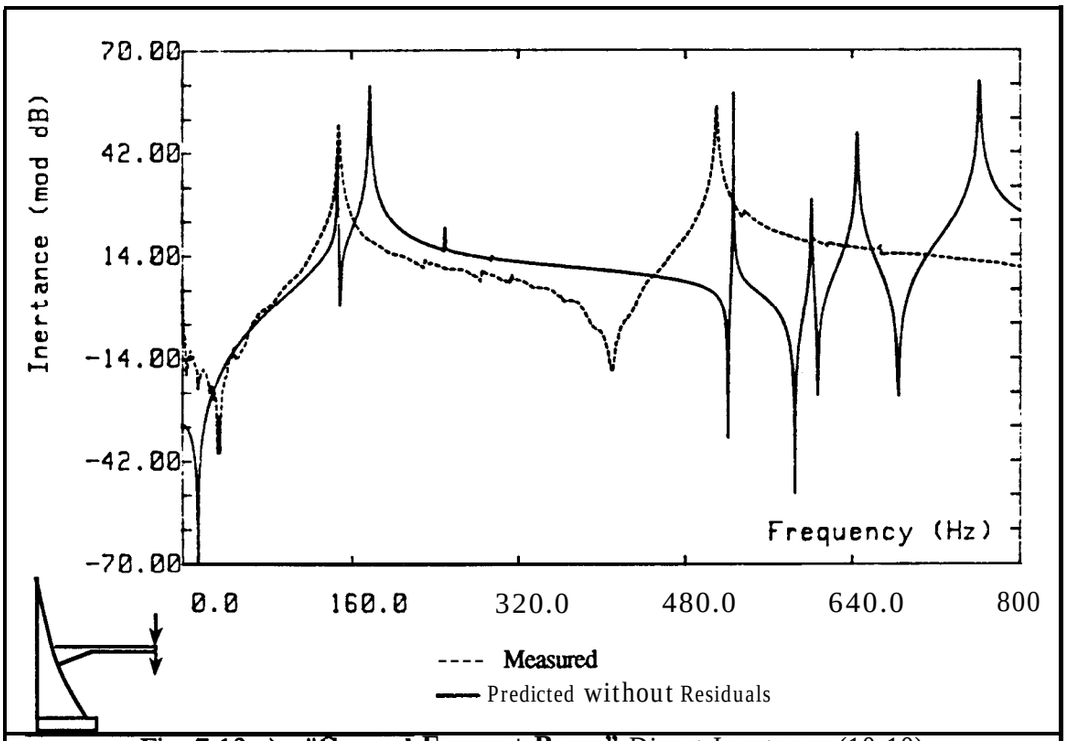

Fig. 7.13 a) - "**Curved Frame + Beam**" Direct Inertance (10-10)
(4 connection coordinates)

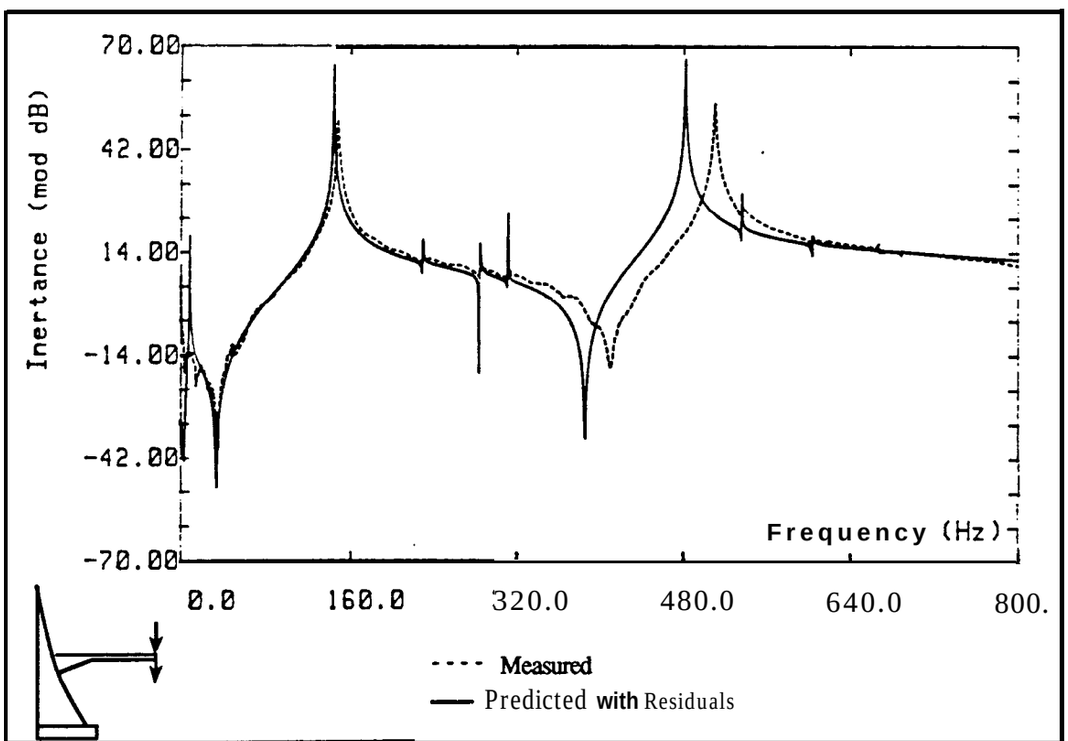

Fig. 7.13 b) - "**Curved Frame + Beam**" Direct Inertance (10-10)
(4 connection coordinates)

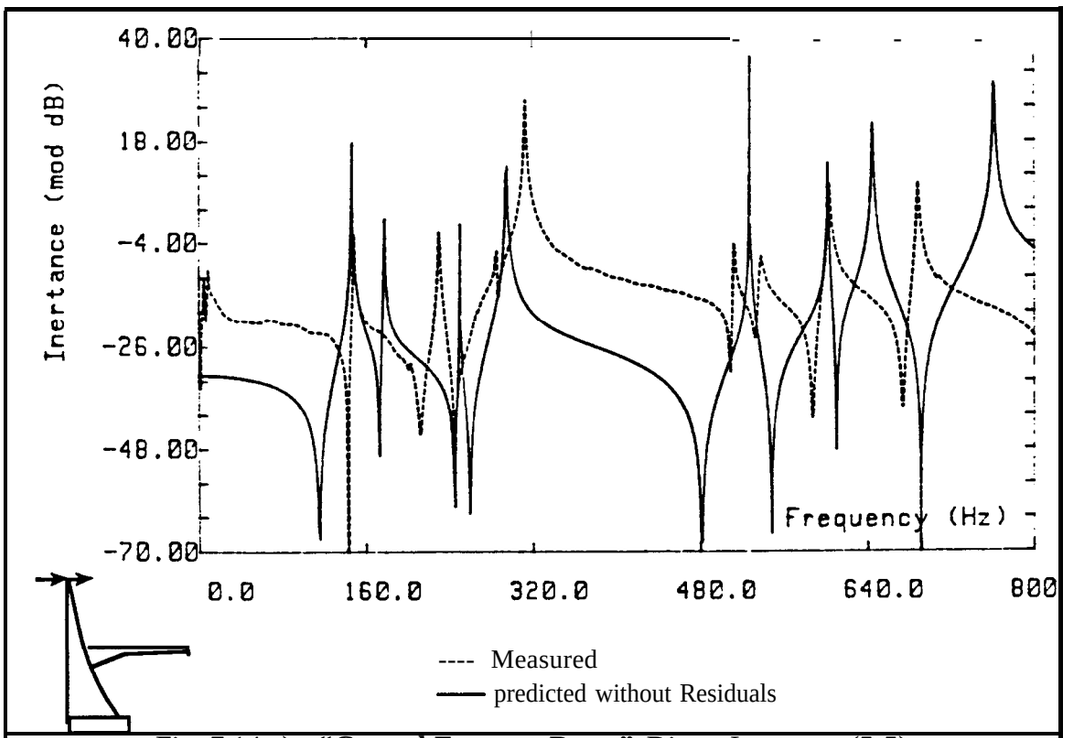

Fig. 7.14 a) - **"Curved Frame + Beam"** Direct Inertance (5-5)
(4 *connection coordinates*)

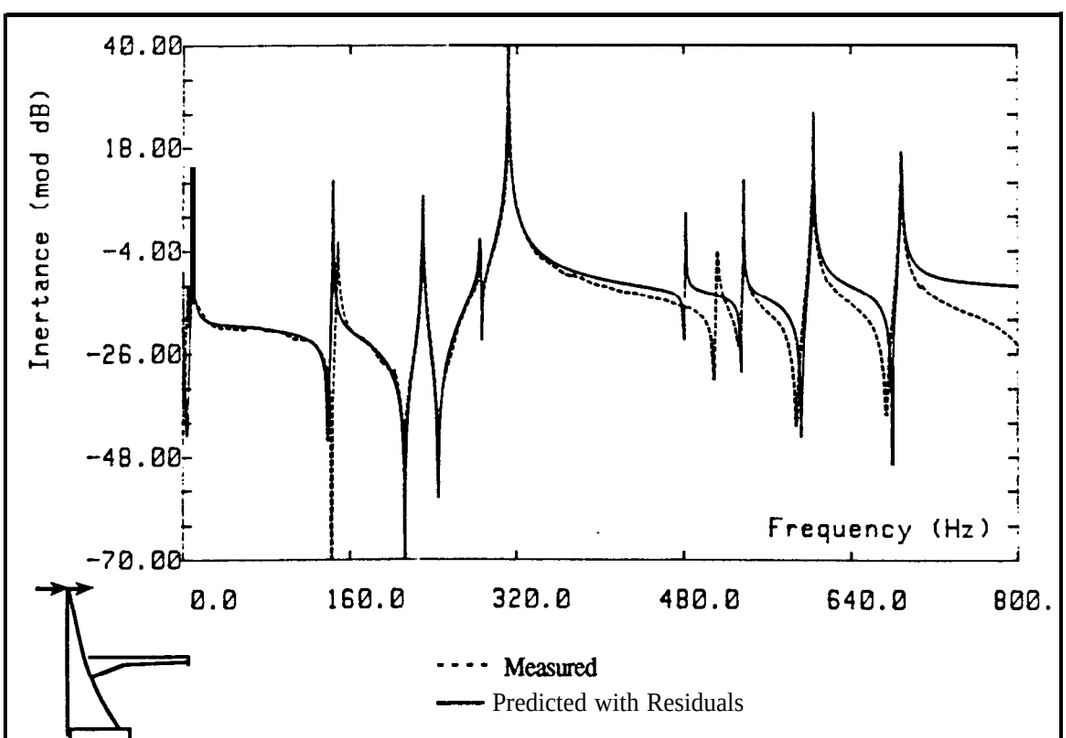

Fig. 7.14 b) - **"Curved Frame + Beam"** Direct Inertance (5-5)
(4 *connection coordinates*)

3 Connecting Coordinates

	1	2	3	4	5	6	7	8
Measured	149	231	286	313	512	537	603	688
Residual 100 %	145.4	229.7	284.6	311.9	488.2	536.9	604.2	688.3
relative *error*	*-2.42*	*-0.56*	*-0.49*	*-0.35*	*-4.65*	*-0.02*	*0.2*	*0.04*
Residual 1 %	177.35	229.8	284.7	312.5	822.5	536	603.4	687.7
relative error	*19.03*	*-0.52*	*-0.45*	*-0.16*	*60.64*	*-0.19*	*-0.07*	*-0.04*
No Residuals	177.7	229.8	284.7	312.5	828.7	536	603.4	687.8
relative error	*19.26*	*-0.52*	*-0.45*	*-0.16*	*61.85*	*-0.19*	*-0.07*	*-0.03*

Table 7.9 - Natural frequencies predicted using 3 coordinates

4 Connecting Coordinates

	1	2	3	4	5	6	7	8
Measured	149	231	286	313	512	537	603	688
Residual 100 %	144.1	229.8	284.6	311.9	481.82	536.9	604.1	688.3
relative error	*-3.29*	*-0.52*	*-0.49*	*-0.35*	*--5.89*	*-0.02*	*0.18*	*0.04*
Residual 1 %	177.3	236.8	289.7	334.9	828.2	536.9	603.4	690.
relative error	*18.99*	*2.51*	*1.29*	*6.99*	*61.76*	*-0.02*	*0.07*	*0.29*
No Residuals	146.89	177.7	249.9	294.5	761.46	526.9	602.2	645.4
relative error	***-1.42***	***--23.1***	***-12.62***	***-5.91***	***48.72***	***-1.88***	***-0.13***	*-6.19*

Table 7.10 - Natural frequencies predicted using 4 coordinates

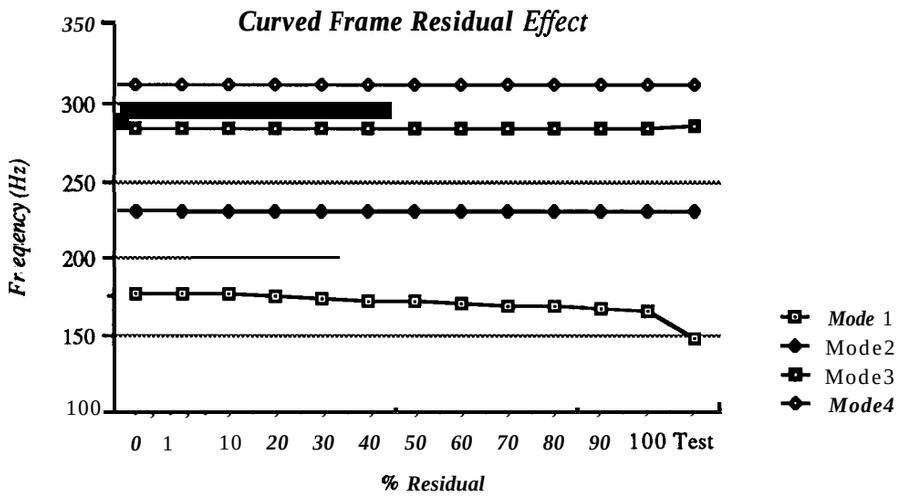

Fig. 7.15 a) - **Curved frame** residual effect on modes 1 2 3 4

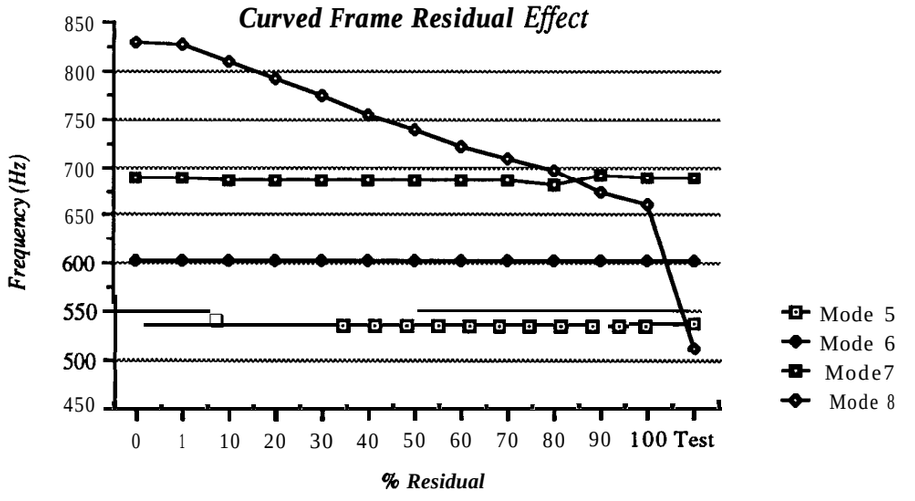

Fig. 7.15 b) - **Curved frame** residual effect on modes 5 6 7 8

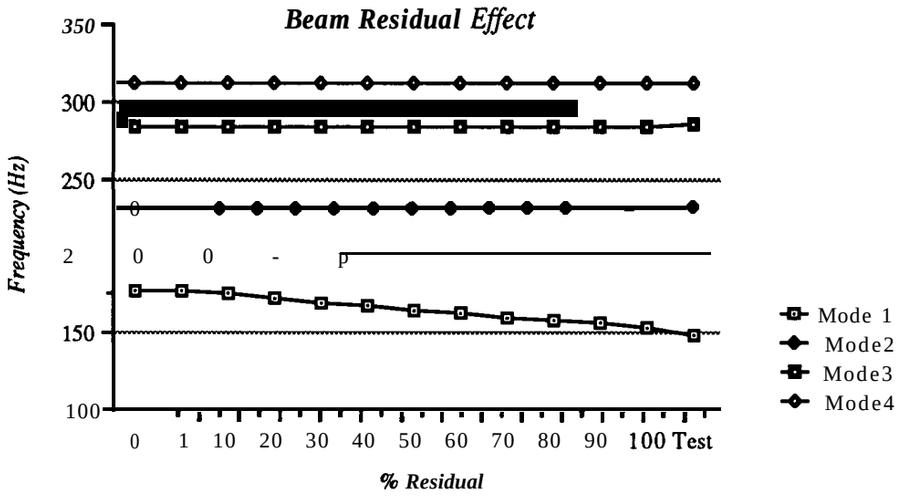

Fig. 7.16 a) - **Beam** residual effect on modes 1 2 3 4

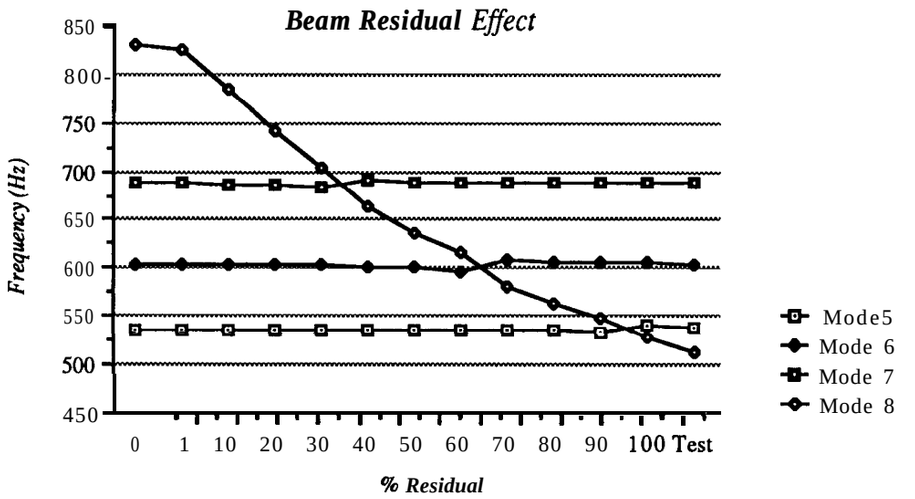

Fig. 7.16 **b) - Beam** residual effect on modes 5 6 7 8

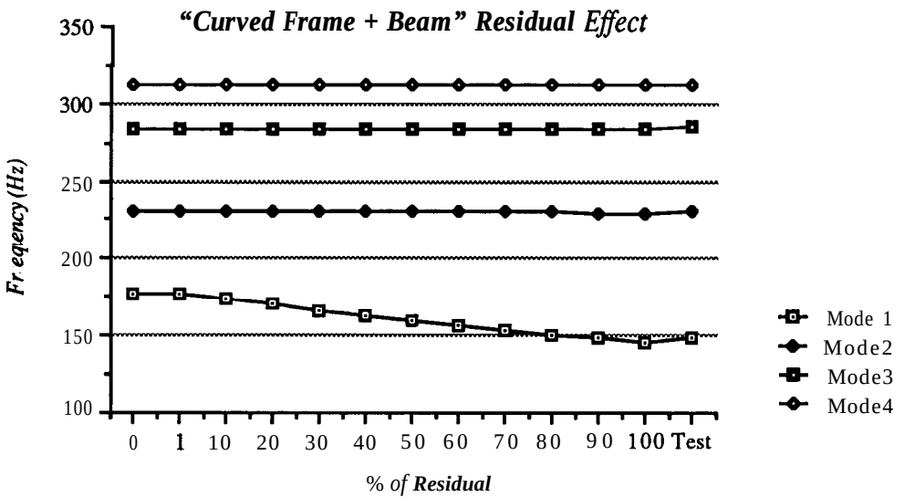

Fig. 7.17 a) - **"Curved frame + Beam"** residual effect on modes 1 2 3 4

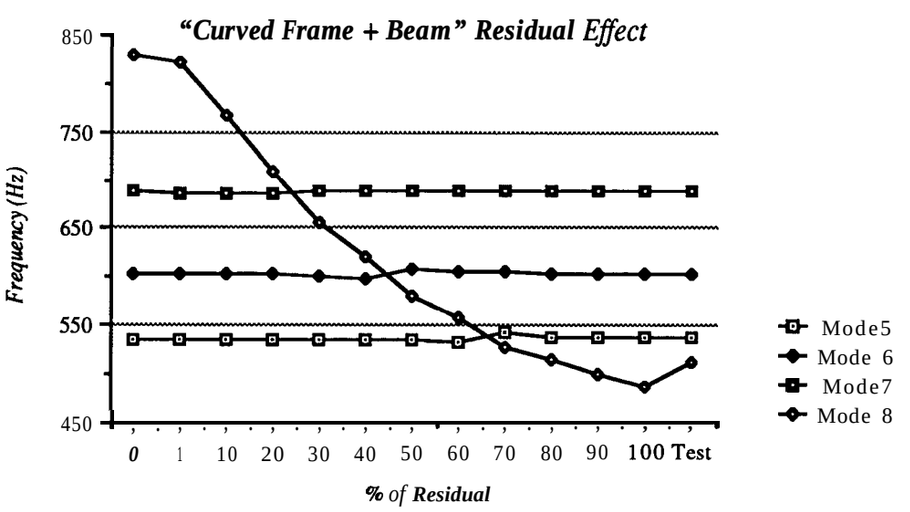

Fig. 7.17 b) - **"Curved frame + Beam"** residual effect on modes 5 6 7 8

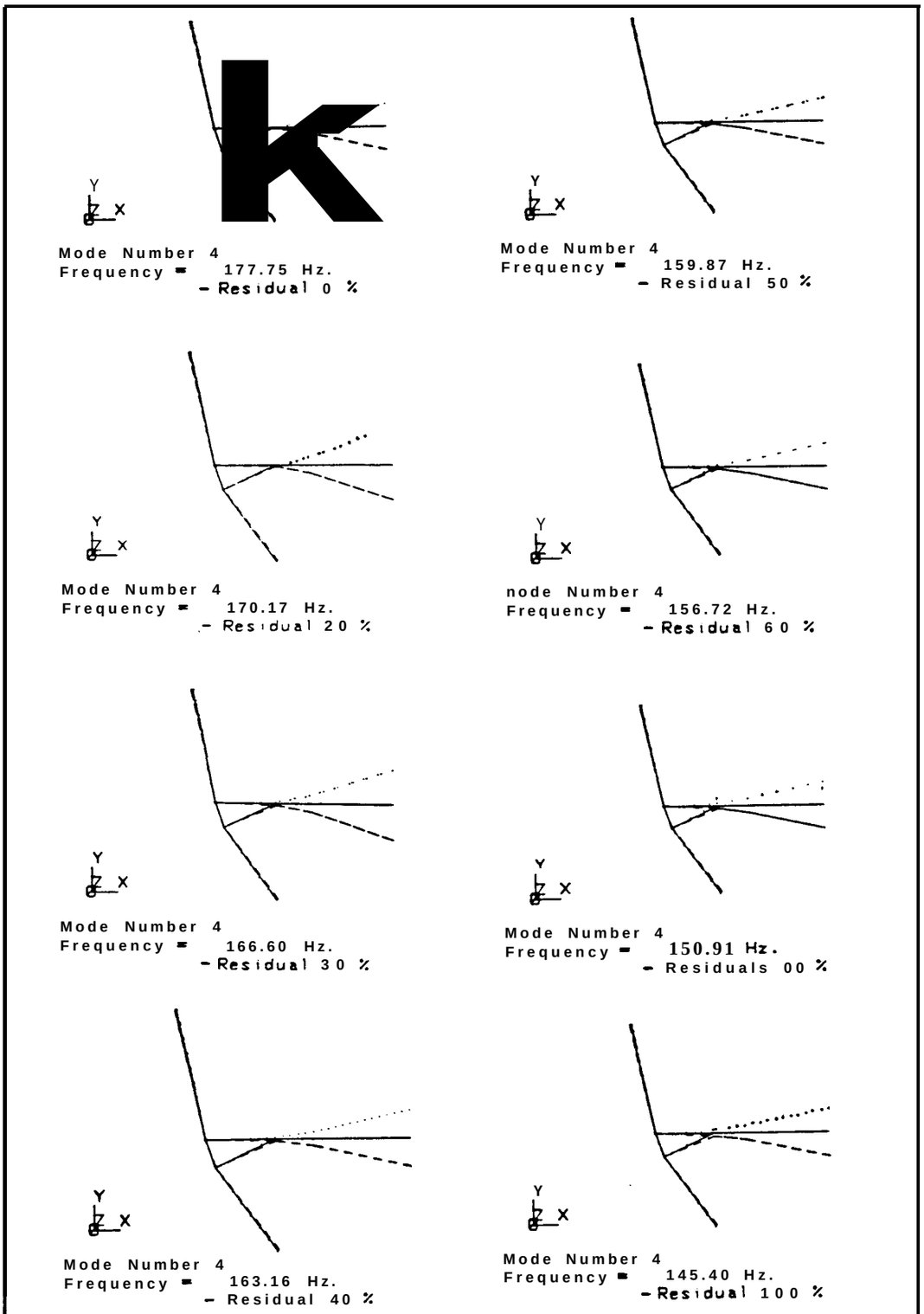

Fig. 7.18 - **"Curved Frame + Beam" -** Predicted **First** elastic mode shape using different percentages of Residuals

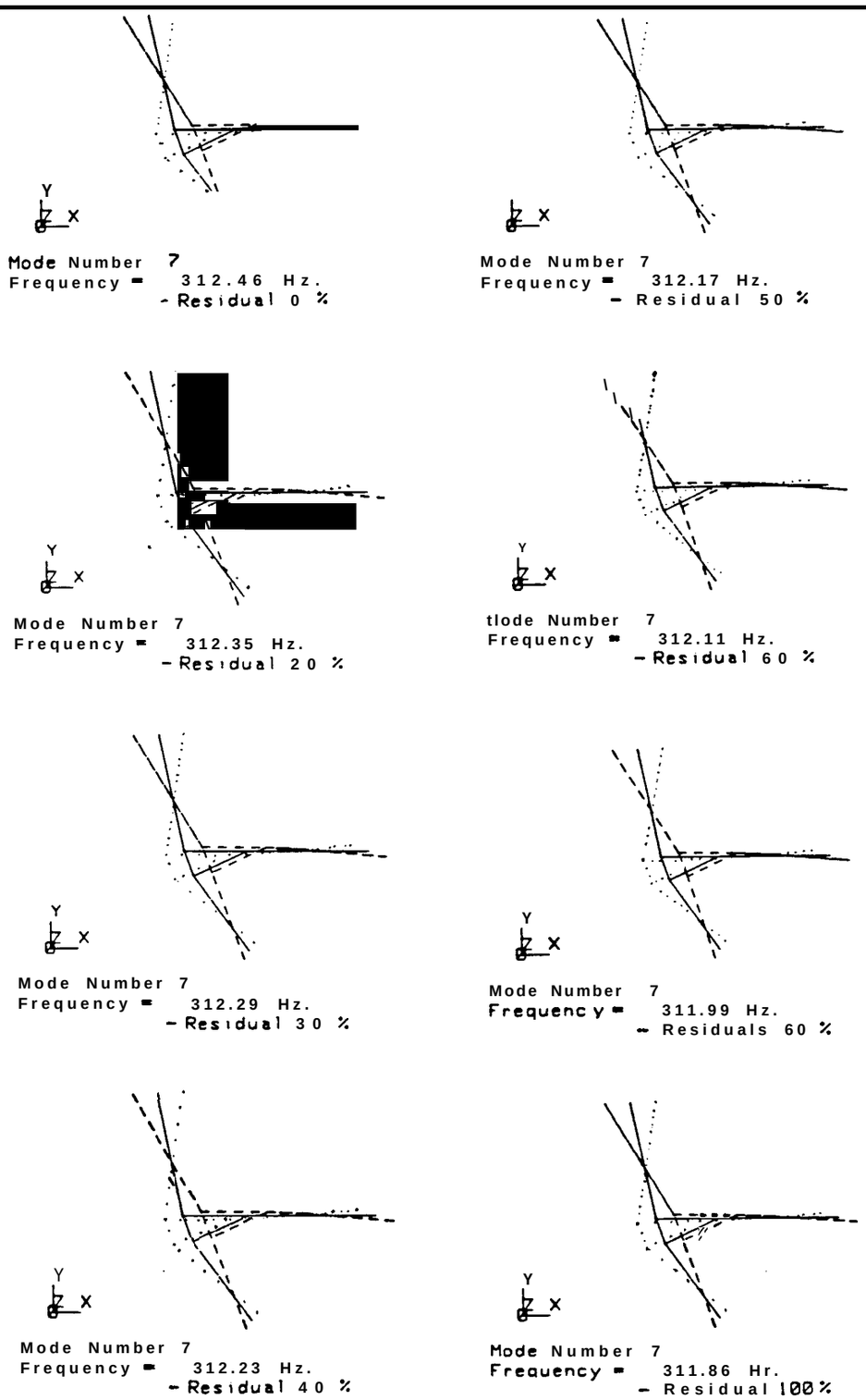

Fig. 7.19 - **"Curved Frame + Beam"** - Predicted **Fourth** elastic mode shape using different percentages of Residuals

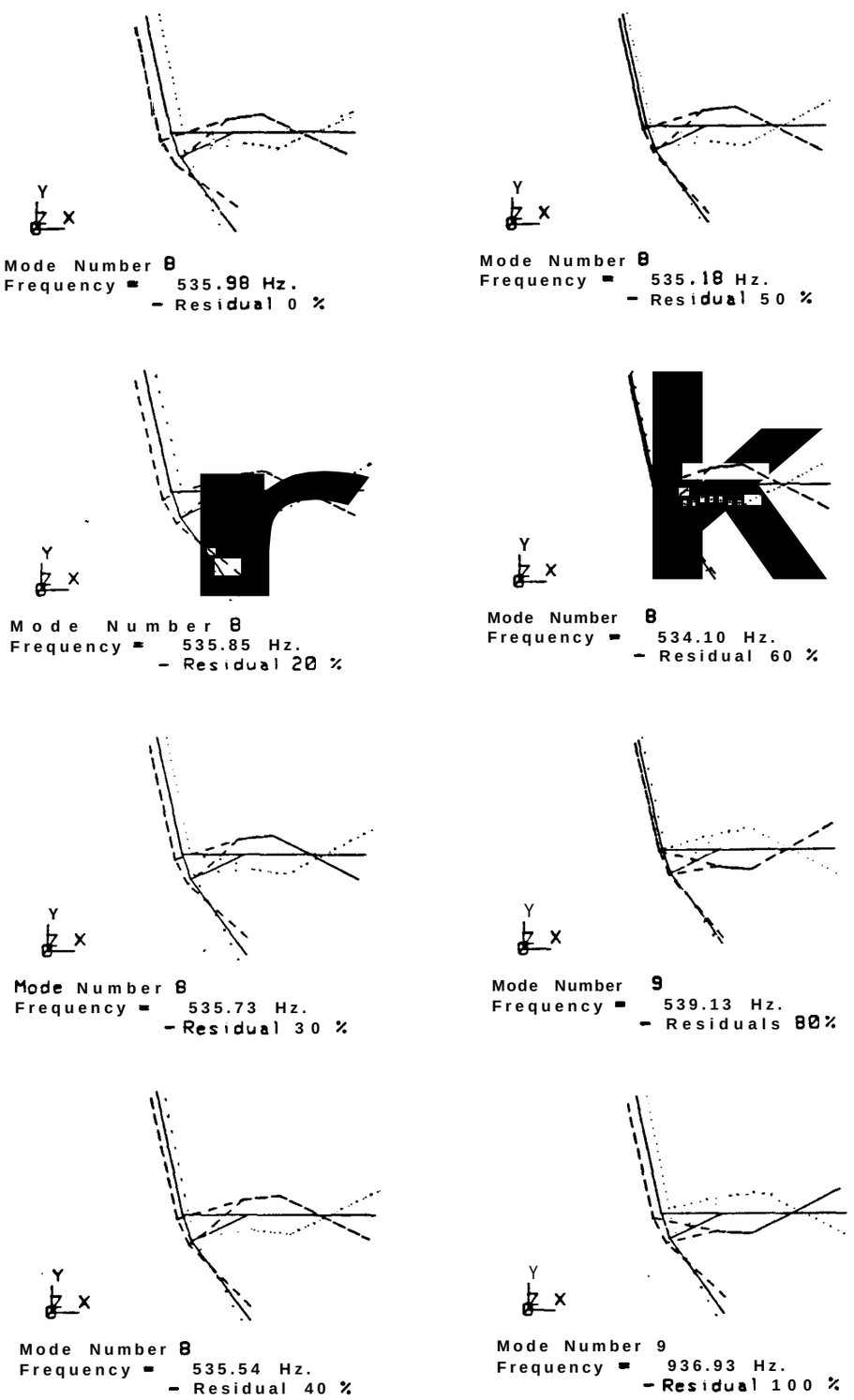

Fig. 7.20 - **"Curved Frame + Beam"** - Predicted **Fifth** elastic mode shape using different percentages of Residuals

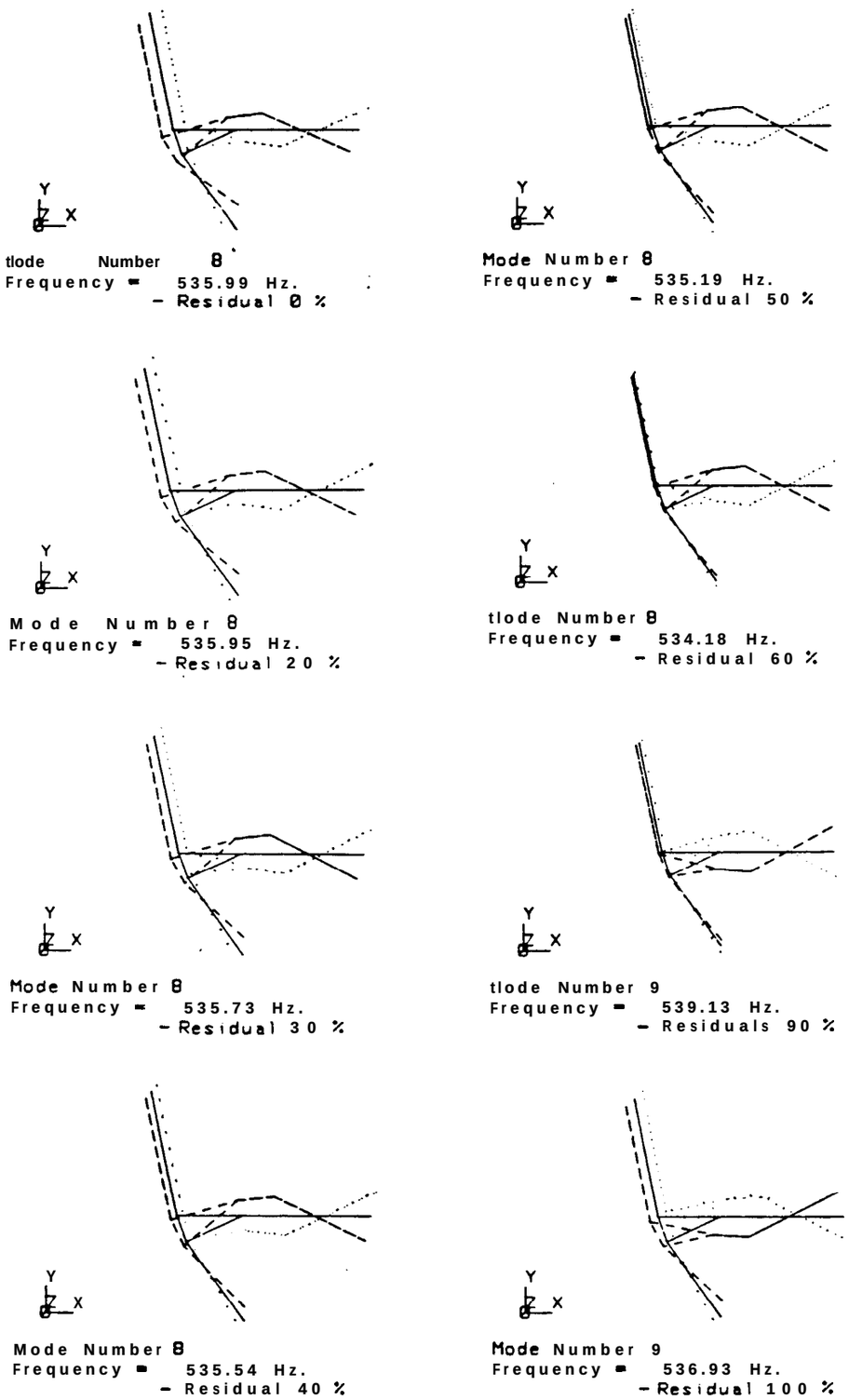

Fig. 7.21 - "Curved Frame + Beam" - Predicted Sixth elastic mode shape using different percentages of Residuals

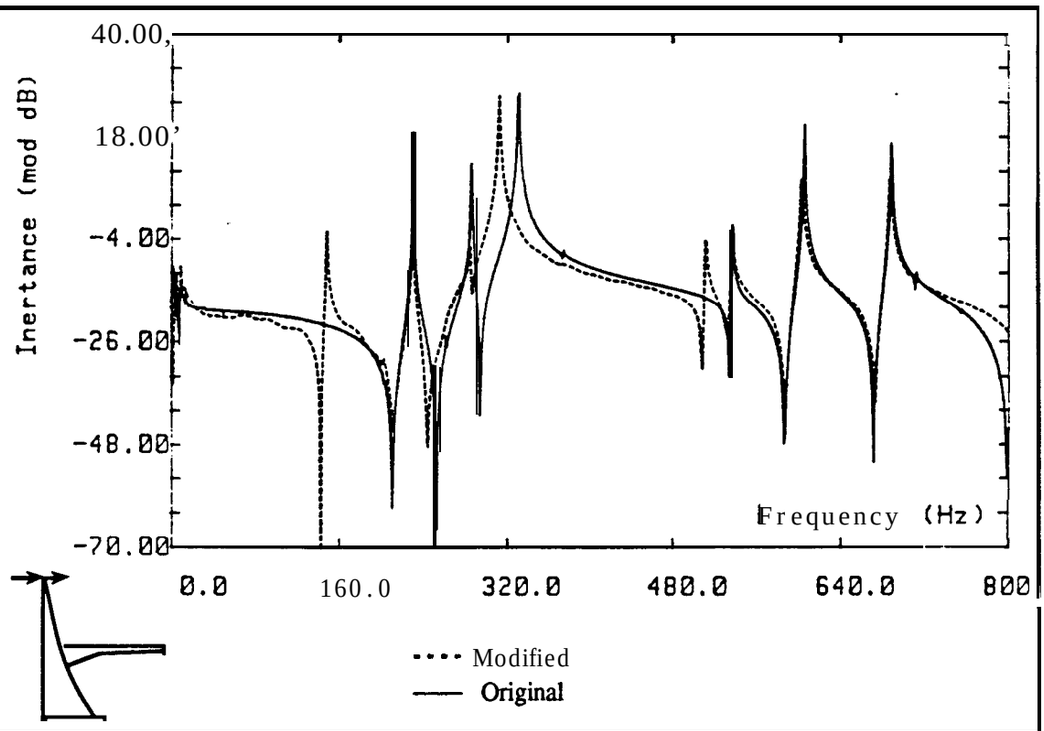

Fig. 7.22 - Original and modified Curved Frame FRFs - Direct Inertance (5-5)

TITLE -->>Curved Frame t l Beam(No Residuals)
FILE Name -->>MDU_HB14NR: ,702
Coord. = 14 Nodes = 11

	1	2	3	4	5	6	7	8	9	10	11
1	+1.57E-01	-4.27E-02	+5.57E-29	+4.86E-03	+8.14E-02	+9.31E-02	-2.08E-01	+3.47E-02	-4.36E-02	-2.27E-02	-7.65E-03
2	-4.50E-20	+4.30E-03	+1.57E-01	-2.24E-02	-4.58E-03	+1.59E-02	-4.88E-02	+2.55E-02	-4.06E-02	-6.79E-03	+1.53E-02
3	+1.57E-01	+4.59E-03	-6.65E-30	-5.43E-03	+7.09E-02	+7.20E-02	-2.12E-01	+1.55E-02	-4.46E-02	-3.18E-02	+2.56E-04
4	-4.43E-20	+6.87E-03	+1.57E-01	-2.36E-02	-9.96E-04	+1.72E-02	-4.02E-02	+2.37E-02	-4.03E-02	-4.34E-03	+1.52E-02
5	+1.57E-01	-2.73E-01	+3.62E-28	+5.62E-02	+6.97E-02	+5.22E-02	+2.91E-01	+3.58E-02	+8.99E-02	+8.20E-02	-5.06E-02
6	-7.02E-20	-8.52E-02	+1.57E-01	-2.25E-03	+9.74E-03	+2.68E-02	+1.24E-02	+3.93E-02	-1.26E-04	+2.99E-02	-9.20E-04
7	+1.57E-01	+1.43E-01	-1.87E-28	-4.20E-02	+2.41E-02	+1.53E-02	+5.92E-02	-3.19E-03	-3.95E-03	-2.13E-02	+1.34E-02
8	-1.58E-20	+1.08E-01	+1.57E-01	-7.89E-02	-2.61E-02	+5.53E-01	+9.78E-02	-8.25E-02	-5.68E-03	-6.32E-01	+4.55E-02
9	+1.57E-01	-4.29E-02	+4.23E-29	-4.35E-02	+7.56E-02	+8.62E-02	-2.12E-01	+3.06E-02	-4.56E-02	-2.51E-02	-6.81E-04
10	+5.37E-20	+3.55E-01	+1.57E-01	+1.73E+00	+1.45E-01	+1.35E-01	+7.38E-02	+7.26E-02	+6.58E-02	+9.44E-02	+1.53E+00
11	+1.57E-01	-4.29E-02	+4.23E-29	-4.35E-02	+7.56E-02	+8.62E-02	-2.12E-01	+3.06E-02	-4.56E-02	-2.51E-02	-6.81E-04
12	+1.84E-20	+2.30E-01	+1.57E-01	+3.26E-01	-4.84E-03	-3.02E-02	-2.86E-02	-5.56E-02	-5.56E-02	-7.69E-02	-1.14E+00
13	+1.57E-01	-4.29E-02	+4.23E-29	-4.35E-02	+7.56E-02	+8.62E-02	-2.12E-01	+3.06E-02	-4.56E-02	-2.51E-02	-6.81E-04
14	+1.12E-22	+1.65E-01	+1.57E-01	+1.54E-02	-2.78E-02	-4.42E-02	-4.63E-02	-4.09E-02	-4.87E-02	-4.60E-02	-3.11E-01

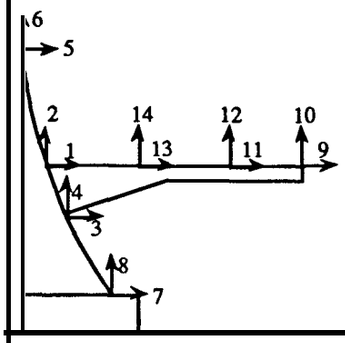

Eigenvalues	Natural Frequencies
1.000E-08	1.592E-05 Hz
4.319E-07	1.046E-04 Hz
1.000E-06	1.592E-04 Hz
1.247E+06	1.777E+02 Hz
2.085E+06	2.298E+02 Hz
3.200E+06	2.847E+02 Hz
3.854E+06	3.125E+02 Hz
1.134E+07	5.360E+02 Hz
1.437E+07	6.034E+02 Hz
1.867E+07	6.878E+02 Hz
2.711E+07	8.287E+02 Hz

Table 7.11 - **"Curved Frame + Beam"** Predicted Modal Matrix **without** Residuals

TITLE -->>Curved Frame + I Beam(Experimental Residuals)
FILE Name-->>MDU_HB14RR: ,702
Coord. = 14 Modes = 14

	1	2	3	4	5	6	7	8	9	10	11
1	-1.57E-01	●	4.28E-02	+1.12E-05	+9.79E-03	+8.15E-02	+9.37E-02	-2.06E-01	-1.37E-02	+3.68E-02	-3.96E-02	-2.06E-02
2	+7.82E-06	-4.31E-03	+1.57E-01	-2.76E-02	-4.23E-03	+1.60E-02	-4.86E-02	+2.13E-02	+2.27E-02	-4.22E-02	-8.51E-03	
3	-1.57E-01	-4.50E-03	+1.04E-05	-2.73E-03	+7.12E-02	+7.26E-02	-2.10E-01	-9.18E-03	+1.67E-02	-4.18E-02	-3.05E-02	
4	+6.21E-06	-6.87E-03	+1.57E-01	-2.87E-02	-6.10E-04	+1.74E-02	-4.00E-02	+2.11E-02	+2.09E-02	-4.20E-02	-6.09E-03	
5	-1.57E-01	+2.73E-01	+1.50E-05	+7.12E-02	+6.87E-02	+5.06E-02	+2.91E-01	-3.13E-02	+4.09E-02	+9.46E-02	+8.69E-02	
6	+6.39E-05	+8.52E-02	+1.57E-01	-3.56E-03	+9.71E-03	+2.66E-02	+1.26E-02	+1.42E-02	+3.76E-02	-4.96E-04	+2.97E-02	
7	-1.57E-01	-1.43E-01	+8.16E-06	-4.34E-02	+2.50E-02	+1.51E-02	+5.97E-02	+8.30E-03	-4.71E-03	-5.12E-03	-2.24E-02	
8	-5.71E-05	-1.08E-01	+1.57E-01	-7.55E-02	-2.31E-02	+5.53E-01	+1.02E-01	-1.75E-02	-7.96E-02	-2.64E-03	-6.34E-01	
9	-1.57E-01	+4.30E-02	+1.12E-05	-5.19E-02	+7.78E-02	+8.92E-02	-2.18E-01	+3.25E-02	+2.93E-02	-5.35E-02	-3.12E-02	
10	-2.12E-04	-3.55E-01	+1.57E-01	+1.57E+00	+8.85E-02	+1.05E-01	+5.28E-02	+1.25E+00	-1.19E-01	-7.94E-02	-2.33E-02	
11	-1.57E-01	+4.30E-02	+1.12E-05	-5.19E-02	+7.78E-02	+8.92E-02	-2.18E-01	+3.25E-02	+2.93E-02	-5.35E-02	-3.12E-02	
12	-1.33E-04	-2.30E-01	+1.57E-01	+4.97E-01	-3.32E-03	-2.31E-02	-2.17E-02	-9.32E-01	+9.60E-02	+6.31E-02	+1.89E-02	
13	-1.57E-01	+4.30E-02	+1.12E-05	-5.19E-02	+7.78E-02	+8.92E-02	-2.18E-01	+3.25E-02	+2.93E-02	-5.35E-02	-3.12E-02	
14	-9.26E-05	-1.65E-01	+1.57E-01	+2.07E-01	-1.71E-02	-3.32E-02	-3.75E-02	-8.48E-01	+8.57E-02	+3.61E-02	+8.27E-03	

Eigenvalues	Natural Frequencies
1.137E-08	1.697E-05 Hz
4.308E-07	1.045E-04 Hz
1.000E-06	1.592E-04 Hz
8.346E+05	1.454E+02 Hz
2.083E+06	2.297E+02 Hz
3.197E+06	2.846E+02 Hz
3.840E+06	3.119E+02 Hz
9.410E+06	4.882E+02 Hz
1.138E+07	5.369E+02 Hz
1.441E+07	6.042E+02 Hz
1.871E+07	6.883E+02 Hz
5.550E+07	1.186E+03 Hz
1.337E+08	1.841E+03 Hz
2.808E+08	2.667E+03 Hz

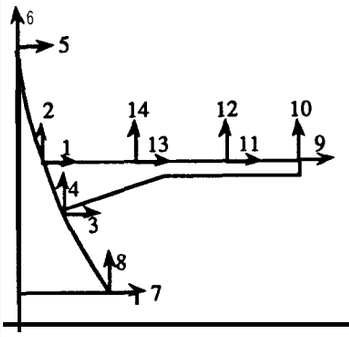

Table 7.12 - **"Curved Frame + Beam"** predicted Modal Matrix **with** Residuals

TITLE -->>Measured Curved Frame t I Beam-(MB101-2 3-4 5-6 10-11 B-9 1-C 1-B)
FILE Ware -->>MDU_MB14XX:,702
Coord. = 14 Modes = 11

	1	2	3	4	5	6	7	8	9	10	11
1	+1.57E-01	+0.00E+00	-1.78E-01	+3.05E-03	+4.28E-02	+4.07E-02	-8.99E-02	+1.13E-02	-6.53E+00	+3.56E+00	+1.35E-02
2	+0.00E+00	+1.57E-01	-3.88E-04	+1.03E-02	-4.13E-03	+6.45E-03	-2.51E-02	-4.12E-03	-3.12E+00	+4.28E+00	+2.07E-03
3	+1.57E-01	+0.00E+00	-1.60E-01	-8.53E-03	+3.61E-02	+4.90E-02	-8.78E-02	-1.73E-02	-3.57E+00	+3.20E+00	+1.66E-02
4	+0.00E+00	+1.57E-01	+3.70E-03	+9.48E-03	-3.43E-03	+3.72E-03	-1.28E-02	-1.17E-02	-4.30E+00	+5.86E+00	+1.09E-03
5	+1.57E-01	+0.00E+00	-2.52E-01	-3.65E-02	+3.87E-02	+1.71E-02	+1.23E-01	-1.24E-02	-5.77E+00	-9.32E+00	-3.81E-02
6	+0.00E+00	+1.57E-01	-1.95E-02	+3.43E-03	+3.69E-03	+1.51E-02	+1.57E-03	+3.37E-03	-2.88E+00	-8.10E-02	-1.23E-02
7	+1.57E-01	+0.00E+00	-1.12E-01	+1.95E-02	+1.24E-02	+8.65E-03	+3.42E-02	+1.00E-02	-1.00E-05	-1.00E-05	+9.57E-03
8	+0.00E+00	+1.57E-01	+3.48E-02	+2.87E-02	-1.84E-02	-1.65E-02	+8.76E-02	+2.18E-02	-5.75E+00	+9.03E+00	+6.78E-03
9	+1.57E-01	+0.00E+00	-1.78E-01	+4.56E-02	+3.83E-02	+4.24E-02	-9.86E-02	+5.86E-03	-4.05E+00	+5.63E+00	+1.65E-02
10	+0.00E+00	+1.57E-01	+1.ICE-01	-8.20E-01	+4.05E-02	+3.26E-02	-2.05E-02	+3.85E-01	+3.10E+01	+1.13E+01	+3.72E-03
11	+1.57E-01	+0.00E+00	-1.78E-01	+3.05E-03	+4.28E-02	+4.07E-02	-8.99E-02	+1.13E-02	-6.53E+00	+3.56E+00	+1.35E-02
12	+0.00E+00	+1.57E-01	+8.06E-02	-3.62E-01	+1.05E-02	-9.17E-04	-6.66E-03	-2.03E-01	-1.41E+01	-3.28E+00	-6.85E-04
13	+1.57E-01	+0.00E+00	-1.78E-01	+3.05E-03	+4.28E-02	+4.07E-02	-8.99E-02	+1.13E-02	-6.53E+00	+3.56E+00	+1.35E-02
14	+0.00E+00	+1.57E-01	+6.43E-02	-1.82E-01	-3.60E-03	-2.35E-03	-4.79E-03	-2.96E-01	-1.89E+01	-4.21E+00	-1.91E-03

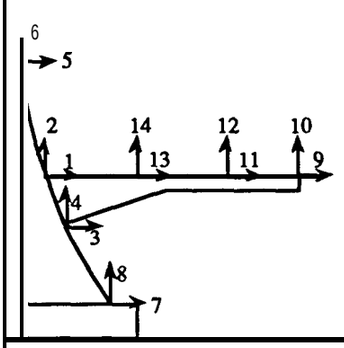

Eigenvalues	Natural Frequencies
1.000E-08	1.592E-05 Hz
1.000E-06	1.592E-04 Hz
3.948E-07	1.000E-04 Hz
8.765E+05	1.490E+02 Hz
2.107E+06	2.310E+02 Hz
3.229E+06	2.860E+02 Hz
3.868E+06	3.130E+02 Hz
1.035E+07	5.120E+02 Hz
1.138E+07	5.370E+02 Hz
1.435E+07	6.030E+02 Hz
1.869E+07	6.880E+02 Hz

Table 7.13 - **"Curved Frame + Beam"** Experimentally-derived Modal Matrix

7.3 EXPERIMENTAL CASE STUDY II

7.3.1 INTRODUCTION

In this case study, an assembled structure formed of two components is dealt with. These components are the two beams which have already been considered in chapter 6, therein seeking to determine experimentally the rotational responses at specified coordinates on the beams. The reason for such an investigation was linked to the need to incorporate the rotational coordinate information in the formulation of constraint equations between the two vibrating subsystems forming a complete structure. In fact, this is not a general rule for all coupling cases, as shown in the previously-presented case study whereby the constraint conditions were formulated without the need of explicit calculation of the rotational responses even with a moment to be transmitted in the interface region of the two components. In that case, the consideration of two coordinates - through which two forces equivalent to a moment can be transmitted - was possible since they were sufficiently spaced from each other on the connecting region to allow, in practical terms, the measurement of the response and the excitation forces.

However, such practical considerations are not possible in the present case study due to the small connecting area between the two beams which, when connected, should constitute a longer continuous beam. Thus, a rotational coordinate should be included at the interface region in order to fullfil the compatibilty between displacements and rotations and equilibrium between forces and moments. Otherwise, the error incurred in neglecting such a coordinate can lead to failure in predictions for the actual response of the assembled beam. The techniques presented in chapter 6 are believed to be suitable for estimating the necessary rotational response in this kind of beam-like elements. Therefore, the results obtained in chapter 6 will be further used in the present case study to construct the necessary Response and Modal models of each beam for subsequent input into the FRF and Modal coupling procedures, respectively.

7.3.2 DESCRIPTION OF THE SUBSYSTEMS

The test components consist of straight steel beams with a uniform rectangular cross-section, as shown in fig. 7.23 . The connection coordinates for each beam are selected to be at their ends which are subsequently connected to another one, forming a longer beam.

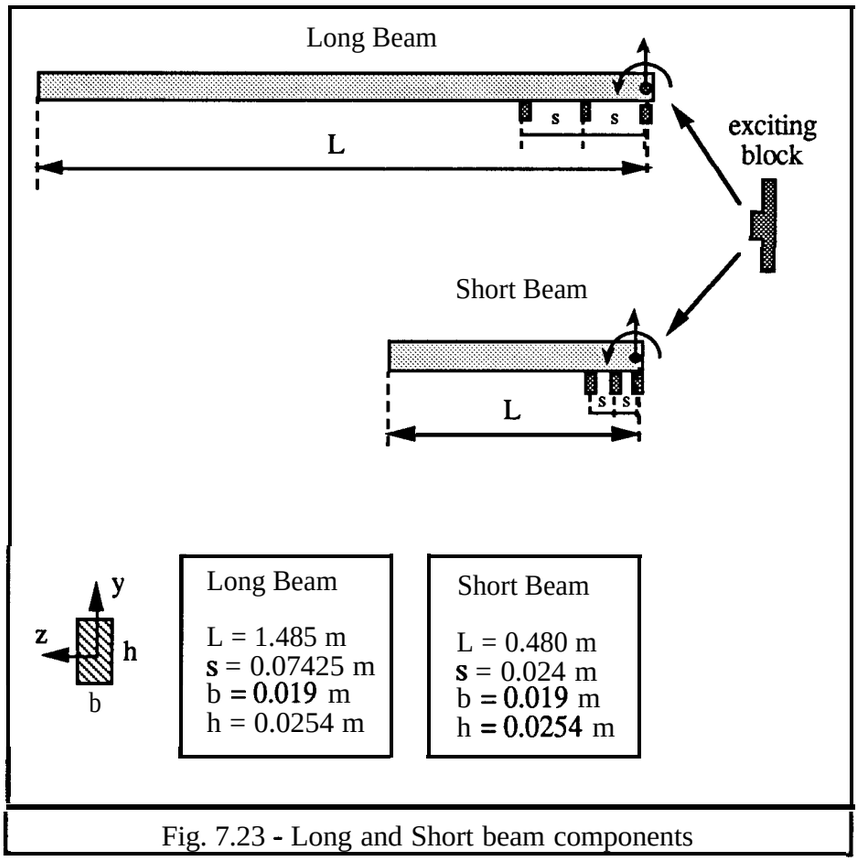

Fig. 7.23 - Long and Short beam components

7.3.3 SUBSYSTEM MODELLING

In chapter 6, the theoretically- and experimentally-derived rotational responses for each beam have already been presented and constituted a topic of discussion in terms of the aptitude of each procedure to estimate accurate rotational properties. In this chapter, various Response and Modal models are constructed by incorporating those estimated rotational responses. These models will differ from each other only by the response of the

rotational coordinate since the transverse response is assumed to be the same for all of them. The various models will be identified according the name given to the procedures used to estimate the rotations in chapter 6, e.g. if one refers to **Long beam 2** it will mean that the corresponding rotational response in the model is estimated following procedure 2. The table containing the information on all the procedures is presented next:

Table 7.14 - Procedures to estimate **Response** and **Modal** models

Procedure	Name	No. Points	Distance (d)	d/L
1	3PS	3	S	0.05
2	3P2S	3	2S	0.1
3	2PS	2	S	0.05
4	2P2S	2	2S	0.1
5	2P4S	2	4S	0.2

and four locations for the accelerometers corresponding to the measured coordinates on each beam are shown in fig. 7.24 (in each procedure, only two or three coordinates are considered when estimating the rotations).

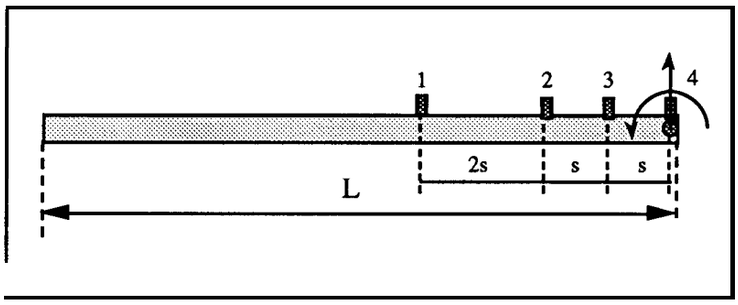

Fig. 7.24 - Beam with 4 accelerometers

7.3.3.1 RESPONSE MODELS

The frequency range of interest for the complete structure's properties is taken to be 0 800 Hz. This requires the measurement of each FRF in both beams to be undertaken in the **same** frequency range, if the FRF coupling technique is used. Only the rotational

shown in fig.7.25, since the corresponding data for the long beam have already been presented in the previous chapter.

7.3.3.2 MODAL MODELS

The Modal models of both beams are derived by following the Modal route described in chapter 6 (vidé section 6.6.3). This route assumes the measurement of FRFs at two or three closely-spaced coordinates, necessary to construct one row (or column) in the **FRF** matrix. Then a modal identification algorithm [71] is applied to convert the Response data into Modal properties. It is important to note that in this case there are no restrictions about the measured frequency ranges on each component since a Modal coupling technique is supposed to be used subsequently.

The ***measured*** Modal models need to be converted into ***estimated*** ones, and this can be done by using the first and second order approximations, whose formulation was presented in chapter 6 (vide 6.3.2.1 and 6.3.2.2). It should be noted that this will express each model's dynamic properties in the measured frequency range only. Should the residual flexibility effect ot the out-of-range modes be taken into account, it is necessary to measure additional FRFs and to identify an extra mode in each of these in order to estimate the residual matrix according to first and second order formulation above mentioned.

The modal and residual flexibility matrices referred to the 4 measured coordinates on both beams are presented next. From these, the corresponding matrices referred to the translational and rotational coordinate at point 4 are estimated, as follows;

Modal and **Residual Flexibility** matrices referred to the **measured (4)** coordinates

.....**Long beam**.....

Modal Matrix

$$[\Phi]_{4x7} = \begin{bmatrix} 4.211E\text{-}1 & 2.845E\text{-}1 & 8.817E\text{-}2 & -2.838E\text{-}1 & -4.720E\text{-}1 & -4.517E\text{-}1 & -2.866E\text{-}1 \\ 4.211E\text{-}1 & 3.734E\text{-}1 & 3.641E\text{-}1 & 1.488E\text{-}1 & -5.902E\text{-}2 & -2.425E\text{-}1 & -3.672E\text{-}1 \\ 4.211E\text{-}1 & 4.241E\text{-}1 & 5.640E\text{-}1 & 4.433E\text{-}1 & 3.053E\text{-}1 & 1.860E\text{-}1 & 3.723E\text{-}2 \\ 4.211E\text{-}1 & 5.001E\text{-}1 & 7.447E\text{-}1 & 7.270E\text{-}1 & 7.076E\text{-}1 & 6.965E\text{-}1 & 6.632E\text{-}1 \end{bmatrix}$$

Natural Frequencies 0, 0, 61. 167, 325. 535, 794 Hz

Identified Residual Matrix

$$[R_{cc}]_{4x4} = \begin{bmatrix} 4.036E\text{-}9 & -4.772E\text{-}9 & -1.661E\text{-}9 & 4.490E\text{-}9 \\ -4.772E\text{-}9 & 9.374E\text{-}9 & 2.453E\text{-}9 & -1.241E\text{-}8 \\ -1.661E\text{-}9 & 2.453E\text{-}9 & 3.034E\text{-}9 & 5.060E\text{-}9 \\ 4.490E\text{-}9 & -1.241E\text{-}8 & 5.060E\text{-}9 & 2.688E\text{-}8 \end{bmatrix}$$

.....**Short beam**.....

Modal Matrix

$$[\Phi]_{4x5} = \begin{bmatrix} 7.387E\text{-}1 & 5.905E\text{-}1 & 5.066E\text{-}2 & -6.084E\text{-}1 & -8.629E\text{-}1 \\ 7.387E\text{-}1 & 8.186E\text{-}1 & 6.053E\text{-}1 & 1.407E\text{-}1 & -2.726E\text{-}1 \\ 7.387E\text{-}1 & 9.344E\text{-}1 & 9.081E\text{-}1 & 6.447E\text{-}1 & 3.670E\text{-}1 \\ 7.387E\text{-}1 & 1.045E00 & 1.236E00 & 1.152E00 & 1.073E00 \end{bmatrix}$$

Natural Frequencies 0, 0, 572, 1528, 2844 Hz

Identified Residual Matrix

$$[R_{cc}]_{4x4} = \begin{bmatrix} 1.013E\text{-}09 & 2.056E\text{-}10 & -2.877E\text{-}10 & -3.868E\text{-}10 \\ 2.056E\text{-}10 & 7.109E\text{-}10 & 2.247E\text{-}10 & -8.998E\text{-}10 \\ -2.877E\text{-}10 & 2.247E\text{-}10 & 2.206E\text{-}10 & 2.377E\text{-}10 \\ -3.868E\text{-}10 & -8.998E\text{-}10 & 2.377E\text{-}10 & 1.483E\text{-}09 \end{bmatrix}$$

Estimated Modal and **Residual Flexibility** matrices
referred to the **end (2)** coordinates

..... **Long beam** .....

Procedure 1 - **3 points, distance=s (5% L)**

$$[\Phi]_{2x7} = \begin{bmatrix} 4.211E\text{-}1 & 5.001E\text{-}1 & 7.447E\text{-}1 & 7.270E\text{-}1 & 7.076E\text{-}1 & 6.965E\text{-}1 & 6.632E\text{-}1 \\ 0.000E00 & 1.192E00 & 2.304E00 & 3.750E00 & 5.672E00 & 7.428E00 & 9.922E00 \end{bmatrix}$$

$$[R_{cc}]_{2x2} = \begin{bmatrix} 2.688E\text{-}09 & 3.232E\text{-}07 \\ 3.232E\text{-}07 & 3.822E\text{-}06 \end{bmatrix}$$

Procedure 2 - **3 points, distance=2s (10% L)**

$$[\Phi]_{2x7} = \begin{bmatrix} 4.211E\text{-}1 & 5.001E\text{-}1 & 7.447E\text{-}1 & 7.270E\text{-}1 & 7.076E\text{-}1 & 6.965E\text{-}1 & 6.632E\text{-}1 \\ 0.000E00 & 9.788E\text{-}1 & 2.915E00 & 4.384E00 & 6.353E00 & 8.780E00 & 1.068E01 \end{bmatrix}$$

$$[R_{cc}]_{2x2} = \begin{bmatrix} 2.688E\text{-}09 & 4.538E\text{-}07 \\ 4.538E\text{-}07 & 8.605E\text{-}06 \end{bmatrix}$$

Procedure 3 - **2 points, distance=s (5% L)**

$$[\Phi]_{2x7} = \begin{bmatrix} 4.211E\text{-}1 & 5.001E\text{-}1 & 7.447E\text{-}1 & 7.270E\text{-}1 & 7.076E\text{-}1 & 6.965E\text{-}1 & 6.632E\text{-}1 \\ 0.000E00 & 1.022E00 & 2.433E00 & 3.822E00 & 5.417E00 & 6.875E00 & 8.430E00 \end{bmatrix}$$

$$[R_{cc}]_{2x2} = \begin{bmatrix} 2.688E\text{-}09 & 2.939E\text{-}07 \\ 2.939E\text{-}07 & 3.590E\text{-}06 \end{bmatrix}$$

Procedure 4 - **2 points, distance=2s (10% L)**

$$[\Phi]_{2x7} = \begin{bmatrix} 4.211E\text{-}1 & 5.001E\text{-}1 & 7.447E\text{-}1 & 7.270E\text{-}1 & 7.076E\text{-}1 & 6.965E\text{-}1 & 6.632E\text{-}1 \\ 0.000E00 & 8.522E\text{-}1 & 2.563E00 & 3.894E00 & 5.162E00 & 6.323E00 & 6.939E00 \end{bmatrix}$$

$$[R_{cc}]_{2x2} = \begin{bmatrix} 2.688E\text{-}09 & 2.646E\text{-}07 \\ 2.646E\text{-}07 & 2.770E\text{-}06 \end{bmatrix}$$

Procedure 5 - **2 points, distance=4s (20% L)**

$$[\Phi]_{2x7} = \begin{bmatrix} 4.211E\text{-}1 & 5.001E\text{-}1 & 7.447E\text{-}1 & 7.270E\text{-}1 & 7.076E\text{-}1 & 6.965E\text{-}1 & 6.632E\text{-}1 \\ 0.000E00 & 7.257E\text{-}1 & 2.210E00 & 3.403E00 & 3.972E00 & 3.866E00 & 3.198E00 \end{bmatrix}$$

$$[R_{cc}]_{2x2} = \begin{bmatrix} 2.688E\text{-}09 & 7.539E\text{-}08 \\ 7.539E\text{-}08 & 2.487E\text{-}07 \end{bmatrix}$$

Estimated Modal and **Residual Flexibility** matrices
referred to the **end (2)** coordinates

.....**Short beam**.....

Procedure 1 - **3 points, distance=s (5% L)**

$$[\Phi]_{2x5} = \begin{bmatrix} -7.387E\text{-}1 & -1.045E00 & -1.236E00 & -1.152E00 & -1.073E00 \\ 0.000E00 & 4.470E00 & 1.418E01 & 2.123E01 & 3.081E01 \end{bmatrix}$$

$$[R_{cc}]_{2x2} = \begin{bmatrix} 1.483E\text{-}09 & -5.412E\text{-}08 \\ -5.412E\text{-}08 & 2.033E\text{-}06 \end{bmatrix}$$

Procedure 2 - **3 points, distance=2s (10% L)**

$$[\Phi]_{2x5} = \begin{bmatrix} -7.387E\text{-}1 & -1.045E00 & -1.236E00 & -1.152E00 & -1.073E00 \\ 0.000E00 & 4.683E00 & 1.393E01 & 2.381E01 & 3.590E01 \end{bmatrix}$$

$$[R_{cc}]_{2x2} = \begin{bmatrix} 1.483E\text{-}09 & -7.980E\text{-}08 \\ -7.980E\text{-}08 & 4.705E\text{-}06 \end{bmatrix}$$

Procedure 3 - **2 points, distance=s (5% L)**

$$[\Phi]_{2x5} = \begin{bmatrix} -7.387E\text{-}1 & -1.045E00 & -1.236E00 & -1.152E00 & -1.073E00 \\ 0.000E00 & 4.588E00 & 1.366E01 & 2.115E01 & 2.942E01 \end{bmatrix}$$

$$[R_{cc}]_{2x2} = \begin{bmatrix} 1.483E\text{-}09 & -5.188E\text{-}08 \\ -5.188E\text{-}08 & 2.132E\text{-}06 \end{bmatrix}$$

Procedure 4 - **2 points, distance=2s (10% L)**

$$[\Phi]_{2x5} = \begin{bmatrix} -7.387E\text{-}1 & -1.045E00 & -1.236E00 & -1.152E00 & -1.073E00 \\ 0.000E00 & 4.706E00 & 1.314E01 & 2.108E01 & 2.804E01 \end{bmatrix}$$

$$[R_{cc}]_{2x2} = \begin{bmatrix} 1.483E\text{-}09 & -4.964E\text{-}08 \\ -4.964E\text{-}08 & 1.733E\text{-}06 \end{bmatrix}$$

Procedure 5 - **2 points, distance=4s (20% L)**

$$[\Phi]_{2x5} = \begin{bmatrix} -7.387E\text{-}1 & -1.045E00 & -1.236E00 & -1.152E00 & -1.073E00 \\ 0.000E00 & 4.729E00 & 1.235E01 & 1.834E01 & 2.017E01 \end{bmatrix}$$

$$[R_{cc}]_{2x2} = \begin{bmatrix} 1.483E\text{-}09 & -1.947E\text{-}08 \\ -1.947E\text{-}08 & 3.548E\text{-}07 \end{bmatrix}$$

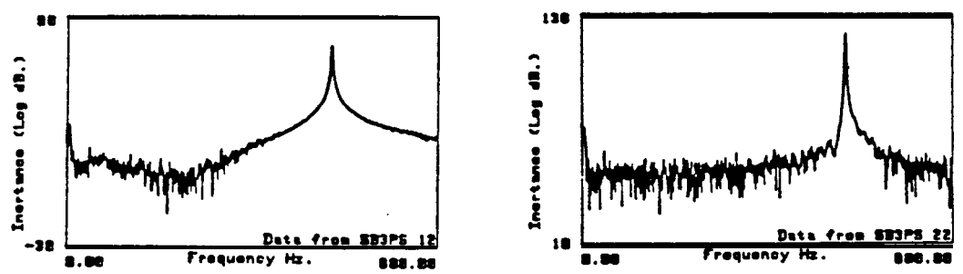

$H_{y\theta}$ **Procedure 1** - 3 accel. dist.= 5% of L $H_{\theta\theta}$

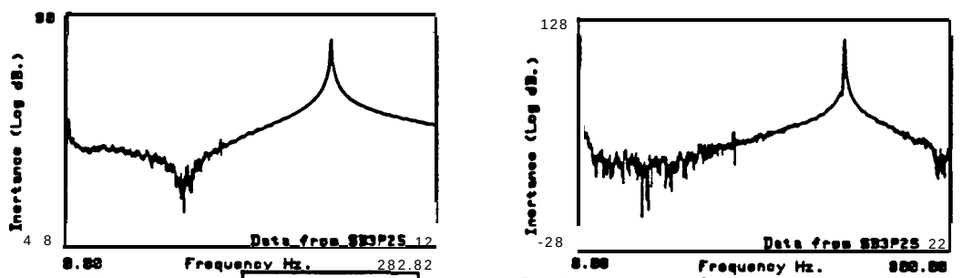

$H_{y\theta}$ **Procedure 2** - 3 accel. dist.= 10% of L $H_{\theta\theta}$

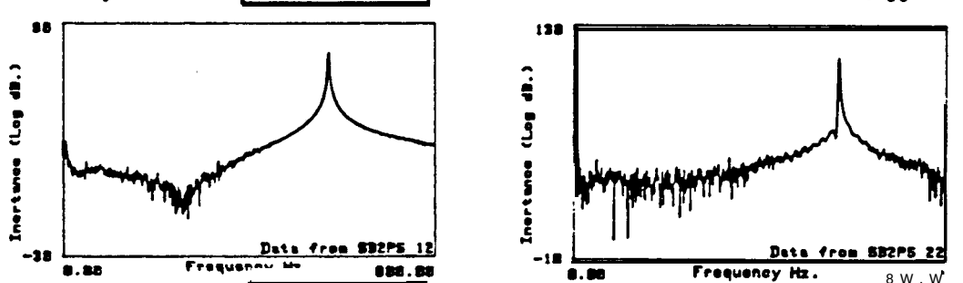

$H_{y\theta}$ **Procedure 3** - 2 accel. dist.= 5% of L $H_{\theta\theta}$

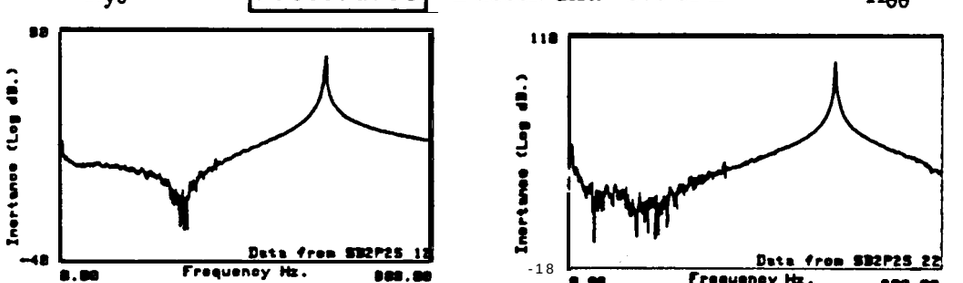

$H_{y\theta}$ **Procedure 4** - 2 accel. dist.= 10% of L $H_{\theta\theta}$

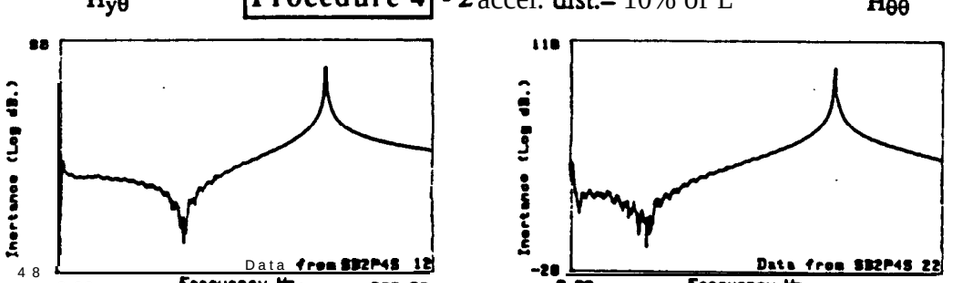

$H_{y\theta}$ **Procedure 5** - 2 accel. dist.= 20% of L $H_{\theta\theta}$

Fig. 7.25 - **Short Beam** estimated **FRFs** using closely-spaced accelerometers

7.3.4 RESULTS FOR THE COUPLED STRUCTURE

Several combinations of models derived according to the previously-mentioned procedures 1 to 5 have been explored in order to predict the coupled structure response. The evaluation of those models, made in chapter 6 just in terms of their rotational responses, gave a good insight into the possible performance of each during a coupling process. For instance, it is expected to have bad results, over the higher frequencies, whenever procedure 5 is utilized to model each beam whereas fairly good results are obtained over the entire range when procedures 2 or 3 are employed. Only the actual results produced by a coupling process can reveal the aptitude of each beam model.

7.3.4.1 DISCUSSION OF IMPEDANCE COUPLING RESULTS

As mentioned in the introduction of this chapter, it is vital to include the rotational coordinate response if reliable results are to be predicted in an assembly of beam-like components. Fig. 7.26 shows the predicted FRF of the assembled beam by considering only the transverse coordinate in the coupling region. It is natural to expect lower resonance frequencies than the true values, since under such a condition the junction is - in effect - assumed to be behaving as pin-joint.

The Response models based on procedure 2 - one of best classified in chapter 6 - were used as a first attempt to predict the coupled structure response. However, the results shown in fig. 7.27 were discouraging since from the conclusions extracted from chapter 6 this procedure was expected to give a fairly accurate modelling of the rotation on the beams. An explanation of the disagreement between the measured and predicted FRFs shown in fig. 7.27, can be made by examining the estimated rotational FRFs of the short beam shown in fig. 7.25, which are here considered over the frequency range O-800 Hz, instead of the O-3200 Hz range assumed in chapter 6. The estimated $H_{\theta\theta}$ FRFs are very noisy for procedures 1 to 3 - there is a rigid-body like behaviour which is not very well defined below the first resonance - and only from procedure 4 onwards does the FRF

become better defined. The misunderstanding about the behaviour of a certain model when drawing conclusions based on the Modal model, as happened in chapter 6, is justified by the fact that only data around the resonance frequency is taken into account in that case, whereas the FRF model data is used at every frequency value, thus being in error over most of the range. Three alternative ways were attempted to improve the prediction. On the one hand, the measured **FRFs** were identified and then regenerated with the inclusion of residual flexibility effects for the out-of-range modes in order to obtain smoothed **FRFs** for input to the estimation process of $H_{y\theta}$ and $H_{\theta\theta}$.**The** results using the smoothed curves for both beams are shown in fig. 7.28, revealing a slight improvement over the previously mentioned ones. *On* the other hand, the short beam model using procedure 4 with raw data, which gives better estimations for $H_{y\theta}$ and $H_{\theta\theta}$ was used and the results, shown in fig. 7.29, are similar to those achieved with procedure 2 and smoothed data. Lastly, the block approach making use of smoothed data was used for modelling short beam and the results, shown in fig. 7.30, were in better agreement than all the previously mentioned predictions.

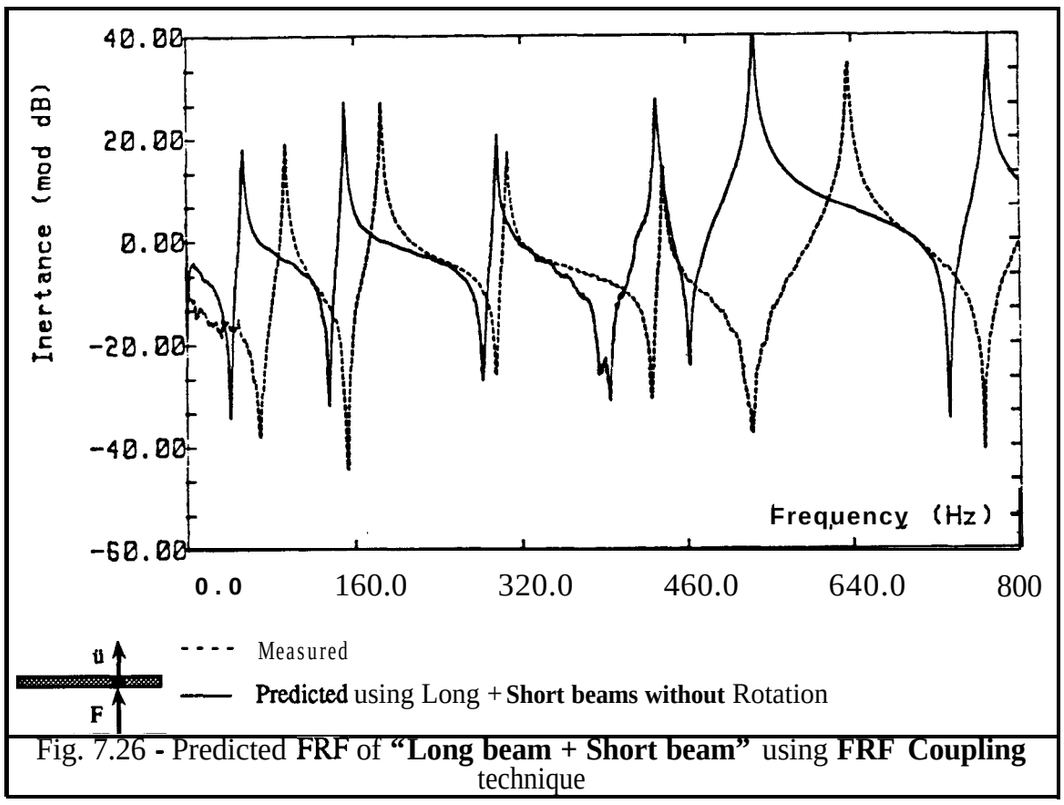

Fig. 7.26 - Predicted **FRF** of **"Long beam + Short beam"** using **FRF Coupling** technique

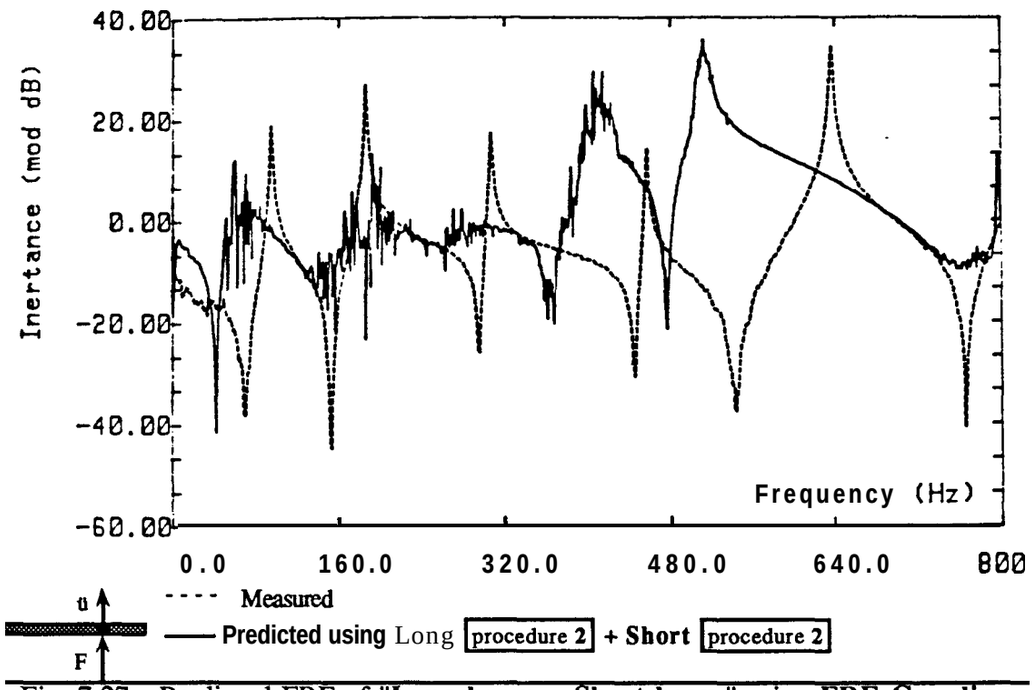

Fig. 7.27 - Predicted FRF of "**Long beam + Short beam**" using **FRF Coupling** technique

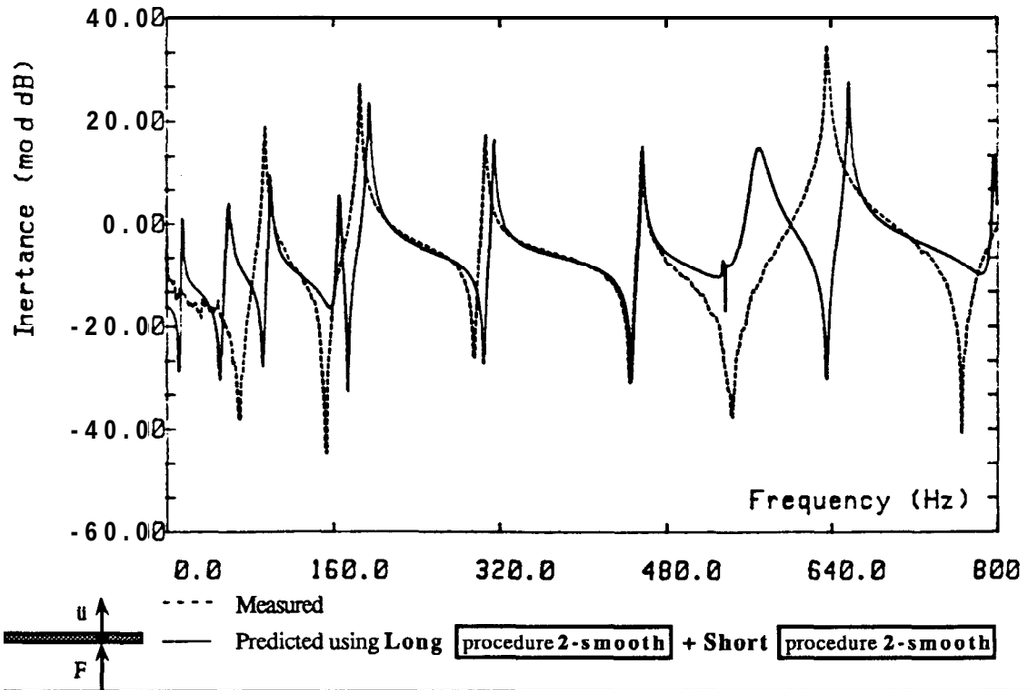

Fig. 7.28 - Predicted FRF of "**Long beam + Short beam**" using **FRF Coupling** technique

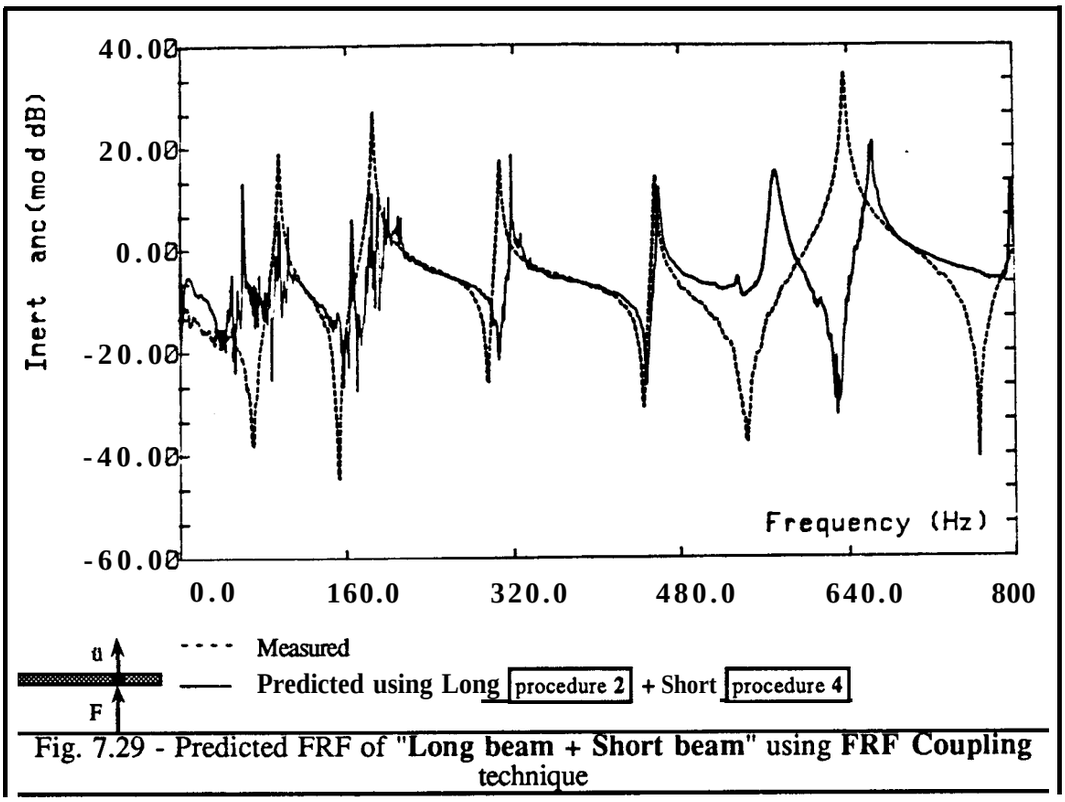

Fig. 7.29 - Predicted FRF of "**Long beam + Short beam**" using **FRF Coupling** technique

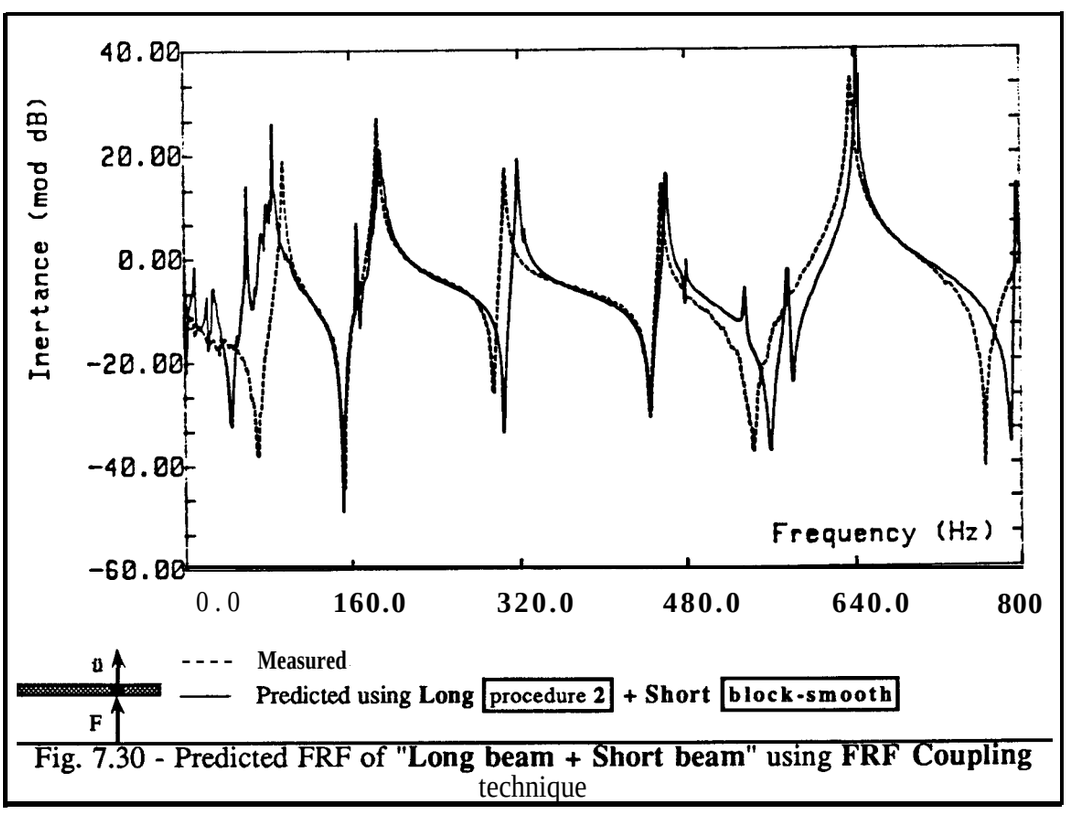

Fig. 7.30 - Predicted FRF of "**Long beam + Short beam**" using **FRF Coupling** technique

7.3.4.2 DISCUSSION OF MODAL COUPLING RESULTS

The Modal models of both beams are used to predict the assembled Modal model from which an FRF at the connection point is generated for comparison with the measured one. As mentioned before, the Modal models of each beam were derived following the Modal route presented in chapter 6 (vidé section 6.6.3) and using different procedures to estimate the rotational amplitude of the mode shapes. One of the procedures which was found to estimate fairly accurate amplitudes of rotations in all the modes and in both beams was procedure 2. Our attention is then focused on the thus-derived Modal models, which include as well the corresponding residual flexibility matrices.

However, in order to compare results coming from a Modal coupling technique with those obtained by using FRF coupling, it was decided that the measured data used to develop the Response and Modal models initially should be obtained under identical conditions. In other words, since the FRF coupling requires both components to be measured over the same frequency range - which is O-800 Hz - the Modal coupling technique will make use of short beam Modal models which contain only one flexural mode - range O-800 Hz - in contrast to what was presented in chapter 6 where those models contain information on three flexural modes (o-3200 Hz). Since the residual flexibility information can be appended to those models, the final result will be similar for either of the Modal models used for the short beam.

Figs. 7.31 and 7.32 show the predicted FRFs using either Modal models without and with residuals, respectively.

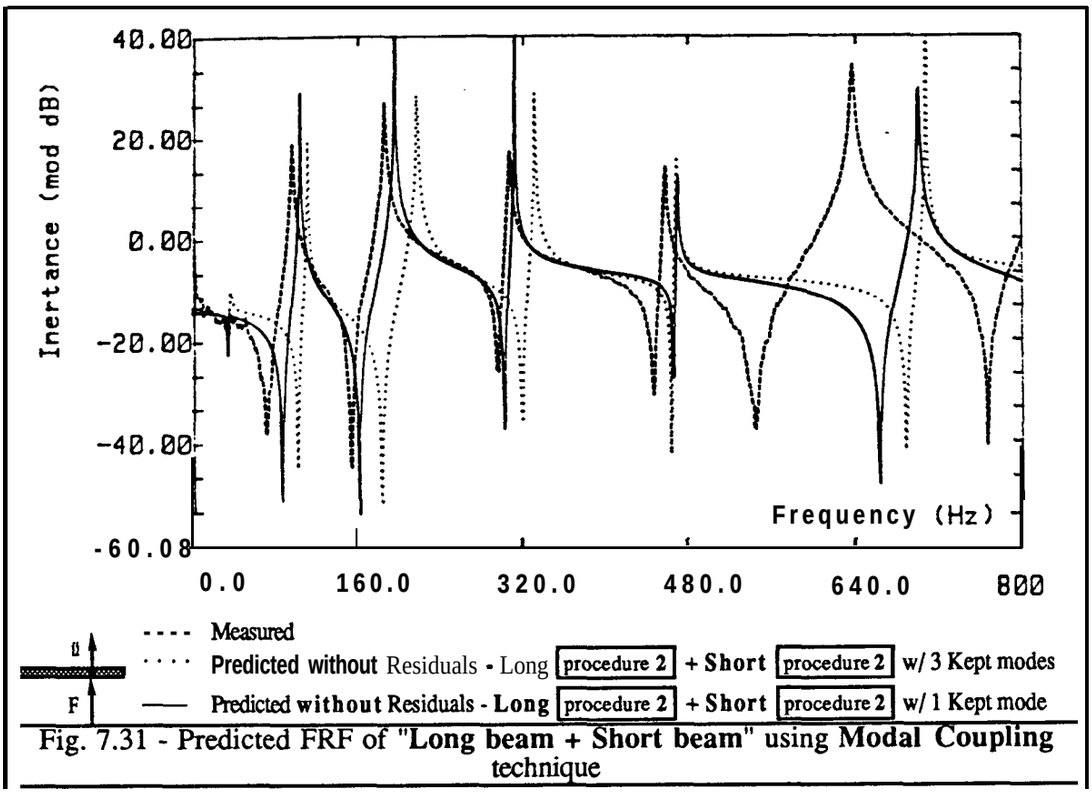

Fig. 7.31 - Predicted FRF of "**Long beam + Short beam**" using **Modal Coupling** technique

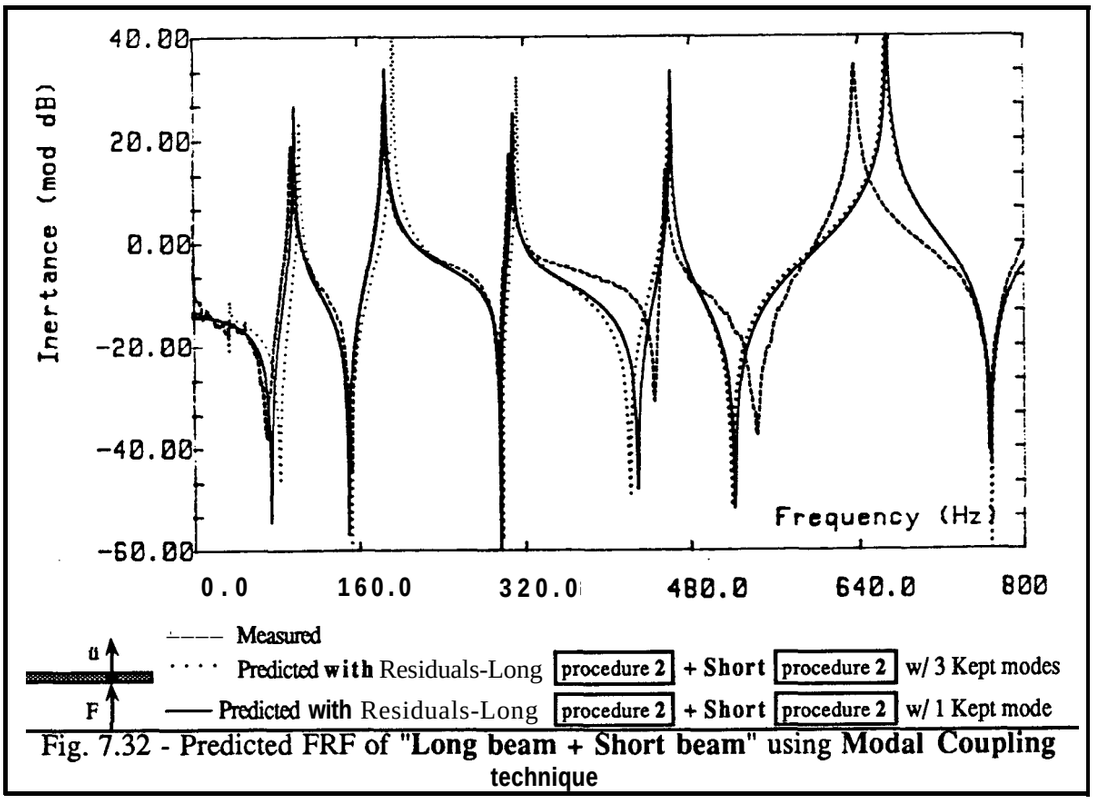

Fig. 7.32 - Predicted FRF of "**Long beam + Short beam**" using **Modal Coupling** technique

7.3.5 COMPARISON OF FRF AND MODAL COUPLING RESULTS

Fig. 7.33 shows one measured and two predicted **FRFs** using the Response and the Modal routes. For the former route, the Response model of both beams was constructed from the smoothed **FRFs.** This requires the original Response model to be converted to a Modal one, which is then used to generate the new Response model (taking into account the residual effects of the out-of-range modes).

In the Modal route, the Modal model derived from the measured **FRFs** (only translations included) was used to estimate a similar model but a this time possessing the explicit rotational information; the algorithms presented in chapter 6, have shown that it is also possible to calculate the residual flexibility information related to the rotational coordinates.

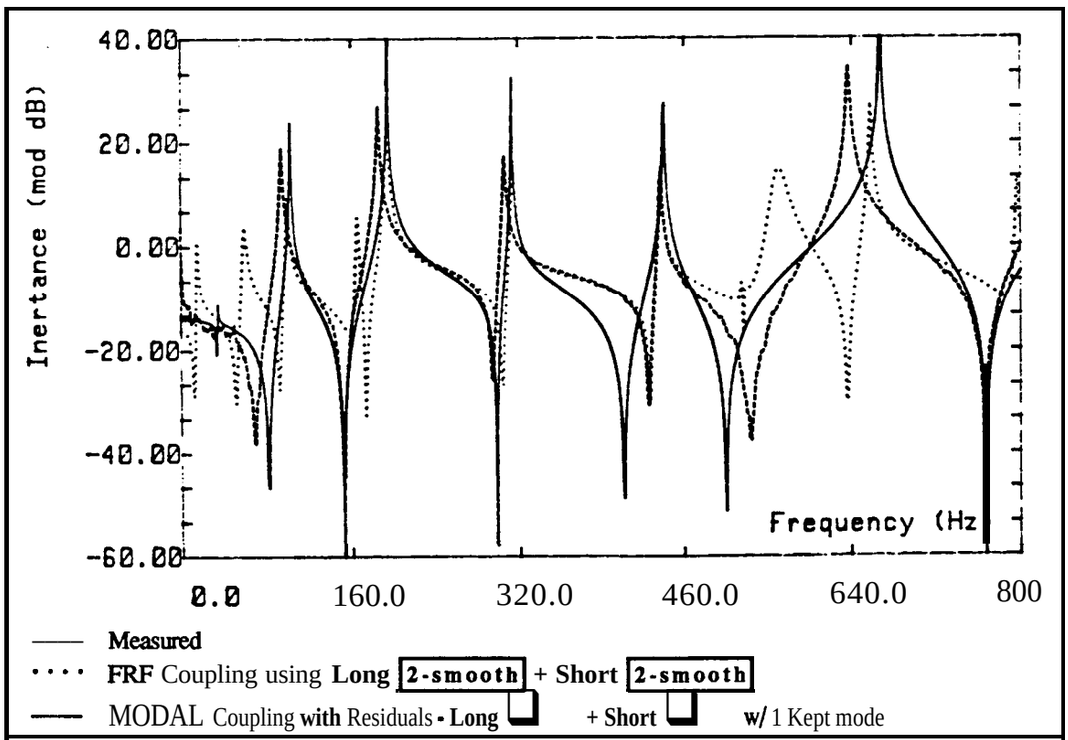

Fig. 7.33 - Predicted FRF of **"Long beam + Short beam"** using **FRF** and **Modal Coupling** techniques

The Modal coupling technique predicted a better response than the FRF coupling technique, mainly due to the fact that former does not require any inversion process. This is the main reason for explaining the errors which arise in the FRF coupling technique which, besides the fact of using a smoothed Response model, is still sensitive to any inherent model inconsistency. This inconsistency is caused by the need to use different locations for the accelerometer to gather data during the measurement stage, and this causes a slight variation of the natural frequencies amongst the measured FRFs.

7.3.6 CONCLUSIONS

In beam-like components it is essential to have a rotational coordinate in the connecting region in order to fulfill the constraint conditions properly, if such a component is linked to another structure. The techniques presented in chapter 6 form the mathematical and experimental tools which permit estimation of the necessary rotational quantities to create either the Response or Modal models for such components. Central to the Modal model, there is also the possibility of estimating the residual flexibility effects related to the rotational parameters (due to the unmeasured modes), which are important ingredients to be used with the refined Modal Coupling technique (vidé chapter 4).

It was found in this work that the Modal route is preferable when predicting the response of an assembled structure formed of two beams, especially when these behave as lightly-damped components. However, it is important to remember at this stage that the Modal coupling technique, which one is concerned with, is restricted to that type of component whose damping can be neglected; should there be a considerable degree of damping, only the FRF coupling technique is able to handle such components with a lower probability of numerical ill-conditioned matrices during the coupling process.

8 CLOSURE

8.1 GENERAL CONCLUSIONS

In this last chapter, the general conclusions of the research are presented following the same general breakdown of topics as used in the main body of the thesis. One of these sections is devoted entirely to the refinement of standard techniques - Impedance and Modal coupling - which was possible ***either*** by reformulating the existing theory ***or*** by making use of more efficient algorithms. Of these algorithms, one resolves the numerical failures during matrix inversions and another is used to detect causes of ill-conditioned matrices, specifically that due to redundant information in the coordinates of a system model. As a consequence of these refinements, more accurate and reliable results can be obtained for the prediction of assembled systems whose models are derived from measured data. Another section in the thesis is dedicated to the experimental determination of the rotational responses which play a vital role in some coupling exercises; the techniques to gather the necessary experimental data and the subsequent mathematical manipulation constitute some of the main topics for conclusions in this chapter.

8.1.1 CONCLUSIONS ON IMPEDANCE COUPLING TECHNIQUES

The Spatial coupling method is used extensively in cases involving theoretical modelling. Reduction methods are presented in chapter 3 to condense Spatial models to the primary (master) coordinates **- coordinate reduction** which inevitably cause a **mode reduction -** in order to decrease the computational needs to solve the global problem. In this context it was found that the selection of those coordinates must be made according to some criterion in order to preserve, as much as possible, the dynamic characteristics of the original unreduced models. The accuracy of the results obtained via the use of static or dynamic reduced subsystem Spatial models depends on the coordinates which are eliminated - it is a question of mass value dependency, so the choice of the secondary coordinates should be made according to the relative mass values. Should a **static reduction be** applied to a spatially described model, the secondary coordinates must possess relatively small mass values. Conversely, if a **dynamic reduction** is applied to a model, the dynamic characteristics of the reduced model are better preserved if relatively high mass values are assigned to the eliminated coordinates.

In contrast to the Spatial coupling method there is the FRF **coupling** technique which is suitable for the use of FRF data measured on the components. It makes use of Response models derived directly from experimental data (seldom from theoretical modelling). Conceptually, one can say that the FRF coupling technique is very attractive since it makes use of models whose dynamic characteristics are fully quantified and thus do not suffer from incompleteness. Furthermore, a reduction performed on the interior coordinates of a given subsystem still preserves the dynamic information necessary for a subsequent use in a FRF coupling procedure.

However, there is a numerical aspect associated with this technique which may cause the coupling procedure to fail. It was shown in chapter 2, that the required FRF matrix of the coupled structure is obtained after three matrix inversions - two of them carried out before and one after the FRF matrices are assembled. Should one of these matrices be near singular, the results will reflect the numerical errors caused by inversion and will predict

the dynamic behaviour of the overall structure erratically. Unfortunately, when dealing with experimentally-derived FRF matrices, one is mostly restricted to use inconsistent models that are inaccurate due to experimental or systematic errors in the measurement stage and this causes the FRF matrix to be ill-conditioned. Another situation which may lead to near singular matrices is caused by local rigidities at the measured coordinates. Over certain frequency ranges the response at some coordinates may tend to be nearly dependent and then the FRF matrix will tend to be rank-deficient.

The alternative algorithms presented in chapter 3 can be used to resolve the numerical difficulties encountered during the coupling process based on the classical algorithm whenever the localised regions are referred to the interior regions of each component or only to one of their connecting regions. In such a situation, the approach making use of algorithm 3 presents a remarkable advantage over the other two, since the inversion is only required once and even then it is applied to a matrix whose order depends only on the number of connecting coordinates.

In the other most extreme situation, when the rigidities are localised in both interface regions, other alternatives are required. For instance, if it is possible to know a priori the number of redundant coordinates or, in other words, the rank for each subsystem FRF at each frequency in the range of interest, the analyst can make a judgement about the possible exclusion of some of the connected coordinates without affecting the constraint formulation of the actual physical connection. It is in this context that the auxiliary mathematical tools presented in chapter 5 should be employed. Of these, the SVD technique proved to be a useful mathematical tool to be used during a coupling process involving subsystems which both possess redundant information (in terms of coordinates) at the interface region. Additionally, it is shown that the common inversion algorithms can still be used provided the redundancy in the connecting region is eliminated by using a suitable algorithm to detect how many and which coordinates are redundant. This may be useful when a large degree of redundancy is present in a multi-point connected system. In such a case, a substantial reduction may be applied to the

initially specified connection matrix, thereby allowing a less time-consuming coupling process while preserving the accuracy in the final result at the same time.

8.1.2 CONCLUSIONS ON MODAL COUPLING TECHNIQUES

Unlike the Impedance-based methods which take advantage on the reduction of the number of coordinates, the Modal coupling methods use a reduction performed on the number of **modes used** to describe each component model while still accounting for all the physical coordinates. A refined Modal coupling technique using free-interface modes was presented in chapter 4. The main achievement of this method was the inclusion of the residual flexibilty effects which compensate for the truncation of the number of kept or measured modes in each component. The lack of flexibility associated with the description of each component displacement in the connection region (which results from this truncation) has caused the classical free-interface methods to predict results with poor accuracy when compared with the fixed-interface methods - in effect, the components are assumed to be stiffer than actually is the case. With the inclusion of the residual flexibility information - in fact, an approximation when experimentally-derived models are dealt with - by using a “dummy” interconnecting flexible system, the two main components are mathematically coupled using the best available information provided by data measured over the frequency range of interest for each component.

The results obtained in the case studies show that the degree of importance of each residual flexibility effect is associated with the relative mass of each component - the lighter the component the more important becomes its residual flexibility. Furthermore, the use of a redundant set of connecting coordinates has not presented any numerical difficulty when using the refined approach, whereas in the classical method, a careful analysis needs to be done, prior to the coupling process, on the dependency amongst the coordinates included.

8.1.3 CONCLUSIONS ON DETERMINATION AND USE OF ROTATIONAL RESPONSES

The laser measurement technique described in chapter 6 can estimate very easily the rotational displacements in the mode shapes when compared with techniques using accelerometers. Additionally, since it is possible to measure in a quasi-continuous way the mode shape patterns over a specified length or area on a structure, it is possible to obtain more accurate estimates of the spatial derivatives, mainly for the higher modes. This constitutes the main drawback to similar data measured with closely-spaced accelerometers since it is impracticable to obtain a precise description of the displacement field near the connection region. Although the rotations obtained by using either technique are only concerned with a very simple case study, it is believed that in more complex structures involving tridimensional measurements, the laser technique will offer the best capability.

There are, however, some drawbacks associated with the measurements carried out with the laser technique. On the one hand, by estimating the rotational responses from the displacement pattern of each mode in the frequency range of interest, there is no possibility of calculating the residual flexibility which represents the out-of-range modes; generally, this knowledge is important whenever Modal models are used and therefore more modes must be measured. On the other hand, the optically-based system may be unable to reach some important areas or points on the structure; for instance, should a shaker be placed near the region of interest it can obstruct the directed laser beam path, or in other cases, the point of measurement can be located at an inaccessible interior surface.

The use of two or three closely-spaced accelerometers near the point of interest constitutes a practicable alternative to the exciting-block approach which in turn, is prone to errors when the cancelled mass is large compared with the mass of the structure, specifically for higher frequencies. In the cases where Modal models have to be derived for each subsystem, the use of closely-spaced accelerometers constitutes an ideal alternative, since it requires the modal identification of the measured curves rather than the estimated ones.

Additionally, it allows estimation of the residual effects of the out-of-range modes for the derived rotational FRFs.

For beam-like components linked to other structures, it is essential to have a rotational coordinate in the connecting region in order to fulfill properly the constraint conditions. The techniques presented in chapter 6 constitute the mathematical and experimental tools which lead to the estimation of the necessary rotational quantities to create either the Response or Modal models of a beam-like component. Central to the Modal model, there is also the possibility of estimating the residual flexibility effects related to the rotational parameters (due to the unmeasured modes), which are important ingredients to be used with the refined Modal Coupling technique presented in chapter 4.

It was found in this case study, that the Modal route is preferable when predicting the response of an assembled structure formed of two beams, especially when these behave as lightly-damped components. However, it is important to remember that the Modal coupling technique, which one is concerned with, is restricted to that type of component whose damping can be neglected; should there be a considerable degree of damping, only the FRF coupling technique is able to handle such components with a lower probability of numerical ill-conditioned matrices during the coupling process.

8.2 SUGESTIONS FOR FUTURE WORK

The study undertaken in this thesis revealed that some further developments may be of interest in future work in the field of Dynamic Analysis of Coupled Structures. Some general sugestions are outlined below.

- The refined Modal Coupling approach can be investigated further in order to extend its applicability to the prediction of the dynamic characteristics of structures in which some of the components possess a non negligible damping.

- The necessity of the mentioned development is still reinforced in the cases of highly dissipative joints between components. In this case, the 'dummy' flexible inter-connecting system which is used to express the information of the residual flexibility effect of the out-of-range modes can yet incorporate the joint charateristics such as flexibility and generally hysteretic damping.

- In this field, a philosophy which may be adopted relies on the assumption of an uncoupling techniques; these make use of the whole structure properties and the component and joint properties can then be determined by uncoupling, step by step, each of the assembled components.

- Further investigation is necessary on the experimental determination of rotational properties. The techniques used in the present work, namely those making use of accelerometer and laser measurements, can be extended to the determination of responses in more than one plane.

- Another interesting topic to be investigated relates to the determination of rotational responses of structures possessing close modes; in this context the laser measurement needs to be explored in more detail.

- In terms of structural modification, it is the author's belief that the SVD has some potential to be used in order to locate the coordinate (or mode) which change is most effective to attain a specific modification on the structure.

REFERENCES

REFERENCES

1 **Ewins, D.J.**
'Modal *Testing: Theory and Practice"*
Research Study Press - 1984

2 **Zienkiewicz, O.C.**
'The Finite Element Method in Engineering Science"
MacGraw-Hill, 197 1

3 **Ewins, D.J.**
"Whys and Wherefores of Modal Testing"
Journal of the Society of Environmental Engineers, September 1979

4 **Bishop, R.E.D.; Johnson, D.C.**
'The *Mechanics of Vibration"*
Cambridge University Press, 1960

5 **Timoshenko, S.; Young, D.H; Weaver, W.**
"Vibration Problems in Engineering"
John Willey and Sons, 1974

6 **Duncan, W.J.**
"Mechanical Admittances and Their Applications to Oscillation Problems"
HMSO R and M2000, 1947

7 **Sykes, A.O.**
"Application of Admittance and Impedance Concepts in the Synthesis of Vibrating Systems"
ASME, Synthesis of Vibrating Systems, 1971

8 **Noiseaux, D.U.; Meyer, E.B.**
"Applicability of Mechanical Admittance Techniques"
Shock and Vibration Bulletin, Vo138 (2), 1968

9 **Ewins, D.J.**
"'Measurement and Application of Mechanical Impedance Data" (3 Parts)
Journal of the Society of Environmental Engineers, Vols. 14(3),15(1), and 15(2), 19751976

10 **Klosterman, A.L.**
"A Combined Experimental and Analytical Procedure for Improving Automotive System Dynamics"
S.A.E. Paper No. 720093, 1972

11 **Sainsbury, M.G.; Ewins, D.J**
"Vibration Analysis of Damped Machinery Foundation Structure Using Dynamic Stiffness Coupling Technique"
A.S.M.E. Paper, 73-DET-136, 1973

12 **Ewins, D.J.; Silva, J.M.M.; Maleci, G.**
"Vibration Analysis of a Helicopter Plus an Externally-Attached Structure"
Shock and Vibration Bulletin, 50 (2), 1980

13 **Hunter, Jr, N.F.; Otts, J.V.**
"The Measurement of Mechanical Impedance and Its Use in Vibration Testing"
Shock and Vibration Bulletin, Vo142 (1), 1972

14 **Heer, E.; Lutes, L.D.**
"Application of the Mechanical Receptance Coupling Principle to Spacecraft Systems"
Shock and Vibration Bulletin, 38 (2), 1968

15 **Lutes, L.D.; Heer, E.**
'Receptance Coupling of Structural Components Near a Component Resonance Frequency"
Jet Propulsion Laboratory Report, October 1968

16 **Ewins, D.J.**
"Modal Test Requirements for Coupled Structue Analysis Using Experimentally-derived Component Models"
Joint ASME/ASCE Appllied Mechanics Conference, Albuquerque, New Mexico, June 1985

17 **Gleeson, P.T.**
"Identification of Spatial Models for the Vibration Analysis of Lightly-Damped Structures"
Ph.D. Thesis, Imperial College, University of London, 1979

18 **Imregun, M.; Robb, D.A.; Ewins, D.J.**
"Structural Modification and Coulping Dynamic Analysis Using FRF Data"
5th International Modal Analysis Conference, 1987

19 **Ewins, D.J.; Sainsbury, M.G.**
"Mobility Measurements for the Vibration Analysis of Connected Structures"
Shock and Vibration Bulletin, 42 (1), 1972

20 **Henderson, F.N.**
"The Influence of Rotational Coordinates in a Dynamic Coupling Analysis"
MSc. Thesis, Imperial College, University of London, 1984

21 **Maleci, G.; Young, J.W.**
"The Effect of Rotational Degrees of Freedom in System Analysis (SA) via Building Block Approach (BBA)"
3rd International Modal Analysis Conference, 1985

22 **Smith, J.E.**
"Measurement of Total Structural Mobility Matrix"
Shock and Vibration Bulletin, 40 (7), 1969

23 **Sainsbury, M.G.**
"Experimental and Theoretical Techniques for Vibration Analysis of Complex Structures"
Ph.D. Thesis, Imperial College, University of London, 1976

24 **Ewins, D.J.;Gleeson, P.T.**
"Experimental Determination of Multi-Directional Mobility Data for Beams"
Journal of Sound and Vibration, Vol. 45 (5), 1975

25 **Licht, T.R.**
"Angular Vibration Measurements Transducers and their Configuration"
3rd International Modal Analysis Conference, 1985

26 **Rorrer, R.A.L.;Wicks, A.L.; Williams, J.**
"Angular Acceleration Measurements of a Free-Free Beam"
7th International Modal Analysis Conference, 1989

27 **Chen, W-H; Cherng, J-S**
"Modal Synthesis Via Combined Experimental and Finite Element Techniques With Consideration of Rotational Effects"
Journal of Sound and Vibration, Vol103 (1), 1985

28 **Sattinger, S.S.**
"A Method for Experimentally Determining Rotational Mobilities of Structures"
Shock and Vibration Bulletin, 50 (1), 1980

29 **Przemieniecki, J.S.**
"Matrix Structural Analysis of Substructures"
AIAA Journal Vol. 1, (1), 1963

30 **Hurty, W.C.**
"Dynamic Analysis of Structural Systems Using Component Modes"
AIAA Journal, Vol.3, (4), 1965

31 **Craig, R.R.; Bampton, M.C.C.**
"Coupling of Substructures for Dynamic Analysis"
AIAA Journal, Vo1.6, (7), 1968

32 **Gladwell, G.M.L.**
"Branch-Mode Analysis of Vibrating Systems"
Journal Sound and Vibration, Vol. 1, 1964

33 **Goldman, R.L.**
"Vibration Analysis by Dynamic Partitioning"
AIAA Journal, Vo1.7, (6), 1969

34 **Hou, S.**
"Review of Modal Synthesis Techniques and a New Approach"
Shock and Vibration Bulletin, Vol. 40 (4), 1969

35 Craig, R.R.
"Methods of Component Mode Synthesis"
Shock and Vibration Digest, Vol.9 (11), 1977

36 Nelson, F.C.
"A Review of Substructure Analysis of Vibrating Systems"
Shock and Vibration Digest, Vol.1 1 (1 1), 1979

37 Goldenberg,S.; Shapiro, M.
"A Study of Modal Coupling Procedures for the Space Shuttle"
NASA CR-l 12252, April 1973

38 Hart, G.C.; Hurty, W.C; Collins, J.D.
"A Survey of Modal Synthesis Methods"
SAE Paper No. 710783, 1971

39 Hurty, W.C.; **Collins,** J.D.; Hart, G.C.
"Dynamic Analysis of Large Structures by Modal Synthesis Techniques"
Computers and Structures, Vol. 1, 1971

40 **MacNeal,** R.H.
"A Hybrid Method of Component Mode Synthesis"
Computers and Structures, Vol. 1, 1971

41 Kuhar, E.J.; **Stahle,** C.V.
"Dynamic Transformation Method for Modal Synthesis"
AIAA Journal, Vo1.12, (5), 1974

42 **Hintz,** R.M.
"Analytical Methods in Component Mode Synthesis"
AIAA Journal, Vol.13, (8), 1975

43 Benfield,W.A.; Hruda, R.F.
"Vibration Analysis of Structures by Component Mode Substitution"
AIAA Journal, Vo1.9, (7), 1971

44 **Rubin,** S.
"Improved Component-Mode Representation for Structural Dynamic Analysis"
AIAA Journal, Vol.13, (8), 1975

45 Klosterman, A.L.
"On the Experimental Determination and Use of Modal Representation of Dynamic Characteristics"
Ph.D. Thesis, University of Cincinnati, 197 1

46 Klosterman, A.L.; Lemon, J.R.
"Dynamic Design Analysis Via Building Block Approach"
Shock and Vibration Bulletin, Vol. 42 (1), 1972

47 Craig, R.R.; Chang, C-J
"On the Use of Attachment Modes in Substructure Coupling for Dynamic Analysis"
Proc. AIAA/ASME 18th SSDM Conference, 1977.

48 **Craig, R.R.**
"Substructure *Coupling for Dynamic Analysis and Testing"*
NASA CR-2781, February 1977

49 **Martinez, D.R.; Carne, T.G.; Miller, A.K.**
"Combined Experimental/Analytical Modeling Using Component Mode Synthesis"
SAND83-1889, Sandia National Laboratories, Albuquerque, New Mexico, April 1984

50 **Martinez, D.R.; Gregory, D.L.**
"A Comparison of Free Component Mode Synthesis Techniques Using MSC / NASTRAN"
SAND83-0025, Sandia National Laboratories, Albuquerque, New Mexico, June 1984

51 **Coppolino, R.N.**
"Employment of Hybrid Experimental/Analytical Modeling in Component Mode Synthesis of Aerospace Structures"
Joint ASME/ASCE Apllied Mechanics Conference, Albuquerque,New Mexico, June 1985

52 **Craig, R.R.**
"A Review of Time-Domain and Frequency-Domain Component Mode Synthesis Methods"
The Intematinal Journal of Analytical and Experimental Modal Analysis, Vol.2 (2), April 1987

53 **Klahs, J.W.; Townley, G.E.**
"Determining Component Loads and Stresses with Improved System Modeling Techniques"
3rd International Modal Analysis Conference, 1985

54 **Guyan, R.J.**
"Reduction of Stiffness and Mass Matrices"
AIAA Journal, Vo1.3, (2), 1965

55 **Press, W.H; Flannery, B.P.; Tenkolsky, S.A.; Vetterling, W.T.**
"Numerical Recipes - The Art of Scientific Computing"
Cambridge University Press, 1986

56 **Martin, K.F.; Ghlaim, K.H.**
"System Prediction Using Reduced Component Modes"
1st International Modal Analysis Conference, 1982

57 **Martin, K.F.; Ghlaim, K.H.**
"On the Solution of Approximated Systems When Using Reduced Component Modes"
Earthquake Engineering and Structural Dynamics, Vol. 12, 1984

58 **Sekimoto, S.**
"A Study on Truncation Error in Substructure Testing"
3rd International Modal Analysis Conference, 1985

59 Gwim, **K.W.; Lauffer, J.P.; Miller,A.K.**
"Component Mode Synthesis Using Experimental Modes Enhanced by Mass Loading"
6th International Modal Analysis Conference, 1988

60 Urgueira, **A.P.V.**
"Coupled Structure Analysis Using Incomplete Models"
Imperial College, Dynamics Section - Internal Report 87012, November 1987

61 Imregun, M.
"Dynamic Condensation : Theory and Applications"
MSc. Thesis, Imperial College, University of London, 1980

62 Imregum, M.
"User's ***Guide to MODALP"***
Imperial College, Dynamics Section, 1987

63 **Larsson, P.O.**
'Methods Using Frequency-Response Functions for the Analysis of Assembled Structures"
3th International Conference on Recent Adavances in Structural Dynamics, University of Southampton, 1988

64 **Henderson, H.V.; Searle, S.R.**
"On Deriving the Inverse of a Sum of Matrices"
SIAM Review, Vol. 23, (1), 1981

65 **Jetmundsen, B.; Bielawa, R.L.; Flannelly, W.G.**
"Generalized Frequency Domain Substructure Synthesis"
Journal of the American Helicopter Society, January 1988

66 **Urgueira, A.P.V.**
"A Modal Coupling Technique Using Experimentally Data"
Imperial College, Dynamics Section - Internal Report 88012, 1988

67 **Urgueira, A.P.V.; Ewins, D.J.**
"A Refined Modal Coupling Technique for Including Residual Effects of Out-of-Range Modes"
7th International Modal Analysis Conference, 1989

68 **Craig, R.R.,Jr.**
"Structural Dynamics - An Introduction to Computer Methods"
John Wiley & Sons, NY, 1981

69 **Hansteen, O.E.; Bell, K.**
"On ***the Accuracy of Mode Superposition Analysis in Structural Dynamics"***
Earthquake Engineering and Structural Dynamics, Vol.7, 1979

70 **Sainsbury, M.G.**
"User's Guide for the Structural Dynamics Computer Program COUPLE" (Revised Form)
Imperial College, Dynamics Section, 1975

71 Maia, N.M.M.
"A New Approach on the Identification of Lightly Damped Structures"
Imperial College - Internal Report no. 87014, Dynamics Section, December 1987

72 Golub, G.H.; Kahan, W.
"Calculating the Singular Values and Pseudo-Inverse of a Matrix"
SIAM J. Numer. Anal., vol 2, 1965

73 Wilkinson, J.H.; Reinsch, C.
"Linear Algebra"
Hand Book of Automatic Computation, Springer Verlag, 1971

74 Francis, J.G.F.
"The QR Transformation - Part 2"
SIAM Review, Vol. 23, (1), 1981

75 Lawson, C.L.; Hanson, R.J.
"Solving Least Squares Problems"
Prentice-Hall, Inc., 1974

76 Chambers J. M.
"Computational Methods for Data Analysis"
John Wiley & Sons, NY, 1977

77 Jacobs D.
"Numerical Software - Needs and Availability"
Academic Press, 1978

78 Miller, W.; Wrathall, C.
"Software for Roundoff Analysis of Matrix Algorithms"
Academic Press, 1980

79 Forsythe, G. E.; Malcolm, M. A.; Moler, C.B.
"Computer Methods for Mathematical Computations"
Prentice-Hall, Inc., 1977

80 Golub, G.H.; Van Loan, C. F.
"Matrix Computations"
North Oxford Academic Publishing Co. Ltd., 1983

81 Golub, G.H.; Reinnsh, C.
"Singular Value Decomposition and Least Squares Solutions"
Numer. Math, Vol 14, pp 403-420, 1970

82 Moore, C.
"Applications of Singular Value Decomposition to the Design, Analysis, and Control of Industrial Processes"
American Control Conference, 1986

83 Klema, V.C.; Laub, **A.J.**
"The Singular Value Decomposition: Its Computation and Some Applications"
IEEE Transactions on Automatic Control, Vol. AC-25, No. 2, 1980

84 **Golub, G.H.; Klema, V.; Stewart, G.W.**
"Rank Degeneracy and Least Squares Problems"
Stanford University, STAN-CS-76-559, 1976

85 **O'Callahan, J.C.; Avitable, P.; Lieu, I-W; Madden, R.**
"An Efficient Method of Determining Rotational Degrees of Freedom from Analytical and Experimental Modal Data"
4th International **Modal** Analysis Conference, 1986

86 **O'Callahan, J.C.; Lieu, I-W; Chou, C-M**
"Determination of Rotational Degrees of Freedom for Moment Transfers in Structural Modifications"
3rd International **Modal** Analysis Conference, 1985

87 Smiley, **R.G.; Brinkman, B.A.**
"Rotational Degrees-of-Freedom in Structural Modification"
2nd International **Modal** Analysis Conference, 1984

88 **Silva, J.M.M.**
"Measurements and Applications of Structural Mobilty Data for the Vibration Analysis of Complex Structures"
Ph.D. Thesis, Imperial College, University of London, 1978

89 Sriram, **P.; Craig, J.I.; Hanagud, S.**
"A Scanning Laser Doppler Vibrometer for Modal Analysis"
7th International Modal Analysis Conference, 1989

90 Oliver, D.
"Non-Contact Vibration Imagerfor Wide Range of Component Sizes and Displacement Amplitudes"
6th International Modal Analysis Conference, 1988

91 Hilary, B.; Ewins, D.J.
"A Preliminary Investigation Into The Receptance Coupling Methods Using Measured Data"
Imperial College, Dynamics Section - Internal Report 515/2, May 1983

92 Sham, W.P.; Ewins, D.J.
"Prediction of Dynamic Response of an Assembled Structure Using Measured Data"
Imperial College, Dynamics Section - Internal Report 515/4, October 1986

93 **Broch,** J.T.
"Mechanical Vibration and Shock Measurement"
B & K edition, April 1984

94 Robb, D.A.
"User's Guide to MODESH"
Imperial College, Dynamics Section, 1987

Benfield,W.A., 256
Bishop, R.E.D., 253
Broch, J.T., 260
Chambers J. M., 259
Chen, W-H, 255
Coppolino, R.N., 257
Craig, R.R., 255, 256,257
Craig, R.R.,Jr., 258
Duncan, W.J., 253
Ewins, D.J., 253, 254, 255
Forsythe, G. E., 259
Francis, J.G.F., 259
Gladwell, G.M.L., 255
Gleeson, P.T., 254
Goldenberg,S., 256
Goldman, R.L., 255
Golub, G.H., 259, 260
Guyan, R.J., 257
Gwim, K.W., 258
Hansteen, O.E., 258
Hart, G.C., 256
Heer, E., 254
Henderson, F.N., 254
Henderson, H.V., 258
Hilary, B., 260
Hintz, R.M., 256
Hou, S., 255
Hunter, Jr, N.F., 254
Hurty, W.C., 255, 256
Imregum, M., 258
Imregun, M., 254,258
Jacobs D., 259
Jetmundsen, B., 258
Klahs, J.W., 257
Klema, V.C., 259
Klosterman, A.L., 254, 256
Kuhar, E.J., 256
Larsson, P.O., 258
Lawson, C.L., 259
Licht, T.R., 255
Lutes, L.D., 254
MacNeal, R.H., 256
Maia, N.M.M., 259
Maleci, G., 254
Martin, K.F., 257
Martinez, D.R., 257
Miller, W., 259
Moore, C., 259
Nelson, F.C., 256
Noiseaux, D.U., 253
O'Callahan, J.C., 260
Oliver, D., 260
Press, W.H, 257
Przemieniecki, J.S., 255
Robb, D.A., 260
Rorrer, R.A.L., 255
Rubin, S., 256
Sainsbury, M.G., 254, 255, 258
Sattinger, S.S., 255
Sekimoto, S., 257
Sham, W.P., 260
Silva, J.M.M., 260
Smiley, R.G., 260
Smith, J.E., 255
Sriram, P., 260
Sykes, A.O., 253
Timoshenko, S., 253
Urgueira, A.P.V., 258
Wilkinson, J.H., 259
Zienkiewicz, O.C., 253

APPENDICES

APPENDIX I

REFORMULATED FRF MATRIX OF IMPEDANCE COUPLING METHOD

Without loss of generality, the FRF matrix which is assumed herein is the Receptance matrix (which can be interrelated with Mobility or Accelerance). It can be partitioned according to the previously selected interior and connection coordinates in each subsystem as follows:

$$\begin{Bmatrix} {}_A\mathbf{u}_i \\ \cdots \\ {}_A\mathbf{u}_c \end{Bmatrix} = \begin{bmatrix} {}_A\mathbf{H}_{ii} & : & {}_A\mathbf{H}_{ic} \\ \cdots & : & \cdots \\ {}_A\mathbf{H}_{ci} & : & {}_A\mathbf{H}_{cc} \end{bmatrix} \begin{Bmatrix} {}_A\mathbf{f}_i \\ \cdots \\ {}_A\mathbf{f}_c \end{Bmatrix} \qquad \textbf{(A1.1)}$$

$$\begin{Bmatrix} {}_B\mathbf{u}_i \\ \cdots \\ {}_B\mathbf{u}_c \end{Bmatrix} = \begin{bmatrix} {}_B\mathbf{H}_{ii} & : & {}_B\mathbf{H}_{ic} \\ \cdots & : & \cdots \\ {}_B\mathbf{H}_{ci} & : & {}_B\mathbf{H}_{cc} \end{bmatrix} \begin{Bmatrix} {}_B\mathbf{f}_i \\ \cdots \\ {}_B\mathbf{f}_c \end{Bmatrix} \qquad \text{(A1.2)}$$

The coordinates in the FRF matrix of the coupled structure can be partitioned according to three regions corresponding to,

- the interior coordinates of component A $({}_A\mathbf{n}_i)$ denoted as **a**
- the interior coordinates of component B $({}_B\mathbf{n}_i)$ denoted as **b**
- the common connection coordinates of component A and B $({}_A\mathbf{n}_c = {}_B\mathbf{n}_c = \mathbf{n}_c)$ denoted as c

The whole system will possess an FRF matrix such as,

$$\begin{Bmatrix} \mathbf{U}_a \\ \cdots \\ \mathbf{U}_c \\ \cdots \\ \mathbf{U}_b \end{Bmatrix} = \begin{bmatrix} \mathbf{H}_{aa} & : & \mathbf{H}_{ac} & : & \mathbf{H}_{ab} \\ \cdots & : & \cdots & : & \cdots \\ \mathbf{H}_{ca} & : & \mathbf{H}_{cc} & : & \mathbf{H}_{cb} \\ \cdots & : & \cdots & : & \cdots \\ \mathbf{H}_{ba} & : & \mathbf{H}_{bc} & : & \mathbf{H}_{bb} \end{bmatrix} \begin{Bmatrix} \mathbf{F}_a \\ \cdots \\ \mathbf{F}_c \\ \cdots \\ \mathbf{F}_b \end{Bmatrix} \qquad \text{(A1.3)}$$

APPENDIX I

REFORMULATED FRF MATRIX OF IMPEDANCE COUPLING METHOD

Without loss of generality, the FRF matrix which is assumed herein is the Receptance matrix (which can be interrelated with Mobility or Accelerance). It can be partitioned according to the previously selected interior and connection coordinates in each subsystem as follows:

$$\begin{Bmatrix} {}_A u_i \\ \cdots \\ {}_A u_c \end{Bmatrix} = \begin{bmatrix} {}_A H_{ii} & : & {}_A H_{ic} \\ \cdots & : & \cdots \\ {}_A H_{ci} & : & {}_A H_{cc} \end{bmatrix} \begin{Bmatrix} {}_A f_i \\ \cdots \\ {}_A f_c \end{Bmatrix} \qquad \text{(Al. 1)}$$

$$\begin{Bmatrix} {}_B u_i \\ \cdots \\ {}_B u_c \end{Bmatrix} = \begin{bmatrix} {}_B H_{ii} & : & {}_B H_{ic} \\ \cdots & : & \cdots \\ {}_B H_{ci} & : & {}_B H_{cc} \end{bmatrix} \begin{Bmatrix} {}_B f_i \\ \cdots \\ {}_B f_c \end{Bmatrix} \qquad \text{(A1.2)}$$

The coordinates in the FRF matrix of the coupled structure can be partitioned according to three regions corresponding to,

- the interior coordinates of component A ($_A n_i$) denoted as **a**
- the interior coordinates of component B ($_B n_i$) denoted as **b**
- the common connection coordinates of component A and B ($_A n_c = {}_B n_c = n_c$) denoted as c

The whole system will possess an FRF matrix such as,

$$\begin{Bmatrix} U_a \\ \cdots \\ U_c \\ \cdots \\ U_b \end{Bmatrix} = \begin{bmatrix} H_{aa} & :H_{ac} & : H_{ab} \\ \cdots & : & \cdots \\ H_{ca} & : H_{cc} & : H_{cb} \\ \cdots & : & \cdots \\ H_{ba} & : H_{bc} & : H_{bb} \end{bmatrix} \begin{Bmatrix} F_a \\ \cdots \\ F_c \\ \cdots \\ F_b \end{Bmatrix} \qquad \text{(A1.3)}$$

The compatibility of displacements and equilibrium of forces between the two subsystems are expressed as,

$$\{U_a\} = \{{}_A u_i\} \tag{A1.4}$$

$$\{U_b\} = \{{}_B u_i\} \tag{A1.5}$$

$$\{U_c\} = \{{}_A u_c\} = \{{}_B u_c\} \tag{A1.6}$$

$$\{F_c\} = \{{}_A f_c\} + \{{}_B f_c\} = \{0\} \tag{A1.7}$$

$$\{F_a\} = \{{}_A f_i\} \tag{A1.8}$$

$$\{F_b\} = \{{}_B f_i\} \tag{A1.9}$$

Denoting the interconnecting force acting on each subsystem as,

$$\{f_c\} = \{{}_A f_c\} = -\{{}_B f_c\} \tag{A1.10}$$

and by invoking equation (A1.6) a relationship between $\{f_c\}$ and the acting forces $\{F_a\}$ and $\{F_b\}$ is given as,

$$\{f_c\} = [[{}_A H_{cc}] + [{}_B H_{cc}]]^{-1} ([{}_B H_{ci}]\{F_b\} - [{}_A H_{ci}]\{F_a\}) \tag{A1.11}$$

If this equation is substituted into the following relationships,

$$\{{}_A u_i\} = [{}_A H_{ii}]\{F_a\} + [{}_A H_{ic}]\{f_c\} \tag{A1.12}$$

$$\{{}_B u_i\} = [{}_B H_{ii}]\{F_b\} - [{}_B H_{ic}]\{f_c\} \tag{A1.13}$$

$$\{{}_A u_c\} = [{}_A H_{ic}]\{F_a\} + [{}_A H_{cc}]\{f_c\} \tag{A1.14}$$

whose displacements ought to be equal to the displacements,

$$\{U_a\} = [H_{aa}]\{F_a\} + [H_{ab}]\{F_b\} \tag{A1.15}$$

$$\{U_b\} = [H_{ba}]\{F_a\} + [H_{bb}]\{F_b\} \tag{A1.16}$$

$$\{U_c\} = [H_{ca}]\{F_a\} + [H_{cb}]\{F_b\} \tag{A1.17}$$

respectively, this leads to the required relationships between the sub-matrices of the whole system FRF matrix and the sub-matrices of each component FRF matrix as presented next,

$$[H_{aa}]_{A n_i \times A n_i} = [{}_A H_{ii}] - [{}_A H_{ic}] \left[[{}_A H_{cc}] + [{}_B H_{cc}] \right]^{-1} [{}_A H_{ci}] \quad \text{(A1.18)}$$

$$[H_{bb}]_{B n_i \times B n_i} = [{}_B H_{ii}] - [{}_B H_{ic}] \left[[{}_A H_{cc}] + [{}_B H_{cc}] \right]^{-1} [{}_B H_{ci}] \quad \text{(A1.19)}$$

$$[H_{ca}]_{n_c \times A n_i} = [{}_A H_{ci}] - [{}_A H_{cc}] \left[[{}_A H_{cc}] + [{}_B H_{cc}] \right]^{-1} [{}_A H_{ci}] \quad \text{(A1.20)}$$

$$[H_{cb}]_{n_c \times B n_i} = [{}_A H_{cc}] \left[[{}_A H_{cc}] + [{}_B H_{cc}] \right]^{-1} [{}_B H_{ci}] \quad \text{(A1.21)}$$

$$[H_{ab}]_{A n_i \times B n_i} = [{}_A H_{ic}] \left[[{}_A H_{cc}] + [{}_B H_{cc}] \right]^{-1} [{}_B H_{ci}] \quad \text{(A1.22)}$$

$$[H_{cc}]_{A n_i \times B n_i} = [{}_B H_{cc}] \left[[{}_A H_{cc}] + [{}_B H_{cc}] \right]^{-1} [{}_A H_{cc}] \quad \text{(A1.23)}$$

or in a condensed expression as,

$$\begin{bmatrix} H_{aa} : H_{ac} : H_{ab} \\ \cdots : \cdots : \cdots \\ H_{ca} : H_{cc} : H_{cb} \\ \cdots : \cdots : \cdots \\ H_{ba} : H_{bc} : H_{bb} \end{bmatrix} = \begin{bmatrix} {}_A H_{ii} : {}_A H_{ic} : 0 \\ \cdots : \cdots : \cdots \\ {}_A H_{ci} : {}_A H_{cc} : 0 \\ \cdots : \cdots : \cdots \\ 0 : 0 : {}_B H_{ii} \end{bmatrix} - \begin{bmatrix} {}_A H_{ic} \\ \cdots \\ {}_A H_{cc} \\ \cdots \\ {}_B H_{ic} \end{bmatrix} \left[[{}_A H_{cc}] + [{}_B H_{cc}] \right]^{-1} \begin{bmatrix} {}_A H_{ic} \\ \cdots \\ {}_A H_{cc} \\ \cdots \\ {}_B H_{ic} \end{bmatrix}^T$$

(A 1.24)

APPENDIX II

RESIDUAL FLEXIBILITY CALCULATION

1 THEORETICAL ROUTE

The equation of motion for an undamped system is represented as,

$$[M]\{\ddot{u}\} + [K]\{u\} = \{F\} \qquad \text{(A2.1-a)}$$

or, in partitioned form:

$$\begin{bmatrix} M_{ii} & : & M_{ic} \\ \cdots & : & \cdots \\ M_{ci} & : & M_{cc} \end{bmatrix} \begin{Bmatrix} \ddot{u}_i \\ \cdots \\ \ddot{u}_c \end{Bmatrix} + \begin{bmatrix} K_{ii} & : & K_{ic} \\ \cdots & : & \cdots \\ K_{ci} & : & K_{cc} \end{bmatrix} \begin{Bmatrix} u_i \\ \cdots \\ u_c \end{Bmatrix} = \begin{Bmatrix} 0 \\ \cdots \\ f_c \end{Bmatrix} \qquad \text{(A2.1-b)}$$

Assuming free harmonic motion, the eigensolution leads to the Modal model, formed of the m=N mass-normalised mode shapes $[\Phi]_n$ and the m natural frequencies $\left[\omega_{rm}^2\right]$. Each coordinate displacement can now be represented as,

$$\{u\} = [\Phi_m]\{p_m\} \qquad \text{(A2.2)}$$

or, by grouping the mode shapes according to the kept modes $[\Phi_k]$ and the eliminated or neglected out-of-range modes $[\Phi_e]$, as:

$$\{u\} = [\Phi_k]\{p_k\} + [\Phi_e]\{p_e\} = [\Phi_k : \Phi_e] \begin{Bmatrix} p_k \\ \cdots \\ p_e \end{Bmatrix} \qquad \text{(A2.3)}$$

Substituting equation (A2.3) into (A2.1) yields,

$$\left[-\omega^2 [I] + \begin{bmatrix} \omega_{rk}^2 & \vdots & 0 \\ \cdots\cdots & \vdots & \cdots\cdots \\ 0 & \vdots & \omega_{re}^2 \end{bmatrix} \right] \begin{Bmatrix} p_k \\ \cdots \\ p_e \end{Bmatrix} = \left[\Phi_k : \Phi_e \right]^T \{F\} \qquad (A2.4)$$

1.1 APPROXIMATE METHOD

Substituting equation (A2.3) into (A2.1-a) leads to,

$$[[K] - \omega^2 [M]] [\Phi_k] \{p_k\} + [[K] - \omega^2 [M]] [\Phi_e] \{p_e\} = \{F\} \quad (A2.5)$$

Pre-multiplying equation (A2.5) $[\Phi_e]^T$ and considering the orthogonality of the natural modes, the following equation is obtained,

$$\left(-\omega^2 [I] + \left[\omega_{re}^2 \right] \right) \{p_e\} = [\Phi_e]^T \{F\} \qquad (A2.6)$$

which gives the modal coordinates associated with the higher modes $\left[\omega_{re}^2 \right]$,

$$\{p_e\} = \left[-\omega^2 [I] + \left[\omega_{re}^2 \right] \right]^{-1} [\Phi_e]^T \{F\} \qquad (A2.7)$$

or, for the respective displacements,

$$\{u_e'\} = [\Phi_e] \left[-\omega^2 [I] + \left[\omega_{re}^2 \right] \right]^{-1} [\Phi_e]^T \{F\} \qquad (A2.8)$$

Since we assume that $\omega_{re}^2 >> \omega_r^2$, this equation can be approximated to,

$$\{u_e'\} = [\Phi_e] \left[\omega_{re}^2 \right]^{-1} [\Phi_e]^T \{F\} \qquad (A2.9)$$

so that the residual flexibility matrix is given by:

$$[R] = [\Phi_e] \left[\omega_{re}^2 \right]^{-1} [\Phi_e]^T \qquad (A2.10)$$

1.2 IMPROVED METHOD

In this case a distinction must be made between constrained and unconstrained structures, always assuming that the system is not constrained in its connection degrees of freedom.

1.2.1 CONSTRAINED STRUCTURES

The following procedure is based on Hansteen's method [69] which permits the calculation of a more accurate residual flexibility matrix.

Let us re-write the second term of equation (A2.4) as,

$$\left[\Phi_k : \Phi_e\right]^T \{F\} = [I]\begin{Bmatrix} f_k \\ \cdots \\ f_e \end{Bmatrix} \qquad \text{(A2.11)}$$

Because of the mass-normalisation of the mode shapes, the following relationship is valid:

$$[I] = \left[\Phi_k : \Phi_e\right]^T [M]\left[\Phi_k : \Phi_e\right] \qquad \text{(A2.12)}$$

which, when substituted into equation (A2.11) gives,

$$\{F\} = [M]\left[\Phi_k : \Phi_e\right]\begin{Bmatrix} f_k \\ \cdots \\ f_e \end{Bmatrix} \qquad \text{(A2.13)}$$

or

$$\{F\} = [M]\left[\Phi_k\right]\{f_k\} + [M]\left[\Phi_e\right]\{f_e\} \qquad \text{(A2.14)}$$

$$\{F\} = \{f_k'\} + \{f_e'\} \qquad \text{(A2.15)}$$

This means that the force vector is composed of two parts; the first one is exciting the kept modes and the second is used to excite the remaining modes. This latter contribuition is

$$\{f_e'\} = \{F\} - [M][\Phi_k]\{f_k\} \quad \text{(A2.16)}$$

$$\{f_e'\} = \left[[I] - [M][\Phi_k][\Phi_k]^T\right]\{F\} \quad \text{(A2.17)}$$

The displacement due to that force is then:

$$\{u_e\} = [[K] - \omega^2[M]]^{-1}\{f_e'\}$$

$$\{u_e\} = [[K] - \omega^2[M]]^{-1}\left[[I] - [M][\Phi_k][\Phi_k]^T\right]\{F\} \quad \text{(A2.18)}$$

In cases where the out-of-range natural frequencies are much greater than the frequencies of interest, it is possible to approximate equation (A2.18) to:

$$\{u_e\} = [K]^{-1}\left[[I] - [M][\Phi_k][\Phi_k]^T\right]\{F\} \quad \text{(A2.19)}$$

The residual flexibility matrix is given by:

$$[R] = [G]\left[[I] - [M][\Phi_k][\Phi_k]^T\right] \quad \text{(A2.20)}$$

or $$[R] = [G] - [\Phi_k][\omega_{rk}^2]^{-1}[\Phi_k]^T$$

with $[G] = [K]^{-1}$ being the total flexibility matrix.

1.2.2 UNCONSTRAINED STRUCTURES

In the case of unconstrained structures, it is not possible to invert the stiffness matrix and so another approach should be employed. Craig [68] suggests the following procedure;

Firstly, the modes are separated into rigid-body and flexible modes such that,

$$\{u\} = [\Phi_r]\{p_r\} + [\Phi_f]\{p_f\} = [\Phi_r : \Phi_f]\begin{Bmatrix} p_r \\ \cdots \\ p_f \end{Bmatrix} \quad \text{(A2.21)}$$

In order to create an invertible stiffness matrix, the rigid body motion must be removed. When equation (A2.21) is substituted into equation (A2.1-a) the uncoupled equations are obtained,

$$[\mathbf{I}]\{\ddot{\mathbf{p}}_r\} = [\Phi_r]^T \{\mathbf{F}\} \qquad \text{(A2.22)}$$

$$[\mathbf{I}]\{\ddot{\mathbf{p}}_f\} + [\omega_{rf}^2]\{\mathbf{p}_f\} = [\Phi_f]^T \{\mathbf{F}\} \qquad \text{(A2.23)}$$

From equation (A2.22) it is seen that, as far as rigid-body motion is concerned, the external forces are reacted by rigid-body inertia forces. Thus, if these forces are subtracted from the applied force there will be no excitation of the rigid-body modes. The net force producing flexible motion is thus given by:

$$\{\mathbf{F}_f\} = \{\mathbf{F}\} + \{\mathbf{f}_i\} = [\mathbf{I}] - [\mathbf{M}][\Phi_r][\Phi_r]^T]\{\mathbf{F}\} \qquad \text{(A2.24)}$$

$$\{\mathbf{F}_f\} = [\mathbf{A}]\{\mathbf{F}\} \qquad \text{(A2.25)}$$

This force will produce a pseudo-static displacement, provided that some arbitrary statically-determinate constraints are imposed. Let $[\mathbf{R}_*]$ be the flexibility matrix relative to the imposed constraints (which includes rows and columns of zeros at the constraint DoF). Then the pseudo-static displacement is:

$$\{\mathbf{u}^*\} = [\mathbf{R}^*]\{\mathbf{F}_f\}$$

$$\{\mathbf{u}^*\} = [\mathbf{R}^*][\mathbf{A}]\{\mathbf{F}\} \qquad \text{(A2.26)}$$

The equation giving the final displacement is then:

$$\{\mathbf{u}\} = [\mathbf{G}]\{\mathbf{F}\} \qquad \text{(A2.27)}$$

with

$$[\mathbf{G}] = [\mathbf{K}]^{-1}[\mathbf{A}]^T[\mathbf{R}^*][\mathbf{A}] \qquad \text{(A2.28)}$$

being the total flexibility matrix which should be substituted into equation (A2.20) for the calculation of the relevant residual flexibility matrix **[R]**.

2. EXPERIMENTAL ROUTE

From the Response model of a given structure, a modal identification may be applied in order to extract the modal parameters **[1]**. For each measured FRF (Frequency Response Function), say the Receptance obtained by measuring the displacement at coordinate j by exciting the structure at coordinate k, a set of modal parameters is extracted for each of the existing modes,

$_rA_{jk}$ -- Modal Constant (Modulus + Phase)

ω_r -- natural frequency

ζ_r -- damping factor

The Receptance for a particular case of a lightly damped structure is theoretically given by,

$$\frac{x_j}{f_k} = \alpha_{jk}(\omega) = \sum_{r=1}^{\infty} \frac{{}_rA_{jk}}{\omega_r^2 - \omega^2} \qquad \text{(A2.29)}$$

Let us suppose that only m_k modes have been measured in the frequency range of interest, but that there are also other modes outside this range at lower frequencies and at higher frequencies. Equation (A2.29) may now be written as,

$$\alpha_{jk}(\omega) = \sum_{r=1}^{m_1} \frac{{}_rA_{jk}}{\omega_r^2 - \omega^2} + \sum_{r=m_1+1}^{m_1+m_k} \frac{{}_rA_{jk}}{\omega_r^2 - \omega^2} + \sum_{r=m_1+m_k+1}^{\infty} \frac{{}_rA_{jk}}{\omega_r^2 - \omega^2} \qquad \text{(A2.30)}$$

At lower frequencies, i.e. for $\omega_r << \omega$, the first term can be approximated as:

$$\sum_{r=1}^{m_1} \frac{{}_rA_{jk}}{-\omega^2} = \frac{S_{jk}}{-\omega^2} \qquad \text{(A2.3 1)}$$

corresponding to a ***residual mass*** which accounts for the out-of-range low frequency terms (S_{jk} has dimension *1/mass* and units ***l/kg***) Conversely, at higher frequencies we have $\omega_r >> \omega$ leading to the approximation for the third term,

$$\sum_{r=m_1+m_k+1}^{\infty} \frac{{}_rA_{jk}}{\omega_r^2} = R_{jk} \qquad \text{(A2.32)}$$

which corresponds to a ***residual compliance*** or ***flexibility,*** accounting for the out-of-range high frequency modes (R_{jk} has dimensions *1/stiffness* and units ***m/N***).

Assuming that the low frequency residual can be represented by a zero-frequency mode, we may write for the **point response** Receptance;

$$\frac{x_j}{f_j} = \alpha_{jj}(\omega) = \sum_{r=1}^{m_k} \frac{{}_rA_{jj}}{\omega_r^2 - \omega^2} + R_{jj} \qquad \text{(A2.33)}$$

The residual flexibility matrix is then constructed by measuring all the necessary R_{jk} values; sometimes, and because transfer residual flexibility values are negligible when compared with the point response residuals, only the diagonal elements are considered.

The ***high-frequency residual*** can be visualised as a ***spring,*** attached to the system at the corresponding coordinates. The high frequency residual is an approximation to the combined effects of a number of modes which can be expressed in terms of a modal constant of a fictitious mode at an assumed ressonance frequency. It is important to note that there is **no** mode shape associated to the fictitious residual mode.

APPENDIX III

MATRIX PROPERTIES

1 MATRIX NORMS

The most frequently-used matrix norms in numerical analysis is the F-norm (Frobenius norm) given as,

$$\| A \|_F = \left[\sum_{i=1}^{m} \sum_{i=1}^{m} | a_{ij} |^2 \right]^{\frac{1}{2}}$$

$$\| A \|_F^2 = \sigma_1^2 + \sigma_2^2 + \ldots + \sigma_n^2 \quad (\sigma_i \text{ are the singular values of } [A])$$

and the p-norms (especially $p=1,2,\infty$)

$$\| A \|_p = \sup_{x \neq 0} \frac{\| Ax \|_p}{\| x \|_p}$$

$$\| A \|_1 = \max_j \sum_{i=1}^{m} | a_{ij} |$$

$$\| A \|_2 = [\text{ max eigen of } [A]^T[A]]^{\frac{1}{2}} = \sigma_1$$

$$\| A \|_\infty = \max_i \sum_{j=1}^{n} | a_{ij} |$$

The Frobenius norms and the p-norms satisfy certain inequalities such as,

$$\| A \|_2 \leq \| A \|_F \leq \sqrt{n} \| A \|_2$$

$$\max | a_{ij} | \leq \| A \|_2 \leq \sqrt{m n} \max | a_{ij} |$$

2 RANK PROPERTIES

The rank of a matrix, r = $\mathrm{rank}([A]_{mxn})$, is the number of linearly independent rows (and columns) in a given matrix. Some of the rank properties of a matrix are presented next:

- r is a positive integer
- $\mathrm{rank}([A]_{mxn}) \leq m$ and $\leq n$: the rank of a matrix equals or is less than the smaller of its number of rows or columns
- $\mathrm{rank}([A]_{nxn}) \leq n$: a square matrix has rank not exceeding its order
- when $r \neq 0$ there is at least one square submatrix of [A] having order r that is non-singular
- when $\mathrm{rank}([A]_{nxn}) = n$ then [A] is non-singular i.e., $[A]^{-1}$ exists and is said to have full rank
- when $\mathrm{rank}([A]_{mxn}) = m < n$ [A] is said to have full row rank
- when $\mathrm{rank}([A]_{mxn}) = n < m$ [A] is said to have full column rank

3 LINEAR COMBINATION OF VECTORS

Let us assume n vectors, all of them of the same order, which we call a set of n vectors $[A] \equiv [\{a_1\}\{a_2\}\cdots\{a_n\}]$ and the scalars $x_1, x_2, \ldots, x_n$. The product $[A]\{x\} = \sum_{i=1}^{n} x_i \{a_i\}$ is called a linear combination of the set of the n vectors.

- [A] {x) is a column vector, a linear combination of the columns of [A]
- $(b\}^T[A]$ is a row vector, a linear combination of the rows of [A]
- [A][B] is matrix with its rows being a linear combination of the rows of [B] and its columns being a linear combination of the columns of [A]

Given a set of vectors, their dependence or independence can be ascertained by attempting to solve [A]{ x} = {0}. If a solution can be found other than {x) = {0} (which is always a solution), then it will be a non-null solution, and the vectors will be dependent. Otherwise they are linearly independent.

A set of linearly independent vectors of order n can not contain more than n such vectors. An important characteristic concerning the independence of rows and columns in a given matrix is that the number of linearly independent rows is the same as the number of linearly independent columns.

4 PERMUTATION MATRICES

An elementary permutation matrix denoted as $[E_{rs}]$ is obtained from an identity matrix by interchanging its r^{th} and s^{th} rows. The pre-multiplication of [A] by $[E_{rs}]$ interchanges rows r and s so does post-multiplication interchange columns.

In general , a permutation matrix is an identity matrix with its rows re-sequenced in some order. Because such a matrix is always a product of elementary matrices [E], it is not necessarily symmetric but it is always orthogonal. One of the great uses of permutation matrices is that they provide a mechanism for re-sequencing columns in a matrix so that a matrix having r linearly independent rows can be re-sequenced into one having its first r rows and its first r columns as linearly independent.

APPENDIX IV

RIGID BODY MOTION

1. DYNAMICS

The basic configuration of a rigid-body is shown in fig. A4.1.

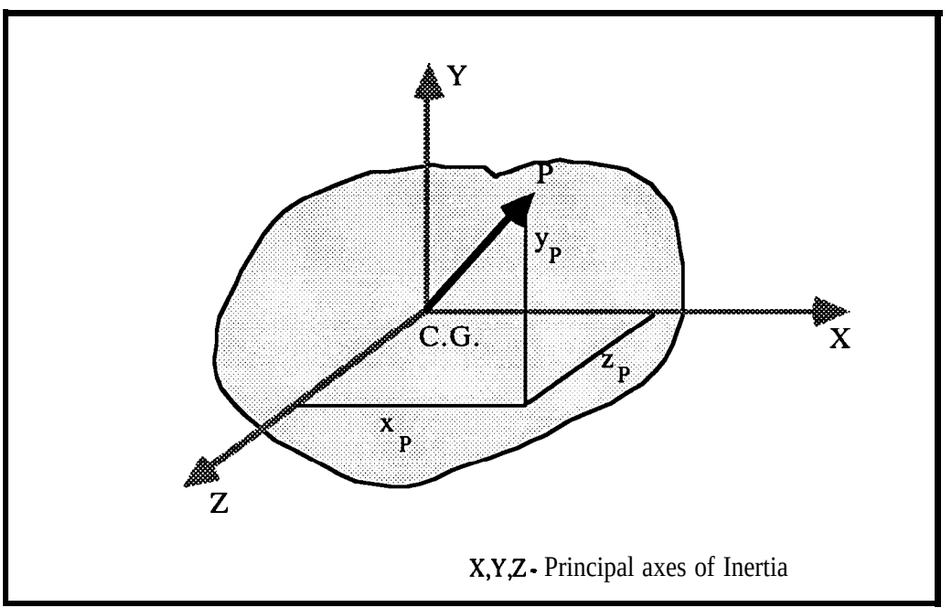

X,Y,Z - Principal axes of Inertia

Let us assume that the inertia characteristics - i.e., the mass m and the principal mass moments of inertia I_{xx}, I_{yy} and I_{zz} - are known.

The dynamic equilibrium equation for an unrestrained body with respect to the principal axes is,

$$\begin{Bmatrix} {}_G F_x \\ {}_G F_y \\ {}_G F_z \\ M_x \\ M_y \\ M_z \end{Bmatrix} = \begin{bmatrix} m & & & & & \\ & m & & & & \\ & & m & & & \\ & & & I_{xx} & & \\ & & & & I_{YY} & \\ & & & & & I_{zz} \end{bmatrix} \begin{Bmatrix} \ddot{x}_G \\ \ddot{y}_G \\ \ddot{z}_G \\ \ddot{\theta}_x \\ \ddot{\theta}_y \\ \ddot{\theta}_z \end{Bmatrix} \qquad \text{(A4. l-a)}$$

$$\{F\}_G = \left[\grave{M}_{GG} \right] \{\ddot{u}\}_G \qquad \text{(A4. l-b)}$$

or in the inverse form

$$\begin{Bmatrix} \ddot{x}_G \\ \ddot{y}_G \\ \ddot{z}_G \\ \ddot{\theta}_x \\ \ddot{\theta}_y \\ \ddot{\theta}_z \end{Bmatrix} = \begin{bmatrix} 1/m & & & & & \\ & 1/m & & & & \\ & & 1/m & & & \\ & & & 1/I_{xx} & & \\ & & & & 1/I_{yy} & \\ & & & & & 1/I_{zz} \end{bmatrix} \begin{Bmatrix} {}_G F_x \\ {}_G F_y \\ {}_G F_z \\ M_x \\ M_y \\ M_z \end{Bmatrix} \qquad \text{(A4.2-a)}$$

$$\{\ddot{u}\}_G = \left[\grave{M}_{GG} \right]^{-1} \{F\}_G \qquad \text{(A4.2-b)}$$

The point P has position coordinates (x_p, y_p, z_p) in the principal reference system. Assuming small axis rotations, the general displacement (acceleration) at point P is related to the centroidal displacements (accelerations) by the equation,

$$\begin{Bmatrix} \ddot{x}_P \\ \ddot{y}_P \\ \ddot{z}_P \\ \ddot{\theta}_x \\ \ddot{\theta}_y \\ \ddot{\theta}_z \end{Bmatrix} = \begin{bmatrix} 1 & 0 & 0 & 0 & z_P & -y_P \\ 0 & 1 & 0 & -z_P & 0 & x_P \\ 0 & 0 & 1 & y_P & -x_P & 0 \\ 0 & 0 & 0 & 1 & 0 & 0 \\ 0 & 0 & 0 & 0 & 1 & 0 \\ 0 & 0 & 0 & 0 & 0 & 1 \end{bmatrix} \begin{Bmatrix} \ddot{x}_G \\ \ddot{y}_G \\ \ddot{z}_G \\ \ddot{\theta}_x \\ \ddot{\theta}_y \\ \ddot{\theta}_z \end{Bmatrix} \qquad \text{(A4.3-a)}$$

$$\{\ddot{u}\}_P = [T_{PG}]\{\ddot{u}\}_G \qquad \text{(A4.3-b)}$$

being the general force vector at point P related to the centroidal vector of general forces by the equation

$$\{F\}_G = [T_{PG}]^T \{F\}_P \qquad \text{(A4.4)}$$

For another point Q, a similar relationships exist,

$$\{\ddot{u}\}_Q = [T_{QG}]\{\ddot{u}\}_G \qquad \text{(A4.5)}$$

$$\{F\}_G = [T_{QG}]^T \{F\}_Q \qquad \text{(A4.6)}$$

If the force is now acting at point Q, the resulting responses at point P will be given as,

$$\{\ddot{u}\}_P = [M_{PQ}]^{-1} \{F\}_Q \qquad \text{(A4.7)}$$

with

$$[M_{PQ}]^{-1} = [T_{PG}] \left[M_{GG} \right]^{-1} [T_{QG}]^T \qquad \text{(A4.8)}$$

This is the matrix of the “transferred” rigid-body Accelerance (Inertance) between points Q and P.

It is interesting to note that the first three diagonal terms contain components corresponding to the three rigid-body modes; one of the components is due to the translational motion whereas the other two are related to rotational motions.

The full transferred Accelerance matrix elements are presented next,

$$[M_{PQ}]^{-1} =$$

$$\begin{bmatrix}
\frac{1}{m}+\frac{z_P z_Q}{I_{YY}}+\frac{y_P y_Q}{I_{zz}} & \frac{-y_P x_Q}{I_{zz}} & \frac{-z_P x_Q}{I_{YY}} & 0 & \frac{z_P}{I_{YY}} & \frac{-y_P}{I_{zz}} \\
\frac{-x_P y_Q}{I_{zz}} & \frac{1}{m}+\frac{z_P z_Q}{I_{xx}}+\frac{x_P x_Q}{I_{zz}} & \frac{-z_P y_Q}{I_{xx}} & \frac{-z_P}{I_{xx}} & 0 & \frac{x_P}{I_{zz}} \\
\frac{-x_P z_Q}{I_{YY}} & \frac{-y_P z_Q}{I_{xx}} & \frac{1}{m}+\frac{y_P y_Q}{I_{xx}}+\frac{x_P x_Q}{I_{YY}} & \frac{y_P}{I_{xx}} & \frac{-x_P}{I_{yy}} & 0 \\
0 & \frac{-z_Q}{I_{xx}} & \frac{y_Q}{I_{xx}} & \frac{1}{I_{xx}} & 0 & 0 \\
\frac{z_Q}{I_{YY}} & 0 & \frac{-x_Q}{I_{YY}} & 0 & \frac{1}{I_{yy}} & 0 \\
\frac{-y_Q}{I_{zz}} & \frac{x_Q}{I_{ZX}} & 0 & 0 & 0 & \frac{1}{I_{zz}}
\end{bmatrix}$$

(A4.9)

The forces applied at point Q may be related to the resulting responses at point P by using the “transferred” Inertia or Mass matrix

$$\{F\}_Q = [M_{PQ}]\{\ddot{u}\}_P \qquad \text{(A4.10)}$$

being the $[M_{PQ}]$ matrix elements presented as follows

$$[M_{PQ}] = \begin{bmatrix}
m & 0 & 0 & 0 & -mz_P & my_P \\
0 & m & 0 & mz_P & 0 & -mx_P \\
0 & 0 & m & -my_P & mx_P & 0 \\
0 & mz_Q & -my_Q & I_{xx}+m(z_P z_Q+y_P y_Q) & -mx_P y_Q & -mx_P z_Q \\
-mz_Q & 0 & mx_Q & -my_P x_Q & I_{yy}+m(z_P z_Q+x_P x_Q) & -my_P z_Q \\
my_Q & -mx_Q & 0 & -mz_P x_Q & -mz_P y_Q & I_{zz}+m(y_P y_Q+x_P x_Q)
\end{bmatrix}$$

(A4.11)

2. RIGID-BODY MODE-SHAPES

For a freely-supported structure, the low-frequency response is dominated by the rigid-body modes, which resonate at zero frequency. From Appendix II, the low-frequency residual receptance due to the six rigid-body modes is given by,

$$\frac{x_j}{f_k} = \alpha_{jk}(\omega) = \sum_{r=1}^{6} \frac{{}_r\phi_j \, {}_r\phi_k}{-\omega^2} = \frac{S_{jk}}{-\omega^2} \qquad \text{(A4.12)}$$

or in terms of Accelerance,

$$\frac{\ddot{x}_j}{f_k} = -\omega^2 \alpha_{jk}(\omega) = I_{jk}(\omega) = -\omega^2 \sum_{r=1}^{6} \frac{{}_r\phi_j \, {}_r\phi_k}{-\omega^2} = S_{jk} \qquad \text{(A4.13)}$$

each term in ${}_r\phi_j$ corresponds to an element in vector ${}_r\{\Phi\}$.

At zero frequency, the six rigid-body modes - three translational and three rotational - may resonate together; thus, depending on the geometrical properties and on the location of the exciting force, the modal constant S_{jk} calculated for the zero frequency mode may contain a combination of the different rigid-body modes. Then, this combined information must be separated before the full matrix $[\Phi]$ can be evaluated. For each point, say P, six possible displacements are considered,

$$\{\Phi\}_P = \begin{Bmatrix} x_P \\ y_P \\ z_P \\ \theta_x \\ \theta_y \\ \theta_z \end{Bmatrix} \qquad \text{(A4.14)}$$

2.1 *Translational* RIGID-BODY MODE-SHAPES

In the rigid-body motion involving only translational motions along the X, Y and Z axis respectively, all the rotational displacements are zero except the corresponding axial displacements. The mode shape vector related to point P is then,

$$_{\text{Transl.}}[\Phi]_P = \left[{}_x\{\Phi\}_P \mid {}_y\{\Phi\}_P \mid {}_z\{\Phi\}_P \right] \qquad \text{(A4.15)}$$

$$_{\text{Transl.}}[\Phi]_P = \left[C_x \begin{Bmatrix} 1 \\ 0 \\ 0 \\ 0 \\ 0 \\ 0 \end{Bmatrix} \vdots \; C_y \begin{Bmatrix} 0 \\ 1 \\ 0 \\ 0 \\ 0 \\ 0 \end{Bmatrix} \vdots \; C_z \begin{Bmatrix} 0 \\ 0 \\ 1 \\ 0 \\ 0 \\ 0 \end{Bmatrix} \right] \qquad \text{(A4.16)}$$

C_x, C_y and C_z being the scaling factors to be calculated according to normalisation process.

2.2 *Rotational* RIGID-BODY MODE-SHAPES

Since we assume small rotations, the corresponding rotational rigid-body mode-shapes are,

$$_{\text{Rot.}}[\Phi]_P = \left[{}_{\theta_x}\{\Phi\}_P \mid {}_{\theta_y}\{\Phi\}_P \mid {}_{\theta_z}\{\Phi\}_P \right] \qquad \text{(A4.17)}$$

$$_{\text{Rot.}}[\Phi]_P = \left[C_{\theta_x} \begin{Bmatrix} 0 \\ -z_P \\ y_P \\ 1 \\ 0 \\ 0 \end{Bmatrix} \vdots \; C_{\theta_y} \begin{Bmatrix} z_P \\ 0 \\ -x_P \\ 0 \\ 1 \\ 0 \end{Bmatrix} \vdots \; C_{\theta_z} \begin{Bmatrix} -y_P \\ x_P \\ 0 \\ 0 \\ 0 \\ 1 \end{Bmatrix} \right] \qquad \text{(A4.18)}$$

where $C_{\theta_x}, C_{\theta_y}$ and C_{θ_z} are the rotational scaling factors.

2.3 Normalised RIGID-BODY MODE-SHAPES

Let us consider the case of the response at point P due to the excitation at the same point. **The** full non-normalised rigid-body mode shape matrix for point P is given by,

$$[\Phi]_P = \left[{}_{\text{Transl.}}[\Phi]_P : \text{Rot.}\,[\Phi]_P \right] \tag{A4.19}$$

The scaling factors are calculated by imposing the orthogonalisation condition with respect to the mass matrix $[M_{PP}]$, which is calculated by using equation (A4.11) for the case of a point excitation (Q=P). Thus,

$$[\Phi]_P^T [M_{PP}] [\Phi]_P = [I] \tag{A4.20}$$

which gives for the scaling factors the following values,

$$C_x = C_y = C_z = \frac{1}{\sqrt{m}}$$

$$C_{\theta_x} = \frac{1}{\sqrt{I_{xx}}} \tag{A4.21}$$

$$C_{\theta_y} = \frac{1}{\sqrt{I_{yy}}}$$

$$C_{\theta_z} = \frac{1}{\sqrt{I_{zz}}}$$

The full mass-normalised rigid-body mode shape matrix is then represented as,

$$\begin{bmatrix} \Phi_{x_P} \\ \Phi_{y_P} \\ \Phi_{z_P} \\ \Phi_{\theta_x} \\ \Phi_{\theta_y} \\ \Phi_{\theta_z} \end{bmatrix} = \left[\frac{1}{\sqrt{m}} \begin{Bmatrix} 1 \\ 0 \\ 0 \\ 0 \\ 0 \\ 0 \end{Bmatrix} \vdots \frac{1}{\sqrt{m}} \begin{Bmatrix} 0 \\ 1 \\ 0 \\ 0 \\ 0 \\ 0 \end{Bmatrix} \vdots \frac{1}{\sqrt{m}} \begin{Bmatrix} 0 \\ 0 \\ 1 \\ 0 \\ 0 \\ 0 \end{Bmatrix} \vdots \right.$$

$$\left. \frac{1}{\sqrt{I_{xx}}} \begin{Bmatrix} 0 \\ -z_P \\ y_P \\ 1 \\ 0 \\ 0 \end{Bmatrix} \vdots \quad \frac{1}{\sqrt{I_{yy}}} \begin{Bmatrix} z_P \\ 0 \\ -x_P \\ 0 \\ 1 \\ 0 \end{Bmatrix} \vdots \frac{1}{\sqrt{I_{zz}}} \begin{Bmatrix} -y_P \\ x_P \\ 0 \\ 0 \\ 0 \\ 1 \end{Bmatrix} \right] \quad \text{(A4.22)}$$